



รายงานวิจัยฉบับสมบูรณ์

(เล่มที่ 3 ของจำนวน 3 เล่ม)

โครงการ

งานวิจัยขั้นสูงทางการให้ส่องสถานะและการเพิ่ม
ความสามารถในการถ่ายทอดความร้อน

โดย

ศ. ดร. สมชาย วงศ์วิเศษ

ภาควิชาวิศวกรรมเครื่องกล คณะวิศวกรรมศาสตร์

มหาวิทยาลัยเทคโนโลยีพระจอมเกล้าธนบุรี

วันที่ 31 มีนาคม 2557

ภาคผนวก ข.

ผลงานการจดสิทธิบัตร

เลขที่สิทธิบัตร 31282



สป/200 - ช

สิทธิบัตรการประดิษฐ์

อาศัยอำนาจตามความในพระราชบัญญัติสิทธิบัตร พ.ศ. 2522

ด้วยมหัศรีพยัลลินทางปัญญาออกแบบสิทธิบัตรฉบับนี้ให้แก่

มหาวิทยาลัยเทคโนโลยีพระจอมเกล้าธนบุรี

สำนักงานกองทุนสนับสนุนการวิจัย

สำหรับการประดิษฐ์ตามรายละเอียดการประดิษฐ์ ข้อดีสิทธิ และรูปเขียน (ถ้ามี)
ภายในสิทธิบัตรนี้

ที่ด้วยเลขที่ 0101005157 (070592)

ขอรับสิทธิบัตร 20 มีนาคม 2544

ประดิษฐ์ นายสมชาย วงศ์เศษ และคณะ

แสดงถึงการประดิษฐ์ อุปกรณ์แลกเปลี่ยนความร้อนแบบท่อขดเบนวง

ให้สูตรจะ พลิกอินโนเก้นท์คามกภูมายาวลักษณ์สิทธิบัตรทุกประการ
ออกให้ 23 เดือน พฤษภาคม พ.ศ. 2554
หมดอายุ 19 เดือน มีนาคม พ.ศ. 2564



พนักงานเจ้าหน้าที่

หมายเหตุ 1. ผู้ทรงสิทธิบัตรต้องชำระค่าธรรมเนียมรายปีเริ่มต้นที่ 5 ของอายุสิทธิบัตร มิฉะนั้นสิทธิบัตรจะสิ้นอายุ
2. ผู้ทรงสิทธิบัตรจะขอชำระค่าธรรมเนียมรายปีล่วงหน้าได้ข้ารรทึ้งหนึ่งเดือนในคราวเดียวที่ได้
3. การอนุญาตให้ใช้สิทธิบัตรและกิจกรรมใดๆ ก็ได้ที่สิทธิบัตรห้ามหั้นห้ามและจดทะเบียนต่อหนังสือ

011198



คำขอรับสิทธิบัตร/อนุสิทธิบัตร

การประดิษฐ์
 การออกแบบผลิตภัณฑ์
 อนุสิทธิบัตร

ข้าพเจ้าผู้ลงลายมือชื่อในคำขอรับสิทธิบัตร/อนุสิทธิบัตรนี้
 ขอรับสิทธิบัตร/อนุสิทธิบัตร ตามพระราชบัญญัติสิทธิบัตร
 พ.ศ. 2522 แก้ไขเพิ่มเติมโดยพระราชบัญญัติสิทธิบัตร (ฉบับ^{ที่ 2}) พ.ศ. 2535 และพระราชบัญญัติสิทธิบัตร (ฉบับที่ 3)
 พ.ศ. 2542

สำหรับเจ้าหน้าที่

วันรับคำขอ 30 ต.ค. 2552	เลขที่คำขอ
วันยื่นคำขอ	0901004855
สัญลักษณ์จำแนกการประดิษฐ์ระหว่างประเทศ	
ให้กับแบบผลิตภัณฑ์ ประเภทผลิตภัณฑ์	
วันประกาศโฆษณา	เลขที่ประกาศโฆษณา
วันออกสิทธิบัตร/อนุสิทธิบัตร	เลขที่สิทธิบัตร/อนุสิทธิบัตร
	ลายมือชื่อเจ้าหน้าที่

1. ชื่อที่แสดงถึงการประดิษฐ์/การออกแบบผลิตภัณฑ์

“กรรมวิธีการเลือกขนาดท่อคานปีกลูต้าไนโตรเจนให้เหมาะสมท่าความเย็นที่ใช้
 สารทำความเย็น R404A, R407B, R407C, R410A, R410B, R502A, R507Aโดยใช้แทนก๊าซ”

2. คำขอรับสิทธิบัตรการออกแบบผลิตภัณฑ์ที่เป็นคำขอส่วนบุคคลผลิตภัณฑ์อย่างเดียวกันและเป็นคำขอลำดับที่
 ในจำนวน คำขอ ที่ยื่นในคราวเดียวกัน

3. ผู้ขอรับสิทธิบัตร/อนุสิทธิบัตร และที่อยู่ (เลขที่ ถนน แขวง ตำบล ประวัติ ไทย)	3.1 สำนักงานวิจัยและพัฒนา มหาวิทยาลัยเทคโนโลยีพระจอมเกล้าธนบุรี 126 ถ.ประชาอุทิศ แขวงบางมด เขตทุ่งครุ กรุงเทพฯ 10140
1. มหาวิทยาลัยเทคโนโลยีพระจอมเกล้าธนบุรี ตั้งอยู่เลขที่ 126 ถ.ประชาอุทิศ แขวงบางมด เขตทุ่งครุ กรุงเทพฯ 10140 2. มหาวิทยาลัยธรรมศาสตร์ ตั้งอยู่เลขที่ 168 ถ. งามวงศ์วาน ต.แสลงสุข อ.เมือง ชลบุรี 20131 3. สถาบันวิจัยและพัฒนาคุณภาพชีวภาพ ตั้งอยู่เลขที่ 979 ชั้น 14 อาคารอสสอท ศูนย์วิจัยและพัฒนาคุณภาพชีวภาพ มหาวิทยาลัยเทคโนโลยีพระจอมเกล้าธนบุรี 126 ถ.ประชาอุทิศ แขวงบางมด เขตทุ่งครุ กรุงเทพฯ 101400	3.2 โทรศพท 0-2470-9685-8
	3.3 โทรศาร 0-2872-9083
	3.4 อีเมล์ research@kmutt.ac.th

4. ผู้ที่ในการขอรับสิทธิบัตร/อนุสิทธิบัตร

ผู้ประดิษฐ์/ผู้ออกแบบ ผู้ขอรับสิทธิโดยเหตุอื่น

5. ตัวแทน (ถ้ามี) / ที่อยู่ (เลขที่ ถนน จังหวัด ประเทศไทย รหัสไปรษณีย์) นางสาวผ่องศรี เวสารัช และ/หรือ นางสาวเชาวนี สนธิธรรม ศูนย์ส่งเสริมงานวิจัยและทรัพย์สินทางปัญญา มหาวิทยาลัยเทคโนโลยีพระจอมเกล้าธนบุรี 126 ถ.ประชาอุทิศ แขวงบางมด เขตทุ่งครุ กรุงเทพฯ 10140	5.1 ตัวแทนเลขที่ 1745,1739
	5.2 โทรศพท 0-2470-9705,0-2470-9685-6
	5.3 โทรศาร 0-2872-9083
	5.4 อีเมล์ research@kmutt.ac.th

6. ผู้ประดิษฐ์/ผู้ออกแบบผลิตภัณฑ์ และที่อยู่ (เลขที่ ถนน จังหวัด ประเทศไทย)

1. นายสมชาย วงศิริเสถย์ ออยู่บ้านเลขที่ 12/5 หมู่ 10 ซอยเพชรเกษม 67/1 บางแค กรุงเทพฯ 10160
 2. นายวรวรษณ์ กิริมย์ภักดี ออยู่บ้านเลขที่ 353 หมู่ที่ 2 ตำบลวังกระยะ อำเภอเมือง จังหวัดตรัง 23000

7. คำขอรับสิทธิบัตร/อนุสิทธิบัตรนี้แยกจากหรือเกี่ยวข้องกับคำขอเดิม

ผู้ขอรับสิทธิบัตร/อนุสิทธิบัตรขอให้ถือว่าได้ยื่นคำขอรับสิทธิบัตร/อนุสิทธิบัตรนี้ไว้ในวันเดียวกับคำขอรับสิทธิบัตรเลขที่
 วันยื่น

เพาะคำขอรับสิทธิบัตร/อนุสิทธิบัตรนี้แยกจากหรือเกี่ยวข้องกับคำขอเดิมเพรา

คำขอเดิมมีการประดิษฐ์หลักอย่าง

ถูกคัดค้านเนื่องจากผู้ขอไม่มีสิทธิ

ขอเปลี่ยนแปลงประเภทของสิทธิ

หมายเหตุ ในการที่ไม่อาจระบุรายละเอียดได้ครบถ้วน ให้จดทำเป็นเอกสารแนบท้ายแบบพิมพ์โดยระบุหมายเหตุกำกับข้อและหัวข้อที่แสดง
 รายละเอียดเพิ่มเติมดังกล่าวด้วย

แบบฟอร์มที่ 1001-1

หน้า ๑ จากทั้งหมด 2 หน้า

คำขอรับสิทธิบัตร/อนุสิทธิบัตร

การประดิษฐ์
 ภาระงานคอมพิวเตอร์
 ยุติสิทธิ์

เข้ามาตั้งแต่ปี พ.ศ.๒๕๕๗ ที่มาในราชบัณฑิตย์โดยวิธีต่อตัวตนนี้
 ขอเรียกอีกอย่างหนึ่งว่าติดตาม ตามที่ระบุไว้ในบัญชีติดตาม
 พ.ศ. ๒๕๒๒ ภัยพิบัติน้ำท่วมภัยติดตาม ๒๕๕๗ (ฉบับ
 ที่ ๒) พ.ศ. ๒๕๓๕ และพระราชบัญญัติสิทธิ์ (ฉบับที่ ๓)
 พ.ศ. ๒๕๔๒

1. ร่องรอยสิทธิ์และการประดิษฐ์/การขออนุสิทธิ์

“แผนภาพที่ห้ามการอพัฒนาครองราชอิ势ิอมิลันท์ ที่บ้านบึงกาฬที่บ้านบึงกาฬในระบบบริการภาครัฐที่ใช้รากทั่วโลก

R134a/R407c/R410a ”

2. ค่าตอบแทนที่ห้ามการอพัฒนาครองราชอิ势ิอมิลันท์เป็นค่าใช้จ่ายที่ห้ามรวมกับค่าใช้จ่ายอื่นๆ

3. ผู้ขอรับสิทธิ์ต้องมีสัญชาติไทย และพำนุฯ (ขอ) ถนน จังหวัด ประเทศไทย

1. พระศรีรัตนราชวิราบที่ ๑๒๘ พระบรมราชูปถัมภ์ ๑๐๑๐ ถนน จังหวัด ประเทศไทย

2. สำนักงานคณะกรรมการสิ่งแวดล้อม ๑๕๗๗ ชั้น ๑๔ ชาราชสห
 เอเชียพาร์ค ถนนพหลโยธิน ๑๐๐๐ ถนน จังหวัด ประเทศไทย

๓. ศูนย์พัฒนาและทดสอบเทคโนโลยี ๑๔๐๐ ถนน จังหวัด ประเทศไทย

4. สิทธิ์ในการห้ามการอพัฒนาครองราชอิ势ิอมิลันท์

□ ผู้ขอรับสิทธิ์ต้องมีสัญชาติไทย และพำนุฯ (ขอ) ถนน จังหวัด ประเทศไทย

5. ค่าตอบแทน (รายปี) ๑๐๐๐ (พัน) ถนน จังหวัด ประเทศไทย

๖. บานสหกรณ์ ๗๕๗๗ ถนน จังหวัด ประเทศไทย

๗. บานสหกรณ์ ๗๕๗๗ ถนน จังหวัด ประเทศไทย

๘. บานสหกรณ์ ๗๕๗๗ ถนน จังหวัด ประเทศไทย

๙. บานสหกรณ์ ๗๕๗๗ ถนน จังหวัด ประเทศไทย

๑๐. บานสหกรณ์ ๗๕๗๗ ถนน จังหวัด ประเทศไทย

๑๑. บานสหกรณ์ ๗๕๗๗ ถนน จังหวัด ประเทศไทย

๑๒. บานสหกรณ์ ๗๕๗๗ ถนน จังหวัด ประเทศไทย

สำหรับเจ้าหน้าที่

ห้องน้ำค้า ๑๕ ช.ส. ๒๕๕๓

ห้องน้ำค้า ๑๕ ช.ส. ๒๕๕๓

สัญญาค้าเจ้าหน้าที่ประดิษฐ์ห้องน้ำค้า

เลขที่ค้า ๑๐๐๑๐๑๙๐๙

ให้กับเจ้าหน้าที่

ประดิษฐ์ห้องน้ำค้า

ห้องน้ำค้าเจ้าหน้าที่

เลขที่ค้าบัตร/บัญชีบัตร



คำขอรับสิทธิบัตร/อนุสิทธิบัตร

การประดิษฐ์
 การออกแบบผลิตภัณฑ์
 อนุสิทธิบัตร

ข้าพเจ้าผู้ลงลายมือชื่อในคำขอรับสิทธิบัตร/อนุสิทธิบัตรนี้
 ขอรับสิทธิบัตร/อนุสิทธิบัตร ตามพระราชบัญญัติสิทธิบัตร
 พ.ศ. 2522 แก้ไขเพิ่มเติมโดยพระราชบัญญัติสิทธิบัตร (ฉบับที่ 2) พ.ศ. 2535 และพระราชบัญญัติสิทธิบัตร (ฉบับที่ 3)
 พ.ศ. 2542

สำหรับเจ้าหน้าที่

วันรับคำขอ 12 ๗/๘/๒๕๕๔	เลขที่คำขอ 1101003266
สัญลักษณ์จำแนกการประดิษฐ์ระหว่างประเทศ	
ให้กับแบบผลิตภัณฑ์ ประเภทผลิตภัณฑ์	
วันประกาศโฆษณา	เลขที่ประกาศโฆษณา
วันออกสิทธิบัตร/อนุสิทธิบัตร	เลขที่สิทธิบัตร/อนุสิทธิบัตร
	ลายมือชื่อเจ้าหน้าที่

1. ข้อที่แสดงถึงการประดิษฐ์/การออกแบบผลิตภัณฑ์

“อุปกรณ์เพิ่มสมรรถนะการถ่ายเทความร้อนชนิดกังหันแบบหมุนได้ภายในท่อ”

2. คำขอรับสิทธิบัตรการออกแบบผลิตภัณฑ์นี้เป็นคำขอสำหรับแบบผลิตภัณฑ์อย่างเดียวกันและเป็นคำขอลำดับที่

ในจำนวน คำขอ ที่ยื่นในคราวเดียวกัน

3. ผู้ขอรับสิทธิบัตร/อนุสิทธิบัตร และที่อยู่ (เลขที่ ถนน จังหวัด ประเทศไทย) มหาวิทยาลัยเทคโนโลยีพระจอมเกล้าธนบุรี 126 ถนนประชาอุทิศ แขวงบางมด เขตทุ่งครุ กรุงเทพฯ 10140	3.1 สัญชาติ ไทย 3.2 โทรศัพท์ 0-2470-9685,9688 3.3 โทรศัพท์ 0-2872-9083 3.4 อีเมล์ ip@kmutt.ac.th
---	---

4. สิทธิในการขอรับสิทธิบัตร/อนุสิทธิบัตร

ผู้ประดิษฐ์/ผู้ออกแบบ ผู้รับโอน ผู้ขอรับสิทธิโดยเหตุอื่น

5. ตัวแทน (ถ้ามี) / ที่อยู่ (เลขที่ ถนน จังหวัด ประเทศไทย รหัสไปรษณีย์) นางสาวผ่องศรี เวสารัช และ/หรือ นางสาวเข้าวันี สนธิธรรม ศูนย์ส่งเสริมงานวิจัยและทรัพย์สินทางปัญญา มหาวิทยาลัยเทคโนโลยีพระจอมเกล้าธนบุรี 126 ถนนประชาอุทิศ แขวงบางมด เขตทุ่งครุ กรุงเทพฯ 10140	5.1 ตัวแทนเลขที่ 1745,1739 5.2 โทรศัพท์ 0-2470-9685,9688 5.3 โทรศัพท์ 0-2872-9083 5.4 อีเมล์ ip@kmutt.ac.th
--	--

6. ผู้ประดิษฐ์/ผู้ออกแบบผลิตภัณฑ์ และที่อยู่ (เลขที่ ถนน จังหวัด ประเทศไทย)

1.นายสมชาย วงศิริชัย อัญชันเลขที่ 12/5 หมู่ 10 ซอยเพชรเกษม 67/1 บางแค กรุงเทพฯ 10160
 2.นายวีระพันธ์ ด้วงทองสุก อัญชันเลขที่ 692 หมู่ 10 แขวงหนองแขม เขตหนองแขม กรุงเทพฯ 10160

7. คำขอรับสิทธิบัตร/อนุสิทธิบัตรนี้แยกจากหรือเกี่ยวข้องกับคำขอเดิม

ผู้ขอรับสิทธิบัตร/อนุสิทธิบัตรขอให้ถือว่าได้ยื่นคำขอรับสิทธิบัตร/อนุสิทธิบัตรนี้ไว้ในวันเดียวกับคำขอรับสิทธิบัตรเลขที่
 วันยื่น

เพราะคำขอรับสิทธิบัตร/อนุสิทธิบัตรนี้แยกจากหรือเกี่ยวข้องกับคำขอเดิมเพราะ

คำขอเดิมมีการประดิษฐ์หลายอย่าง ถูกคัดค้านเนื่องจากผู้ขอไม่มีสิทธิ ขอเปลี่ยนแปลงประเภทของสิทธิ

หมายเหตุ ในกรณีที่ไม่อาจระบุรายละเอียดได้ครบถ้วน ให้จัดทำเป็นเอกสารแนบท้ายแบบพิมพ์หนึ่งโดยระบุหมายเลขคำขอและหัวข้อที่แสดง
 รายละเอียดเพิ่มเติมตั้งแต่ตัวอักษร

 คำขอรับสิทธิบัตร/อนุสิทธิบัตร <input checked="" type="checkbox"/> การประดิษฐ์ <input type="checkbox"/> การออกแบบผลิตภัณฑ์ <input type="checkbox"/> อนุสิทธิบัตร ข้าพเจ้าผู้ลงลายมือชื่อในคำขอรับสิทธิบัตร/อนุสิทธิบัตรนี้ ขอรับสิทธิบัตร/อนุสิทธิบัตร ตามพระราชบัญญัติสิทธิบัตร พ.ศ. 2522 แก้ไขเพิ่มเติมโดยพระราชบัญญัติสิทธิบัตร (ฉบับที่ 2) พ.ศ. 2535 และพระราชบัญญัติสิทธิบัตร (ฉบับที่ 3) พ.ศ. 2542	สำหรับเจ้าหน้าที่	
	วันรับคำขอ วันที่รับคำขอ	เลขที่คำขอ 1101003634
สัญลักษณ์เจ้าหน้าที่ในการประดิษฐ์ระหว่างประเทศ		
ใช้แบบนี้ก็ได้ ประดิษฐ์		
วันประภาคโฆษณา	เลขที่ประภาคโฆษณา	
วันออกสิทธิบัตร/อนุสิทธิบัตร	เลขที่สิทธิบัตร/อนุสิทธิบัตร	
ลายมือชื่อเจ้าหน้าที่		
1. รือที่แสดงถึงการประดิษฐ์/การออกแบบผลิตภัณฑ์ ห่อเพิ่มสมรรถนะการถ่ายเทความร้อนแบบร่องเกลียว		
2. คำขอรับสิทธิบัตรการออกแบบผลิตภัณฑ์เป็นคำขอสำหรับแบบผลิตภัณฑ์อย่างเดียวแก้ไขและเป็นคำขอลำดับที่ ในจำนวน คำขอ ที่ยื่นในความเดียวกัน		
3. ผู้ขอรับสิทธิบัตร/อนุสิทธิบัตร และที่อยู่ (เลขที่ ถนน แขวง หัวหมาก กรุงเทพฯ) มหาวิทยาลัยเทคโนโลยีพระจอมเกล้าธนบุรี 126 ถ.ประชาอุทิศ แขวงบางมด เขตทุ่งครุ กรุงเทพฯ 10140		
3.1 สัญชาติ ไทย 3.2 โทรศัพท์ 0-2470-9685-8 3.3 โทรสาร 0-2872-9083 3.4 อีเมล์ ip@kmutt.ac.th		
4. สิทธิในการขอรับสิทธิบัตร/อนุสิทธิบัตร <input checked="" type="checkbox"/> ผู้ประดิษฐ์/ผู้ออกแบบ <input checked="" type="checkbox"/> ผู้รับโอน <input type="checkbox"/> ผู้ขอรับสิทธิโดยเหตุอื่น		
5. ตัวแทน (ถ้ามี) ที่อยู่ (เลขที่ ถนน แขวง หัวหมาก กรุงเทพฯ รหัสไปรษณีย์) นางสาวผ่องศรี เวสาวัช และ/หรือ นางสาวเชวานี สนธิธรรม ศูนย์ส่งเสริมงานวิจัยและพัฒนาสิ่งที่มีคุณค่า มหาวิทยาลัยเทคโนโลยีพระจอมเกล้าธนบุรี 126 ถ.ประชาอุทิศ แขวงบางมด เขตทุ่งครุ กรุงเทพฯ 10140		
5.1 ตัวแทนเลขที่ 1745,1739 5.2 โทรศัพท์ 0-2470-9685-8 5.3 โทรสาร 0-2872-9083 5.4 อีเมล์ IP@kmutt.ac.th		
6. ผู้ประดิษฐ์/ผู้ออกแบบผลิตภัณฑ์ และที่อยู่ (เลขที่ ถนน แขวง หัวหมาก กรุงเทพฯ) นายสมชาย วงศ์พันธุ์ อยู่บ้านเลขที่ 12/5 หมู่ 10 ซอยเพชรเกษม 67/1 ถนนเพชรเกษม แขวงบางแคเขตบางนา กรุงเทพฯ 10160		
7. คำขอรับสิทธิบัตร/อนุสิทธิบัตรนี้แยกจากหรือเกี่ยวข้องกับคำขอเดิม ผู้ขอรับสิทธิบัตร/อนุสิทธิบัตรขอให้ถือว่าได้ยื่นคำขอรับสิทธิบัตร/อนุสิทธิบัตรนี้ไว้ในวันเดียวกับคำขอรับสิทธิบัตรเลขที่ วันที่นี่ เพื่อจะคำขอรับสิทธิบัตร/อนุสิทธิบัตรนี้แยกจากหรือเกี่ยวข้องกับคำขอเดิมเพร哉 <input type="checkbox"/> คำขอเดิมมีการประดิษฐ์หลายอย่าง <input type="checkbox"/> ถูกตัดค้านเนื่องจากผู้ขอไม่มีสิทธิ <input type="checkbox"/> ขอเปลี่ยนแปลงประเภทของสิทธิ		

หมายเหตุ ในการพิจารณาจะต้องมีเอกสารแนบท้ายที่มีลายเซ็นของผู้ขอรับสิทธิบัตรและผู้รับโอน รวมถึงเอกสารที่แสดงถึงความสามารถเชิงวิชาการของผู้ขอรับสิทธิบัตร

สำเนา



ที่ ศธ 5810.3/55035

มหาวิทยาลัยเทคโนโลยีพระจอมเกล้าธนบุรี
แขวงบางมด เขตทุ่งครุ กรุงเทพฯ 10140

17 กุมภาพันธ์ 2555

ป้ายรับคำขอที่ ๑
ลำดับดิจิทัล
เลขที่ 1201000625
วันที่ 17 กุมภาพันธ์ 2555
ภาค

เรื่อง ขอผ่อนผันการส่งเอกสารประกอบคำขอรับสิทธิบัตร

เรียน ผู้อำนวยการสำนักสิทธิบัตร

ด้วย มหาวิทยาลัยเทคโนโลยีพระจอมเกล้าธนบุรี มีความประสงค์จะยื่นคำขอรับสิทธิบัตร ภายใต้ชื่อ ที่แสดงถึงการประดิษฐ์ “อุปกรณ์เพิ่มสมรรถนะการถ่ายเทความร้อนชนิดกั้งหันหมุนองได เหนือพื้นผิวของ การเดือด” ต่อสำนักสิทธิบัตร กรมทรัพย์สินทางปัญญา แต่เนื่องจาก ไม่สามารถนำส่งเอกสารประกอบคำขอรับสิทธิบัตร ณ วันที่ยื่นได้ จึงขอยื่นคำขอรับสิทธิบัตรต่อกรมทรัพย์สินทางปัญญา ก่อนและขอผ่อนผันระยะเวลาการนำส่งเอกสารคงกล่าวออกไปเป็นเวลา 90 วัน เพื่อให้การดำเนินการยื่นคำขอไม่ล่าช้าจน ก่อให้เกิดความเสียหายแก่ราชการ

จึงเรียนมาเพื่อโปรดพิจารณาอนุเคราะห์ด้วย จักอนพระคุณยิ่ง

ขอแสดงความนับถือ

(นางสาวผ่องศรี เวสารัช)

ตัวแทนสิทธิบัตร

ศูนย์ส่งเสริมงานวิจัยและทรัพย์สินทางปัญญา
สำนักวิจัยและบริการวิทยาศาสตร์และเทคโนโลยี
โทร. 0-2470-9685, 9688
โทรสาร 0-2872-9083



คำขอรับสิทธิบัตร/อนุสิทธิบัตร

การประดิษฐ์
 การออกแบบผลิตภัณฑ์
 อนุสิทธิบัตร

ข้าพเจ้าผู้ลงลายมือชื่อในคำขอรับสิทธิบัตร/อนุสิทธิบัตรนี้ ขอรับสิทธิบัตร/อนุสิทธิบัตร ตามพระราชบัญญัติ สิทธิบัตร พ.ศ. 2522 แก้ไขเพิ่มเติมโดยพระราชบัญญัติ สิทธิบัตร (ฉบับที่ 2) พ.ศ. 2535 และพระราชบัญญัติ สิทธิบัตร (ฉบับที่ 3) พ.ศ. 2542

สำหรับเจ้าหน้าที่	
วันรับคำขอ ๑๗ ๐๓ ๒๕๖๖	เลขที่คำขอ
วันยื่นคำขอ ๑๗ ๐๓ ๒๕๖๖	1201000625
สัญลักษณ์จำแนกการประดิษฐ์ระหว่างประเทศ	
ใช้กับแบบผลิตภัณฑ์ ประเภทผลิตภัณฑ์	วันประกาศโฉนดนา
	เลขที่ประกาศโฉนดนา
วันออกสิทธิบัตร/อนุสิทธิบัตร	เลขที่สิทธิบัตร/อนุสิทธิบัตร
	ลายมือชื่อเจ้าหน้าที่
<p>1. ข้อที่แสดงถึงการประดิษฐ์/การออกแบบผลิตภัณฑ์ “อุปกรณ์เพิ่มสมรรถนะการถ่ายเทความร้อนชนิดกั้นหันหน้าเอียงได้เหนือเพิ่มความของการเดือด”</p> <p>ห้องเด็กนรนเป็น</p>	
<p>2. คำขอรับสิทธิบัตรการออกแบบผลิตภัณฑ์นี้เป็นคำขอส่วนหนึ่งแบบผลิตภัณฑ์อ่อนย่างเดียว กันและเป็นคำขอลำดับที่ ในจำนวน คำขอ ที่ยื่นในคราวเดียวกัน</p>	
3. ผู้ขอรับสิทธิบัตร/อนุสิทธิบัตร นางสาวอรุณรัตน์ ภัทรมานะ ที่ อ.เมือง จ.นนทบุรี ว่าด้วยเครื่องซ่อมแซมเครื่องจักรและท่อส่งน้ำ ที่อยู่ (เลขที่ ถนน จังหวัด ประเทศไทย) มหาวิทยาลัยเทคโนโลยีพระจอมเกล้าธนบุรี 126 ถ.ประชาอุทิศ แขวงบางมด เขตทุ่งครุ กรุงเทพฯ 10140	<p>3.1 สัญชาติ ไทย 3.2 โทรศัพท์ 0-2470-9685, 9688 3.3 โทรสาร 0-2872-9083 3.4 อีเมล์ ip@kmutt.ac.th</p>
<p>4. สิทธิในการขอรับสิทธิบัตร/อนุสิทธิบัตร</p> <p><input type="checkbox"/> ผู้ประดิษฐ์/ผู้ออกแบบ <input checked="" type="checkbox"/> ผู้รับโอน <input type="checkbox"/> ผู้ขอรับสิทธิโดยเหตุอื่น</p>	
5. ตัวแทน (ถ้ามี)/ ที่อยู่ (เลขที่ ถนน จังหวัด ประเทศไทย รหัสไปรษณีย์) นางสาว芳 อรุณรัตน์ เวสารัช และ/หรือ นางสาวเชาวน์ สันติธรรม ศูนย์ส่งเสริมงานวิจัยและทรัพย์สินทางปัญญา มหาวิทยาลัยเทคโนโลยีพระจอมเกล้าธนบุรี 126 ถ.ประชาอุทิศ แขวงบางมด เขตทุ่งครุ กรุงเทพฯ 10140	<p>5.1 ตัวแทนเลขที่ 1745, 1739 5.2 โทรศัพท์ 0-2470-9685, 9688 5.3 โทรสาร 0-2872-9083 5.4 อีเมล์ IP@kmutt.ac.th</p>
6. ผู้ประดิษฐ์/ผู้ออกแบบผลิตภัณฑ์ และที่อยู่ (เลขที่ ถนน จังหวัด ประเทศไทย) นายสมชาย วงศิริ อยู่บ้านเลขที่ 12/5 หมู่ 10 ซอยเพชรเกษม 67/1 ถนนเพชรเกษม แขวงบางแค เขตบางแค กรุงเทพฯ 10160	
<p>7. คำขอรับสิทธิบัตร/อนุสิทธิบัตรนี้แยกจากหรือเกี่ยวข้องกับคำขอเดิม ผู้ขอรับสิทธิบัตร/อนุสิทธิบัตรขอให้ถือว่าได้ยื่นคำขอรับสิทธิบัตร/อนุสิทธิบัตรนี้ไว้ในวันเดียวกับคำขอรับสิทธิบัตรเลขที่ วันยื่น เพราะคำขอรับสิทธิบัตรนี้แยกจากหรือเกี่ยวข้องกับคำขอเดิมเพรา <input type="checkbox"/> คำขอเดิมมีการประดิษฐ์หลายอย่าง <input type="checkbox"/> ถูกคัดค้านเนื่องจากผู้ขอไม่มีสิทธิ <input type="checkbox"/> ขอเปลี่ยนแปลงประเภทของสิทธิ</p>	

หมายเหตุ ในกรณีที่ไม่อาจระบุรายละเอียดได้ครบถ้วน ให้จัดทำเป็นเอกสารแนบท้ายแบบพิมพ์นี้โดยระบุหมายเหตุกับข้อและหัวข้อที่แสดงรายละเอียดเพิ่มเติมดังกล่าวด้วย

ภาคผนวก ค.

ผลงานการจดลิขสิทธิ์



ร.ล.ช.01

ทะเบียนข้อมูลเลขที่ ว.1. 1755

หนังสือรับรองการแจ้งข้อมูล
ลิขสิทธิ์
ออกให้เพื่อแสดงว่า
มหาวิทยาลัยเทคโนโลยีพระจอมเกล้าธนบุรี

ได้แจ้งข้อมูลลิขสิทธิ์ ประเภทงาน วรรณกรรม

ลักษณะงาน

โปรแกรมคอมพิวเตอร์

ชื่อผลงาน

โปรแกรมคำนวณหาขนาดท่อคิวปิลารีแบบแอลกอริทึม

Program for sizing adiabatic capillary tube

ไวต์ต์อัลฟ์สินทางปัญญา

ตามคำขอแจ้งข้อมูลลิขสิทธิ์ เลขที่ 098447 เมื่อวันที่ 25 เดือน เมษายน พ.ศ. 2548

ให้ไว้ ณ วันที่ 15 เดือน ชั้นวาร์ค พ.ศ. 2553

ลงชื่อ.....

(นายสุรภูมิ ตีระนันทน์)

นักวิชาการพานิชย์ชำนาญการ

ปฏิบัติราชการแทนผู้อำนวยการสำนักลิขสิทธิ์

หมายเหตุ การเปลี่ยนแปลงรายการข้างต้น ให้คุณดูด้วย



สำเนา

คำขอแจ้งข้อมูลลิขสิทธิ์

ประเภทงานอันมีลิขสิทธิ์

<input checked="" type="checkbox"/> วรรณกรรม	<input type="checkbox"/> ดนตรีกรรม
<input type="checkbox"/> นาฏกรรม	<input type="checkbox"/> ภาพยนตร์
<input type="checkbox"/> ศิลปกรรม	<input type="checkbox"/> งานแฟร์สีียงแฟร์ภาค
<input type="checkbox"/> โศกทศนวัสดุ	<input type="checkbox"/> งานอื่นใดในแผนกวารณคดี
<input type="checkbox"/> ลิ้งบันทึกเสียง	แผนกวิทยาศาสตร์หรือแผนกที่ดิน

1. ชื่อเจ้าของลิขสิทธิ์

มหาวิทยาลัยเทคโนโลยีพระจอมเกล้าธนบุรี
สัญชาติ ไทย

เลขประจำตัวประชาชน/นิติบุคคล 111111111111111111

2. ชื่อตัวแทน

ชื่อ นางสาวผ่องศรี เวสาชัย สัญชาติ ไทย
เลขประจำตัวประชาชน/นิติบุคคล 31102400462834
และ/หรือ นางสาวเชวนี สนธิธรรม สัญชาติ ไทย
เลขประจำตัวประชาชน/นิติบุคคล 3110101334536

ที่อยู่

126 ถนนประชาอุทิศ แขวงบางมด เขตทุ่งครุ กรุงเทพฯ
รหัสไปรษณีย์ 10140

ที่อยู่ ศูนย์ส่งเสริมงานวิจัยและทรัพย์สินทางปัญญา

มหาวิทยาลัยเทคโนโลยีพระจอมเกล้าธนบุรี
126 ถนนประชาอุทิศ แขวงบางมด เขตทุ่งครุ กรุงเทพฯ
รหัสไปรษณีย์ 10140

โทรศัพท์ 0-2470-9685-8

โทรสาร 0-2872-9083

โทรศัพท์ 0-2470-9685-8

โทรสาร 0-2872-9083

3. สถานที่ติดต่อในประเทศไทย ศูนย์ส่งเสริมงานวิจัยและทรัพย์สินทางปัญญา มหาวิทยาลัยเทคโนโลยีพระจอมเกล้าธนบุรี

4. ชื่อผู้สร้างสรรค์ หรือนามแฝง

ชื่อ นายสมชาย วงศิริเดช
สัญชาติ ไทย
เกิดวันที่ 3 ตุลาคม 2502

เลขประจำตัวประชาชน/นิติบุคคล 3104401207618

5. ชื่อผู้สร้างสรรค์ร่วม หรือนามแฝง

ชื่อ นายศิวิว พวงสันเทียะ
สัญชาติ ไทย
เกิดวันที่ 26 กันยายน 2529

เลขประจำตัวประชาชน/นิติบุคคล 111014007705031

ที่อยู่ เลขที่ 12/5 หมู่ 10 ซอยเพชรเกษม 67/1 ถนนเพชรเกษม
แขวงบางแคน เขตบางแคน กรุงเทพฯ

รหัสไปรษณีย์ 10160

ที่อยู่ เลขที่ 160/17 ต路口บ้านช่างทองหล่อ แขวงบ้านช่างทองหล่อ
เขตบางกอกน้อย กรุงเทพฯ

รหัสไปรษณีย์ 10700

โทรศัพท์ โทรสาร

โทรศัพท์ โทรสาร -

วัน เดือน ปี ที่ขอลงทะเบียนนิติบุคคล -

วัน เดือน ปี ที่จดทะเบียนนิติบุคคล -

วัน เดือน ปีที่ผู้สร้างสรรค์ตาย (เฉพาะนิติบุคคลธรรมชาติ) -

วัน เดือน ปีที่ผู้สร้างสรรค์ตาย (เฉพาะนิติบุคคลธรรมชาติ) -

สำหรับเจ้าหน้าที่	เลขที่ 189622
รับวันที่ - 3 พ.ค. 2551	
ทะเบียนข้อมูลเลขที่	
เอกสารแนบ	
<input checked="" type="checkbox"/> สำเนาค่าขอ ฉบับ.01 <input checked="" type="checkbox"/> หนังสือรับรองความเป็นเจ้าของลิขสิทธิ์ <input checked="" type="checkbox"/> ผลงานหรือภาพถ่าย <input checked="" type="checkbox"/> สำเนาตัวประจําตัวหรือหนังสือรับรองนิติบุคคล <input checked="" type="checkbox"/> หนังสือมอบอำนาจ (ถ้ามี) <i>ด้านขวา</i> <input checked="" type="checkbox"/> เอกสารอื่น ๆ (ถ้ามี) <i>ด้านขวา</i> <i>สำเนาหนังสือรับรองนิติบุคคล</i>	

9. ลักษณะการสร้างสรรค์

สร้างสรรค์ขึ้นเองทั้งหมด สร้างสรรค์บ้างส่วน (ระบุ)
 อื่นๆ (ระบุ)

10. สถานที่สร้างสรรค์ สร้างสรรค์ในประเทศไทย (ระบุ) มหาวิทยาลัยเทคโนโลยีพระจอมเกล้าธนบุรี ประเทศไทย

11. ปีที่สร้างสรรค์ (ระบุ) 2548.....

12. การโฆษณา (การนำเสนอเนื้อหาโดยความยินยอมของผู้สร้างสรรค์ โดยสามารถมีจำนวนมากพอสมควร)

ยังไม่ได้โฆษณา
 ได้โฆษณาแล้วโดยโฆษณาครั้งแรกเมื่อวันที่ เดือน พ.ศ.
 ณ ประเทศไทย

13. การแจ้ง/จดทะเบียนลิขสิทธิ์ในต่างประเทศ

ไม่เคยแจ้งหรือจดทะเบียน แจ้งหรือจดทะเบียนไว้แล้วที่ประเทศไทย (ระบุ)

14. การอนุญาตให้ใช้ลิขสิทธิ์/โอนลิขสิทธิ์

ไม่ขออนุญาตให้ใช้ลิขสิทธิ์ / โอนลิขสิทธิ์
 อนุญาตให้ใช้ลิขสิทธิ์ / โอนลิขสิทธิ์ให้แก่ เมื่อวันที่ เดือน พ.ศ.
 อนุญาต/โอนลิขสิทธิ์ (แนบสำเนาสัญญาหรือนิติกรรม)
 ลิขสิทธิ์ทั้งหมด ลิขสิทธิ์ส่วน (ระบุ)

อนุญาต/โอนลิขสิทธิ์ (แนบสำเนาสัญญาหรือนิติกรรม)
 ตลอดอายุลิขสิทธิ์ มีกำหนดเวลา (ระบุ) ปี

15. การเผยแพร่ข้อมูลลิขสิทธิ์

ข้าพเจ้าอนุญาตให้กันอื่นตรวจสอบได้ในแนบคำขอแจ้งข้อมูลลิขสิทธิ์และผลงานของข้าพเจ้าได้
 ข้าพเจ้าไม่ขออนุญาตให้บุคคลใดตรวจสอบได้ในแนบคำขอแจ้งคำขอ และผลงานของข้าพเจ้า
 อื่นๆ (โปรดระบุ)

ทั้งนี้ข้าพเจ้ารับทราบว่า กรณี ให้บุกรุกตรวจสอบคำขอของข้าพเจ้าได้ในแนบคำขอที่ได้ระบุไว้ในแบบ จช.01

ข้าพเจ้าขอรับรองว่าข้อความข้างต้นเป็นความจริงทุกประการและหลักฐานที่ส่งประกอบคำขอเป็นหลักฐานที่ถูกต้อง หากปรากฏภายหลังว่าข้าพเจ้าไม่ได้เป็นเจ้าของลิขสิทธิ์หรือลักษณะของข้าพเจ้าไม่ถูกต้องตามที่ได้ระบุไว้ในแบบ จช.01 ข้าพเจ้าขอรับผิดชอบทุกประการ

ลงชื่อ..... ๘๒๘๔ ใบอนุญาตฯ ของลิขสิทธิ์ / ตัวแทน
 (นางสาวผ่องศรี เวสารัช และ/หรือ นางสาวเชาวนี สนธิธรรม)
 - ๓ ก.ค. 2551

หมายเหตุ ในการที่ได้แบบ จช.01 นี้เนื้อที่ไม่ขอ และต้องการระบุรายละเอียดเพิ่ม ให้ไว้ในค่องท้าย จช.01

ด้วยบุหນายเลขที่กันข้อ และหัวข้อที่แสดงรายละเอียดเพิ่มเติมดังกล่าวด้วย

การดำเนินการตามคำขอที่ไม่ต้องเสียค่าธรรมเนียมใด ๆ ทั้งสิ้น

กำນอเลhibit.....
ทะเบียนข้อมูล เลขที่.....

ใบต่อท้ายคำขอแจ้งข้อมูลลิขสิทธิ์

แบบ ឌ.01

ชื่อผู้สร้างสรรค์ร่วม หรือนามแฝง (ต่อ)

ชื่อ นายอรรถพล วงศ์แสง

สัมมชาติ ไทย

เก็บวันที่ 10 กรกฎาคม 2528

ເລກປະຈຳດ້ວຍປະຈານ/ນິທີບຸກຄົດ 1510100055910

ที่ ๑ เลขที่ 179 หมู่ 4 ตำบลไส้ไทย อำเภอเมือง จังหวัดกระนี

รหัสไปรษณีย์ 81000

ชื่อ นายเอกรัฐ ลิบิตกิจรง

สัมชาดิ ไทย

เก็บวันที่ 10 เมษายน 2528

ເລກປະຈຳເຫັນປະຈາບນ/ນິດົນກອກ 1959900041771

ที่ดินเลขที่ 58 ถนนพิพิธภัคดี ตำบลสะเตง อ่าเภอเมือง จังหวัดยะลา

รหัสไปรษณีย์ 95000

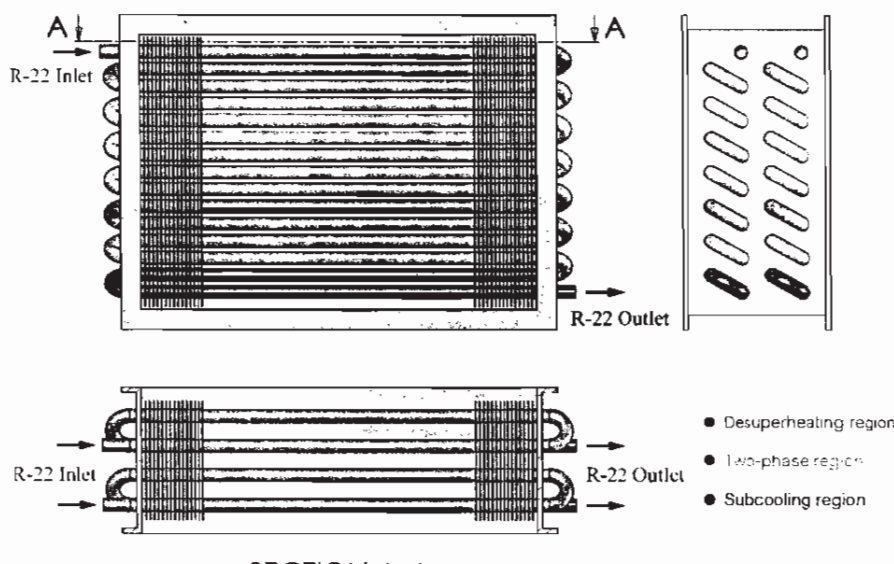
ลงชื่อ..... ลักษณ์ ใจดี ภานุชัย ลงนามรับทราบข้อบังคับดังต่อไปนี้

(นางสาวผ่องศรี เวสารัช และ/หรือ นางสาวเจวนี สนธิธรรม)

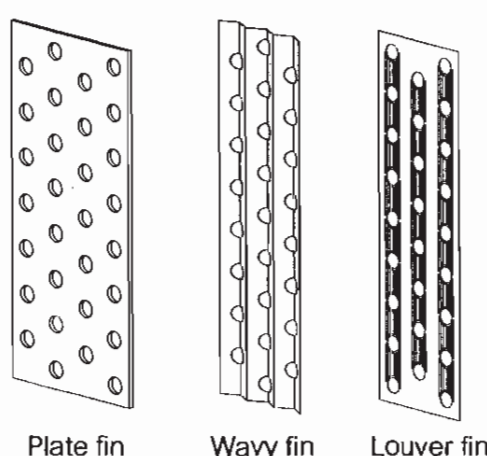
- 3 0.0. 2551

โปรแกรมการออกแบบค้อนเดนเซอร์แบบห่อติดครีบที่ระบายน้ำร้อนด้วยอากาศ

โปรแกรมจำลองการทำงานของค้อนเดนเซอร์ที่ระบายน้ำร้อนด้วยอากาศ เป็นโปรแกรมที่ถูกสร้างขึ้นเพื่อการออกแบบค้อนเดนเซอร์ที่ระบายน้ำร้อนด้วยอากาศ โดยในการวิจัยเรื่องการหาสมรรถนะของค้อนเดนเซอร์ที่ระบายน้ำร้อนด้วยอากาศ เพื่อได้มาซึ่งความถูกต้องและแม่นยำ จำเป็นต้องใช้เวลาและต้นทุนสูง ดังนั้นจึงคิดวิธีแก้ปัญหาโดยการสร้างโปรแกรมเพื่อหาผลลัพธ์ที่ต้องการโดยไม่จำเป็นต้องทำการทดลอง สำหรับการคำนวณจะอาศัยหลักการพื้นฐานทางเทอร์โมไดนามิกส์ และการถ่ายเทความร้อน โดยจะพิจารณาสารทำความเย็นออกเป็น 3 ช่วง คือ ช่วงไอร้อนยวดยิ่ง, ช่วงการไอนลส่องสถานะ และช่วงของเหลวเย็นเยือก ดังแสดงในรูปที่ 1 สำหรับครีบระบายน้ำร้อนที่ให้มี 3 ชนิด คือ Plate fin, Wavy fin และ Louver fin ดังแสดงในรูปที่ 2



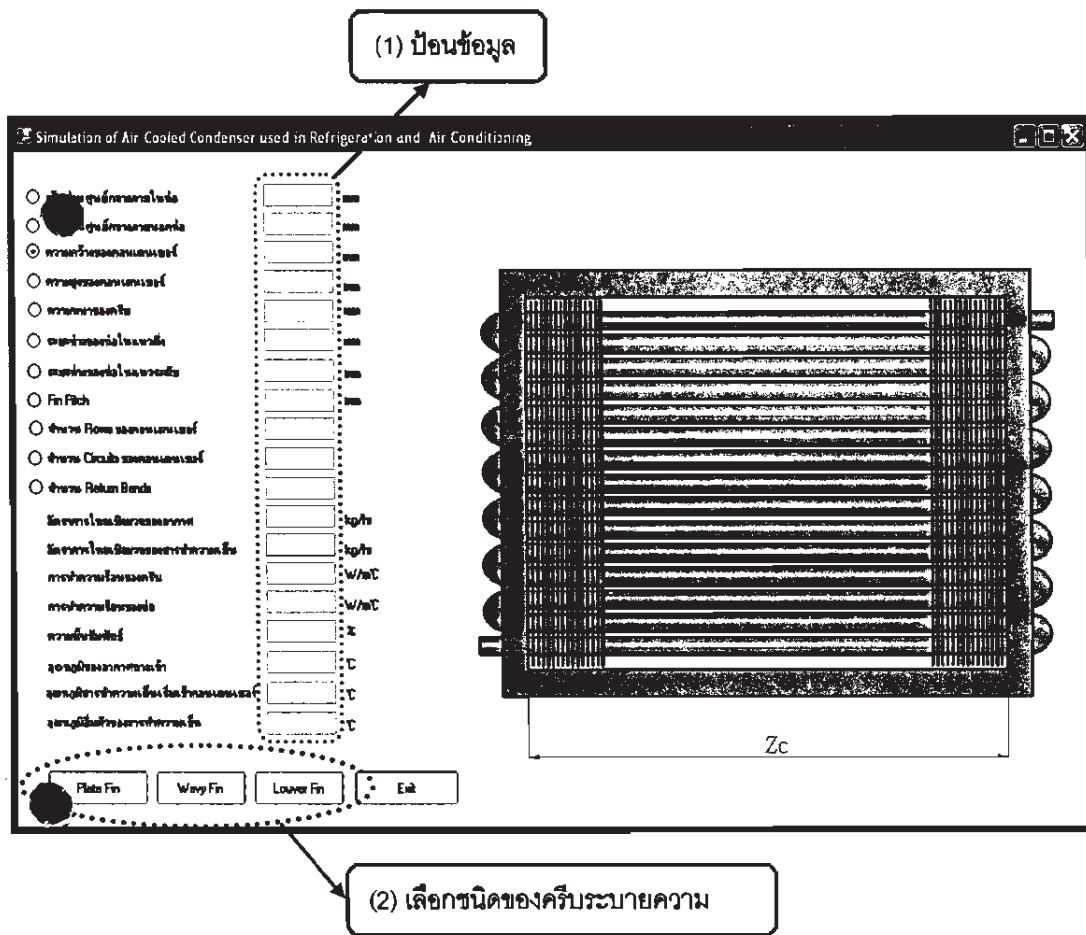
รูปที่ 1 ภาพแสดงสถานะของสารทำความเย็นที่ในผ่านค้อนเดนเซอร์



รูปที่ 2 ภาพแสดงลักษณะของครีบระบายน้ำร้อนชนิดต่าง ๆ

แบบแสดงรายละเอียดเกี่ยวกับการสร้างสรรค์ผลงานโดยย่อ (ต่อ)

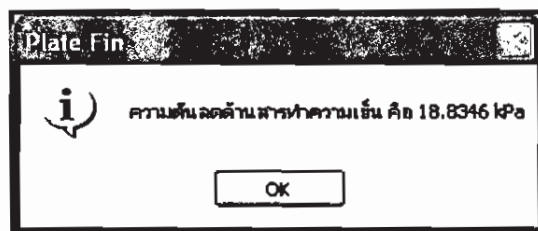
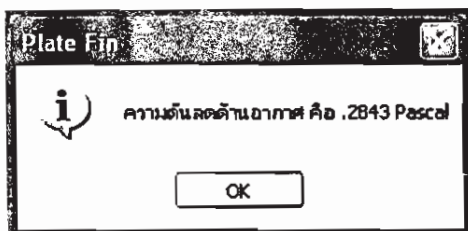
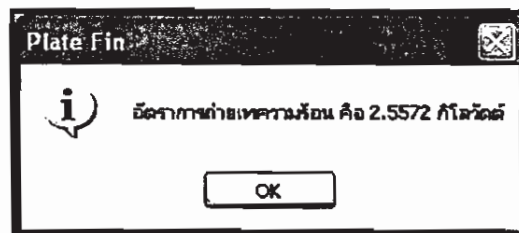
เมื่อเข้าสู่โปรแกรมการใช้งาน จะมีลักษณะดังรูปที่ 3 โดยในการใช้งานโปรแกรมจะต้องทำการป้อนข้อมูลที่จำเป็นในการออกแบบคอนเดนเซอร์ให้กับโปรแกรม จากนั้นจะทำการเลือกชนิดของครีบระบายความร้อนที่ใช้ ซึ่งผลลัพธ์ที่จะคำนวณได้ คือ ขั้นตอนการถ่ายเทความร้อน, ความดันลดทางด้านสารทำความเย็น (R-22) และความดันลดด้านอากาศ ดังแสดงในรูปที่ 4



รูปที่ 3 หน้าต่างแสดงลักษณะโปรแกรมและการใช้งาน

แบบคำขอ ฉบับ เลขที่
ทะเบียนข้อมูล เลขที่

แบบแสดงรายละเอียดเกี่ยวกับการสร้างสรรค์ผลงานโดยย่อ (ต่อ)



รูปที่ 4 ผลลัพธ์ที่คำนวณได้จากโปรแกรม

สำหรับข้อมูลที่ป้อนให้กับโปรแกรมและผลลัพธ์ที่คำนวณได้จะสามารถนำไปออกแบบบนคอมพิวเตอร์ได้ทันที และนอกเหนือไปจากการดังกล่าวข้างต้นสามารถนำไปประยุกต์ใช้กับสารทั่วความ เช่น นิตติศาสตร์ ฯ รวมถึงการพัฒนาการจำลองการทำงานของงานวิจัยอื่นๆ ได้อีกด้วย อาทิเช่น จีวโนป്�ปิเตอร์

ลงชื่อ..... ผู้ดูแล นางน้ำดี รักนิติกร นางสาวจิตาธิชี/ตัวแทน
(นางสาวพ่องศรี เวชารัช และ/หรือ นางสาวเขาวนี ษนธิธรรม)
ลงชื่อ..... ผู้ดูแล นางน้ำดี รักนิติกร นางสาวจิตาธิชี/ตัวแทน
วันที่ ๒๕/มิถุนายน/๒๕๕๑ ลงวันที่ ๒๕/๖/๕๑
- ๓ บ.บ. ๒๕๕๑

หนังสือหลักฐานแสดงความเป็นเจ้าของงานลิขสิทธิ์

โดยหนังสือฉบับนี้ มหาวิทยาลัยเทคโนโลยีพระจอมเกล้าธนบุรี โดย นายไกรวุฒิ เกียรติโภมล ตำแหน่ง อธิการบดี ตั้งอยู่เลขที่ 126 ถนน ประชาอุทิศ แขวงบางมด เขตทุ่งครุ กทม. 10140 ทะเบียนนิติบุคคลเลขที่ (ถ้ามี) _____ ขอรับรองว่าเป็นเจ้าของลิขสิทธิ์ในงานอันมีลิขสิทธิ์ ประเภท โปรแกรมคอมพิวเตอร์ ชื่อผลงาน “โปรแกรมการออกแบบคอนเดนเซอร์แบบท่อติดครีบกีรษนา ระบบความร้อนด้วยอากาศ” ที่ยื่นคำขอแจ้งข้อมูลลิขสิทธิ์ไว้ด้วยกรรมทรัพย์สินทางปัญญา เมื่อวันที่ ๒๕๕๔ แต่เพียงผู้เดียว
วันที่ ๗ ก.ค. ๒๕๕๑

ข้าพเจ้าขอรับรองว่าข้อความข้างต้นเป็นจริงทุกประการ หากปรากฏภายหลังว่า ข้าพเจ้าไม่ได้ เป็นเจ้าของลิขสิทธิ์และก่อให้เกิดความเสียหายแก่บุคคลหนึ่ง บุคคลใดหรือกรรมทรัพย์สินทางปัญญา ข้าพเจ้าขอ เป็นผู้รับผิดชอบในความเสียหายที่เกิดขึ้น

ลงชื่อ

ไกรวุฒิ เกียรติโภมล

(นายไกรวุฒิ เกียรติโภมล อธิการบดีมหาวิทยาลัยเทคโนโลยีพระจอมเกล้าธนบุรี)

- ๓ ก.ค. ๒๕๕๑

วันที่ ๔ เดือน ก.ค. พ.ศ. ๒๕๕๑

X ลักษณะ ✓

รายงาน





รบ.01

ทะเบียนข้อมูลเลขที่ ว1. 2873

หนังสือรับรองการแจ้งข้อมูล

ลิขสิทธิ์

ออกให้เพื่อแสดงว่า

มหาวิทยาลัยเทคโนโลยีพระจอมเกล้าธนบุรี

ได้แจ้งข้อมูลลิขสิทธิ์ ประเภทงาน วรรณกรรม

ลักษณะงาน

โปรแกรมคอมพิวเตอร์

ชื่อผลงาน โปรแกรมการออกแบบหน้าจอที่ติดเครื่องที่ระบายน้ำร้อนด้วยอากาศ

ไว้ต่อกรอบทรัพย์สินทางปัญญา

ตามคำขอแจ้งข้อมูลลิขสิทธิ์ เลขที่ 189622

เมื่อวันที่ 3 เดือน กรกฎาคม พ.ศ. 2551

ให้ไว้ ณ วันที่ 10 เดือน กรกฎาคม พ.ศ. 2551

ลงชื่อ.....

(นายสุรภูมิ ตีระนันทน์)

นักวิชาการพัฒนาระบบ 72

ปฏิบัติราชการแทนผู้อำนวยการสำนักลิขสิทธิ์

หมายเหตุ

การเปลี่ยนแปลงรายก ารซ ำจ ด ให้ด ค า น หลัง

รลบ.01



ทะเบียนข้อมูลเลขที่ ว.1.4613

หนังสือรับรองการแจ้งข้อมูล

ศิษย์เก่า

ออกให้เพื่อแสดงว่า

มหาวิทยาลัยเทคโนโลยีพระจอมเกล้าธนบุรี

ได้แจ้งข้อมูลศิษย์เก่า ประจำงาน วรรณกรรม

ลักษณะงาน

โปรดเกณฑ์พิเศษ

ชื่อผลงาน โปรแกรมการคำนวณอัตราการไฟฟ้าของสารทำความเย็นที่ให้ผลผ่านอุริพิชท่อสัน

วิศวกรรมทรัพย์สินทางปัญญา

ตามคำขอแจ้งข้อมูลศิษย์เก่า เลขที่ 287701

เมื่อวันที่ 11 เดือน กุมภาพันธ์ พ.ศ. 2556

ให้ไว้ ณ วันที่ 19 เดือน มีนาคม พ.ศ. 2556

ลงชื่อ.....
.....

(นายสุรภูมิ ศีระนันทน์)

นักวิชาการพัฒน์ชีวนาฏกรรม

ปฏิบัติราชการแทนผู้อำนวยการสำนักศิษย์เก่า

หมายเหตุ 1. เอกสารนี้มิได้รับรองความถูกต้องของศิษย์เก่า

2. การเปลี่ยนแปลงรายการข้างต้น ให้ดูด้านหลัง

รด.01



ทะเบียนข้อมูลเลขที่ ว.1. 2873

หนังสือรับรองการแจ้งข้อมูล
ลิขสิทธิ์
ออกให้เพื่อแสดงว่า
มหาวิทยาลัยเทคโนโลยีพระจอมเกล้าธนบุรี

ให้แจ้งข้อมูลลิขสิทธิ์ ประจำงาน วรรณกรรม

ลักษณะงาน

โปรแกรมคอมพิวเตอร์

ชื่อผลงาน โปรแกรมการออกแบบองค์เครื่องท่อติดเครื่องที่ระบบความร้อนด้วยอากาศ

"ไว้ต่อกรุนท์รัพย์สินทางปัญญา

ตามคำขอแจ้งข้อมูลลิขสิทธิ์ เลขที่ 189622

เมื่อวันที่ 3 เดือน กรกฎาคม พ.ศ. 2551

ให้ไว้ ณ วันที่ 10 เดือน กรกฎาคม พ.ศ. 2551

ลงชื่อ.....

(นายสุรภูมิ ตีระนันทน์)

นักวิชาการพาณิชย์ 7ว

ปฏิบัติราชการแทนผู้อำนวยการสำนักลิขสิทธิ์

หมายเหตุ

การเปลี่ยนแปลงรายละเอียดข้างต้น ให้คุ้มกันหลัง

ภาคผนวก ง.

ผลงานการเขียน ตำรา หนังสือ



ที่ ศธ 0512.2.75/ 6155

13 ฤกษาพันธ์ 2557

เรื่อง ผลการพิจารณาหนังสือชื่อ “กลศาสตร์ของไฟล เล่ม 1”

เรียน ศาสตราจารย์ ดร.สมชาย วงศิริเดช และ ผู้ช่วยศาสตราจารย์สุเทพ แก้วน้อย

สิ่งที่ส่งมาด้วย 1. หนังสือสัญญาลิขสิทธิ์ จำนวน 2 ฉบับ

ตามที่ท่านได้แก้ไขปรับปรุงต้นฉบับหนังสือชื่อ “กลศาสตร์ของไฟล” และขอปรับเปลี่ยนหนังสือเล่ม ดังกล่าวเป็นจำนวน 2 เล่มย่อย และขอเปลี่ยนชื่อเป็น “กลศาสตร์ของไฟล เล่ม 1 และ เล่ม 2” ตามผลการตรวจสอบคุณภาพเนื้อหาของสำนักพิมพ์นั้น จากการพิจารณาแล้วสำนักพิมพ์เห็นสมควรจัดพิมพ์หนังสือเล่มดังกล่าว จำนวน 1,000 - 2,000 เล่ม สำนักพิมพ์โครงข่ายเรื่องลิขสิทธิ์ คือ จะจ่ายค่าลิขสิทธิ์ร้อยละ 20 ของราคากำหนดโดยจะจ่ายตามยอดขาย ทุก ๆ 6 เดือน

อนึ่ง ตามมติที่ประชุมคณะกรรมการบริหารสำนักพิมพ์ ครั้งที่ 6/2550 เมื่อวันพุธที่ 16 สิงหาคม 2550 ที่ประชุมได้พิจารณาแล้วมีมติเห็นสมควรให้สำนักพิมพ์ดำเนินการจ่ายเงินรางวัลประจำปีให้กับผู้เขียน ดังเกณฑ์ต่อไปนี้

เรื่อง “เกณฑ์การจ่ายเงินรางวัลประจำปีให้กับผู้เขียน”

1. พิมพ์ครั้งที่ 2 เป็นต้นไป และพิมพ์ 2 ครั้งภายใน 1 ปี

หรือ 2. ขายได้มากกว่า 2,500 เล่ม/ชื่อเรื่อง ในปีงบประมาณนั้นโดยจะได้ค่าลิขสิทธิ์

เพิ่มขึ้นร้อยละ 5 หลังจากปีดับบลิช และรับรองงบในปีนั้น

3. เป็นข้อตกลงของผู้เขียนแต่ละราย

4. เห็นสัญญาลิขสิทธิ์ร้อยละ 20 ตามปกติ การจ่ายเพิ่มร้อยละ 5 จ่ายเป็นรางวัล

ตามเงื่อนไข ข้อ 1-2 ทั้งนี้เงินรางวัลจะจ่ายเมื่อสำนักพิมพ์ดำเนินการมีผลกำไร

ลังเรียนมาเพื่อโปรดทราบ และโปรดดำเนินการต่อไปด้วย จักขอบคุณยิ่ง

ขอแสดงความนับถือ

(ผู้ช่วยศาสตราจารย์มานิต จิวโนดม)

กรรมการผู้อำนวยการ

Director@cupress.chula.ac.th

งานธุรการ

ติดต่อวิชาชนา สำเร็น

wasana.su@chula.ac.th

โทร. 0-2218-3269 โทรสาร 0-2218-3266 www.ChulaPress.com

	สำนักพิมพ์แห่งจุฬาลงกรณ์มหาวิทยาลัย
แบบหนังสือสัญญามอบลิขสิทธิ์ให้พิมพ์หนังสือ	FM-AD-10 หน้า 1/2

สัญญาทำที่ จุฬาลงกรณ์มหาวิทยาลัย
เมื่อวันที่ 18 กุมภาพันธ์ 2557

หนังสือสัญญาฉบับนี้ทำขึ้นระหว่าง ศาสตราจารย์ ดร.สมชาย วงศิริเศษ
อายุ 54 ปี อายุบ้านเลขที่ 12/5 หมู่ 10 บ้านไ閣 ถนน 10160 และ^{.....}
ผู้ช่วยศาสตราจารย์สุเทพ แก้วน้อย อายุ 59 ปี อายุบ้านเลขที่ 32/349 หมู่ 7 ถนน 10160
ซึ่งต่อไปในสัญญานี้จะเรียกว่า “คู่สัญญาฝ่ายที่หนึ่ง” กับ สำนักพิมพ์แห่งจุฬาลงกรณ์มหาวิทยาลัย โดย^{.....}
ผู้ช่วยศาสตราจารย์มานิต จิวิโรคม (กรรมการผู้อ่านวิการสำนักพิมพ์แห่งจุฬาลงกรณ์มหาวิทยาลัย) ผู้รับ^{.....}
มอบอำนาจซึ่งต่อไปในสัญญานี้จะเรียกว่า “คู่สัญญาฝ่ายที่สอง” ทั้งสองฝ่ายได้ตกลงทำสัญญาผูกพันกัน ดังต่อไปนี้
ข้อ 1. คู่สัญญาฝ่ายที่หนึ่ง ซึ่งเป็นผู้ประพันธ์หนังสือ

“กลศาสตร์ของไฟล เล่ม 1”

ตกลงมอบลิขสิทธิ์ให้คู่สัญญาฝ่ายที่สองพิมพ์หนังสือดังกล่าวออกจำหน่ายและส่งเดียวเฉพาะ การพิมพ์ครั้งนี้ เป็น^{.....}
กำหนดเวลา 4 ปี นับตั้งแต่วันที่หนังสือออกสู่ตลาด หรือเมื่อจำหน่ายหนังสือหมด

ข้อ 2. ภายในการกำหนดเวลาข้อ 1. คู่สัญญาฝ่ายที่หนึ่งสัญญาจะไม่พิมพ์ซ้ำ หรือร่วมกับ หรือมอบให้^{.....}
บุคคลหรือนิติบุคคลอื่นพิมพ์ซ้ำ และจะไม่ประพันธ์หรือร่วมกับบุคคลหรือนิติบุคคลอื่นประพันธ์หนังสือใด ๆ ซึ่งเป็น^{.....}
ประเภทเดียวกับหนังสือดังกล่าวในสัญญานี้

ข้อ 3. เพื่อเป็นการตอบแทนแก่คู่สัญญาฝ่ายที่หนึ่ง คู่สัญญาฝ่ายที่สองตกลงจะจ่ายค่าลิขสิทธิ์แก่^{.....}
คู่สัญญาฝ่ายที่หนึ่ง เป็นจำนวน ร้อยละห้าสิบ ของราคากำหนด
จำนวนหนังสือที่ขายได้ทุก 6 เดือน

ข้อ 4. ในกรณีพิมพ์ครั้งนี้คู่สัญญาฝ่ายที่หนึ่งยินยอมให้คู่สัญญาฝ่ายที่สองเป็นผู้กำหนดราคากำหนด
ครั้งแรก และราคาจำนวนครั้งต่อ ๆ ไป ซึ่งอาจมีขึ้น

ข้อ 5. คู่สัญญาฝ่ายที่หนึ่งตกลงทำการตรวจสอบและรื้อหนังสือดังกล่าว ในระหว่างพิมพ์โดยไม่คิด
ค่าการงานใด ๆ ทั้งสิ้น และในการพิมพ์หนังสือดังกล่าวในทุกครั้งคู่สัญญาฝ่ายที่หนึ่ง ตกลงยินยอมแก้ไขปรับปรุง
หนังสือดังกล่าว โดยไม่คิดค่าการงานใด ๆ เน้นเดียวกัน

ข้อ 6. การจัดรูปเล่มและการออกแบบหนังสือให้อยู่ในดุลพินิจของคู่สัญญาฝ่ายที่สอง คู่สัญญา
ฝ่ายที่หนึ่งจะตัดแปลงแก้ไขสิ่งที่คู่สัญญาฝ่ายที่สองพิจารณาแล้วว่าดี เว้นแต่จะได้รับอนุญาตจากคู่สัญญาฝ่ายที่สองก่อน

ข้อ 7. เมื่อต้นฉบับหนังสือเข้าสู่โรงพิมพ์แล้ว ถือว่าคู่สัญญาฝ่ายที่หนึ่งได้ยินยอมมอบลิขสิทธิ์ให้แก่^{.....}
คู่สัญญาฝ่ายที่สองโดยสมมุติ หากคู่สัญญาฝ่ายที่หนึ่งขอถอนเรื่อง ต้องจ่ายค่าเสียหายที่เกิดขึ้นทั้งหมด ตั้งคู่สัญญาฝ่าย
ที่หนึ่งไม่ยินยอมจ่ายค่าเสียหาย คู่สัญญาฝ่ายที่สองมีสิทธิ์พิมพ์หนังสือดังกล่าวตามที่ตกลงกันไว้ในสัญญา

ข้อ 8. การแก้ไขเปลี่ยนแปลงใด ๆ หลังจากที่ต้นฉบับพร้อมพิมพ์เข้าสู่โรงพิมพ์แล้ว หากมีค่าใช้จ่าย^{.....}
เกิดขึ้น คู่สัญญาฝ่ายที่หนึ่งต้องรับผิดชอบค่าใช้จ่ายดังกล่าวทั้งหมด



สำนักพิมพ์แห่งจุฬาลงกรณ์มหาวิทยาลัย

แบบหนังสือสัญญามอบลิขสิทธิ์ให้พิมพ์หนังสือ

FM-AD-10

หน้า 2/2

ข้อ 9. ถ้าคู่สัญญาฝ่ายที่หนึ่งได้ส่งละเมิดลิขสิทธิ์ของผู้หนึ่งผู้ใด ไม่ว่าทั้งหมดหรือแต่บางส่วนอันเกี่ยวน์กับหนังสือในสัญญานี้เป็นเหตุให้เกิดความเสียหายแก่ผู้อื่น คู่สัญญาฝ่ายที่หนึ่งต้องรับผิดชอบของทั้งสิ้น โดยที่คู่สัญญาฝ่ายที่สองมิได้รู้เห็นหรือยินยอมหรือร่วมในการละเมิดลิขสิทธิ์นั้นด้วย

หากคู่สัญญาฝ่ายที่สองต้องเสียหายด้วยประการใด ๆ ในกรณี คู่สัญญาฝ่ายที่หนึ่งตกลงจะชดใช้ให้ทั้งสิ้น

ข้อ 10. ถ้าคู่สัญญาฝ่ายใดฝ่ายหนึ่งผิดสัญญานี้ข้อหนึ่งข้อใด คู่สัญญาอีกฝ่ายหนึ่งตกลงชดใช้ค่าเสียหายทั้งสิ้นให้แก่คู่สัญญาฝ่ายที่เสียหาย

ข้อ 11. สัญญานี้จะสิ้นสุดลงก็ต่อเมื่อคู่สัญญาฝ่ายที่สองมีหนังสือบอกกล่าวล่วงหน้าอย่างน้อย 30 วัน ไปยังคู่สัญญาฝ่ายที่หนึ่งว่าจะยุติการพิมพ์หนังสือดังกล่าวในสัญญานี้

แต่หนังสือบอกกล่าวนี้จะมีผลเป็นการเลิกสัญญาต่อเมื่อหนังสือดังกล่าวซึ่งพิมพ์ครั้งล่าสุดได้ดำเนินการจัดทำล่วงหน้าแล้ว

ข้อ 12. กรณีหนังสือที่ดำเนินการไม่หมดภายในระยะเวลา 5 ปี นับแต่วันที่หนังสือนี้ออกสูตลด หรือหนังสือปีพิมพ์เก่าที่มีปีพิมพ์ใหม่ข้อมูลทันสมัยกว่าจะดำเนินการออกสูตลดแล้ว และผู้จัดดำเนินการทำการส่งคืนให้คู่สัญญาฝ่ายที่สอง คู่สัญญาฝ่ายที่หนึ่งยินยอมมอบลิขสิทธิ์ให้คู่สัญญาฝ่ายที่สองดำเนินการอย่างทั่วไปโดยไม่ได้อ่าวเป็นการดำเนินการ

หนังสือสัญญานี้มีผลบังคับตั้งแต่วันที่ลงนามในสัญญานี้

หนังสือสัญญานี้ทำขึ้นเป็น 2 ฉบับ โดยคู่สัญญาทั้งสองฝ่ายลงนามไว้เป็นหลักฐานต่อหน้าพยาน

ลงนาม.....พงษ์ชัย วงศิริ.....คู่สัญญาฝ่ายที่หนึ่ง

(ศาสตราจารย์ ดร.สมชาย วงศิริ)

ลงนาม.....พงษ์ชัย.....คู่สัญญาฝ่ายที่หนึ่ง

(ผู้ช่วยศาสตราจารย์สุเทพ แก้วนัย)

ลงนาม.....พงษ์ชัย.....คู่สัญญาฝ่ายที่สอง

(ผู้ช่วยศาสตราจารย์มานด รุจิรวรดม)

ลงนาม.....พงษ์ชัย.....พยาน

ลงนาม.....พงษ์ชัย.....พยาน

ภาคผนวก จ.

ผลงานการเขียน Book Chapter

Two-Phase Heat Transfer Coefficients of R134a Condensation in Vertical Downward Flow at High Mass Flux

A.S. Dalkilic¹ and S. Wongwises²

¹*Heat and Thermodynamics Division, Department of Mechanical Engineering, Yildiz Technical University, Yildiz, Istanbul 34349*

²*Fluid Mechanics, Thermal Engineering and Multiphase Flow Research Lab. (FUTURE), Department of Mechanical Engineering, King Mongkut's University of Technology Thonburi, Bangkok 10140*

¹Turkey

²Thailand

1. Introduction

The transfer process of heat between two or more fluids of different temperatures in a wide variety of applications is usually performed by means of heat exchangers e.g. refrigeration and air-conditioning systems, power engineering and other thermal processing plants. In refrigeration equipment, condensers' duty is to cool and condense the refrigerant vapor discharged from a compressor by means of a secondary heat transfer fluid such as air and fluid. Examinations and improvements on the effectiveness of condenser have importance in case there is a design error which can cause the heat transfer failure occurrence in the condenser.

Industries have been trying to improve the chemical features of alternative refrigerants of CFCs due to the depletion of the earth's ozone layer. Because of the similar thermo-physical properties of HFC-134a to those of CFC-12, an intensive support from the refrigerant and air-conditioning industry has given to the refrigerant HFC-134a as a potential replacement for CFC-12. On the other hand, even though there isn't much difference in properties between these two refrigerants, the overall system performance may be affected significantly by these differences. For that reason, the detailed investigation of the properties of HFC-134a should be performed before it is applied.

A large number of researchers focused on the heat transfer and pressure drop characteristics of refrigerants over the years, both experimentally and analytically, mostly in a horizontal straight tube. The CFCs' heat transfer and pressure drop studies inside small diameter vertical either smooth or micro-fin tubes for downward condensation has been concerned comparatively little in the literature. Briggs et al. (1998) have studied on in-tube condensation using large diameter tubes of approximately 20.8 mm with CFC113. Shah (1979) used some smooth tubes up to 40 mm i.d. at horizontal, inclined and vertical positions to have a well-known wide-range applicable correlation. Finally, it has been compared by researchers

commonly for turbulent condensation conditions and it is considered to be the most predictive condensation model for the annular flow regime in a tube. Oh and Revankar (2005) developed the Nusselt theory (1916) to investigate the PCCS condenser using 47.5 mm i.d. and 1.8 m long vertical tube in their experimental study for the validation of their theoretical calculations. Maheshwari et al. (2004) simulated PCCS condensers used in water-cooled reactors using a 42.77 mm i.d. vertical tube during downward condensation presence of non-condensable gas. The prediction of heat transfer considering mass transfer along the tube length was performed by means of a computer code in their study.

Convective condensation in annular flow occurs for many applications inside tubes such as film heating and cooling processes, particularly in power generation and especially in nuclear reactors. The one of the most important flow regimes is annular flow which is characterized by a phase interface separating a thin liquid film from the gas flow in the core region. This flow regime is the most investigated one either analytically or experimentally, because of its practical significance and common usage.

Akers et al. (1959) focused on the similarity between two phase and single phase flows and developed a correlation using two-phase multiplier to predict frictional two phase pressure drop which is same rationale as the Lockhart-Martinelli (1949) two-phase multiplier. His model is known as "equivalent Reynolds number model" in the literature. According to this model, an equivalent all liquid flow, which produces the same wall shear stress as that of the two phase flow, is replaced instead of annular flow inside a tube. Many researchers benefitted from his model such as Moser et al. (1998) and Ma and Rose (2004). Moser et al. (1998) predicted heat transfer coefficient in horizontal conventional tubes developing a model. Ma and Rose (2004) studied heat transfer and pressure drop characteristics of R113 in a 20.8 i.d. vertical smooth and enhanced tubes.

Dobson et al. (1998) used zeotropic refrigerants in their condensation tests including the wide range of mass flux in horizontal tubes and benefitted from the two-phase multiplier approach for annular flow. In their study, heat transfer coefficient increased with increasing mass flux and vapor quality in annular flow due to increased shear and thinner liquid film than other flow regimes. Sweeney (1996) modified their model their model for R407C considering the effect of mass flux.

Cavallini et al. (1974) have some significant theoretical analysis on the in-tube condensation process regarding the investigation of heat transfer and pressure drop characteristics of refrigerants condensing inside various commercially manufactured tubes with enhanced surfaces using a number of correlations in the literature. Lately, Cavallini et al. (2003) prepared a review paper on the most recent condensation works in open literature including the condensation inside and outside smooth and enhanced tubes.

Valladares (2003) presented a review paper on in-tube condensation heat transfer correlations for smooth and micro-fin tubes including the comparison of experimental data belong to various experimental conditions from different researchers. Wang and Honda (2003) made a comparison of well-known heat transfer models with experimental data belong to various refrigerants from literature and proposed some models, valid for the modified annular and stratified flow conditions, for micro-fin tubes. Bassi and Bansal (2003) compared various empirical correlations and proposed two new empirical models for the determination of condensation heat transfer coefficients in a smooth tube using R134a with lubricant oil. Jung et al. (2003, 2004) did condensation tests of many refrigerants such as R12, R22, R32, R123, R125, R134a, and R142b inside a smooth tube. They paid attention not only comparison of their experimental data with various well-known correlations but also proposition on a new correlation to predict condensation heat transfer coefficients.

Generally, the condensation heat transfer coefficients and pressure drops in tubes have been computed by empirical methods. The modifications of the Dittus-Boelter single-phase forced convection correlation (1930) are used in the literature, as in Akers et al. (1959), Cavallini and Zecchin (1974), and Shah (1979). Dalkilic et al. (2010a) made a comparison of thirteen well-known two-phase pressure drop models with the experimental results of a condensation pressure drop of R600a and R134a in horizontal and vertical smooth copper tubes respectively and revealed the main parameters of related models and correlations. Dalkilic et al. (2008a) used the equivalent Reynolds number model (1998) to propose a new correlation for the two-phase friction factor of R134a and also discussed the effect of main parameters such as heat flux, mass flux and condensation temperature on the pressure drop. Dalkilic et al. (2009b) made a comparison of eleven well-known correlations for annular flow using a large amount of data obtained under various experimental conditions to have a new correlation based on Bellinghausen and Renz's method (1992) for the condensation heat transfer coefficient of high mass flux flow of R134a. The effects of heat flux, mass flux and condensation temperature on the heat transfer coefficients also exist in their paper. Dalkilic et al. (2009c) showed the significance of the interfacial shear effect for the laminar condensation heat transfer of R134a using Carey's analysis (1992), which is the improved version of Nusselt's theory (1916), and proposed a new correlation based on Bellinghausen and Renz's method (1992) for the condensation heat transfer coefficient during annular flow of R134a at low mass flux in a vertical tube. Dalkilic et al. (2008b) investigated thirty-three void fraction models and correlations from the available literature and compared them each other using relevant data. The friction factors, based on the analysis of Ma et al. (2004), are obtained from various void fraction models and correlations and a comparison was made with each other and also with those determined from graphical information provided by Bergelin et al. (1946). The presentation for the effect of void fraction alteration on the momentum pressure drop was also shown in their paper. Dalkilic et al. (2009a) compared some simple void fraction models of the annular flow pattern for the forced convection condensation of pure R134a taking into account the effect of the different saturation temperatures in high mass flux conditions. The calculated film thickness from void fraction models and correlations and those from Whalley's annular flow model (1987) were compared each other using their experimental database. Dalkilic and Wongwises (2010b) used Barnea et al. (1982)'s mathematical model, based on the momentum balance of liquid and vapour phases, in order to determine the condensation film thickness of R134a in their paper. The discussions for the effects of heat flux, mass flux and condensation temperature on the film thickness and condensation heat transfer coefficient were also made for laminar and turbulent flow conditions. Six well-known flow regime maps from the literature were found to be in good agreement for the annular flow conditions in the test tube in spite of their different operating conditions. Dalkilic et al. (2010e) used Kosky and Staub's model (1971) to predict flow pattern transitions and validate the results of void fraction models and correlations proposed in their previous publications and also show the identification of flow regimes in data corresponding to annular flow downward condensation of R134a in a vertical smooth copper tube. Furthermore, investigation of twelve number of well-known flow regime correlations from the literature is performed to identify the flow regime occurring in the test tube. Dalkilic et al. (2010d) calculated the average predicted heat transfer coefficient of the refrigerant using Kosky and Staub's model (1971) and the Von Karman universal velocity distribution correlations by means of different interfacial shear stress equations valid for annular flow in horizontal and vertical tubes in order to validate

Chen et al.'s annular flow theory (1987). The discussions for the effects of heat flux, mass flux and condensation temperature on the pressure drop were also made in their paper. A new correlation including dimensionless parameters such as the equivalent Reynolds number, Prandtl number, R number ($\rho\cdot\mu$ ratio), Lockhart and Martinelli parameter, Bond number and Froude number was proposed in their paper using a large number of data points for the determination of turbulent condensation heat transfer coefficient. Dalkilic et al. (2010c) proposed a new experimental approach on the determination of condensation heat transfer coefficient in a vertical tube by means of von Karman's universal velocity distribution and Kosky and Staub's annular flow film thickness model (1971). They benefitted from thirteen numbers of frictional pressure drop models and thirty five numbers of void fraction models in their model. Dalkilic and Wongwises (2009d) reported a detailed review of research on in-tube condensation by reason of its significance in refrigeration, air conditioning and heat pump applications. The heat transfer and pressure drop investigations for the in-tube condensation were included and almost all relevant research subjects were summarized, such as condensation heat transfer and pressure drop studies according to tube orientation (horizontal, vertical, inclined tubes) and tube geometry (smooth and enhanced tubes), flow pattern studies of condensation, void fraction studies, and refrigerants with oil. Besides to the above, various other conference papers (2008, 2009, 2010) were used to support and validate their proposed models and correlations in their papers. It can be seen from above studies, Dalkilic and Wongwises studied in-tube condensation process comprehensively using their experimental facility whose test section is working as a double-tube heat exchanger.

In spite of the existence of some available information in the literature, there still remains room for further research. As a result, the major aim in the present chapter of the book is to investigate the appliance of well-known empirical annular flow correlations to the annular flow condensation at high mass flux in a vertical double tube heat exchanger. The independency of annular flow heat transfer empirical correlations from tube orientation (1987) and the general applicability for a vertical short tube is also proved in this chapter.

2. Data reduction

Fig. 1 shows the steady-state physical model of downward film condensation in a vertical tube. Nusselt-type analysis is valid under some assumptions such as: laminar film flow; saturated state for the vapour of R134a; condensed film of R134a along the tube surface; constant physical properties corresponding to inlet pressure and temperature conditions; no entrainment. It should be noted that there is an interfacial shear effect at the interface occurred due to the much greater vapour velocity than the film velocity. The solution of the problem can be started from the calculation of the force balance in Eq. (1) for the differential element in the control volume neglecting the inertia and downstream diffusion contributions as shown in Dalkilic et al.'s study (2009c).

The force balance for the differential element in the control volume can be expressed as follows:

$$\rho_1 g dxdydz + \tau_\delta(y + dy) dxdz + P(z) dxdy = \tau_\delta(y) dxdz + P(z + dz) dxdy \quad (1)$$

It should be noted that the solution of the investigated case in this chapter will be different from Nusselt's solution (1916) due to the high mass flux condition of the condensate flow in the tube.

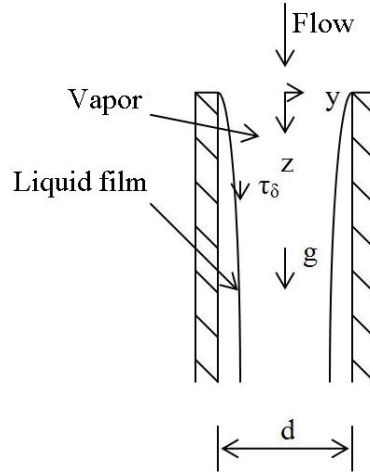


Fig. 1. System model for analysis of downward condensation

2.1 Experimental heat transfer coefficient

The details of determination of the experimental heat transfer coefficient by means of experimental setups can be seen in many papers given in references.

$$h_{\text{exp}} = \frac{Q_{\text{TS}}}{A_i(T_{\text{ref,sat}} - T_{w,i})} \quad (2)$$

where h_{exp} is the experimental average heat transfer coefficient, Q_{TS} is the heat transfer rate in the test section, $T_{w,i}$ is the average temperature of the inner wall, $T_{\text{ref,sat}}$ is the average temperature of the refrigerant at the test section inlet and outlet, and A_i is the inside surface area of the test section:

$$A_i = \pi d L \quad (3)$$

where d is the inside diameter of the test tube. L is the length of the test tube.

2.2 Uncertainties

The uncertainties of the Nusselt number and condensation heat transfer coefficient in the test tube, which belongs to a refrigerant loop consisting of an evaporator, test section and condenser, varied from $\pm 7.64\%$ to $\pm 10.71\%$. The procedures of Kline and McClintock (1953) were used for the calculation of all uncertainties. Various uncertainty values of the study can be seen from Table 1 in detail.

Based on this usual method, suppose that a set of measurement is made and the uncertainty in each may be expressed with same odds. These measurements are then used to calculate some desired result of the experiments. The result P is a given function of the independent variables $x_1, x_2, x_3, \dots, x_n$. Thus:

$$P = P(x_1, x_2, x_3, \dots, x_n) \quad (4)$$

Parameters	Uncertainty
$T_{ref,sat}$ (°C)	0.19
x_i	±6.96-8.24%
ΔT (K)	±0.191
$(T_{w,out} - T_{w,in})_{TS}$ (K)	±0.045
$(T_{w,in} - T_{w,out})_{ph}$ (K)	±0.13
m_{ref} (g s ⁻¹)	±0.023
$m_{w,TS}$ (g s ⁻¹)	±0.35
$m_{w,pre}$ (g s ⁻¹)	±0.38
q_{TS} (W m ⁻²)	±6.55-8.93%
q_{pre} (W m ⁻²)	±12-14.81%
h_{ref} (W m ⁻² K ⁻¹)	±7.64-10.71%.
ΔP (kPa)	±0.15

Table 1. Uncertainty of experimental parameters

Let w_p be the uncertainty in the result, and $w_1, w_2, w_3, \dots, w_n$ be the uncertainties in each independent variables. If the uncertainties in the independent variables are given with some odds, then the uncertainty in the result can be given as followed:

$$w_p = \pm \left[\left(\frac{\partial P}{\partial x_1} w_1 \right)^2 + \left(\frac{\partial P}{\partial x_2} w_2 \right)^2 + \left(\frac{\partial P}{\partial x_3} w_3 \right)^2 + \dots + \left(\frac{\partial P}{\partial x_n} w_n \right)^2 \right]^{1/2} \quad (5)$$

2.2.1 Vapor quality (x_{in})

The vapor quality entering the test section is calculated from an energy balance, which gives the total heat transfer rate from hot water to liquid R134a in the evaporator as the sum of sensible and latent heat transfer rates, on the pre-heater:

$$x_{in} = \frac{1}{i_{ref,fg}} \left[\frac{Q}{m_{ref,T}} - C_{p_{ref}} (T_{ref,sat} - T_{ref,pre,in}) \right] \quad (6)$$

$$w_{x_{in}} = \pm \left[\left(\frac{\partial x_{in}}{\partial Q} w_Q \right)^2 + \left(\frac{\partial x_{in}}{\partial m_{ref,T}} w_m \right)^2 + \left(\frac{\partial x_{in}}{\partial T_{ref,sat}} w_{T_{ref,sat}} \right)^2 + \left(\frac{\partial x_{in}}{\partial T_{ref,pre,in}} w_{T_{ref,pre,in}} \right)^2 \right]^{1/2} \quad (7)$$

$$w_{x_{in}} = \pm \left[\left(\frac{1}{m_{ref,T} i_{ref,fg}} w_Q \right)^2 + \left(\frac{Q}{i_{ref,fg} m_{ref,T}^2} w_{m_{ref,T}} \right)^2 + \left(\frac{C_{p,ref}}{i_{ref,fg}} w_{T_{ref,sat}} \right)^2 + \left(\frac{C_{p,ref}}{i_{ref,fg}} w_{T_{ref,pre,in}} \right)^2 \right]^{1/2} \quad (8)$$

2.2.2 Heat flux (Q)

The outlet quality of R134a from the evaporator is equal to the quality of R134a at the test section inlet. The total heat transferred in the test section is determined from an energy balance on the cold water flow in the annulus:

$$Q = m_w C_p (T_{w,out} - T_{w,in}) \quad (9)$$

$$w_Q = \pm \left[\left(\frac{\partial Q}{\partial m_w} w_{m_w} \right)^2 + \left(\frac{\partial Q}{\partial T_{w,in}} w_{T_{w,in}} \right)^2 + \left(\frac{\partial Q}{\partial T_{w,out}} w_{T_{w,out}} \right)^2 \right]^{1/2} \quad (10)$$

2.2.3 Average heat transfer coefficient (h_i)

The refrigerant side heat transfer coefficient in Eq. (2) is determined from the total heat transferred in the test section which is a vertical counter-flow tube-in-tube heat exchanger with refrigerant flowing in the inner tube and cooling water flowing in the annulus:

$$w_{h_i} = \left[\left(\frac{\partial h_i}{\partial Q} w_Q + \frac{\partial h_i}{\partial (T_{ref,sat} - T_{ref,w,i})} w_{(T_{ref,sat} - T_{ref,w,i})} \right) \right] \quad (11)$$

2.2.4 Nusselt number (Nu)

Nusselt number can be expressed as follows:

$$Nu = \frac{h_i L}{k_l} \quad (12)$$

$$w_{Nu} = \pm \left[\left(\frac{\partial Nu}{\partial h_i} w_{h_i} \right)^2 \right]^{1/2} \quad (13)$$

2.2.5 Temperature difference

The temperature measurements for the determination of outer surface temperature of the test tube are evaluated as an average value for the uncertainty analysis and calculation procedure can be seen as follows:

$$T_0 = \frac{T_1 + T_2 + T_3 + \dots + T_{10}}{10} \quad (14)$$

$$w_{T_0} = \pm \left[\left(\frac{\partial T_0}{\partial T_1} w_{T_1} \right)^2 + \left(\frac{\partial T_0}{\partial T_2} w_{T_2} \right)^2 + \dots + \left(\frac{\partial T_0}{\partial T_{10}} w_{T_{10}} \right)^2 \right]^{1/2} \quad (15)$$

$$w_{T_0} = \pm \left[\left(\frac{1}{10} w_{T_1} \right)^2 + \left(\frac{1}{10} w_{T_2} \right)^2 + \dots + \left(\frac{1}{10} w_{T_{10}} \right)^2 \right]^{1/2} \quad (16)$$

3. Heat transfer correlations in this chapter

The comparison of convective heat transfer coefficients with Shah correlation (1979) has been done by researchers commonly for turbulent condensation conditions especially in vertical tubes (2000) and it is found to be the most comparative condensation model during annular flow regime in a tube (2002). Shah correlation (1979) is based on the liquid heat transfer coefficient and is valid for $Re_l \geq 350$. A two-phase multiplier is used for the annular flow regime of high pressure steam and refrigerants (2000, 2002) in the equation.

Dobson and Chato (1998) used a two-phase multiplier to develop a correlation for an annular flow regime. A correlation is also provided for a wavy flow regime. The researchers used commonly their correlations for zeotropic refrigerants. Its validated mass flux (G) covers the values more than $500 \text{ kg m}^{-2} \text{ s}^{-1}$ for all qualities in horizontal tubes.

Sweeney (1996) developed the Dobson and Chato model (1998) using zeotropic mixtures for annular flow.

Cavallini et al. (1974) used various organic refrigerants for the condensation inside tubes in both vertical and horizontal orientations and developed a semi empirical correlation as a result of their study.

Bivens and Yokozeki (1994) modified Shah correlation (1979) benefitted from various flow patterns of R22, R502, R32/R134a, R32/R125/R134a.

Tang et al. (2000) developed the Shah [(1979) equation for the annular flow condensation of R410A, R134a and R22 in i.d. 8.81 mm tube with $Fr_{so} > 7$.

Fujii (1995) modified the correlation in Table 2 for shear-controlled regimes in smooth tubes. There is also another correlation belong to Fujii (1995) for gravity controlled regimes.

Chato (1961) used a two-phase multiplier to modify Dittus-Boelter's correlation (1930) for an annular flow regime.

Traviss et al. (1972) focused on the flow regime maps for condensation inside tubes. Their correlation was suggested for the condensation of R134a inside tubes specifically. Their model takes into account of the variation in the quality of the refrigerant using Lockhart-Martinelli parameter.

Akers and Rosson (1960) developed the Dittus-Boelter (1930)'s single-phase forced convection correlation. Their correlation's validity range covers the turbulent annular flow in small diameter circular tubes and rectangular channels.

Tandon et al. (1995) developed the Akers and Rosson (1960) correlation for shear controlled annular and semi-annular flows with $Re_g > 30000$. There is another correlation of Tandon et al. (1995) for gravity-controlled wavy flows with $Re_g < 30000$.

4. Results and discussion

It should be noted that it is possible for researcher to identify the experimental data of condensation by means of both flow regime maps and sight glass at the inlet and outlet of the test section. Dalkilic and Wongwises (2009b, 2010b, 2010e) checked the data shown in all figures and formulas that they were in an annular flow regime by Hewitt and Robertson's (1969) flow pattern map and also by sight glass in their experimental setup. The vapor quality range approximately between 0.7-0.95 in the 0.5 m long test tube was kept in order to obtain annular flow conditions at various high mass fluxes of R134a.

In Table 2, the list of correlations is evaluated to show the similarity of annular flow correlations which are independent of tube orientation (horizontal or vertical). Chen et al. (1987) also developed a general correlation to discuss this similarity in their article by relating the interfacial shear stress to flow conditions for annular film condensation inside tubes.

Researcher	Model/Correlation
Shah (1979)	$\text{Re}_l \geq 350$ $\text{Re}_l = \frac{Gd(1-x)}{\mu_l}$ $h_{shah} = h_{sf} \left(\frac{1.8}{Co^{0.8}} \right)$ $P_{red} = \frac{P_{sat}}{P_{critic}}$ $h_{sf} = h_l(1-x)^{0.8}$ $Co = \left(\frac{1}{x} - 1 \right)^{0.8} \left(\frac{\rho_g}{\rho_l} \right)^{0.5}$ $h_l = \frac{k_l}{d} \left(0.023 \left(\frac{\text{Re}_l}{1-x} \right)^{0.8} \text{Pr}_l^{0.4} \right)$
Dobson and Chato (1998)	$\text{For } G > 500 \text{ kg m}^{-2} \text{ s}^{-1}$ $Nu = 0.023 \text{Re}_l^{0.8} \text{Pr}_l^{0.4} \left[1 + \frac{2.22}{X^{0.89}} \right]$ $Ga = \frac{\rho_l(\rho_l - \rho_g)gd^3}{\mu_l^2}$ $X = \left(\frac{1-x}{x} \right)^{0.9} \left(\frac{\rho_g}{\rho_l} \right)^{0.5} \left(\frac{\mu_l}{\mu_g} \right)^{0.1}$ $Fr_{so} = c_3 \text{Re}_l^{c_4} \left(\frac{1 + 1.09X^{0.039}}{X} \right)^{1.5} \frac{1}{Ga^{0.5}}$ $\text{Re}_l = \frac{Gd(1-x)}{\mu_l}$ $\text{For } \text{Re}_l > 1250 \text{ and } Fr_{so} > 18$ $Nu = 0.023 \text{Re}_l^{0.8} \text{Pr}_l^{0.3} \frac{2.61}{X^{0.805}}$
Sweeney (1996)	$Nu = 0.7 \left(\frac{G}{300} \right)^{0.3} Nu_{Dobson-Chato}$
Cavallini et al. (1974)	$Nu_l = 0.05 \text{Re}_{eq}^{0.8} \text{Pr}^{0.33}$ $\text{Re}_{eq} = \text{Re}_g \left(\mu_g / \mu_l \right) \left(\rho_l / \rho_g \right)^{0.5} \text{Re}_l$ $\text{Re}_g = Gdx / \mu_g$
Bivens and Yokozeki (1994)	$Nu = Nu_{Shah} \left(0.78738 + \frac{6187.89}{G^2} \right)$ $P_{red} = P_{sat} / P_{critic}$ $Nu_{Shah} = 0.023 \text{Re}_l^{0.8} \text{Pr}_l^{0.4} \left[1 + \frac{3.8}{P_{red}^{0.38}} \left(\frac{x}{1-x} \right)^{0.76} \right]$
Tang et al. (2000)	$Nu = 0.023 \text{Re}_l^{0.8} \text{Pr}_l^{0.4} \left[1 + 4.863 \left(\left(-\ln(P_{red}) \frac{x}{1-x} \right)^{0.836} \right) \right]$ $\text{Re}_l \leq 1250$ $c_3 = 0.025$ $c_4 = 1.59$ $Fr_{so} = c_3 \text{Re}_l^{c_4} \left(\frac{1 + 1.09X^{0.039}}{X} \right)^{1.5} \frac{1}{Ga^{0.5}}$ $\text{Re}_l > 1250$ $c_3 = 1.26$ $c_4 = 1.04$
Fujii (1995)	$Nu_l = 0.0125 \left(\text{Re}_l \sqrt{\rho_l / \rho_g} \right)^{0.9} \left(\frac{x}{1-x} \right)^{0.1x+0.8} \text{Pr}_l^{0.63}$
Chato (1961)	$Nu = 0.023 \text{Re}_l^{0.8} \text{Pr}_l^{0.4} \left[\frac{2.47}{X^{1.96}} \right]$
Traviss et al. (1972)	$Nu = \text{Re}_l^{0.9} \text{Pr}_l \frac{F_1(X)}{F_2(\text{Re}_l, \text{Pr}_l)}$ $F_1(X) = 0.15 \left[\frac{1}{X} + \frac{2.83}{X^{0.476}} \right]$ $\text{Re}_l > 1125$ $F_2 = 5 \text{Pr}_l + 5 \ln(1 + 5 \text{Pr}_l) + 2.5 \ln(0.00313 \text{Re}_l^{0.812})$
Akers and Rosson (1960)	$Nu = 0.0265 \text{Re}_{eq}^{0.8} \text{Pr}_l^{1/3}$ $\text{Re}_{eq} = \frac{G_{eq}d}{\mu_l}$ $G_{eq} = G \left[(1-x) + x \left(\rho_l / \rho_g \right)^{0.5} \right]$
Tandon et al. (1995)	$\text{Re}_g > 30000$ $Nu = 0.084 \text{Re}_g^{0.67} \text{Pr}_l^{1/3} \left[\frac{1}{Ja_l} \right]^{1/6}$ $Ja_l = \frac{Cp_l \Delta T_{sat}}{i_{fg}}$

Table 2. Annular flow heat transfer correlations and models

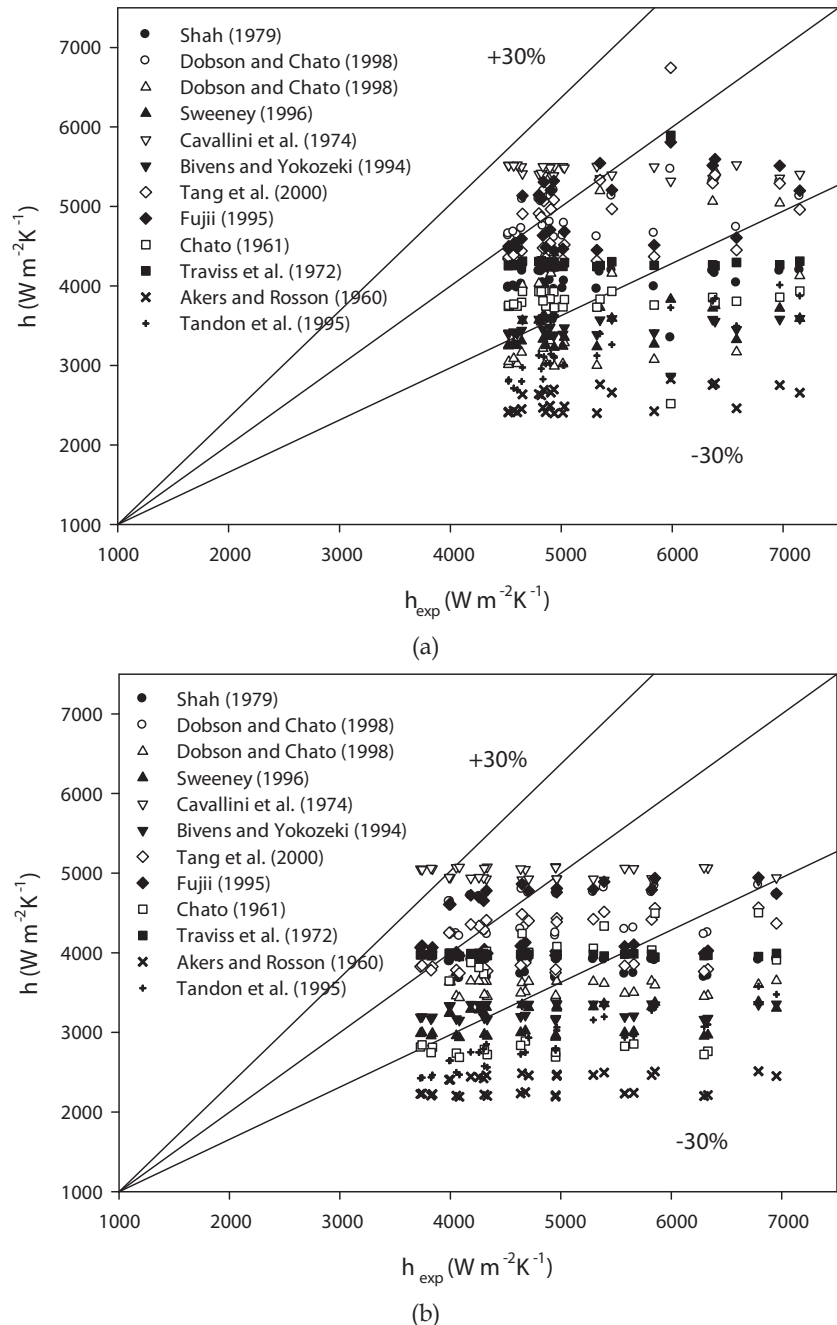


Fig. 2. Comparison of experimental condensation heat transfer coefficient vs. various correlations for $G=300 \text{ kg m}^{-2} \text{ s}^{-1}$ (a) $T_{\text{sat}}=40 \text{ }^{\circ}\text{C}$ and (b) $T_{\text{sat}}=50 \text{ }^{\circ}\text{C}$

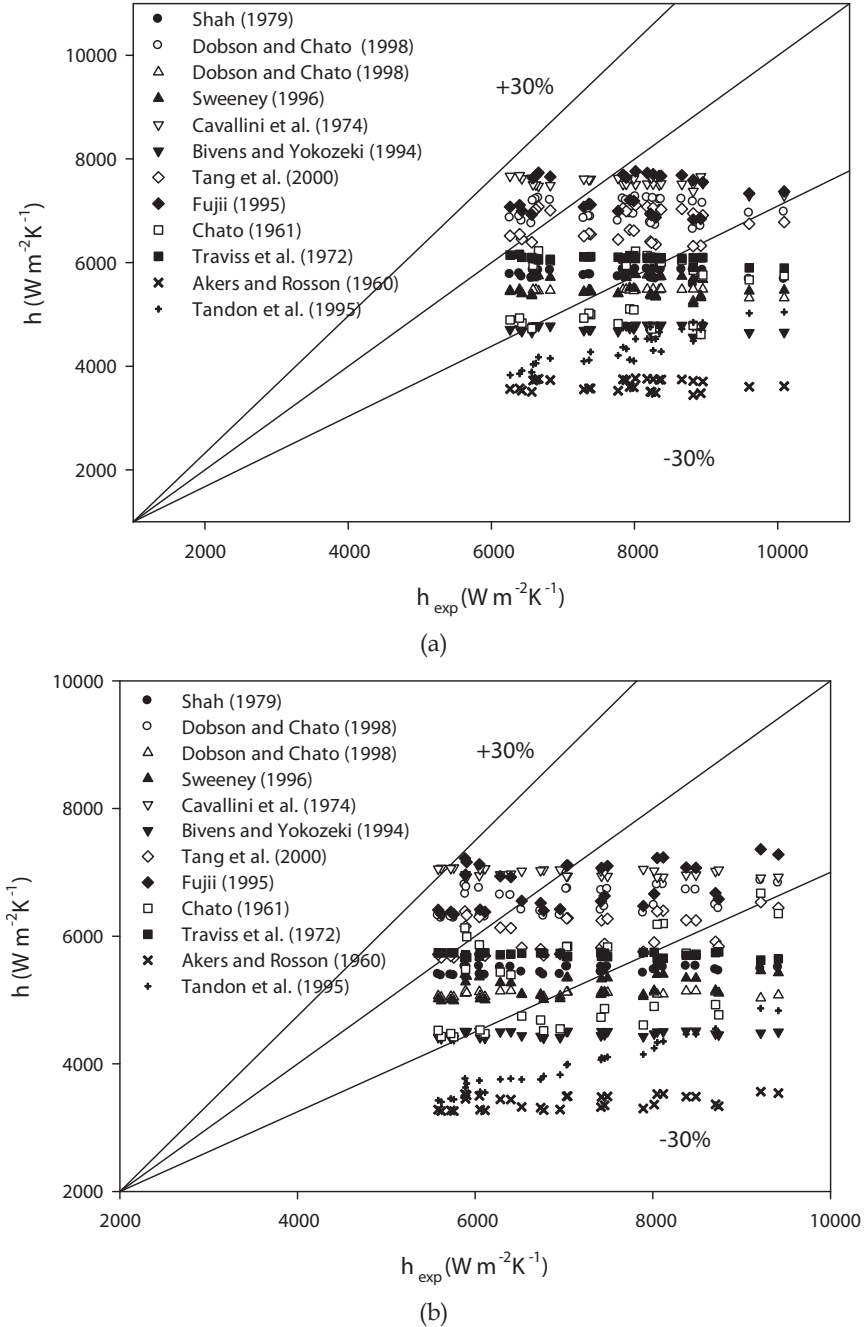


Fig. 3. Comparison of experimental condensation heat transfer coefficient vs. various correlations for $G=456 \text{ kg m}^{-2} \text{ s}^{-1}$ (a) $T_{sat}=40^\circ\text{C}$ and (b) $T_{sat}=50^\circ\text{C}$

The comparison of experimental heat transfer coefficients with various annular flow correlations are shown in Figs. 2-3 in a 30% deviation line for the condensation temperatures of 40 and 50 °C and mass fluxes of 300 and 456 kg m⁻²s⁻¹ respectively. It can be clearly seen from these figures that the Dobson and Chato (1998) correlation, Cavallini et al. (1974) correlation, Fujii (1995) correlation are in good agreement with the experimental data. In addition to this, the majority of the data calculated by Shah (1979) correlation, Dobson and Chato (1998) correlation, Tang et al. (2000) correlation, Traviss et al. (1972) correlation fall within ±30%, whereas, Tandon et al. (1995) correlation and Akers and Rosson (1960) correlation are found to be incompatible with the experimental data. Nonetheless, the Chato (1961) correlation, the Sweeny (1996) correlation, and the Bivens and Yokozeki (1994) correlation are found to have poor agreement with experimental data.

In the literature, some correlations are developed for gravity-controlled regimes such as Fujii (1995) and Tandon et al. (1995) correlations. In this chapter, the correlations, proposed for gravity-controlled regimes, are not found to be in good agreement with the data as expected for annular flow regime. These kinds of correlations do not exist in this chapter due to their large deviations and validity for wavy flow. Chen et al. (1987) reported that the vapor shear stress acting on the interface of vapor-liquid phases affects the forced convective condensation inside tubes especially at high vapor flow rates. On that account, Fujii (1995) and Tandon et al. (1995)'s shear-controlled correlations were used to predict condensation heat transfer coefficient of R134a. Furthermore, Valladares (2003) obtained similar results on these explanations in this chapter for the condensation of various refrigerants in horizontal tubes by Valladares (2003).

5. Conclusion

In this chapter of the book, the method to determine the average heat transfer coefficient of R134a during condensation in vertical downward flow at high mass flux in a smooth tube is proposed. The comparison between the various annular flow heat transfer correlations and experimental heat transfer coefficients is shown with ±30% deviation line. It can be noted that the Dobson and Chato (1998) correlation, the Cavallini et al. (1974) correlation, the Fujii (1995) correlation are found to have the most predictive results than others in an 8.1 mm i.d. copper tube for the mass fluxes of 300 and 456 kg m⁻²s⁻¹ and condensation temperatures of 40 and 50 °C. As a result of the analysis in this chapter, it is proven that annular flow models are independent of tube orientation provided that annular flow regime exists along the tube length and capable of predicting condensation heat transfer coefficients inside the vertical test tube although most of these correlations were developed for the annular flow condensation in horizontal tubes.

6. Acknowledgements

The authors would like to thank King Mongkut's University of Technology Thonburi (KMUTT), the Thailand Research Fund, the Office of Higher Education Commission and the National Research University Project for the financial support. Especially, the first author wishes to thank KMUTT for providing him with a Post-doctoral fellowship.

7. Nomenclature

A	surface area, m ²
C _p	specific heat, J kg ⁻¹ K ⁻¹
d	internal tube diameter, m
Fr	Froude number
G	mass flux, kg m ⁻² s ⁻¹
Ga	Galileo number
g	gravitational constant, m s ⁻²
h	convective heat transfer coefficient, W m ⁻² K ⁻¹
i	enthalpy, J kg ⁻¹
i _{fg}	latent heat of condensation, J kg ⁻¹
Ja	Jakob number
k	thermal conductivity, W m ⁻¹ K ⁻¹
L	length of test tube, m
m	mass flow rate, kg s ⁻¹
Nu	Nusselt number
P	pressure, MPa
Pr	Prandtl number
Re	Reynolds number
T	temperature
Q	heat transfer rate, W
q	mean heat flux, kW m ⁻²
y	wall coordinate
x	mean vapor quality
y	radial coordinate
z	axial coordinate
X	Lockhart-Martinelli parameter
w	uncertainty

Greek Symbols

ΔT	vapor side temperature difference, T _{ref,sat} - T _{wi} , °C
ρ	density, kg m ⁻³
μ	dynamic viscosity, kg m ⁻¹ s ⁻¹
τ	shear stress, N m ⁻²

Subscripts

eq	equivalent
exp	experimental
g	gas/vapor
i	inside
in	inlet
l	liquid
out	outlet
pre	preheater
red	reduced
ref	refrigerant

sat	saturation
so	Soliman
T	total
TS	test section
w	water
w _i	inner wall
δ	film thickness

8. References

Akers, W.W., Rosson, H.F. (1960). Condensation inside a horizontal tube, *Chemical Engineering Progress Symposium Series*, Vol. 56, No. 30, 145-149.

Akers, W.W., Deans, A., Crosser, O.K. (1959). Condensing heat transfer within horizontal tubes. *Chemical Engineering Progress Symposium Series*, Vol. 55, No. 29, 171-176.

Barnea, D., Shoham, O., Taitel, Y. (1982). Flow pattern transition for vertical downward two phase flow. *Chemical Engineering Science*, Vol. 37, No. 5, 741-744.

Bassi, R., Bansal, P.K. (2003). In-tube condensation of mixture of R134a and ester oil: empirical correlations. *International Journal of Refrigeration*, Vol. 26, No. 4, 402-409.

Bellinghausen, R., Renz, U. (1992). Heat transfer and film thickness during condensation of steam flowing at high velocity in a vertical pipe. *International Journal of Heat and Mass Transfer*, Vol. 35, No. 3, 683-689.

Bivens, D.B., Yokozeki, A. (1994). Heat transfer coefficient and transport properties for alternative refrigerants. *Proc. 1994 Int. Refrigeration Conference*, 299-304, Indiana.

Bergelin, O.P., Kegel, P.K., Carpenter, F.G., Gazley, C. (1946). Co-current gas-liquid flow. II. Flow in vertical tubes. *ASME Heat Transfer and Fluid Mechanic Institute*, 19-28.

Briggs, A., Kelemenis, C., Rose, J.W. (2000). Heat transfer and pressure drop measurements for in-tube condensation of CFC-113 using microfin tubes and wire inserts. *Experimental Heat Transfer*, Vol. 13, No. 3, 163-181.

Briggs, A., Kelemenis, C., Rose, J.W. (1998). Condensation of CFC-113 with downflow in vertical, internally enhanced tubes. *Proceedings of 11th IHTC*, August 23-28, Kyongju.

Carey, V.P. (1992). Liquid-Vapor Phase Change Phenomena, *Hemisphere Publishing*, 1992.

Cavallini, A., Zecchin, R. (1974). A dimensionless correlation for heat transfer in forced convection condensation. *6th International Heat Transfer Conference*, Vol. 3, 309-313, Tokyo.

Cavallini, A., Censi, G., Del Col, D., Doretti, L., Longo, G.A., Rossetto, L., Zilio, C. (2003). Condensation inside and outside smooth and enhanced tubes - a review of recent research. *International Journal of Refrigeration*, Vol. 26, No. 4, 373-392.

Chato, J.C. (1961). Laminar Condensation inside horizontal and inclined tubes. *ASHRAE Journal*, Vol. 4, 52-60.

Chen, S.L., Gerner, F.M., Tien, C.L. (1987). General film condensation correlations. *Experimental Heat Transfer*, Vol. 1, No. 2, 93-107.

Dalkilic, A.S., Laohalertdecha, S., Wongwises, S. (2008). A comparison of the void fraction correlations of R134a during condensation in vertical downward laminar flow in

a smooth and microfin tube. *Proceedings of the Micro/Nanoscale Heat Transfer International Conference*, Parts A-B, 1029-1040, Tainan.

Dalkilic, A.S., Laohalertdecha, S., Wongwises, S. (2008). Two-phase friction factor obtained from various void fraction models of R-134a during condensation in vertical downward flow at high mass flux. *Proceedings of the ASME Summer Heat Transfer Conference*, Vol. 2, 193-206, Jacksonville.

Dalkilic, A.S., Laohalertdecha, S., Wongwises, S. (2008). Two-phase friction factor in vertical downward flow in high mass flux region of refrigerant HFC-134a during condensation. *International Communications in Heat and Mass Transfer*, Vol. 35, No. 9, 1147-1152. (a)

Dalkilic, A.S., Laohalertdecha, S., Wongwises, S. (2008). Effect of void fraction models on the two-phase friction factor of R134a during condensation in vertical downward flow in a smooth tube. *International Communications in Heat and Mass Transfer*, Vol. 35, No. 8, 921-927. (b)

Dalkilic, A.S., Laohalertdecha, S., Wongwises, S. (2009). Experimental investigation on the condensation heat transfer and pressure drop characteristics of R134a at high mass flux conditions during annular flow regime inside a vertical smooth tube. *ASME Summer Heat Transfer Conference*, July 19-23, San Francisco.

Dalkilic, A.S., Agra, O. (2009). Experimental apparatus for the determination of condensation heat transfer coefficient for R134a and R600a flowing inside vertical and horizontal tubes. *ASME Summer Heat Transfer Conference*, July 19-23, San Francisco.

Dalkilic, A.S., Laohalertdecha, S., Wongwises, S. (2009). Experimental research on the similarity of annular flow models and correlations for the condensation of R134a at high mass flux inside vertical and horizontal tubes. *ASME International Mechanical Engineering Congress and Exposition*, November 13-19, Lake Buena Vista.

Dalkilic, A.S., Wongwises, S. (2009). A heat transfer model for co-current downward laminar film condensation of R134a in a vertical micro-fin tube during annular flow regime. *The Eleventh UK National Heat Transfer Conference*, Queen Mary University of London, September 6-8, London.

Dalkilic, A.S., Laohalertdecha, S., Wongwises, S. (2009). Effect of void fraction models on the film thickness of R134a during downward condensation in a vertical smooth tube. *International Communications in Heat and Mass Transfer*, Vol. 36, No. 2, 172-179. (a)

Dalkilic, A.S., Laohalertdecha, S., Wongwises, S. (2009). Experimental investigation of heat transfer coefficient of R134a during condensation in vertical downward flow at high mass flux in a smooth tube. *International Communications in Heat and Mass Transfer*, Vol. 36, No. 10, 1036-1043. (b)

Dalkilic, A.S., Yildiz, S., Wongwises, S. (2009). Experimental investigation of convective heat transfer coefficient during downward laminar flow condensation of R134a in a vertical smooth tube. *International Journal of Heat and Mass Transfer*, Vol. 52, No. 1-2, 142-150. (c)

Dalkilic, A.S., Wongwises, S. (2009). Intensive literature review of condensation inside smooth and enhanced tubes. *International Journal of Heat and Mass Transfer*, Vol. 52, No. 15-16, 3409-3426. (d)

Dalkilic, A.S., Laohalertdecha, S., Wongwises, S. (2010). Comparison of condensation frictional pressure drop models and correlations during annular flow of R134a inside a vertical tube. *ASME-ATI-UTI Thermal and Environmental Issues in Energy Systems*, May 16-19, Sorrento.

Dalkilic, A.S., Wongwises, S. (2010). Experimental study on the flow regime identification in the case of co-current condensation of R134a in a vertical smooth tube. *ASME International Heat Transfer Conference*, August 8-13, Washington.

Dalkilic, A.S., Agra, O., Teke, I., Wongwises, S. (2010). Comparison of frictional pressure drop models during annular flow condensation of R600a in a horizontal tube at low mass flux and of R134a in a vertical tube at high mass flux, *International Journal of Heat and Mass Transfer*, Vol. 53, No. 9-10, 2052-2064. (a)

Dalkilic, A.S., Wongwises, S. (2010). An investigation of a model of the flow pattern transition mechanism in relation to the identification of annular flow of R134a in a vertical tube using various void fraction models and flow regime maps. *Experimental Thermal and Fluid Science*, Vol. 34, No. 6, 692-705. (b)

Dalkilic, A.S., Laohalertdecha, S., Wongwises, S. (2010). New experimental approach on the determination of condensation heat transfer coefficient using frictional pressure drop and void fraction models in a vertical tube. *Energy Conversion and Management*, Vol. 51, No. 12, 2535-2547. (c)

Dalkilic, A.S., Wongwises, S. (2011). Experimental study on the modeling of condensation heat transfer coefficients in high mass flux region of refrigerant HFC-134a inside the vertical smooth tube during annular flow regime. *Heat Transfer Engineering*, Vol. 32, No. 1, 1-12. (d)

Dalkilic, A.S., Wongwises, S. (2010). Validation of void fraction models and correlations using a flow pattern transition mechanism model in relation to the identification of annular vertical downflow in-tube condensation of R134a. *International Communications in Heat and Mass Transfer* Vol. 37, No. 7, 827-834. (e)

Dittus, F.W., Boelter, L.M.K. (1930). Heat transfer in automobile radiators of the tubular type, *University of California Publications on Engineering*, Berkeley, CA, Vol. 2, No. 13, 443-461.

Dobson, M.K., Chato, J.C. (1998). Condensation in smooth horizontal tubes. *Journal of Heat Transfer-Transactions of ASME*, Vol. 120, No. 1, 193-213.

Fujii, T. (1995). Enhancement to condensing heat transfer-new developments, *Journal of Enhanced Heat Transfer*, Vol. 2, No. 1-2, 127-137.

Hewitt, G.F., Robertson, D.N. (1969). Studies of two-phase flow patterns by simultaneous x-ray and flash photography. Rept AERE-M2159, UKAEA, Harwell.

Jung, D., Song, K., Cho, Y., Kim, S. (2003). Flow condensation heat transfer coefficients of pure refrigerants. *International Journal of Refrigeration*, Vol. 26, No. 1, 4-11.

Jung, D., Cho, Y., Park, K. (2004). Flow condensation heat transfer coefficients of R22, R134a, R407C and R41A inside plain and micro-fin tubes. *International Journal of Refrigeration*, Vol. 27, No. 5, 25-32.

Kim, S.J., No, H.C. (2000). Turbulent film condensation of high pressure steam in a vertical tube. *International Journal of Heat and Mass Transfer*, Vol. 43, No. 21, 4031-4042.

Kline, S.J., McClintock, F.A. (1953). Describing uncertainties in single sample experiments. *Journal of the Japan Society of Mechanical Engineers*, Vol. 75, No. 1, 3-8.

Kosky, P.G., Staub, F.W. (1971). Local condensing heat transfer coefficients in the annular flow regime, *AIChE Journal*, Vol. 17, No. 5, 1037-1043.

Liebenberg, L., Bukasa, J.P., Holm, M.F.K., Meyer, J.P., Bergles, A.E. (2002). Towards a unified approach for modelling of refrigerant condensation in smooth tubes. *Proceedings of the International Symposium on Compact Heat Exchangers*, 457-462, Grenoble.

Lockhart, R.W., Martinelli, R.C. (1949). Proposed correlation of data for isothermal two-phase, two-component flow in pipes. *Chemical Engineering Progress*, Vol. 45, No. 1, 39-48.

Ma, X., Briggs, A., Rose, J.W. (2004). Heat transfer and pressure drop characteristics for condensation of R113 in a vertical micro-finned tube with wire insert. *International Communications in Heat and Mass Transfer*, Vol. 31, No. 5, 619-627.

Maheshwari, N.K., Sinha, R.K., Saha, D., Aritomi, M. (2004). M., Investigation on condensation in presence of a noncondensable gas for a wide range of Reynolds number. *Nuclear Engineering and Design*, Vol. 227, No. 2, 219-238.

Moser, K., Webb, R.L., Na, B. (1998). A new equivalent Reynolds number model for condensation in smooth tubes. *International Journal of Heat Transfer*, Vol. 120, No. 2, 410-417.

Nusselt, W. (1916). Die oberflachen-kondensation des wasserdampfer. *Zeitschrift des Vereines Deutscher Ingenieure*, Vol. 60, No. 27, 541-569.

Oh, S., Revankar, A. (2005). Analysis of the complete condensation in a vertical tube passive condenser. *International Communications in Heat and Mass Transfer*, Vol. 32, No. 6, 716-722.

Shah, M.M. (1979). A general correlation for heat transfer during film condensation inside pipes. *International Journal of Heat and Mass Transfer*, Vol. 22, No. 4, 547-556. (3)

Sweeney, K.A. (1996). The heat transfer and pressure drop behavior of a zeotropic refrigerant mixture in a micro-finned tube. *M.S. thesis*, Dept. of Mechanical and Industrial Engineering, University of Illinois at Urbana-Champaign.

Tandon, T.N., Varma, H.K., Gupta, C.P. (1995). Heat transfer during forced convection condensation inside horizontal tube. *International Journal of Refrigeration*, Vol. 18, No. 3, 210-214.

Tang, L., Ohadi, M.M., Johnson, A.T. (2000). Flow condensation in smooth and microfin tubes with HCFC-22, HFC-134a, and HFC-410 refrigerants. part II: Design equations. *Journal of Enhanced Heat Transfer*, Vol. 7, No. 5, 311-325.

Travis, D.P., Rohsenow, W.M., Baron, A.B. (1972). Forced convection inside tubes: a heat transfer equation for condenser design. *ASHRAE Transactions*, Vol. 79, No. 1, 157-165.

Valladeres, O.G. (2003). Review of in-tube condensation heat transfer coefficients for smooth and microfin tubes. *Heat Transfer Engineering*, Vol. 24, No. 4, 6-24.

Wang, H.S., Honda, H. (2003). Condensation of refrigerants in horizontal microfin tubes: comparison of prediction methods for heat transfer. *International Journal of Refrigeration*, Vol. 26, No. 4, 452-460.

Whalley, P.B. (1987). Boiling, condensation, and gas-liquid flow, *Oxford University Press*.

Optimum Fin Profile under Dry and Wet Surface Conditions

Balaram Kundu¹ and Somchai Wongwises²

¹*Department of Mechanical Engineering
Jadavpur University, Kolkata – 700 032*

²*Fluid Mechanics, Thermal Engineering and Multiphase
Flow Research Lab (FUTURE), Department of Mechanical Engineering
King Mongkut's University of Technology Thonburi (KMUTT)
Bangmod, Bangkok 10140*

¹*India*

²*Thailand*

1. Introduction

Fins or extended surfaces are frequently employed in heat exchangers for effectively improving the overall heat transfer performance. The simple design of fins and their stability in different surface conditions have created them a popular augmentation device. The different fin shapes are available in the literature. The geometry of the fin may be dependent upon the primary surface also. For circular primary surface, the attachment of circumferential fins is a common choice. The longitudinal and pin fins are generally used to the flat primary surface. However, due to attachment of fins with the primary surface, the heat transfer augments but the volume, weight, and cost of the heat exchanger equipments increase as well. Hence, it is a challenge to the designer to minimize the cost for the attachment of fins. This can be done by determining the optimum shape of a fin satisfying the maximization of heat transfer rate for a given fin volume. In general, two different approaches are considered for the optimization of any fin design problem. Through a rigorous technique, the profile of a fin for a particular geometry (flat or curved primary surface) may be obtained such that the criteria of the maximum heat transfer for a given fin volume or equivalently minimum fin volume for a given heat transfer duty is satisfied. In a parallel activity, the optimum dimensions of a fin of given profile (rectangular, triangular etc.) are determined from the solution of the optimality criteria. The resulting profile obtained from the first case of optimum design is superior in respect to heat transfer rate per unit volume and thus it is very much important in fin design problems. However, it may be limited to use in actual practice because the resulting profile shape would be slightly difficult to manufacture and fabricate. Alternatively, such theoretical shape would first be calculated and then a triangular profile approximating the base two thirds of the fin would be used. Such a triangular fin transfers heat per unit weight, which is closer to that of the analytical optimum value.

Under a convective environmental condition, Schmidt (1926) was the first researcher to forward a systematic approach for the optimum design of fins. He proposed heuristically that for an optimum shape of a cooling fin, the fin temperature must be a linear function

with the fin length. Later, through the calculus of variation, Duffin (1959) exhibited a rigorous proof on the optimality criteria of Schmidt. Liu (1961) extended the variational principle to find out the optimum profile of fins with internal heat generation. Liu (1962) and Wilkins (1961) addressed for the optimization of radiating fins. Solov"ev (1968) determined the optimum radiator fin profile. The performance parameter of annular fins of different profiles subject to locally variable heat transfer coefficient had been investigated by Mokheimer (2002). From the above literature works, it can be indicated that the above works were formulated based on the "length of arc idealization (LAI)."

Maday (1974) was the first researcher to eliminate LAI and obtained the optimum profile through a numerical integration. It is interesting to note that an optimum convecting fin neither has a linear temperature profile nor possesses a concave parabolic shape suggested by Maday. The profile shape contains a number of ripples denoted as a "wavy fin". The same exercise was carried out for radial fins by Guceri and Maday (1975). Later Razelos and Imre (1983) applied Pontryagin's minimum principle to find out the minimum mass of convective fins with variable heat transfer coefficient. Zubair et al. (1996) determined the optimum dimensions of circular fins with variable profiles and temperature dependent thermal conductivity. They found an increasing heat transfer rate through the optimum profile fin by 20% as compare to the constant thickness fin.

A variational method was adopted by Kundu and Das (1998) to determine the optimum shape of three types of fins namely the longitudinal fin, spine and disc fin. A generalized approach of analysis based on a common form of differential equations and a set of boundary conditions had been described. For all the fin geometries, it was shown that the temperature gradient is constant and the excess temperature at the tip vanishes. By taking into account the LAI, Hanin and Campo (2003) forecasted a shape of a straight cooling fin for the minimum envelop. From the result, they have highlighted that the volume of the optimum circular fin with consideration of LAI found is 6.21-8 times smaller than the volume of the corresponding Schmidt's parabolic optimum fin. A new methodological determination for the optimum design of thin fins with uniform volumetric heat generation had been done by Kundu and Das (2005).

There are ample of practical applications in which extended surface heat transfer is involved in two-phase flow conditions. For example, when humid air encounter into a cold surface of cooling coils whose temperature is maintained below the dew point temperature, condensation of moisture will take place, and mass and heat transfer occur simultaneously. The fin-and-tube heat exchangers are widely used in conventional air conditioning systems for air cooling and dehumidifying. In the evaporator of air conditioning equipment, the fin surface becomes dry, partially or fully wet depending upon the thermogeometric and psychrometric conditions involved in the design process. If the temperature of the entire fin surface is lower than the dew point of the surrounding air, there may occur both sensible and latent heat transferred from the air to the fin and so the fin is fully wet. The fin is partially wet if the fin-base temperature is below the dew point while fin-tip temperature is above the dew point of the surrounding air. If the temperature of the entire fin surface is higher than the dew point, only sensible heat is transferred and so the fin is fully dry. For wet surface, the moisture is condensed on the fin surface, latent heat evolves and mass transfer occurs simultaneously with the heat transfer. Thermal performance of different surface conditions of a fin depends on the fin shape, thermophysical and psychrometric properties of air.

Many investigations have been devoted to analyze the effect of condensation on the performance of different geometric fins. It is noteworthy to mention that for each instance, a

suitable fin geometry has been selected a priori to make the analysis. For the combined heat and mass transfer, the mathematical formulation becomes complex to determine the overall performance analysis of a wet fin. Based on the dry fin formula, Threlkeld (1970) and McQuiston (1975) determined the one-dimensional fin efficiency of a rectangular longitudinal fin for a fully wet surface condition. An analytical solution for the efficiency of a longitudinal straight fin under dry, fully wet and partially wet surface conditions was introduced elaborately by Wu and Bong (1994) first with considering temperature and humidity ratio differences as the driving forces for heat and mass transfer. For the establishment of an analytical solution, a linear relationship between humidity ratio and the corresponding saturation temperature of air was taken. Later an extensive analytical works on the performance and optimization analysis of wet fins was carried out by applying this linear relationship. A technique to determine the performance and optimization of straight tapered longitudinal fins subject to simultaneous heat and mass transfer has been established analytically by Kundu (2002) and Kundu and Das (2004). The performance and optimum dimensions of a new fin, namely, SRC profile subject to simultaneous heat and mass transfer have been investigated by Kundu (2007a; 2009a). In his work, a comparative study has also been made between rectangular and SRC profile fins when they are operated in wet conditions. Hong and Web (1996) calculated the fin efficiency for wet and dry circular fins with a constant thickness. Kundu and Barman (2010) have studied a design analysis of annular fins under dehumidifying conditions with a polynomial relationship between humidity ratio and saturation temperature by using differential transform method. In case of longitudinal fins of rectangular geometry, approximate analytic solution for performances has been demonstrated by Kundu (2009b). Kundu and Miyara (2009) have established an analytical model for determination of the performance of a fin assembly under dehumidifying conditions. Kundu et al. (2008) have described analytically to predict the fin performance of longitudinal triangular fins subject to simultaneous heat and mass transfer.

The heat and mass transfer analysis for dehumidification of air on fin-and-tube heat exchangers was done experimentally by the few authors. The different techniques, namely, new reduction method, tiny circular fin method, finite circular fin method and review of data reduction method used for analyzing the heat and mass transfer characteristics of wavy fin-and-tube exchangers under dehumidifying conditions had been investigated by Pirompugd et al. (2007a; 2007b; 2008; 2009).

The above investigations had been focused on determination of the optimum profile subjected to convective environment. However a thorough research works have already been devoted for analyzing the performance and optimization of wet fins. To carryout these analyses, suitable fin geometry has been chosen a priori. However, the optimum profile fin may be employed in air conditioning apparatus, especially, in aircrafts where reduction of weight is always given an extra design attention. Kundu (2008) determined an optimum fin profile of thin fins under dehumidifying condition of practical interest formulated with the treatment by a calculus of variation. Recently, Kundu (2010) focused to determine the optimum fin profile for both fully and partially wet longitudinal fins with a nonlinear saturation curve.

In this book chapter, a mathematical theory has been developed for obtaining the optimum fin shape of three common types of fins, namely, longitudinal, spine and annular fins by satisfying the maximizing heat transfer duty for a given either fin volume or both fin volume and length. The analysis was formulated for the dry, partially and fully wet surface conditions. For the analytical solution of a wet fin equation, a relationship between humidity ratio and temperature of the saturation air is necessary and it is taken a linear variation. The influence of

wet fin surface conditions on the optimum profile shape and its dimensions has also been examined. From the analysis, it can be mentioned that whether a surface is dry, partially or fully wet at an optimum condition, the air relative humidity is a responsible factor. The optimum fin profile and design variables have been determined as a function of thermropsychrometric parameters. The dry surface analysis can be possible from the present fully wet surface fin analysis with considering zero value of latent heat of condensation. From the analysis presented, it can be highlighted that unlike dry and partially wet fins, tip temperature for fully wet fins is below the ambient temperature for the minimum profile envelop fin.

2. Variational formulations for the optimum fin shape

For determination of the optimum fin shape, it can be assumed that the condensate thermal resistance to heat flow is negligibly small as the condensate film is much thinner than the boundary layer in the dehumidification process. Under such circumstances, it may follow that the heat transfer coefficient is not influenced significantly with the presence of condensation. The condensation takes place when fin surface temperature is below the dew point of the surrounding air and for its calculation, specific humidity of the saturated air on the wet surface is assumed to be a linear function with the local fin temperature. This assumption can be considered due to the smaller temperature range involved in the practical application between fin base and dew point temperatures and within this small range, saturation curve on the psychometric chart is possible to be an approximated by a straight line (Wu and Bong, 1994; Kundu, 2002; Kundu, 2007a; Kundu, 2007b; Kundu, 2008; Kundu, 2009). Owing to small temperature variation in the fin between fin-base and fin-tip, it can be assumed that the thermal conductivity of the fin material is a constant. The different types of fins, namely, longitudinal, spine and annular fin are commonly used according to the shape of the primary surfaces. Depending upon the fin base, fin tip and dew point temperatures, fin-surface can be dry, partially and fully wet. The analysis for determination of an optimum profile of fully and partially wet fins for longitudinal, spine and annular fin geometries are described separately in the followings:

2.1 Fully wet longitudinal fins

The schematic diagram of an optimum shape of longitudinal fins is illustrated in Fig. 1. The governing energy equation for one-dimensional temperature distribution on fully wet surface fins can be written under steady state condition as follows:

$$\frac{d}{dx} \left(y \frac{dT}{dx} \right) = \frac{h}{k} \left[(T - T_a) + h_m (\omega - \omega_a) h_{fg} / h \right] \quad (1)$$

h_m is the average mass transfer coefficient based on the humidity ratio difference, ω is the humidity ratio of saturated air at temperature T , ω_a is the humidity ratio of the atmospheric air, and h_{fg} is the latent heat of condensation. For the mathematical simplicity, the following dimensionless variables and parameters can be introduced:

$$X = hx/k; Y = hy/k; L = hl/k; \theta = (T_a - T)/(T_a - T_b); Le = (h/h_m C_p)^{3/2} \quad (2)$$

where, Le is the Lewis number. The relationship between heat and mass transfer coefficients can be obtained from the Chilton-Colburn analogy (Chilton and Colburn, 1934). The relationship between the saturated water film temperature T and the corresponding

saturated humidity ratio ω is approximated by a linear function (Wu and Bong, 1994; Kundu, 2002; Kundu, 2007a; Kundu, 2007b; Kundu, 2008; Kundu, 2009) in this study:

$$\omega = a + bT \quad (3)$$

where, a and b are constants determined from the conditions of air at the fin base and fin tip. Eq. (1) is written in dimensionless form by using Eqs. (2) and (3) as follows:

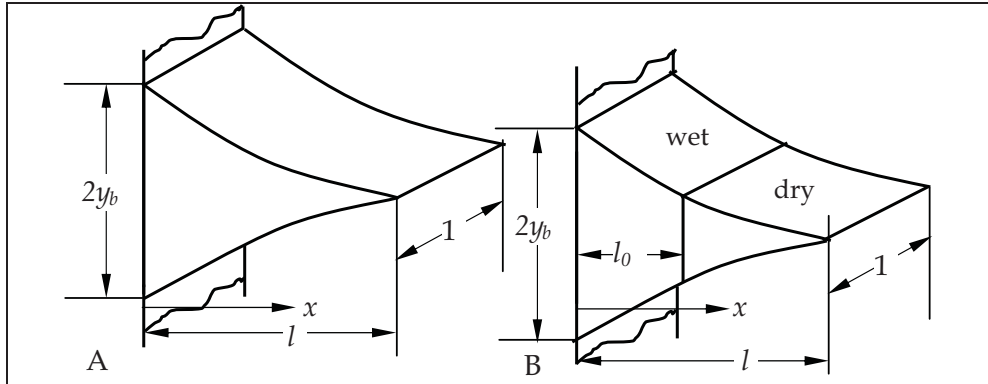


Fig. 1. Schematic diagram of an optimum longitudinal fin under dehumidifying conditions: A. Fully wet; and B. Partially wet.

$$d/dX(Y d\phi/dX) = (1 + b\xi)\phi \quad (4)$$

where

$$\phi = \theta + \theta_p; \quad \theta_p = (\omega_a - a - bT_a) / [(T_a - T_b)(1 + b\xi)]; \quad \xi = h_{fg}/C_p L e^{2/3} \quad (5)$$

Eq. (4) is subjected to the following boundary conditions:

$$\text{at } X = 0, \quad \phi = 1 + \theta_p = \phi_0 \quad (6a)$$

$$\text{at } X = L, \quad Y d\phi/dX = 0 \quad (6b)$$

For determination of the heat transfer duty through fins, Eq. (4) is multiplied by ϕ , and then integrated, the following expression are obtained with the help of the corresponding boundary conditions:

$$-[Y \phi d\phi/dX]_{X=0} = \int_{X=0}^L \left[Y \left(d\phi/dX \right)^2 + (1 + b\xi)\phi^2 \right] dX \quad (7)$$

The heat transfer rate through the fins can be calculated by applying the Fourier's law of heat conduction at the fin base:

$$Q = \frac{q}{2k(T_a - T_b)} = -[Y d\phi/dX]_{X=0} = \frac{1}{\phi_0} \int_{X=0}^L \left[Y \left(d\phi/dX \right)^2 + (1 + b\xi)\phi^2 \right] dX \quad (8)$$

The fin volume is obtained from the following expression:

$$U = \frac{V(h/k)^2}{2} = \int_{X=0}^L Y dX \quad (9)$$

The profile shape of a fin has been determined from the variational principle after satisfying the maximization of heat transfer rate Q for a design condition. In the present study, either the fin volume or both the fin volume and length are considered as a constraint condition. A functional F may be constructed from Eqs. (8) and (9) by employing Lagrange multiplier λ :

$$F = Q - \lambda U = \frac{1}{\phi_0} \int_{X=0}^L \left[Y(d\phi/dX)^2 + (1 + b\xi)\phi^2 - \lambda \phi_0 Y \right] dX \quad (10)$$

The relation between the variation of F and that of Y is obtained from the above equation and for maximum value of F , δF is zero for any admissible variation of δY . Thus

$$\delta F = \frac{1}{\phi_0} \int_{X=0}^L Y^{-1} \left[Y(d\phi/dX)^2 - \lambda \phi_0 Y \right] \delta Y dX = 0 \quad (11)$$

From the above equation, the following optimality criteria are obtained:

$$Y(d\phi/dX)^2 - \lambda \phi_0 Y = 0 \quad (12)$$

From Eq. (12), it is obvious that the temperature gradient in the longitudinal fin for the optimum condition is a constant.

2.1.1 Optimum longitudinal fin for the volume constraint

Here the fin length L is not a constant and thus it can be taken as a variable. From Eq. (10), the variation of function F with L is as follows:

$$\delta F = \frac{1}{\phi_0} \left[Y(d\phi/dX)^2 + (1 + b\xi)\phi^2 - \lambda \phi_0 Y \right] \delta X \Big|_{X=0}^L = 0 \quad (13)$$

At $X = 0$, the above term vanishes as $\delta X = 0$. At $X = L$, δX is not zero; therefore, at the tip, the following optimality conditions can be obtained:

$$Y(d\phi/dX)^2 + (1 + b\xi)\phi^2 - \lambda \phi_0 Y = 0 \quad (14)$$

Combining Eqs. (4), (6), (12) and (14), yields the tip condition $\phi = 0$. The tip thickness of a fin may be determined from the tip condition and the optimality criterion and boundary condition (Eqs. (12) and (6b)). It can be seen that the tip thickness is zero. The tip temperature for fully wet surface $\theta_t = -\theta_p$, which is slightly less than the ambient value and this temperature is obvious as a function of psychometric properties of the surrounding air. From Eqs. (4), (6), (12) and tip condition, the temperature distribution and fin profile are written as follows:

$$\theta = 1 - (1 + \theta_p) X / L \quad (15)$$

and

$$Y = \frac{(1 + b\xi)}{2} (L - X)^2 \quad (16)$$

The optimum fin length L_{opt} can be obtained from Eqs. (9) and (16). The maximum heat transfer rate through the fin can be written by the design variables as follows:

$$\begin{bmatrix} L_{opt} \\ Q_{opt} \end{bmatrix} = \begin{bmatrix} \{6 U / (1 + b\xi)\}^{1/3} \\ \phi_0 \{3U(1 + b\xi)^2 / 4\}^{1/3} \end{bmatrix} \quad (17a)$$

$$(17b)$$

2.1.2 Optimum longitudinal fin for both length and volume constraints

In fin design, sometimes the length of the fin is required to specify due to restricted space and ease of manufacturing. Under this design consideration, both length (fixed L) and volume may be adopted as a constraint. For obtaining the temperature distribution and fin profile, Eqs. (6), (9) and (12) can be combined:

$$\theta = 1 - \alpha X \quad (18)$$

and

$$Y = \frac{(1 + b\xi)}{2\alpha} [2\phi_0(L - X) - \alpha(L^2 - X^2)] \quad (19)$$

where

$$\alpha = \frac{3 L^2 (1 + b\xi) \phi_0}{6U + 2L^3 (1 + b\xi)} \quad (20)$$

Here, it may be noted that the optimum fin shape for dry surface fins can be determined by using the above formula.

2.2 Partially wet longitudinal fins

There are two regions dry and wet in partially wet fins shown in Fig. 1B. For partially wet longitudinal fins, the energy equations are in the followings:

$$\begin{bmatrix} \frac{d}{dx} \left(y \frac{dT}{dx} \right) \\ \frac{d}{dx} \left(y \frac{dT}{dx} \right) \end{bmatrix} = \begin{bmatrix} \frac{h}{k} (T - T_a) \\ \frac{h}{k} \{ (T - T_a) + h_m (\omega - \omega_a) h_{fg} / h \} \end{bmatrix} \quad \begin{array}{l} \text{for dry surface } T > T_d \\ \text{for wet surface } T \leq T_d \end{array} \quad (21a)$$

$$(21b)$$

By using Eqs. (2) and (3), Eq. (21) is made in normalized form and it can be expressed as follows:

$$\left[\frac{d}{dX} \left(Y \frac{d\theta}{dX} \right) \right] = \left[\begin{array}{c} \theta \\ (1+b\xi)\phi \end{array} \right] \quad \text{for dry domain } \theta > \theta_d \quad (22a)$$

$$\left[\frac{d}{dX} \left(Y \frac{d\phi}{dX} \right) \right] = \left[\begin{array}{c} \theta \\ (1+b\xi)\phi \end{array} \right] \quad \text{for wet domain } \theta \leq \theta_d \quad (22b)$$

The heat transfer through the tip is negligibly small in comparison to that through the lateral surfaces and fin base temperature is taken as a constant. In addition, continuity of temperature and heat conduction satisfies at the section where dry and wet separates. Thus, for solving Eq. (22) the following boundary conditions are taken:

$$\text{at } X = 0, \phi = \phi_0 \quad (23a)$$

$$\text{at } X = L_0, \begin{cases} \theta = \theta_d \\ d\theta/dX = d\phi/dX \end{cases} \quad (23b)$$

$$\text{at } X = L, Yd\theta/dX = 0 \quad (23c)$$

$$\text{at } X = L, Yd\theta/dX = 0 \quad (23d)$$

Eq. (22) are multiplied by respective variables θ and ϕ , and the following relationships are obtained by integration and using boundary conditions:

$$-[Y\phi d\phi/dX]_{X=0} = -[Y\phi d\phi/dX]_{X=L_0} + \int_{X=0}^{L_0} \left[Y \left(\frac{d\phi}{dX} \right)^2 + (1+b\xi)\phi^2 \right] dX \quad (24a)$$

and

$$-[Y\theta d\theta/dX]_{X=L_0} = \int_{X=L_0}^L \left[Y \left(\frac{d\theta}{dX} \right)^2 + \theta^2 \right] dX \quad (24b)$$

Combining Eqs. (24a) and (24b), one can get

$$-[Y\phi d\phi/dX]_{X=0} = \frac{\phi_d}{\theta_d} \int_{X=L_0}^L \left[Y \left(\frac{d\theta}{dX} \right)^2 + \theta^2 \right] dX + \int_{X=0}^{L_0} \left[Y \left(\frac{d\phi}{dX} \right)^2 + (1+b\xi)\phi^2 \right] dX \quad (25)$$

The heat transfer rate through the fins is calculated by applying the Fourier's law of heat conduction at the fin base and it can be written by using Eq. (25) as

$$\begin{aligned} Q &= \frac{q}{2k(T_a - T_b)} = - \left(Y \frac{d\phi}{dX} \right)_{X=0} = \frac{\phi_d}{\theta_d \theta_d} \int_{X=L_0}^L \left[Y \left(\frac{d\theta}{dX} \right)^2 + \theta^2 \right] dX \\ &+ \frac{1}{\phi_0} \int_{X=0}^{L_0} \left[Y \left(\frac{d\phi}{dX} \right)^2 + (1+b\xi)\phi^2 \right] dX \end{aligned} \quad (26)$$

The fin volume per unit width can be obtained from the following expressions:

$$U = \frac{V(h/k)^2}{2} = \int_{X=0}^{L_0} Y dX + \int_{X=L_0}^L Y dX \quad (27)$$

The optimum profile shape of a fin can be determined from the variational principle by constructing a functional F from Eqs. (26) and (27) using Lagrange multiplier λ .

$$\begin{aligned} F = Q - \lambda U = & \frac{1}{\phi_0} \int_{X=0}^{L_0} \left[Y(d\phi/dX)^2 + (1+b\xi)\phi^2 - \lambda \phi_0 Y \right] dX \\ & + \frac{\phi_d}{\phi_0 \theta_d} \int_{X=L_0}^L \left[Y(d\theta/dX)^2 + \theta^2 - \lambda \phi_0 \theta_d Y / \phi_d \right] dX \end{aligned} \quad (28)$$

For maximizing value of F , the following condition is obtained from Eq. (28).

$$\begin{aligned} \delta F = & \frac{1}{\phi_0} \int_{X=0}^{L_0} Y^{-1} \left[Y(d\phi/dX)^2 - \lambda \phi_0 Y \right] \delta Y dX \\ & + \frac{\phi_d}{\phi_0 \theta_d} \int_{X=L_0}^L Y^{-1} \left[Y(d\theta/dX)^2 - \lambda \phi_0 \theta_d Y / \phi_d \right] \delta Y dX = 0 \end{aligned} \quad (29)$$

From Eq. (29), the optimality criterion is derived as follows:

$$\begin{bmatrix} Y(d\theta/dX)^2 - \lambda \phi_0 \theta_d Y / \phi_d \\ Y(d\phi/dX)^2 - \lambda \phi_0 Y \end{bmatrix} = \begin{bmatrix} 0 \\ 0 \end{bmatrix} \quad \theta > \theta_d \quad (30a)$$

$$\begin{bmatrix} Y(d\theta/dX)^2 - \lambda \phi_0 \theta_d Y / \phi_d \\ Y(d\phi/dX)^2 - \lambda \phi_0 Y \end{bmatrix} = \begin{bmatrix} 0 \\ 0 \end{bmatrix} \quad \theta \leq \theta_d \quad (30b)$$

2.2.1 Optimum longitudinal fin for volume constraint

The variation of F with a function of L and L_0 yields the following expressions from Eq. (29):

$$\begin{bmatrix} \delta F \\ \delta F \end{bmatrix} = \begin{bmatrix} \frac{1}{\phi_0} \left\{ Y(d\phi/dX)^2 + (1+b\xi)\phi^2 - \lambda \phi_0 Y \right\} \delta X \\ \frac{\phi_d}{\theta_d \phi_0} \left\{ Y(d\theta/dX)^2 + \theta^2 - \lambda Y \phi_0 \theta_d / \phi_d \right\} \delta X \end{bmatrix} \Bigg|_{X=0}^{X=L_0} = \begin{bmatrix} 0 \\ 0 \end{bmatrix} \quad \theta \leq \theta_d \quad (31a)$$

$$\begin{bmatrix} \delta F \\ \delta F \end{bmatrix} = \begin{bmatrix} \frac{1}{\phi_0} \left\{ Y(d\phi/dX)^2 + (1+b\xi)\phi^2 - \lambda \phi_0 Y \right\} \delta X \\ \frac{\phi_d}{\theta_d \phi_0} \left\{ Y(d\theta/dX)^2 + \theta^2 - \lambda Y \phi_0 \theta_d / \phi_d \right\} \delta X \end{bmatrix} \Bigg|_{X=L_0}^L = \begin{bmatrix} 0 \\ 0 \end{bmatrix} \quad \theta > \theta_d \quad (31b)$$

At $X = 0$, the above term should vanish as $\delta X = 0$. At $X = L_0$ and $X = L$, δX is nonzero; thus, the location for both dry and wet surfaces coexist and the fin tip satisfies are the optimality conditions:

$$\begin{bmatrix} Y(d\theta/dX)^2 + \theta^2 - \lambda \theta_d \phi_0 Y / \phi_d \\ Y(d\phi/dX)^2 + (1+b\xi)\phi^2 - \lambda \phi_0 Y \end{bmatrix} = \begin{bmatrix} 0 \\ 0 \end{bmatrix} \quad \text{at } X = L_0 \quad (32a)$$

$$(32b)$$

and

$$Y(d\theta/dX)^2 + \theta^2 - \lambda \theta_d \phi_0 Y / \phi_d = 0 \quad \text{at } X = L \quad (33)$$

Combining Eqs. (4), (6b), (30), (32) and (33), the tip temperature vanishes. Using optimality criteria, the temperature distribution and fin profile can be expressed as

$$\theta = \begin{cases} 1 - (1 - \theta_d)X/L_0 & 0 \leq X \leq L_0 \\ \theta_d(L - X)/(L - L_0) & L_0 \leq X \leq L \end{cases} \quad (34a)$$

$$(34b)$$

and

$$Y = \frac{1}{2} \left[(L - L_0)^2 + \frac{(1 + b\xi)}{(1 - \theta_d)} \left\{ 2L_0\phi_0(L_0 - X) - (1 - \theta_d)(L_0^2 - X^2) \right\} \right] \quad \text{for } 0 \leq X \leq L_0 \quad (35a)$$

$$Y = \frac{1}{2}(L - X)^2 \quad \text{for } L_0 \leq X \leq L \quad (35b)$$

The length of the wet region L_0 can be determined by using an energy balance at that length where dry and wet sections live together.

$$L_0 = L(1 - \theta_d) \quad (36)$$

Here L is not a constraint. L can be obtained from Eqs. (27), (35) and (36). The optimum length and the maximum heat transfer rate through a fin can be written as

$$L_{opt} = \frac{(6U)^{1/3}}{\left[\theta_d^2(3 - 2\theta_d) + (1 + b\xi)(1 - \theta_d)^2(3\phi_0 + 2\theta_d - 2) \right]^{1/3}} \quad (37a)$$

and

$$Q_{opt} = \frac{\left[\theta_d^2 + (1 + b\xi)(2\phi_0 + \theta_d - 1)(1 - \theta_d) \right]^2 (6U)^{1/3}}{\left[\theta_d^2(3 - 2\theta_d) + (1 + b\xi)(1 - \theta_d)^2(3\phi_0 + 2\theta_d - 2) \right]^{1/3}} \quad (37b)$$

2.2.2 Optimum longitudinal fin for both length and volume constraints

The temperature distribution and fin profile can be determined by using Eqs. (4), (6) and (13):

$$\begin{bmatrix} \theta \\ \theta \end{bmatrix} = \begin{bmatrix} 1 - \alpha X \\ \theta_d - \alpha(X - L_0) \end{bmatrix} \quad \begin{array}{l} 0 \leq X \leq L_0 \\ L_0 \leq X \leq L \end{array} \quad (38a)$$

$$(38b)$$

and

$$Y = \frac{1}{2\alpha} \left[2(\theta_d + \alpha L_0)(L - L_0) - \alpha(L^2 - L_0^2) + (1 + b\xi) \left\{ 2\phi_0(L_0 - X) - \alpha(L_0^2 - X^2) \right\} \right] \quad (0 \leq X \leq L_0) \quad (39a)$$

$$Y = \frac{1}{2\alpha} \left[2(\theta_d + \alpha L_0)(L - X) - \alpha(L^2 - X^2) \right] \quad (L_0 \leq X \leq L) \quad (39b)$$

where

$$\alpha = \frac{3\theta_d(L^2 - L_0^2) + 3\phi_0(1 + b\xi)L_0^2}{6U + 2L_0^3(1 + b\xi) + 2L^3 - L_0(3L^2 - L_0^2) + 4(L^3 - L_0^3)} \quad (40)$$

and

$$L_0 = (1 - \theta_d)/\alpha \quad (41)$$

2.3 Fully wet annular fins

Figure 2a is drawn for a schematic representation of an optimum annular fin under condensation of saturated vapor on its surfaces. The energy equation for one-dimensional temperature distribution in fully wet annular fins can be written under steady state condition as

$$\frac{d}{dx} \left[y(r_i + x) \frac{dT}{dx} \right] = \frac{h}{k} (r_i + x) \left[(T - T_a) + h_m(\omega - \omega_a)h_{fg}/h \right] \quad (42)$$

Eq. (42) is made in dimensionless form by using Eqs. (2) and (3) as

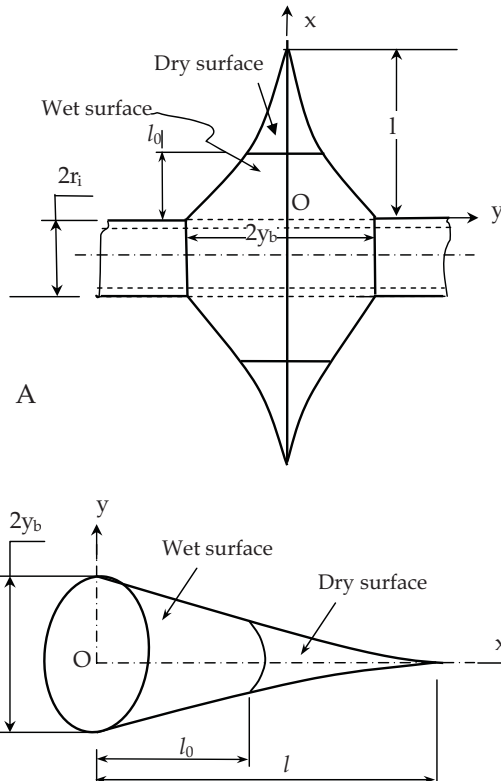


Fig. 2. Typical configuration of wet fins: A. Annular fin; and B. Spine

$$\frac{d}{dX} \left[Y(R_i + X) \frac{d\phi}{dX} \right] = (R_i + X)(1 + b\xi)\phi; \quad R_i = h r_i / k \quad (43)$$

The boundary conditions for annular fins for temperature distribution are considered same as taken longitudinal fins described in Eq. (6). The actual nondimensional heat transfer rate is calculated from the following formula:

$$Q = \frac{q(h/\pi)}{4k^2(T_a - T_b)} = - \left[Y(R_i + X) \frac{d\phi}{dX} \right]_{X=0} = \frac{1}{\phi_0} \int_{X=0}^L (R_i + X) \left[Y(d\phi/dX)^2 + (1 + b\xi)\phi^2 \right] dX \quad (44)$$

The fin volume in dimensionless form can be written as

$$U = \frac{V(h/k)^3}{4\pi^2} = \int_{X=0}^L (R_i + X) Y dX \quad (45)$$

For the application of variational principle, a function F can be constructed by using Lagrange multiplier λ in the followings :

$$F = Q - \lambda U = \frac{1}{\phi_0} \int_{X=0}^L (R_i + X) \left[Y(d\phi/dX)^2 + (1 + b\xi)\phi^2 - \lambda \phi_0 Y \right] dX \quad (46)$$

For maximizing value of F , Eq. (46) is differentiated with respect to Y and finally it becomes to zero.

$$\delta F = \frac{1}{\phi_0} \int_{X=0}^L Y^{-1} (R_i + X) \left[Y(d\phi/dX)^2 - \lambda \phi_0 Y \right] \delta Y dX = 0 \quad (47)$$

From Eq. (47), the following optimality condition for fully wet annular fins is obtained.

$$Y(d\phi/dX)^2 - \lambda \phi_0 Y = 0 \quad (48)$$

From the above optimality condition, it is to mention that the temperature gradient for fully wet annular fins is a constant and it does not depend upon the wetness condition of the fin.

2.3.1 Optimum annular fin for volume constraint

For volume constraint, fin length is variable. The variation of function F with length L is determined from this expression.

$$\delta F = \frac{(R_i + X)}{\phi_0} \left[Y(d\phi/dX)^2 + (1 + b\xi)\phi^2 - \lambda \phi_0 Y \right] \delta X \Big|_{X=0}^L = 0 \quad (49)$$

At $X = L$, the following optimality conditions are obtained:

$$Y(d\phi/dX)^2 + (1 + b\xi)\phi^2 - \lambda \phi_0 Y = 0 \quad (50)$$

Using Eqs. (6), (43), (48) and (50), the condition for temperature at the tip is $\phi = 0$. The thickness of fin profile at the tip is also zero. The temperature distribution and fin profile for the optimum annular fin for fully wet surface conditions is obtained from Eqs. (6), (43), (48) and optimum tip conditions as follows:

$$\theta = 1 - (1 + \theta_p) X / L \quad (51)$$

and

$$Y = \frac{(1 + b\xi)}{6(R_i + X)} \left[(L^3 - 3LX^2 + 2X^3) + 3R_i(L - X)^2 \right] \quad (52)$$

The optimum length and the maximum heat transfer rate through the fin can be determined as a function of design variables in the followings:

$$\begin{bmatrix} L_{opt} \\ Q_{opt} \end{bmatrix} = \begin{bmatrix} L_{opt}^4 + 2R_i L_{opt}^3 - 12U/(1 + b\xi) = 0 \\ \phi_0 L_{opt} (3R_i - L_{opt}) (1 + b\xi) / 6 \end{bmatrix} \quad (53)$$

$$(54)$$

The optimum length can be possible to calculate by a numerical technique. The Newton-Raphson method can be applied for the solution of Eq. (53) to determine the optimum fin length.

2.3.2 Optimum annular fin for both length and volume constraints

The temperature and fin profile for an optimum annular fin under length and volume constraints is determined from Eqs. (6), (43), (45) and (48) and they can be expressed as

$$\theta = 1 - \alpha X \quad (55)$$

and

$$Y = \frac{(1 + b\xi)}{6\alpha(R_i + X)} \left[6R_i \phi_0 (L - X) + 3(\phi_0 - \alpha R_i) (L^2 - X^2) - 2\alpha (L^3 - X^3) \right] \quad (56)$$

where

$$\alpha = \frac{2(3R_i + 2L)L^2(1 + b\xi)\phi_0}{12U + L^3(1 + b\xi)(4R_i + 3L)} \quad (57)$$

2.4 Partially wet annular fins

The energy equations for dry and wet regions in partially wet fins can be written separately in the followings:

$$\left[\frac{d}{dx} \left\{ y(r_i + x) \frac{dT}{dx} \right\} \right] = \left[\frac{h}{k} (r_i + x) (T - T_a) \right] \quad \text{dry domain } T > T_d \quad (58a)$$

$$\left[\frac{d}{dx} \left\{ y(r_i + x) \frac{dT}{dx} \right\} \right] = \left[\frac{h}{k} (r_i + x) \left\{ (T - T_a) + h_m (\omega - \omega_a) h_{fg} / h \right\} \right] \quad \text{wet domain } T \leq T_d \quad (58b)$$

Eq. (58) can be expressed in normalized form as

$$\left[\frac{d}{dX} \left\{ Y(R_i + X) \frac{d\theta}{dX} \right\} \right] = \begin{cases} (R_i + X)\theta & \theta > \theta_d \\ (R_i + X)(1 + b\xi)\phi & \theta \leq \theta_d \end{cases} \quad (59a)$$

$$\left[\frac{d}{dX} \left\{ Y(R_i + X) \frac{d\phi}{dX} \right\} \right] = \begin{cases} (R_i + X)(1 + b\xi)\phi & \theta > \theta_d \\ (R_i + X)\theta & \theta \leq \theta_d \end{cases} \quad (59b)$$

For solving Eq. (59), four boundary conditions are required and these are already written in Eq. (23). Heat transfer equation is obtained from Eq. (59) and boundary conditions in the followings:

$$\begin{aligned} Q = \frac{q(h/\pi)}{4k^2(T_a - T_b)} &= - \left[Y(R_i + X) \frac{d\phi}{dX} \right]_{X=0} = \frac{\phi_d}{\phi_0 \theta_d} \int_{X=L_0}^L (R_i + X) \left[Y \left(\frac{d\theta}{dX} \right)^2 + \theta^2 \right] dX \\ &+ \frac{1}{\phi_0} \int_{X=0}^{L_0} (R_i + X) \left[Y \left(\frac{d\phi}{dX} \right)^2 + (1 + b\xi)\phi^2 \right] dX \end{aligned} \quad (60)$$

The dimensionless fin volume for the partially wet fin can be formulated in the following:

$$U = \frac{V(h/k)^3}{4\pi} = \int_{X=0}^{L_0} (R_i + X) Y dX + \int_{X=L_0}^L (R_i + X) Y dX \quad (61)$$

To apply variational principle, a functional F is constructed by using heat transfer rate and fin volume expressions.

$$\begin{aligned} F = Q - \lambda U &= \frac{1}{\phi_0} \int_{X=0}^{L_0} (R_i + X) \left[Y \left(\frac{d\phi}{dX} \right)^2 + (1 + b\xi)\phi^2 - \lambda \phi_0 Y \right] dX \\ &+ \frac{\phi_d}{\phi_0 \theta_d} \int_{X=L_0}^L (R_i + X) \left[Y \left(\frac{d\theta}{dX} \right)^2 + \theta^2 - \lambda \phi_0 \theta_d Y / \phi_d \right] dX \end{aligned} \quad (62)$$

The optimality criterion can be derived by differentiating functional F with respect to Y and then equating to zero.

$$\begin{aligned} \delta F &= \frac{1}{\phi_0} \int_{X=0}^{L_0} Y^{-1} (R_i + X) \left[Y \left(\frac{d\phi}{dX} \right)^2 - \lambda \phi_0 Y \right] \delta Y dX \\ &+ \frac{\phi_d}{\phi_0 \theta_d} \int_{X=L_0}^L Y^{-1} (R_i + X) \left[Y \left(\frac{d\theta}{dX} \right)^2 - \lambda \phi_0 \theta_d Y / \phi_d \right] \delta Y dX = 0 \end{aligned} \quad (63)$$

Therefore from Eq. (63), the following optimality criterion is found:

$$\left[\begin{array}{l} \left(\frac{d\theta}{dX} \right)^2 - \lambda \phi_0 \theta_d / \phi_d \\ \left(\frac{d\phi}{dX} \right)^2 - \lambda \phi_0 \end{array} \right] = \begin{cases} [0] & \theta > \theta_d \\ [0] & \theta \leq \theta_d \end{cases} \quad (64a)$$

$$(64b)$$

2.4.1 Optimum annular fin for volume constraint

The following expression is obtained for variation of F with length L from Eq. (62)

$$\begin{bmatrix} \delta F \\ \delta F \end{bmatrix} = \begin{bmatrix} \frac{(R_i + X)}{\phi_0} \left\{ Y(d\phi/dX)^2 + (1 + b\xi)\phi^2 - \lambda \phi_0 Y \right\} \delta X \\ \frac{(R_i + X)\phi_d}{\theta_d \phi_0} \left\{ Y(d\theta/dX)^2 + \theta^2 - \lambda Y \phi_0 \theta_d / \phi_d \right\} \delta X \end{bmatrix} \Bigg|_{\substack{X=0 \\ X=L_0}} = \begin{bmatrix} 0 \\ 0 \end{bmatrix} \quad \begin{array}{l} \theta \leq \theta_d \\ \theta > \theta_d \end{array} \quad (65a) \quad (65b)$$

From Eq. (65), the following conditions are determined:

$$\begin{bmatrix} Y(d\theta/dX)^2 + \theta^2 - \lambda \theta_d \phi_0 Y / \phi_d \\ Y(d\phi/dX)^2 + (1 + b\xi)\phi^2 - \lambda \phi_0 Y \end{bmatrix} = \begin{bmatrix} 0 \\ 0 \end{bmatrix} \quad \text{at } X = L_0 \quad (66a)$$

$$\begin{bmatrix} Y(d\theta/dX)^2 + \theta^2 - \lambda \theta_d \phi_0 Y / \phi_d \\ Y(d\phi/dX)^2 + (1 + b\xi)\phi^2 - \lambda \phi_0 Y \end{bmatrix} = \begin{bmatrix} 0 \\ 0 \end{bmatrix} \quad (66b)$$

and

$$Y(d\theta/dX)^2 + \theta^2 - \lambda \theta_d \phi_0 Y / \phi_d = 0 \quad \text{at } X = L \quad (67)$$

From the above analysis, one can determine the dimensionless tip temperature and tip thickness, both are zero for the optimum design condition. The fin temperature and fin profile are obtained as follows:

$$\theta = \begin{cases} 1 - (1 - \theta_d)X/L_0 & 0 \leq X \leq L_0 \\ \theta_d(L - X)/(L - L_0) & L_0 \leq X \leq L \end{cases} \quad (68a)$$

$$(68b)$$

and

$$Y = \frac{1}{6(R_i + X)} \left[6LR_i(L - L_0) + 3(L - R_i)(L^2 - L_0^2) - 2(L^3 - L_0^3) \right. \\ \left. + \frac{(1 + b\xi)}{(1 - \theta_d)} \left\{ 6R_i L_0 \phi_0 (L_0 - X) + 3(\phi_0 L_0 - (1 - \theta_d)R_i)(L_0^2 - X^2) - 2(1 - \theta_d)(L_0^3 - X^3) \right\} \right] \quad (69a)$$

for $(0 \leq X \leq L_0)$

$$Y = \frac{1}{6(R_i + X)} \left[6LR_i(L - X) + 3(L - R_i)(L^2 - X^2) - 2(L^3 - X^3) \right] \quad \text{for } L_0 \leq X \leq L \quad (69b)$$

The length of the optimum annular fin can be determined from the following equation given below:

$$\begin{bmatrix} 2\theta_d^2(1 - \theta_d) + (1 + b\xi) \left\{ 4\phi_0 - 4\theta_d \phi_0 - 3(1 - \theta_d)^2 \right\} (1 - \theta_d)^2 + \theta_d^3(2 - \theta_d) \\ + \left[6\theta_d^2(1 - \theta_d) + 2(1 + b\xi)(3\phi_0 + 2\theta_d - 2)(1 - \theta_d)^2 + 2\theta_d^3 \right] R_i L^3 - 12U = 0 \end{bmatrix} L^4 \quad (70)$$

Eq. (70) can be solved numerically. The Newton-Raphson iterative method can be employed to determine the optimum length of the fin after satisfying the necessary convergence criterion. After estimating L_{opt} value, one can calculate the maximum or optimum actual heat transfer rate which can be determined from the expression give below:

$$Q_{opt} = \frac{L_{opt}}{6} \left[6R_i\theta_d + 3(L_{opt} - R_i) \left\{ 1 - (1 - \theta_d)^2 \right\} - 2L_{opt} \left\{ 1 - (1 - \theta_d)^3 \right\} + (1 - \theta_d)(1 + b\xi)L_{opt}^2 \left\{ 6R_i\phi_0 + 3(\phi_0 L_{opt} - R_i)(1 - \theta_d) - 2L_{opt}(1 - \theta_d)^2 \right\} \right] \quad (71)$$

2.4.2 Optimum annular fin for both length and volume constraints

The temperature distribution and fin profile for the annular fin can be determined by using Eqs. (6), (59), (61) and (64) as

$$\begin{bmatrix} \theta \\ \theta \end{bmatrix} = \begin{bmatrix} 1 - \alpha X \\ \theta_d - \alpha(X - L_0) \end{bmatrix} \quad \begin{array}{l} 0 \leq X \leq L_0 \\ L_0 \leq X \leq L \end{array} \quad (72a)$$

$$(72b)$$

and

$$Y = \frac{1}{6\alpha(R_i + X)} \left[6R_i(\theta_d + \alpha L_0)(L - L_0) + 3(\theta_d - \alpha R_i + \alpha L_0)(L^2 - L_0^2) - 2\alpha(L^3 - L_0^3) + (1 + b\xi) \left\{ 6\phi_0 R_i (L_0 - X) + 3(\phi_0 - \alpha R_i)(L_0^2 - X^2) - 2\alpha(L_0^3 - X^3) \right\} \right] \quad (0 \leq X \leq L_0) \quad (73a)$$

$$Y = \frac{1}{6\alpha(R_i + X)} \left[6(R_i\theta_d + \alpha R_i L_0)(L - X) + 3(\alpha L_0 - \alpha R_i + \theta_d)(L^2 - X^2) - 2\alpha(L^3 - X^3) \right] \quad (L_0 \leq X \leq L) \quad (73b)$$

where

$$\alpha = \frac{6R_i\theta_d(L^2 - L_0^2) + 2\phi_0(1 + b\xi)(3R_i + 2L_0)L_0^2 + 4\theta_d(L^3 - L_0^3)}{12U + L_0^3(1 + b\xi)(4R_i + 3L_0) - 2R_iL_0(3L^2 - L_0^2) + L^3(4R_i + 3L) - L_0(4L^3 - L_0^3)} \quad (74a)$$

and

$$L_0 = (1 - \theta_d)/\alpha \quad (74b)$$

Combining Eqs. (74a) and (74b), the following transcendental equation is obtained:

$$\begin{bmatrix} (1 + b\xi)(3 - 3\theta_d - 4\phi_0) + 3\theta_d + 1 \\ 12U + 4R_iL^3 + 3L^4 \end{bmatrix} L_0^4 + 2R_i \left[(1 - \theta_d)(3 + 2b\xi) - 3\phi_0(1 + b\xi) + 3\theta_d \right] L_0^3 - 2L^2L_0 + (1 - \theta_d)(12U + 4R_iL^3 + 3L^4) = 0 \quad (75)$$

In order to determine the wet length in the fin L_0 , Eq. (75) can be solved by using Newton-Raphson iterative technique.

2.5 Fully wet pin fins

A schematic diagram of a pin fin is shown in Fig. 2B. The energy equation for pin fins subject to condensation of vapor under fully wet condition is written below:

$$\frac{d}{dx} \left(y^2 \frac{dT}{dx} \right) = \frac{2h}{k} y \left[(T - T_a) + h_m (\omega - \omega_a) h_{fg} / h \right] \quad (76)$$

Eq. (76) is expressed in nondimensional form as

$$\frac{d}{dX} \left(Y^2 \frac{d\phi}{dX} \right) = 2Y(1 + b\xi)\phi \quad (77)$$

For the solution of Eq. (77), the boundary conditions expressed in Eq. (7) are taken. The actual heat transfer rate is calculated from the following expression:

$$Q = \frac{2q(h/\pi)}{2k^2(T_a - T_b)} = - \left[Y^2 \frac{d\phi}{dX} \right]_{X=0} = \frac{1}{\phi_0} \int_{X=0}^L Y \left[Y \left(\frac{d\phi}{dX} \right)^2 + 2(1 + b\xi)\phi^2 \right] dX \quad (78)$$

The fin volume of a pin fin is written in dimensionless form as

$$U = \frac{V(h/k)^3}{\pi} = \int_{X=0}^L Y^2 dX \quad (79)$$

For determination of the optimum shape, a functional F is defined as

$$F = Q - \lambda U = \frac{1}{\phi_0} \int_{X=0}^L Y \left[Y \left(\frac{d\phi}{dX} \right)^2 + 2(1 + b\xi)\phi^2 - \lambda \phi_0 Y \right] dX \quad (80)$$

The above equation gives a relationship between F and Y . The optimum condition can be obtained by differentiating functional F with respect to Y .

$$\delta F = \frac{1}{\phi_0} \int_{X=0}^L 2 \left[Y \left(\frac{d\phi}{dX} \right)^2 + (1 + b\xi)\phi^2 - \lambda \phi_0 Y \right] \delta Y dX = 0 \quad (81)$$

The following expression is obtained from Eq. (81).

$$Y \left(\frac{d\phi}{dX} \right)^2 + (1 + b\xi)\phi^2 - \lambda \phi_0 Y = 0 \quad (82)$$

Multiplying on both sides in Eq. (77) by $d\phi/dX$ yields the following expression after some manipulations:

$$d \left[Y^2 \left(\frac{d\phi}{dX} \right)^2 \right] / dX + \left(\frac{d\phi}{dX} \right)^2 d(Y^2) / dX = 2(1 + b\xi)Y \left(\frac{d\phi^2}{dX} \right) / dX \quad (83)$$

Eliminating ϕ^2 from Eq. (82) by using Eq. (83) and then integrating, the following expression is obtained.

$$3Y^2(d\phi/dX)^2 - \lambda\phi_0Y^2 = C \quad (84)$$

where, C is an integration constant determined by using boundary conditions.

2.5.1 Optimum fully wet pin fin for volume constraint

The variation of F with a function of L yields from Eq. (80) as

$$\delta F = \frac{Y}{\phi_0} \left[Y(d\phi/dX)^2 + 2(1+b\xi)\phi^2 - \lambda\phi_0Y \right] \delta X \bigg|_{X=0}^L = 0 \quad (85)$$

As δX is nonzero at $X = L$, the following tip condition can be achieved :

$$Y(d\phi/dX)^2 + 2(1+b\xi)\phi^2 - \lambda\phi_0Y = 0 \quad (86)$$

From Eqs. (6), (77), (82) and (86) the dimensionless temperature ϕ at the tip vanishes and it can be indicated that the same condition is obtained in the case of longitudinal and annular fins with fully wet condition. Using Eqs. (6), (77), (82) and (86), temperature distribution and fin profile for the optimum fin can be written as

$$\theta = 1 - (1 + \theta_p)X/L \quad (87a)$$

and

$$Y = \frac{(1+b\xi)(L-X)^2}{2} \quad (87b)$$

The optimum fin length and heat transfer rate are determined as follows:

$$\begin{bmatrix} L_{opt} \\ Q_{max} \end{bmatrix} = \begin{bmatrix} \left\{ 20U/(1+b\xi)^2 \right\}^{1/5} \\ \phi_0 \left\{ 125U^3(1+b\xi)^4/8 \right\}^{1/5} \end{bmatrix} \quad (88a)$$

$$(88b)$$

2.5.2 Optimum fully wet pin fin for both length and volume constraints

The temperature distribution and fin profile can be found from Eqs. (6), (77) and (84) as

$$\phi = \phi_0 \sqrt{Y_b(Y_t^2 Y^{-1} + 2Y) / (Y_t^2 + 2Y_b^2)}, \quad Y_t \leq Y \leq Y_b \quad (89)$$

and

$$\int_{Y_t}^Y \frac{(2Y^2 - Y_t^2) dY}{\sqrt{(Y^2 - Y_t^2)(Y_t^2 + 2Y^2)} Y} = 2\sqrt{(1+b\xi)} (L-X) \quad (90)$$

In order to determine the temperature profile and fin profile from the above two equations, the unknown variables Y_t and Y_b are required to calculate apriori. These can be determined by constructing two constraint equations as follows:

$$U = \int_{Y=Y_t}^{Y_b} \frac{(2Y^2 - Y_t^2)Y^2 dY}{2\sqrt{(1+b\xi)} \sqrt{(Y^2 - Y_t^2)(Y_t^2 + 2Y^2)} Y} \quad (91a)$$

and

$$\int_{Y=Y_t}^{Y_b} \frac{(2Y^2 - Y_t^2)dY}{\sqrt{(Y^2 - Y_t^2)(Y_t^2 + 2Y^2)} Y} = 2\sqrt{(1+b\xi)} L \quad (91b)$$

A simultaneous solution of Eqs. (91a) and (91b) is provided to get the fin thickness at the base and tip. The above all integration can be performed by Simson's 1/3 rule.

2.6 Partially wet pin fins

The energy equations for partially wet pin fins are written as

$$\left[\frac{d}{dx} \left(y^2 \frac{dT}{dx} \right) \right] = \left[\frac{2h}{k} y (T - T_a) \right] \quad \text{for dry domain } T > T_d \quad (92a)$$

$$\left[\frac{d}{dx} \left(y^2 \frac{dT}{dx} \right) \right] = \left[\frac{2h}{k} y \left\{ (T - T_a) + h_m (\omega - \omega_a) h_{fg} / h \right\} \right] \quad \text{for wet domain } T \leq T_d \quad (92b)$$

Eq. (92) can be expressed in dimensionless form as

$$\left[\frac{d}{dX} \left(Y^2 \frac{d\theta}{dX} \right) \right] = \left[\begin{array}{ll} 2Y\theta & \text{dry domain } \theta > \theta_d \\ 2Y(1+b\xi)\phi & \text{wet domain } \theta \leq \theta_d \end{array} \right] \quad (93a)$$

$$(93b)$$

Boundary conditions are required to solve Eq. (93) which can be taken as longitudinal fins expressed in Eq. (23). The actual heat transfer rate is calculated from the following equation:

$$Q = \frac{q(h/\pi)}{k^2(T_a - T_b)} = - \left[Y^2 \frac{d\phi}{dX} \right]_{X=0} = \frac{\phi_d}{\phi_0 \theta_d} \int_{X=L_0}^L Y \left[Y \left(\frac{d\theta}{dX} \right)^2 + 2\theta^2 \right] dX \quad (94)$$

$$+ \frac{1}{\phi_0} \int_{X=0}^{L_0} Y \left[Y \left(\frac{d\phi}{dX} \right)^2 + 2(1+b\xi)\phi^2 \right] dX$$

The fin volume for a partially wet pin fin is written in an integral form as

$$U = \frac{V(h/k)^3}{\pi} = \int_{X=0}^{L_0} Y^2 dX + \int_{X=L_0}^L Y^2 dX \quad (95)$$

For the application of variational method, a functional F is constructed from heat transfer rate and fin volume expressions:

$$F = Q - \lambda U = \frac{1}{\phi_0} \int_{X=0}^{L_0} Y \left[Y \left(\frac{d\phi}{dX} \right)^2 + 2(1+b\xi)\phi^2 - \lambda \phi_0 Y \right] dX + \frac{\phi_d}{\phi_0 \theta_d} \int_{X=L_0}^L Y \left[Y \left(\frac{d\theta}{dX} \right)^2 + \theta^2 - \lambda \phi_0 \theta_d Y / \phi_d \right] dX \quad (96)$$

For maximizing value of F condition, the following expression is obtained:

$$\delta F = \frac{1}{\phi_0} \int_{X=0}^{L_0} \left[Y \left(\frac{d\phi}{dX} \right)^2 + (1+b\xi)\phi^2 - \lambda \phi_0 Y \right] \delta Y dX + \frac{\phi_d}{\phi_0 \theta_d} \int_{X=L_0}^L \left[Y \left(\frac{d\theta}{dX} \right)^2 + \theta^2 - \lambda \phi_0 \theta_d Y / \phi_d \right] \delta Y dX = 0 \quad (97)$$

Therefore, from Eq. (97), the following optimality criterion is derived:

$$\begin{bmatrix} Y \left(\frac{d\theta}{dX} \right)^2 + \theta^2 - \lambda \phi_0 \theta_d Y / \phi_d \\ Y \left(\frac{d\phi}{dX} \right)^2 + (1+b\xi)\phi^2 - \lambda \phi_0 Y \end{bmatrix} = \begin{bmatrix} 0 \\ 0 \end{bmatrix} \quad \theta > \theta_d \quad (98a)$$

$$\begin{bmatrix} Y \left(\frac{d\theta}{dX} \right)^2 + \theta^2 - \lambda \phi_0 \theta_d Y / \phi_d \\ Y \left(\frac{d\phi}{dX} \right)^2 + (1+b\xi)\phi^2 - \lambda \phi_0 Y \end{bmatrix} = \begin{bmatrix} 0 \\ 0 \end{bmatrix} \quad \theta \leq \theta_d \quad (98b)$$

The following expressions is obtained from Eq. (93) after multiplying on both sides of Eqs. (93a) and (93b) by $d\theta/dX$ and $d\phi/dX$, respectively.

$$\begin{bmatrix} d \left\{ Y^2 \left(\frac{d\theta}{dX} \right)^2 \right\} / dX + \left(\frac{d\theta}{dX} \right)^2 d(Y^2) / dX \\ d \left\{ Y^2 \left(\frac{d\phi}{dX} \right)^2 \right\} / dX + \left(\frac{d\phi}{dX} \right)^2 d(Y^2) / dX \end{bmatrix} = \begin{bmatrix} 2 Y d \left(\theta^2 \right) / dX \\ 2 (1+b\xi) Y d \left(\phi^2 \right) / dX \end{bmatrix} \quad \theta > \theta_d \quad (99a)$$

$$\begin{bmatrix} d \left\{ Y^2 \left(\frac{d\theta}{dX} \right)^2 \right\} / dX + \left(\frac{d\theta}{dX} \right)^2 d(Y^2) / dX \\ d \left\{ Y^2 \left(\frac{d\phi}{dX} \right)^2 \right\} / dX + \left(\frac{d\phi}{dX} \right)^2 d(Y^2) / dX \end{bmatrix} = \begin{bmatrix} 2 (1+b\xi) Y d \left(\phi^2 \right) / dX \\ 2 Y d \left(\theta^2 \right) / dX \end{bmatrix} \quad \theta \leq \theta_d \quad (99b)$$

Elminating θ^2 and ϕ^2 from Eq. (99) with the help of Eq. (98), the following equations are obtained:

$$\begin{bmatrix} 3Y^2 \left(\frac{d\theta}{dX} \right)^2 - \lambda \phi_0 \theta_d Y^2 / \phi_d \\ 3Y^2 \left(\frac{d\phi}{dX} \right)^2 - \lambda \phi_0 Y^2 \end{bmatrix} = \begin{bmatrix} C_1 \\ C_2 \end{bmatrix} \quad \theta > \theta_d \quad (100a)$$

$$\begin{bmatrix} 3Y^2 \left(\frac{d\theta}{dX} \right)^2 - \lambda \phi_0 \theta_d Y^2 / \phi_d \\ 3Y^2 \left(\frac{d\phi}{dX} \right)^2 - \lambda \phi_0 Y^2 \end{bmatrix} = \begin{bmatrix} C_1 \\ C_2 \end{bmatrix} \quad \theta \leq \theta_d \quad (100b)$$

The integration constants C_1 and C_2 are determined from the boundary conditions.

2.6.1 Optimum partially wet pin fin for volume constraint only

The variation of functional F with length parameter L for partially wet pin fins is given below:

$$\begin{bmatrix} \delta F \\ \delta F \end{bmatrix} = \begin{bmatrix} \frac{Y}{\phi_0} \left\{ Y \left(\frac{d\phi}{dX} \right)^2 + 2(1+b\xi)\phi^2 - \lambda \phi_0 Y \right\} \delta X \\ \frac{Y\phi_d}{\theta_d \phi_0} \left\{ Y \left(\frac{d\theta}{dX} \right)^2 + \theta^2 - \lambda \phi_0 \theta_d Y / \phi_d \right\} \delta X \end{bmatrix} \Bigg|_{X=0}^{X=L_0} = \begin{bmatrix} 0 \\ 0 \end{bmatrix} \quad \theta \leq \theta_d \quad (101a)$$

$$\begin{bmatrix} \delta F \\ \delta F \end{bmatrix} = \begin{bmatrix} \frac{Y}{\phi_0} \left\{ Y \left(\frac{d\phi}{dX} \right)^2 + 2(1+b\xi)\phi^2 - \lambda \phi_0 Y \right\} \delta X \\ \frac{Y\phi_d}{\theta_d \phi_0} \left\{ Y \left(\frac{d\theta}{dX} \right)^2 + \theta^2 - \lambda \phi_0 \theta_d Y / \phi_d \right\} \delta X \end{bmatrix} \Bigg|_{X=L_0}^L = \begin{bmatrix} 0 \\ 0 \end{bmatrix} \quad \theta > \theta_d \quad (101b)$$

For $X=0$, the above terms vanish as $\delta X=0$. For $X=L_0$ and $X=L$, δX is not zero; therefore, the location where dry and wet surfaces present, and the tip, the following optimality conditions are achieved:

$$\begin{bmatrix} Y(d\theta/dX)^2 + 2\theta^2 - \lambda\theta_d\phi_0Y/\phi_d \\ Y(d\phi/dX)^2 + 2(1+b\xi)\phi^2 - \lambda\phi_0Y \end{bmatrix} = \begin{bmatrix} 0 \\ 0 \end{bmatrix} \quad \text{at } X = L_0 \quad (102a)$$

$$Y(d\theta/dX)^2 + 2\theta^2 - \lambda\theta_d\phi_0Y/\phi_d = 0 \quad \text{at } X = L \quad (102b)$$

$$Y(d\phi/dX)^2 + 2(1+b\xi)\phi^2 - \lambda\phi_0Y = 0 \quad \text{at } X = L \quad (102c)$$

The temperature distribution and fin profile for an optimum pin fin for volume constraint only are same with that of the longitudinal fin. The fin length and heat transfer rate for the optimum profile fin is obtained from the following equations :

$$L_{opt} = \frac{(60U)^{1/5}}{\left[3\theta_d^4(5-2\theta_d) + Z_1 \left\{ Z_2 + 10\theta_d^2 + 1 \right\} (3\phi_0 + 2\theta_d - 2) \right]^{1/5}} \quad (103a)$$

$$Q_{opt} = \frac{\left[\theta_d^2 + (1+b\xi)(2\phi_0 + \theta_d - 1)(1-\theta_d) \right]^2 (60U)^{3/5}}{\left[3\theta_d^4(5-2\theta_d) + Z_1 \left\{ Z_2 + 10\theta_d^2 + 1 \right\} (3\phi_0 + 2\theta_d - 2) \right]^{3/5}} \quad (103b)$$

where

$$Z_1 = (1+b\xi)(1-\theta_d)^2 \quad (104a)$$

$$Z_2 = (1-\theta_d)(1+b\xi) \left\{ 5(2\phi_0 + \theta_d - 1)(5-6\phi_0 - 2\theta_d) + 5\phi_0(4\phi_0 + 3\theta_d - 3) + 3(1-\theta_d)^2 \right\} \quad (104b)$$

2.6.2 Optimum partially wet pin fin for both length and volume constraints

The temperature distribution and fin profile can be found from Eqs. (6), (93), (95) and (100) for the partially wet conditions as follows:

$$\phi = \phi_0 \sqrt{\frac{Y_b}{Y} \left[\frac{2\phi_d Y^2 + (\phi_d - \theta_d)Y_0^2 + \theta_d Y_t^2}{2\phi_d Y_b^2 + (\phi_d - \theta_d)Y_0^2 + \theta_d Y_t^2} \right]}, \quad Y_0 \leq Y \leq Y_b \quad (105a)$$

$$\theta = \theta_d \sqrt{Y_0 \left(Y_t^2 Y^{-1} + 2Y \right) / \left(Y_t^2 + 2Y_0^2 \right)}, \quad Y_0 \leq Y \leq Y_t \quad (105b)$$

and

$$\int_{Y_0}^Y \frac{(2Y^2 - Y_0^2) dY}{\sqrt{(Y^2 - Y_0^2)(Y_0^2 + 2Y^2)Y}} = 2\sqrt{(1+b\xi)} (L_0 - X) \quad (106a)$$

$$\int_{Y_t}^Y \frac{(2Y^2 - Y_t^2)dY}{\sqrt{(Y^2 - Y_t^2)(Y_t^2 + 2Y^2)}Y} = 2(L - X) \quad (106b)$$

From the above equations for obtaining temperature distribution and fin profile, it is worthy to mention that the design variables Y_0 , Y_t , Y_b and L_0 are required to determine first. The Y_t and Y_b can be determined from the constraint equations taken in the design as

$$U = \int_{Y=Y_0}^{Y_t} \frac{(2Y^2 - Y_0^2)Y^2 dY}{2\sqrt{(1+b\xi)}\sqrt{(Y^2 - Y_0^2)(Y_0^2 + 2Y^2)}Y} + \int_{Y=Y_t}^{Y_b} \frac{(2Y^2 - Y_t^2)Y^2 dY}{2\sqrt{(Y^2 - Y_t^2)(Y_t^2 + 2Y^2)}Y} \quad (107a)$$

$$\int_{Y=Y_0}^{Y_b} \frac{(2Y^2 - Y_0^2)dY}{\sqrt{(Y^2 - Y_0^2)(Y_0^2 + 2Y^2)}Y} + \int_{Y=Y_t}^{Y_0} \frac{(2Y^2 - Y_t^2)dY}{\sqrt{(Y^2 - Y_t^2)(Y_t^2 + 2Y^2)}Y} = 2\sqrt{(1+b\xi)}L_0 + 2(L - L_0) \quad (107b)$$

The parameters L_0 and Y_0 are determined from the dewpoint temperature section where dry and wet part coexist and one can take the continuity of temperature and heat conduction at this section.

3. Results and discussion

The humid air is a mixture of dry air and water vapor. Three properties of air are used to calculate a thermodynamic state point to show the influence of dehumidification of air on the optimizing shape of three common type of fins, namely, Longitudinal, annular and pin fins. The air properties such as pressure, temperature, and relative humidity of air are used to determine a psychrometric state. The effect of the psychrometric properties of air on the optimization study is investigated. Two constraints, namely, fin volume, and both fin volume and length have been adopted to furnish the result for any designed application.

Fig. 3 is depicted the profile shape and temperature distribution in an optimum fin under different surface conditions as a function of fin length for a constraint fin volume. For the dry surface fin, the optimum fin shape can be determined from the fully wet fin analysis presented above by taking zero value of latent heat parameter ξ . To make a comparison between dry and wet surface fins, the results for the dry surface fin has been plotted in the same figure. From the figure, it can be noticeable that the temperature distribution in the fin at an optimum condition under dry, partially wet, and fully wet surfaces varies linearly (Fig. 3A). For the same fin base temperature for all the surface conditions adopted here, temperature on the fin surface of wet fins differs from that of the dry surface fin and the difference increases gradually from the fin base to fin tip. The discrepancy in temperature occurs due to evolving of latent heat of condensation of moisture on the fin surface in the case of wet fins. This difference in temperature becomes maximum for the 100% relative humidity of air as the maximum value of latent heat released for this relative humidity. From the analysis, it can be highlighted that for the dry and partially wet fin at an optimum condition, the tip temperature equalizes to the ambient temperature. However, for fully wet fin, the tip temperature is slightly less than the ambient value. Figure 3B is illustrated the optimum fin profile for dry, partially wet and fully wet conditions. For the dry fin, the optimum length and

optimum base thickness are larger and smaller, respectively than that for the any wet fin for the same fin volume and the difference is maximum for the fully wet fin of 100% relative humidity of air. Nevertheless, the effect of relative humidity on the optimum fin profile for a wet fin is marginal. The same trend for temperature distribution and the optimum fin profile of the annular and pin fins, are found and they are displayed in Figs. 4 and 5, respectively. In the case of annular fins, it can be mentioned that the optimum temperature distribution and fin profile are also function of the tube outer radius parameter R_i .

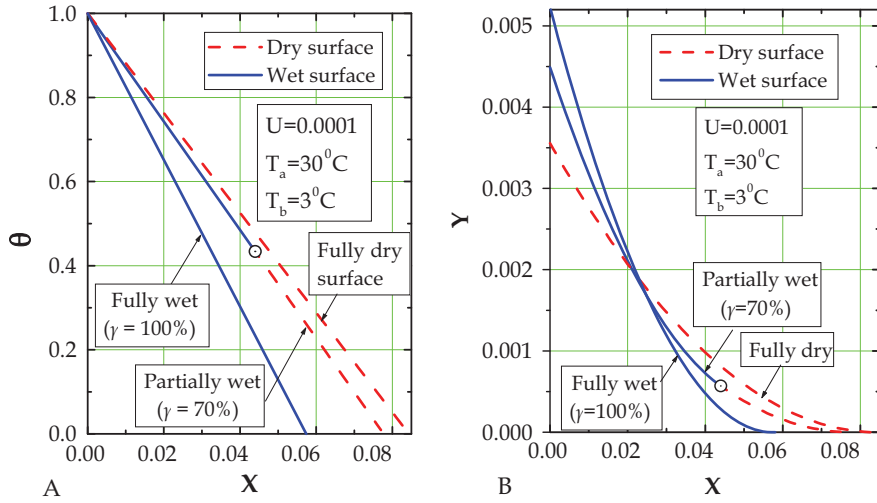


Fig. 3. Variation of temperature distribution and fin profile of an optimum longitudinal fin for the different surface conditions under a volume constraint: A. fin temperature; and B. fin profile

With satisfying either maximizing heat transfer rate for a given fin volume or minimizing fin volume for a given heat transfer duty, the optimization of any fin is studied. Depending upon the requirement of design, any one of these two constraints is used but they give the same result. The optimum profile shape is determined from the solution of the optimality criteria of the fin design and the constraint condition taken. The result from the optimization study of wet fins is depicted in Figs. 6, 7 and 8 as a function of fin volume for longitudinal, annular and spine, respectively. The optimum result for the dry surface condition of each fin, in comparison, is plotted in the corresponding figure. From these illustrations, it is understandable that the optimum parameters, namely, heat transfer rate, fin length, and fin thickness at the base, enhance continually with the fin volume. The maximum rate of heat transfer is not only as a function of the fin material but also as a function of the condition of the surface. A fully wet surface with 100% relative humidity predicts a maximum optimum heat transfer rate per unit volume in comparison with that transferred by any other surfaces. A partially wet surface transfers a less amount of heat per unit volume in comparison to that by fully wet surface fin and heat transfer rate decreases gradually with the decremented relative humidity. A dry surface fin at an optimum condition transfers least amount of heat per unit fin volume in comparison with the wet surface fin. This is happen due to latent heat evolved in wet fin heat transfer mechanism. For a lower value of fin volume, difference in heat transfer among fully wet, partially wet and dry surfaces may not so much important

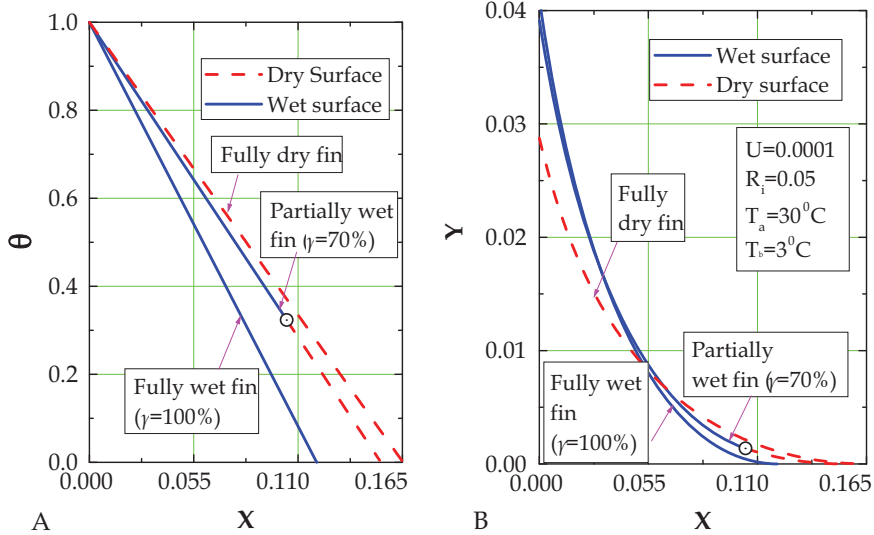


Fig. 4. Variation of temperature distribution and fin profile of an optimum annular fin for the different surface conditions for a volume constraint: A. fin temperature; and B. fin profile.

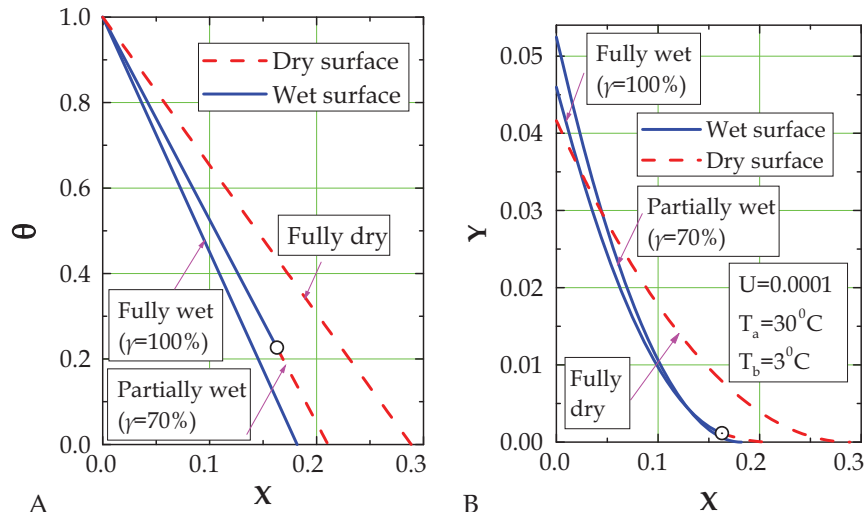


Fig. 5. Variation of temperature distribution and fin profile of an optimum spine for the different surface conditions under a volume constraint: A. fin temperature; and B. fin profile

than that for a higher value of fin volume as shown in Fig. 6A. Irrespective of any surface condition, the length and fin thickness at the base of an optimum fin increases with the fin volume. The optimum fin length for fully wet fins is always shorter than that for the partially wet as well as dry fins. The optimum length is a maximum for the dry surface condition under the same fin volume (Fig. 6B). Nevertheless, an opposite trend is noticed for

the variation of fin thickness at the base with the fin volume in comparison with the variation of fin length with volume for different surface condition as shown in Fig. 6C. A similar exercise has been made for the annular fin and spine by plotting Figs. 7 and 8. In the case of annular fin, the above parameters also function of the thermogeometric parameter R_i . With the increase in R_i , the optimum heat transfer rate increases as well as the optimum length and optimum base thickness decreases, separately with the same fin volume.

From the above optimum results, it can be emphasized to highlight that the optimum fin shape obtained from an optimization technique with the consideration of only one constraint either fin volume or heat transfer rate, is a complex in nature and fragile shape at the tip as already shown in Fig. 3 and hence, it is difficult surely in manufacturing process. To overcome this problem and to restrict the length of the fin, fin length can be taken as an additional constraint with the fin volume. In this case, the shape of the fin profile and fragile

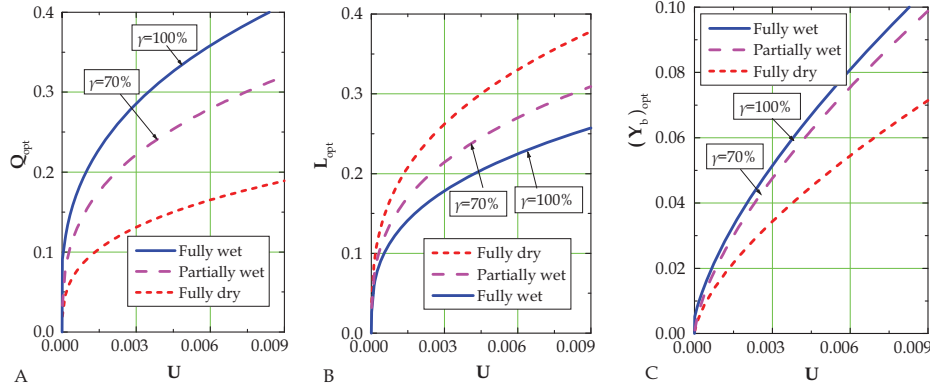


Fig. 6. Design parameters of an optimum longitudinal fin as a function of fin volume: A. maximum heat transfer rate; B. optimum length; and C. optimum semi-fin thickness at the base

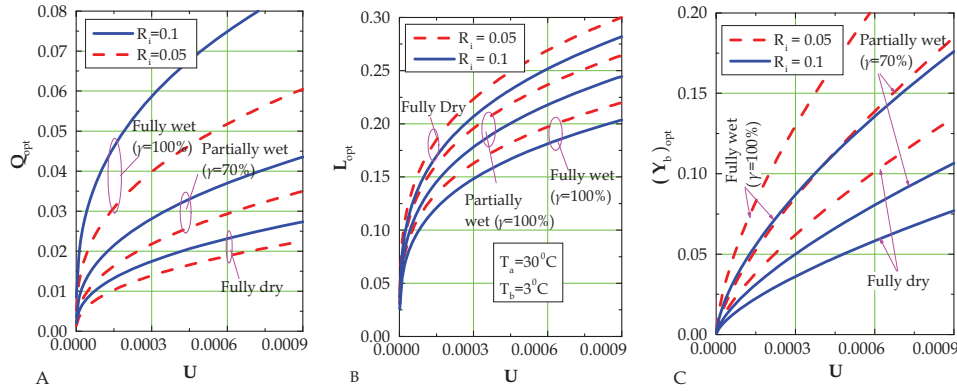


Fig. 7. Design parameters of an optimum annular fin as a function of fin volume: A. maximum heat transfer rate; B. optimum length; and C. optimum semi-fin thickness at the base

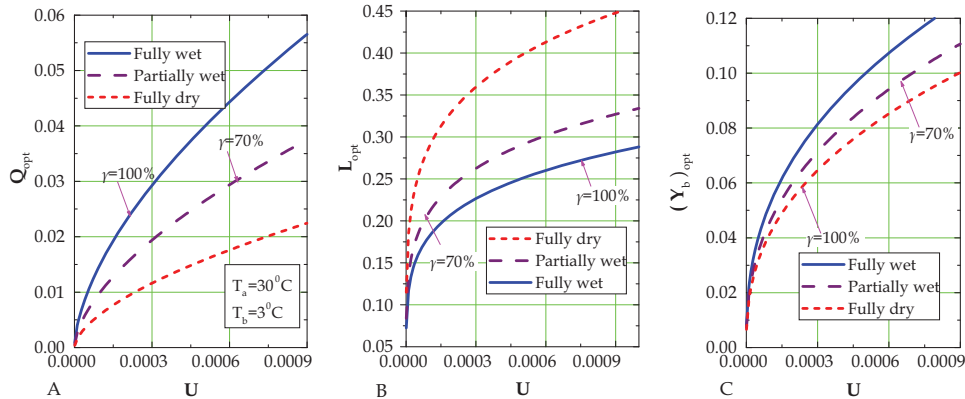


Fig. 8. Design parameters of an optimum pin fin as a function of fin volume: A. maximum heat transfer rate; B. optimum length; and C. optimum fin thickness at the base

geometry at the tip can be improved significantly. To avoid the same nature of the result, the optimum result under both volume and length constraint is illustrated only for the longitudinal fin. The variation of temperature and fin profile is determined under the aforementioned constraint, which is displayed in Fig. 9. From the temperature distribution, it can be mentioned that temperature at the tip of an optimum fin does not vanish and depends upon the magnitude of constraints chosen. For a fully wet surface, temperature at the tip may be closer to the ambient value in comparison with that for the partially and dry surface conditions. With the increase in relative humidity of air, condensation of moisture increases and as a result fin surface temperature increases. This observation can be found in Fig. 9A. The profile shape under both volume and length constraints for various surface conditions is illustrated as a function of dimensionless fin length shown in Fig. 9B. From this figure, it is clear that the profile shape is improved significantly with respect to a profile obtained from only volume constraint chosen, with the consideration of a suitable compatibility in the manufacturing technique. However, there is slightly different in shape between dry and wet surface optimum fin profiles under the same design constants.

4. Conclusions

The fin surface may be dry, fully wet or partially wet depending upon the psychometric conditions of the surrounding air participated as well as the constraints taken in the design. Owing to mass transfer occurred with the heat transfer mechanism, the wet surface fin differs from that of dry surface fin. The optimum-envelop shape of wet fins is different with respect to that of dry surface fins. This deviation may be increased with the increase in relative humidity of air. In this chapter, the optimum profile shape of different fins, namely, longitudinal, spine and annular are evaluated for dry, fully wet, and partially wet surface conditions using variational principle. The analysis has also included for different constraint conditions, namely, fin volume and both fin length and fin volume presented for possible requirements of an optimum design. From the results, the optimum design variable for wet fins is not only function of the design constraints but also is a function of psychometric properties of air. Unlike dry and partially wet surface fins, tip temperature for the fully wet

optimum fins under the volume constraint is less than the surrounding temperature. A significant change in optimum design variables has been noticed with the design constants such as fin volume and surface conditions. In order to reduce the complexity of the optimum profile fins under different surface conditions, the constraint fin length can be selected suitably with the constraint fin volume.

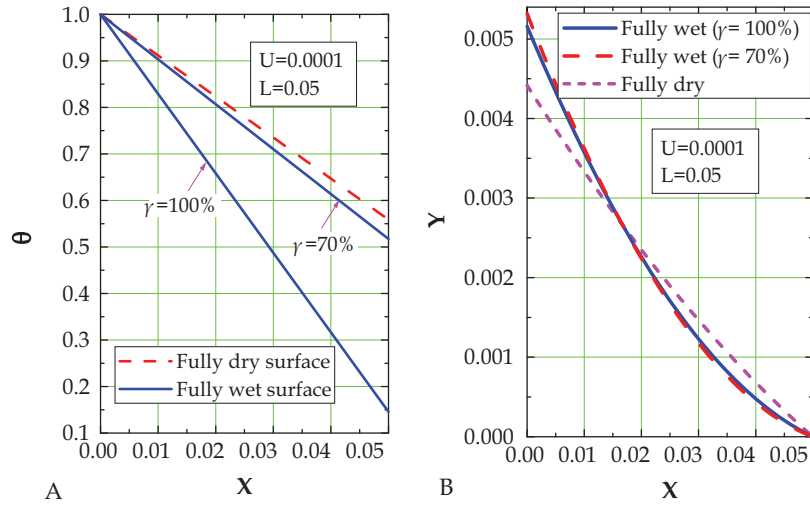


Fig. 9. Variation of temperature and fin profile in a longitudinal fin as a function of length for both volume and length constraints: A. Temperature distribution; and B. Fin profile

5. Acknowledgement

The authors would like to thank King Mongkut's University of Technology Thonburi (KMUTT), the Thailand Research Fund, the Office of Higher Education Commission and the National Research University Project for the financial support.

6. Nomenclatures

a	constant determined from the conditions of humid air at the fin base and fin tip
b	slop of a saturation line in the psychometric chart, K^{-1}
C	non-dimensional integration constant used in Eq. (84)
C_p	specific heat of humid air, $J \text{ kg}^{-1} \text{ K}^{-1}$
F	functional defined in Eqs. (10), (28), (46), (62), (80) and (96)
h	convective heat transfer coefficient, $\text{W m}^{-2} \text{K}^{-1}$
h_m	mass transfer coefficient, $\text{kg m}^{-2} \text{ S}^{-1}$
h_{fg}	latent heat of condensation, J kg^{-1}
k	thermal conductivity of the fin material, $\text{W m}^{-1} \text{K}^{-1}$
l	fin length, m

l_0	wet length in partially wet fins, m
L	dimensionless fin length, hl/k
L_0	dimensionless wet length in partially wet fins, hl_0/k
Le	Lewis number
q	heat transfer rate through a fin, W
Q	dimensionless heat transfer rate
r_i	base radius for annular fins, m
R_i	dimensionless base radius, hr_i/k
T	temperature, K
U	dimensionless fin volume, see Eqs. (9), (27), (45), (61), (79), (91a) and (95)
V	fin volume (volume per unit width for longitudinal fins), m ³
x, y	coordinates, see Figs. 1 and 2, m
X, Y	dimensionless coordinates, hx/k and hy/k , respectively
y_0	semi-thickness of a fin at which dry and wet parts separated, m
Y_0	dimensionless thickness, hy_0/k
Z_1, Z_2	dimensionless parameters defined in Eqs. (104a) and (104b), respectively

Greek Letters

α	parameter defined in Eqs. (20), (40), (57) and (74a)
λ	Lagrange multiplier
ω	specific humidity of air, kg w. v. / kg. d. a.
ξ	Latent heat parameter
ϕ	dimensionless temperature, $\theta + \theta_p$
ϕ_0	dimensionless temperature at the fin base, $1 + \theta_p$
θ	dimensionless fin temperature, $(T_a - T)/(T_a - T_b)$
θ_p	dimensionless temperature parameter, see Eq. (5)
γ	Relative humidity

Subscripts

a	ambient
b	base
d	dewpoint
opt	optimum
t	tip

7. References

Chilton, T.H. & Colburn, A.P. (1934). Mass transfer (absorption) coefficients—prediction from data on heat transfer and fluid friction. *Ind. Eng. Chem.*, Vol. 26, 1183.

Duffin, R. J. (1959). A variational problem relating to cooling fins with heat generation. *Q. Appl. Math.*, Vol. 10, 19-29.

Guceri, S. & Maday, C. J. (1975). A least weight circular cooling fin. *ASME J. Eng. Ind.*, Vol. 97, 1190-1193.

Hanin, L. & Campo, A. (2003). A new minimum volume straight cooling fin taking into account the length of arc. *Int. J. Heat Mass Transfer*, Vol. 46, 5145-5152.

Hong, K. T. & Webb, R. L. (1996). Calculation of fin efficiency for wet and dry fins. *HVAC&R Research*, Vol. 2, 27-40.

Kundu, B. & Das, P.K. (1998). Profiles for optimum thin fins of different geometry - A unified approach. *J. Institution Engineers (India): Mechanical Engineering Division*, Vol. 78, No. 4, 215-218.

Kundu, B. (2002). Analytical study of the effect of dehumidification of air on the performance and optimization of straight tapered fins. *Int. Comm. Heat Mass Transfer*, Vol. 29, 269-278.

Kundu, B. & Das, P.K. (2004). Performance and optimization analysis of straight taper fins with simultaneous heat and mass transfer. *ASME J. Heat Transfer*, Vol. 126, 862-868.

Kundu, B. & Das, P. K. (2005). Optimum profile of thin fins with volumetric heat generation: a unified approach. *J. Heat Transfer*, Vol. 127, 945-948.

Kundu, B. (2007a). Performance and optimization analysis of SRC profile fins subject to simultaneous heat and mass transfer. *Int. J. Heat Mass Transfer*, Vol. 50, 1645-1655.

Kundu, B. (2007b). Performance and optimum design analysis of longitudinal and pin fins with simultaneous heat and mass transfer: Unified and comparative investigations. *Applied Thermal Engg.*, Vol. 27, Nos. 5-6, 976-987.

Kundu, B. (2008). Optimization of fins under wet conditions using variational principle. *J. Thermophysics Heat Transfer*, Vol. 22, No. 4, 604-616.

Kundu, B., Barman, D. & Debnath, S. (2008). An analytical approach for predicting fin performance of triangular fins subject to simultaneous heat and mass transfer, *Int. J. Refrigeration*, Vol. 31, No. 6, 1113-1120.

Kundu, B. (2009a). Analysis of thermal performance and optimization of concentric circular fins under dehumidifying conditions, *Int. J. Heat Mass Transfer*, Vol. 52, 2646-2659.

Kundu, B. (2009b). Approximate analytic solution for performances of wet fins with a polynomial relationship between humidity ratio and temperature, *Int. J. Thermal Sciences*, Vol. 48, No. 11, 2108-2118.

Kundu, B. & Miyara, A. (2009). An analytical method for determination of the performance of a fin assembly under dehumidifying conditions: A comparative study, *Int. J. Refrigeration*, Vol. 32, No. 2, 369-380.

Kundu, B. (2010). A new methodology for determination of an optimum fin shape under dehumidifying conditions. *Int. J. Refrigeration*, Vol. 33, No. 6, 1105-1117.

Kundu, B. & Barman, D. (2010). Analytical study on design analysis of annular fins under dehumidifying conditions with a polynomial relationship between humidity ratio and saturation temperature, *Int. J. Heat Fluid Flow*, Vol. 31, No. 4, 722-733.

Liu, C. Y. (1961). A variational problem relating to cooling fins with heat generation. *Q. Appl. Math.*, Vol. 19, 245-251.

Liu, C. Y. (1962). A variational problem with application to cooling fins. *J. Soc. Indust. Appl. Math.*, Vol. 10, 19-29.

Maday, C. J. (1974). The minimum weight one-dimensional straight fin. *ASME J. Eng. Ind.*, Vol. 96, 161-165.

McQuiston, F. C. (1975). Fin efficiency with combined heat and mass transfer. *ASHRAE Transaction*, Vol. 71, 350-355.

Mokheimer, E. M. A. (2002). Performance of annular fins with different profiles subject to variable heat transfer coefficient. *Int. J. Heat Mass Transfer*, Vol. 45, 3631-3642.

Pirompugd, W., Wang, C. C. & Wongwises, S. (2007a). Heat and mass transfer characteristics of finned tube heat exchangers with dehumidification. *J. Thermophysics Heat transfer*, Vol. 21, No. 2, 361-371.

Pirompugd, W., Wang, C. C. & Wongwises, S. (2007b). A fully wet and fully dry tiny circular fin method for heat and mass transfer characteristics for plain fin-and-tube heat exchangers under dehumidifying conditions. *J. Heat Transfer*, Vol. 129, No. 9, 1256-1267.

Pirompugd, W., Wang, C. C. & Wongwises, S. (2008). Finite circular fin method for wavy fin-and-tube heat exchangers under fully and partially wet surface conditions. *Int. J. Heat Mass Transfer*, Vol. 51, 4002-4017.

Pirompugd, W., Wang, C. C. & Wongwises, S. (2009). A review on reduction method for heat and mass transfer characteristics of fin-and-tube heat exchangers under dehumidifying conditions. *Int. J. Heat Mass Transfer*, Vol. 52, 2370-2378.

Razelos, P. & Imre, K. (1983). Minimum mass convective fins with variable heat transfer coefficient. *J. Franklin Institute*, Vol. 315, 269-282.

Schmidt, E. (1926). *Wärmeübertragung durch Rippen*. Z. Deustsh Ing., Vol. 70, 885-951.

Solov'ev, B.A. (1968). An optimum radiator-fin profile. *Inzhenerno Fizicheskii Jurnal*, Vol. 14, No. 3, 488-492.

Threlkeld, J. L. (1970). *Thermal environment engineering*. Prentice-Hall, New York.

Wilkins, J. E. Jr. (1961). Minimum mass thin fins with specified minimum thickness. *J. Soc. Ind. Appl. Math.*, Vol. 9, 194-206.

Wu, G. & Bong, T. Y. (1994). Overall efficiency of a straight fin with combined heat and mass transfer. *ASRAE Transation*, Vol. 100, No. 1, 365-374.

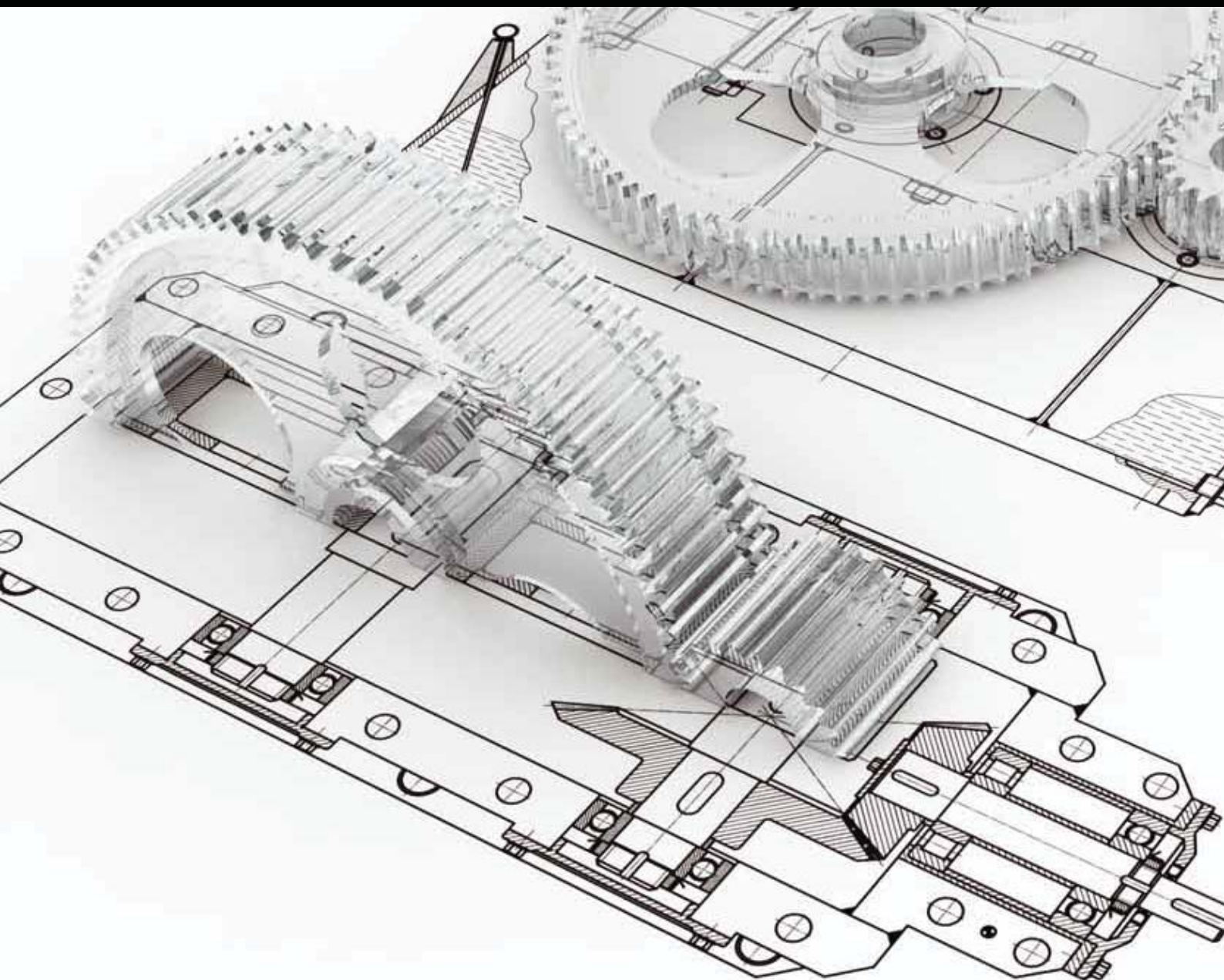
Zubair, S. M.; Al-Garni, A. Z. & Nizami, J. S. (1996). The optimum dimensions of circular fins with variable profile and temperature-dependent thermal conductivity. Vol. 39, No. 16, 3431-3439.

ภาคผนวก ฉ.

ผลงานการนำไปใช้ประโยชน์ เชิงสารสนเทศ

Two-Phase Flow and Heat Transfer Enhancement

Guest Editors: Somchai Wongwises, Afshin J. Ghajar, Kwok-wing Chau, Octavio García Valladares, Balaram Kundu, Ahmet Selim Dalkılıç, and Godson Asirvatham Lazarus





Two-Phase Flow and Heat Transfer Enhancement

Advances in Mechanical Engineering

Two-Phase Flow and Heat Transfer Enhancement

Guest Editors: Somchai Wongwises, Afshin J. Ghajar,
Kwok-wing Chau, Octavio García Valladares, Balaram Kundu,
Ahmet Selim Dalkılıç, and Godson Asirvatham Lazarus



Copyright © 2013 Hindawi Publishing Corporation. All rights reserved.

This is a special issue published in "Advances in Mechanical Engineering." All articles are open access articles distributed under the Creative Commons Attribution License, which permits unrestricted use, distribution, and reproduction in any medium, provided the original work is properly cited.

Editorial Board

Koshi Adachi, Japan	Luís Godinho, Portugal	D. R. Salgado, Spain
Mehdi Ahmadian, USA	Tian Han, China	Mohammad Reza Salimpour, Iran
Rehan Ahmed, UK	Francisco J. Huera-Huarte, Spain	Sunetra Sarkar, India
Muhammad Tahir Akhtar, Japan	D. Jalali-Vahid, Iran	Pietro Scandura, Italy
Nacim Alilat, France	Jiin Yuh Jang, Taiwan	A. Seshadri Sekhar, India
M. Affan Badar, USA	Zhongmin Jin, UK	Ahmet Selim Dalkılıç, Turkey
Luis Baeza, Spain	Xiaodong Jing, China	Liyuan Sheng, China
R. Balachandran, UK	S.-W. Kang, Republic of Korea	Xi Shi, China
Claude Bathias, France	Xianwen Kong, UK	Seiichi Shiga, Japan
Adib Becker, UK	Michał Kuciej, Poland	C. S. Shin, Taiwan
Leonardo Bertini, Italy	Yaguo Lei, China	Ray W. Snidle, UK
L. A. Blunt, UK	Zili Li, The Netherlands	Margaret M. Stack, UK
Noël Brunetière, France	Cheng-Xian Lin, USA	Neil Stephen, UK
Marco Ceccarelli, Italy	Jaw-Ren Lin, Taiwan	Kumar K. Tamma, USA
Fakher Chaari, Tunisia	S. Nima Mahmoodi, USA	Yaya Tan, China
Chin-Lung Chin, Taiwan	Oronzo Manca, Italy	Anand Thite, UK
H. H. Cho, Republic of Korea	Ramiro Martins, Portugal	Cho W. Solomon To, USA
Seung-Bok Choi, Korea	Aristide Fausto Massardo, Italy	Yoshihiro Tomita, Japan
Kangyao Deng, China	Francesco Massi, Italy	Shan-Tung Tu, China
Francisco D. Denia, Spain	T. H. New, Singapore	Sandra Velarde-Suárez, Spain
T. S. Dhanasekaran, USA	Kim Choon Ng, Singapore	Moran Wang, China
Nihad Dukhan, USA	C. T. Nguyen, Canada	Junwu Wang, China
Farzad Ebrahimi, Iran	Hirosi Noguchi, Japan	Jia-Jang Wu, Taiwan
Ali El Wahed, UK	Hakan F. Oztop, Turkey	Fengfeng Xi, Canada
Bogdan I. Epureanu, USA	Duc Truong Pham, UK	Gongnan Xie, China
M. R. Eslami, Iran	Jurij Prezelj, Slovenia	Wei Mon Yan, Taiwan
Ali Fatemi, USA	Xiaotun Qiu, USA	Jianqiao Ye, UK
Mario L. Ferrari, Italy	Pascal Ray, France	Byeng D. Youn, USA
Siegfried Fourny, France	Robert L. Reuben, UK	Jianbo Yu, China
Ian Frigaard, Canada	Pedro A. R. Rosa, Portugal	Bo Yu, China
Mergen H. Ghayesh, Canada	Elsa de Sá Caetano, Portugal	Zhongrong Zhou, China

Contents

Two-Phase Flow and Heat Transfer Enhancement, Somchai Wongwises, Afshin J. Ghajar, Kwok-wing Chau, Octavio García Valladares, Balaram Kundu, Ahmet Selim Dalkılıç, and Godson Asirvatham Lazarus
Volume 2013, Article ID 256839, 2 pages

Two-Phase Flow and Heat Transfer during Steam Condensation in a Converging Microchannel with Different Convergence Angles, Ben-Ran Fu, T. H. Chang, and Chin Pan
Volume 2013, Article ID 372898, 10 pages

Computational Analysis of Droplet Mass and Size Effect on Mist/Air Impingement Cooling Performance, Zhenglei Yu, Tao Xu, Junlou Li, Tianshuang Xu, and Tatsuo Yoshino
Volume 2013, Article ID 181856, 8 pages

Economic Analysis for Rebuilding of an Aged Pulverized Coal-Fired Boiler with a New Boiler in an Aged Thermal Power Plant, Burhanettin Cetin and Merve Abacioglu
Volume 2013, Article ID 270159, 6 pages

Simulation and Experimental Investigation of Thermal Performance of a Miniature Flat Plate Heat Pipe, R. Boukhanouf and A. Haddad
Volume 2013, Article ID 474935, 8 pages

Numerical Determination of Effects of Wall Temperatures on Nusselt Number and Convective Heat Transfer Coefficient in Real-Size Rooms, Ozgen Acikgoz and Olcay Kincay
Volume 2013, Article ID 287963, 9 pages

Editorial

Two-Phase Flow and Heat Transfer Enhancement

Somchai Wongwises,¹ Afshin J. Ghajar,² Kwok-wing Chau,³ Octavio García Valladares,⁴ Balaram Kundu,⁵ Ahmet Selim Dalkılıç,⁶ and Godson Asirvatham Lazarus⁷

¹ *Fluid Mechanics, Thermal Engineering and Multiphase Flow Research Lab. (FUTURE), Department of Mechanical Engineering, Faculty of Engineering, King Mongkut's University of Technology Thonburi, Bangkok 10140, Thailand*

² *School of Mechanical and Aerospace Engineering, Oklahoma State University, Stillwater, OK 74078, USA*

³ *Department of Civil & Environmental Engineering, The Hong Kong Polytechnic University Hunghom, Kowloon, Hong Kong*

⁴ *Department of Energy Systems, Centro de Investigación en Energía, CIE-UNAM, Privada Xochicalco S/N, 62580 Temixco, MOR, Mexico*

⁵ *Department of Mechanical Engineering, Jadavpur University, Kolkata 700032, India*

⁶ *Heat and Thermodynamics Division, Department of Mechanical Engineering, Yildiz Technical University, Yildiz, 34349 Istanbul, Turkey*

⁷ *Department of Mechanical Engineering, Karunya University, Coimbatore, Tamil Nadu 641 114, India*

Correspondence should be addressed to Somchai Wongwises; somchai.won@kmutt.ac.th

Received 2 December 2013; Accepted 2 December 2013

Copyright © 2013 Somchai Wongwises et al. This is an open access article distributed under the Creative Commons Attribution License, which permits unrestricted use, distribution, and reproduction in any medium, provided the original work is properly cited.

Gas-liquid two-phase flow and heat transfer processes are commonly encountered in a wide variety of applications, for example, refrigeration and air-conditioning systems, power engineering, and other thermal processing plants. The advantage of high thermal performance in comparison to the single-phase applications leads to various engineering applications including the cooling systems of various types of equipment such as high performance microelectronics, supercomputers, high-powered lasers, medical devices, high heat-flux compact heat exchangers in spacecraft and satellites, and so forth. The aim of this special issue was to collect the original research and review papers on the recent developments in the field of two-phase flow and heat transfer enhancement. Potential topics included advanced heat pipe technologies, boiling and condensation heat transfer, CHF and post-CHF heat transfer, cooling of electronic system, Heat and mass transfer in phase change processes, instabilities of two-phase flow, measurements and modeling of two-phase flow in microchannel, microgravity in two-phase flow, nanofluids science and technology, nuclear reactor applications, passive and active heat transfer enhancement techniques, Refrigeration and air-conditioning technology, two-phase flow with heat and mass transfer, two-phase

refrigerant flow, and special topics on the latest advances in two-phase flow and heat transfer. In this special issue, we have invited a few papers that address such issues.

First paper of special issue investigates the effect of convergence angle of microchannel on two-phase flow and heat transfer during steam condensation experimentally. The experimental results show that the condensation heat flux increases with an increase in the convergence angle and/or the steam mass flux at a given coolant flow rate but decreases with an increase in the coolant flow rate at a given steam mass flux. Second paper focuses on simulating mist impingement cooling under typical gas turbine operating conditions of high temperature and pressure in a double chamber model. The results of this paper can provide guidance for corresponding experiments and serve as the qualification reference for future more complicated studies with convex surface cooling. In third paper, economic analysis of rebuilding an aged pulverized coal-fired boiler with a new pulverized coal-fired boiler including flue gas desulfurization unit and a circulating fluidized bed boiler is investigated in existing old thermal power plants. The fourth paper presents the results of a CFD analysis and experimental tests of two identical miniature flat plate heat pipes using sintered and screen

mesh wicks and a comparative analysis and measurement of two solid copper base plates 1 mm and 3 mm thick. In fifth paper, a modeled room was numerically heated from a wall and cooled from the opposite wall in order to create a real-room simulation. The cooled wall simulated heat loss of the room, and the heated wall simulated the heat source of enclosure. The effects of heated and cooled wall temperatures on convective heat transfer coefficient and Nusselt number in the enclosure were investigated numerically for two- and three-dimensional (3D) modeling states.

In summary, this special issue reflects a variety of contemporary research in heat transfer and is expected to promote further research activities and development opportunities.

Acknowledgment

We thank the authors who prepared the paper within the stringent length and time requirements. We thank the reviewers who provided meaningful suggestions on short notice.

Somchai Wongwises

Afshin J. Ghajar

Kwok-wing Chau

Octavio García Valladares

Balaram Kundu

Ahmet Selim Dalkılıç

Godson Asirvatham Lazarus

Research Article

Two-Phase Flow and Heat Transfer during Steam Condensation in a Converging Microchannel with Different Convergence Angles

Ben-Ran Fu,¹ T. H. Chang,² and Chin Pan^{2,3,4}

¹ Green Energy and Environment Research Laboratories, Industrial Technology Research Institute, Hsinchu 31040, Taiwan

² Department of Engineering and System Science, National Tsing Hua University, Hsinchu 30013, Taiwan

³ Institute of Nuclear Engineering and Science, National Tsing Hua University, Hsinchu 30013, Taiwan

⁴ Low Carbon Energy Research Center, National Tsing Hua University, Hsinchu 30013, Taiwan

Correspondence should be addressed to Chin Pan; cpan@ess.nthu.edu.tw

Received 15 June 2013; Revised 30 September 2013; Accepted 30 September 2013

Academic Editor: Ahmet Selim Dalkılıç

Copyright © 2013 Ben-Ran Fu et al. This is an open access article distributed under the Creative Commons Attribution License, which permits unrestricted use, distribution, and reproduction in any medium, provided the original work is properly cited.

The present study experimentally investigates the effect of convergence angle of microchannel on two-phase flow and heat transfer during steam condensation. Three condensation regimes, from the inlet to the outlet, are identified: mist/annular flow, injection flow, and slug-bubbly flow. Flow pattern maps are constructed using superficial vapor and liquid velocities as the coordinates, wherein relatively distinct boundaries between the flow patterns can be identified. The experimental results show that the condensation heat flux increases with an increase in the convergence angle and/or the steam mass flux at a given coolant flow rate but decreases with an increase in the coolant flow rate at a given steam mass flux. The results further demonstrate that the local condensation heat transfer coefficient in the mist/annular flow region is much higher than that in other condensation regimes. Moreover, the local condensation heat transfer coefficient in the mist/annular flow and injection flow region decreases with an increase in the convergence angle.

1. Introduction

Condensation in microchannels is of significant fundamental interest and has diversified applications, such as in microchannel heat exchangers and micro-fuel cells. In recent years, many studies on the characteristics of two-phase flow and heat transfer during condensation in microchannels were reported. For example, Wu and Cheng [1] visualized the condensation flow patterns of steam flowing through 10 parallel microchannels with a hydraulic diameter of $82.8\text{ }\mu\text{m}$ and a trapezoidal cross-sectional area. They categorized the flow patterns observed as follows: droplet flow (mist flow), annular flow, injection flow, and slug-bubbly flow. The injection flow pattern appears periodically because of its upstream flow patterns alternate between the droplet two-phase flow and the vapor flow. Wu et al. [2] further carried out experimental studies on injection flow during steam condensation in microchannels with hydraulic diameters ranging from $53\text{ }\mu\text{m}$

to $128.5\text{ }\mu\text{m}$. They proposed that the location of the injection flow corresponds to the Reynolds number (Re), condensation number (Co), and diameter-to-length ratio (D_h/L) and obtained a dimensionless correlation for the location of injection flow in silicon microchannels.

Quan et al. [3] investigated the effects of the mass flux and cooling flow rate on the occurrence frequency of the injection flow in a single microchannel with hydraulic diameters of 120 and $128\text{ }\mu\text{m}$. Their study revealed that the shape of the microchannels has a critical influence on the instability of the condensation flow mechanisms. Furthermore, Wu et al. [4] conducted an experimental study on heat transfer and flow friction during steam condensation in trapezoidal silicon microchannels with hydraulic diameters of 77.5, 93.0, and $128.5\text{ }\mu\text{m}$. Their experimental results demonstrated that the condensation Nusselt number increases with an increase in the Re, Co, and D_h/L , and the condensation two-phase

frictional multiplier decreases with an increase in the Re and D_h/L or a decrease in the Co .

Chen et al. [5] performed a visualization experiment to investigate the steam condensation in triangular microchannels with hydraulic diameters of 100 and 250 μm . The experimental results indicated that the droplet, annular, injection, and slug-bubbly flows are the dominant flow patterns during steam condensation in microchannels. In addition, they proposed the correlations for injection location, injection frequency, and condensation Nusselt number. Wu et al. [6] presented a visualization study on steam condensation in wide rectangular microchannels. Three typical flow patterns were identified in their study, namely, droplet-annular compound flow, injection flow, and vapor slug-bubbly flow. They demonstrated that the injection location moves to the channel outlet with an increase in the Re , and the injection frequency increases with increasing the Re and condensate Weber number. In addition, the results showed that the injection frequency is lower than that in the triangular microchannel with the same hydraulic diameter, indicating that the cross-sectional shape of the microchannel plays an important role in the instability of condensation flow.

Agarwal et al. [7] reported the condensation heat transfer coefficients of R134a in six noncircular horizontal microchannels with different shapes (barrel-shaped, N-shaped, rectangular, square, and triangular tubes, and a channel with a W-shaped corrugated insert). For square, rectangular, and barrel-shaped channels, an annular-flow-based heat transfer model was developed. On the other hand, for triangular, N-shaped, and W-insert channels (i.e., those with sharp corner), a mist-flow-based heat transfer model was proposed. Ma et al. [8] investigated the two-phase flow patterns and transition characteristics during steam condensation in trapezoidal microchannels. Annular flow, droplet flow, injection flow, and bubbly flow were observed in their study. Two-phase flow pattern maps were constructed using coordinates of steam mass flux and steam quality. They also reported that the flow pattern transition from annular flow to bubbly flow occurs earlier in the smaller microchannel. In addition, criteria for transitions between flow patterns were also proposed in the form of nondimensional groups (steam quality, condensation number, Reynolds number, Weber number, Bond number, and width-to-diameter ratio).

Fang et al. [9] investigated the effect of wall hydrophobicity on the steam condensation in the rectangular microchannel. They found that the channel surface wettability has a significant impact on the condensation flow pattern, pressure drop, and heat transfer characteristics. At a given inlet vapor flux and temperature, the hydrophobic microchannel presents higher heat transfer rate and pressure drop than those in the hydrophilic one. Odaymet and Louahlia-Gualous [10] reported the local heat transfer coefficient and flow visualization during condensation in a square microchannel. They identified the following flow regimes: mist flow, churn flow, annular flow, slug flow, liquid ring flow, and annular/bubbly flow. Their results indicated that the local condensation heat transfer coefficient increases with an increase in the steam mass flux. Recently, Odaymet et al. [11] investigated the local heat transfer and flow patterns during

steam condensation in a single silicon-based microchannel. They further modified condensation flow patterns as follows (from upstream to downstream): mist flow, churn flow, elongated bubbly flow followed by a bubbly sequence, and slug flow. In addition, they also found that local thermal performance of condensation flow for mist flow and upstream elongated bubbly flow is better than slug and bubbly flows.

Kim et al. [12] carried out an experimental study on condensation of FC-72 in parallel microchannels. Smooth-annular, wavy-annular, transition, slug, and bubbly flows were identified in their experimental observation. Furthermore, they discussed the condensation two-phase flow pressure drop using both two-phase homogenous and separated flow models and found that the homogenous model unexpectedly provides better predictions than the separated flow model. Furthermore, Kim and Mudawar [13] demonstrated that the local condensation heat transfer coefficient is the highest near the channel inlet and decreases along the microchannel due to an increase in the film thickness. In addition, a correlation of condensation heat transfer coefficient for annular condensation in microchannels was also proposed.

Based on the above literature reviews on microchannel condensation, it is clearly found that significant effects of microchannel cross-sectional shape on the condensation flow patterns and heat transfer are demonstrated. In our previous study [14], convective steam condensation in uniform, converging, and diverging microchannels with a mean hydraulic diameter of 117 μm was experimentally investigated. The steam flow in the microchannel was cooled by a still water bath. Flow patterns, two-phase flow pressure drop, outlet temperature, bubbly emission frequency, and bubbly velocity in the three different cross-section designs of microchannels were reported. The experimental results demonstrated that, for a given steam mass flow rate, the two-phase flow pressure drop in the diverging microchannel is considerably higher than that in the uniform and converging microchannels. The converging microchannel presents the lowest two-phase flow pressure drop, suggesting its merit for removing the two-phase fluids during steam condensation.

Furthermore, Kuo and Pan [15] investigated steam condensation in uniform and converging microchannels with a mean hydraulic diameter of 135 μm . The steam flow in the microchannels was cooled by water cross-flowing along its bottom surface, which is different from other methods reported in the literature. The flow patterns, two-phase flow pressure drop, and local condensation heat transfer coefficient were examined. The results demonstrated that although the uniform microchannel presents a higher heat transfer coefficient than those in the converging microchannel under mist/annular flow regimes, the total heat transfer rate is higher for the microchannel with the converging cross-section than that with the uniform cross-section. Moreover, empirical correlations of local condensation heat transfer for the mist and annular flow regions and a two-phase frictional multiplier in the form of the Lockhart-Martinelli correlation were developed.

This work investigates the effect of convergence angle (half of the included angle) of microchannel experimentally

on two-phase flow and heat transfer during steam condensation. Flow pattern maps are constructed using coordinates of superficial vapor and liquid velocities. In addition, the effects of convergence angle on local heat transfer coefficient as well as condensation heat transfer rate are explored.

2. Experimental Details

2.1. Experimental Setup. Figure 1 shows the experimental setup, which is similar to that employed in our previous study [15], that consists of a water tank, a high-performance liquid chromatography (HPLC) pump (P680: Dionex), a heating module, a test section, a cooling water circulation system, a condensate collecting container, an electronic balance (XS625 M: Precisa Gravimetrics), a flow visualization system, and related control and measurement systems. Before conducting experiments, the deionized water in the water tank was boiled to evacuate dissolved gas. Then, water was driven by the HPLC pump through the helical tube immersed in the silicone oil bath and heated and stirred by a heating module to vaporize the water to steam. The steam subsequently flowed into the test section. Three K-type thermocouples were placed in the bath to measure the oil temperature. A cooling water circulation system combined with a metering pump (FEM03KT: KNF) drove water with a constant inlet temperature of 22°C at a specific flow rate in the cross-flow direction along the backside surface of the test section. The condensate was collected by a container at atmosphere pressure and condensate was weighed using an electronic balance to verify the steam mass flow rates (m_s). The steam mass flow rates in the present study ranged from 2.36×10^{-6} kg/s to 5.28×10^{-6} kg/s.

The test section with a converging microchannel was a silicon strip with dimensions of 10 mm \times 48 mm. Three convergence angles ($\beta = 0.5^\circ$, 1.0° , and 1.5°) of the microchannel with the same mean hydraulic diameter (D_h) of 135 μm were employed to study the effect of convergence angle. Here, the mean hydraulic diameter of the converging microchannel was calculated based on the following definition [16]:

$$D_h = \frac{1}{L} \int_0^L \frac{4 \times H \times W(x)}{2 \times [H + W(x)]} dx \quad (1)$$

$$= 2H \left[1 - \frac{H}{W_{\text{out}} - W_{\text{in}}} \ln \left(\frac{H + W_{\text{out}}}{H + W_{\text{in}}} \right) \right].$$

Figures 2 and 3 depict schematics of the test section and cooling chamber, respectively. The detailed dimensions of the microchannels with different convergence angles are summarized in Table 1. Two T-type thermocouples and a differential pressure transducer (692: Huba) were employed to measure the inlet and outlet temperatures and the pressure drop between the inlet and outlet chambers. Three T-type thermocouples were embedded in the backside surface of the test section (facing the coolant) to measure the local wall temperature (T_w), which is then used to evaluate the local heat transfer coefficient. These three thermocouples were located at $z = 9.5$, 17.5, and 25.5 mm, respectively, in reference to the channel inlet. The data of the thermocouples

TABLE 1: Detailed dimensions of the microchannels with different convergence angles.

Test section	Ref. [15]	No. 1	No. 2	No. 3
β ($^\circ$)	0	0.5	1.0	1.5
W_{in} (μm)	675	1022	1445	1933
W_{out} (μm)	675	410	220	100
L (mm)	35	35	35	35
H (μm)	75	75	75	75
D_h (μm)	135	135	135	135

and the differential pressure transducer were recorded by a data acquisition system (MXI100: Yokogawa) with a sampling rate of 2 Hz.

The flow visualization system included a high-speed digital camera (XS-4: IDT) mounted with a microlens (zoom 125C: OPTEM) and a computer. In addition, an x - y - z mechanism was installed to hold the CCD and microlens with an accurate position on the test plane (x - y plane) and focus in the z -direction. The typical frame rate employed in the study was 4000 frames/s. A 250 W fiber optic illuminator (FOI-250: TechniQuip) was used as the light source.

2.2. Fabrication of the Test Section. To prepare the microchannel with a uniform depth, the test section was made of P-type (100) orientation silicon on insulator (SOI) wafer, which consisted of three layers (from bottom to top): (1) handle layer (P-type (100) bare wafer, thickness: $525 \pm 25 \mu\text{m}$); (2) box layer (SiO_2 , thickness: 0.5 μm); and (3) device layer (P-type (100) silicon wafer, thickness: $75 \pm 1 \mu\text{m}$). The converging microchannels with inlet and outlet chambers were etched on the surface of the device layer. The fabrication processes of the test section employed deep reactive ion etching (DRIE) with photolithography, laser-cutting technology, and anodic bonding processes. The etching stop mechanism on the box layer for the DRIE process ensured a uniform depth for the microchannels and chambers. Subsequently, an excimer laser micromachining technology was applied to make through holes, which were used as the inlet and outlet chambers for the working fluid to flow through the microchannel. Finally, to enable flow visualization the test section was covered with the Pyrex no. 7740 glass through anodic bonding.

2.3. Uncertainty Analysis. The measurement uncertainty for the liquid volumetric flow rate through the HPLC pump in the microchannels after calibration was estimated to be $\pm 0.2\%$. The accuracy of the metering pump was $\pm 2\%$. The measurement uncertainty of the pressure transducer was 0.5% over the full scale, resulting in an actual uncertainty of ± 1.25 kPa. The uncertainties in the temperature measurements were $\pm 0.2^\circ\text{C}$ and $\pm 0.5^\circ\text{C}$ for T-type and K-type thermocouples, respectively. The ambient temperature was controlled at about 25°C by an air conditioner during experiments. The uncertainties for the temperature of the cooling water, ambient condition, and steam were estimated to be $\pm 0.5^\circ\text{C}$. The uncertainty analysis methodology developed by Moffat [17] was used to estimate the uncertainty for the total condensation heat transfer rate and the local condensation

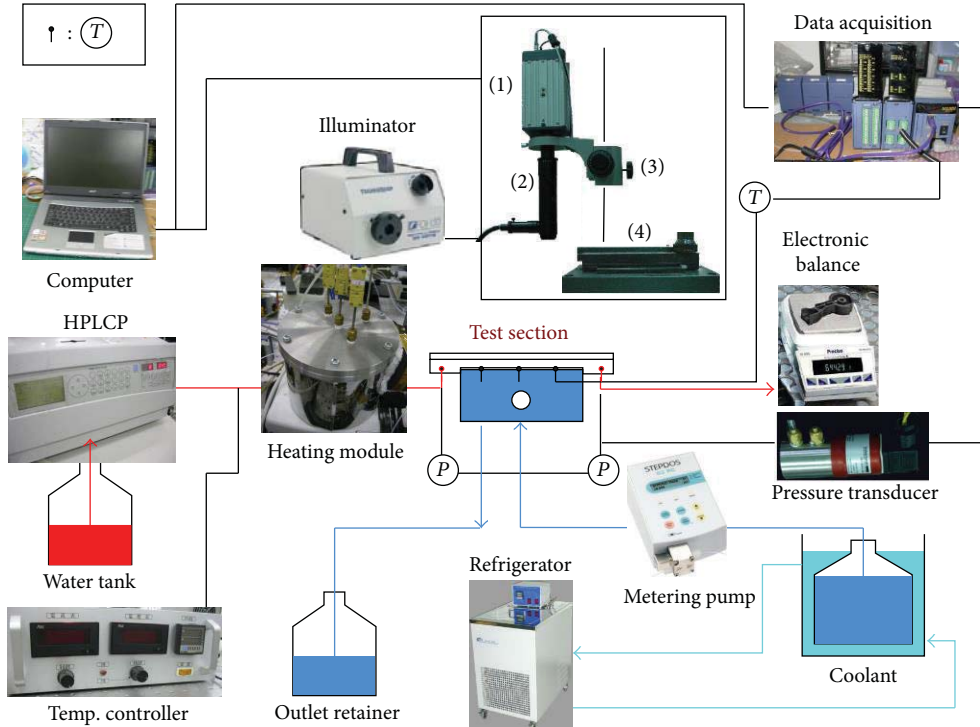


FIGURE 1: Experimental setup: (1) CCD, (2) microscope, and (3) and (4) x - y - z mechanism.

heat transfer coefficient, which were 1.9% and 6.6%, respectively. In addition, the uncertainty of the void fraction of 0.52 is about 9.6%, estimated from our previous study [18], which is due to the image analysis tool. As shown in Fu et al. [18], the uncertainty of the void fraction decreases with an increase in the void fraction. Consequently, the uncertainty for the void fraction of 0.8, which is corresponding to transition location between mist/annular flow and injection flow, will be smaller than 9.6%. And the highest uncertainty of the condensation heat transfer rate for a particular flow region is 9.8%, which is higher than that of total condensation heat transfer rate.

3. Data Reduction

In the present study, the heat released by the steam is mainly carried away by the forced convection to the cooling water flowing underneath the test section, defined as q_c , and a small fraction may be lost by natural convection via the top glass surface of the test section to the ambient air. In the present study, the estimated heat transfer by natural convection is less than 0.1% of the measured heat dissipation. Thus, the total heat (q_t) released by the steam can be reasonably considered to be absorbed totally by the coolant (q_c); that is, $q_t = q_c$. Thermal radiation to the ambient is considered to be negligible. Here, q_c is estimated by the following equations:

$$q_c = m_c c_{p,c} (T_{c,out} - T_{c,in}). \quad (2)$$

Following a methodology developed by Kuo and Pan [15], the total condensation heat transfer rate along the microchannel is divided into three parts, that is, q_1 , q_2 , and q_3 ,

corresponding to three distinct two-phase flow regimes: (1) the mist/annular flow, (2) injection flow, and (3) slug/bubbly flow regions, respectively, as depicted in Figure 4. These three regions can be distinguished clearly by flow visualization. Consider

$$q_t = q_1 + q_2 + q_3. \quad (3)$$

The distributions of the condensation heat transfer rate in regions (1) and (3) are assumed to be uniform. For region (1), mist/annular flow prevails and the void fraction is close to unity. Therefore, it is reasonable to assume a uniform condensation heat transfer rate there. On the other hand, for region (3) bubbly flow appears, and thus the condensation heat transfer rate is low and is also uniformly distributed. The condensation heat transfer rates in regions (1) and (3) can be evaluated by the following equations based on the energy balance with a vapor quality (x) determined from the void fraction (α) data:

$$q_1 = (x_{in} - x_1) m_s i_{LV} \quad (4)$$

$$q_3 = (x_2 - x_{out}) m_s i_{LV},$$

where vapor quality at any axial location, z , can be estimated from the following equations:

$$\alpha_z = \frac{0.03 \alpha_{h,z}^{0.5}}{1 - 0.97 \alpha_{h,z}^{0.5}}, \quad (5)$$

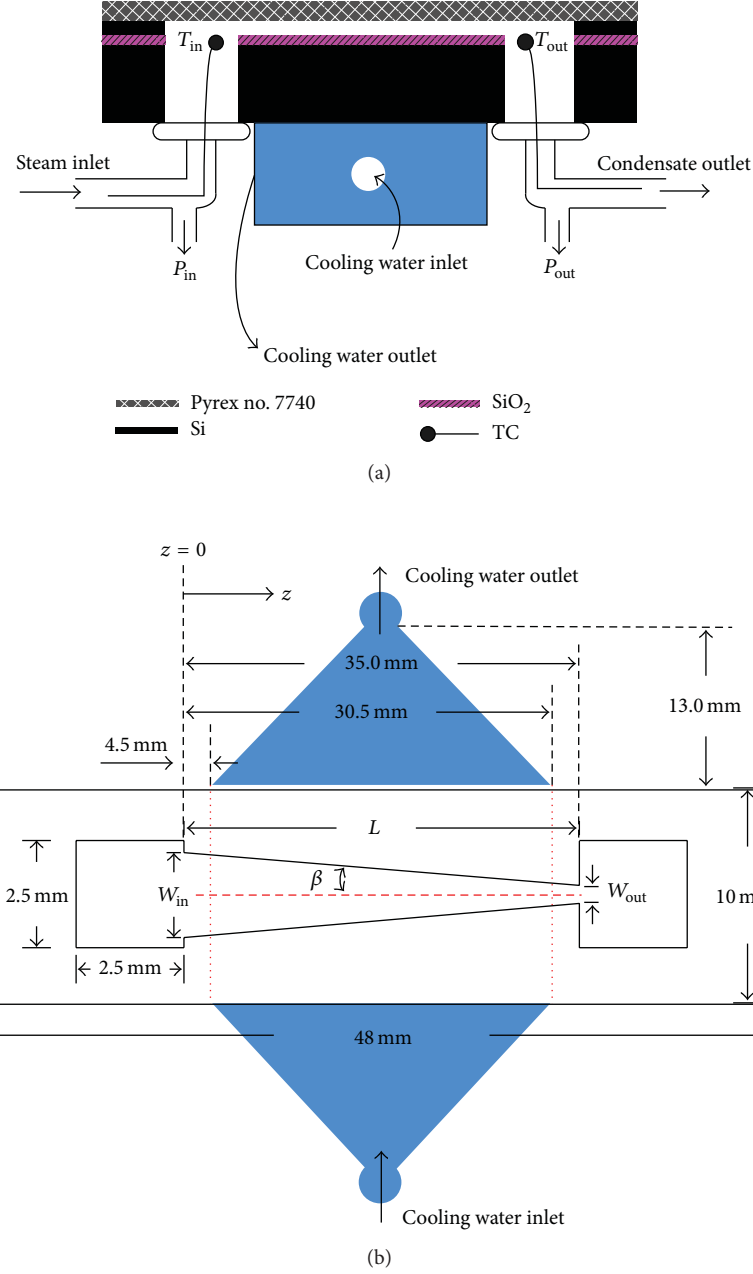


FIGURE 2: Schematic of the test section: (a) side view and (b) top view.

proposed by Kawahara et al. [19]. Consider

$$\alpha_{h,z} = \frac{j_{V,z}}{j_{V,z} + j_{L,z}} = \frac{1}{1 + (1/x_z - 1) \rho_V/\rho_L} \quad (6)$$

$$x_{in} = x_{out} + \frac{q_t}{m_s i_{LV}}.$$

For the present study, the void fraction for a particular region is determined by the mean value of the projected area of vapor bubbles on the bottom wall of 100 frames, randomly selected from the flow visualization of different conditions, divided by the bottom surface area of the

region [18]. The present results demonstrate that the void fraction decreases sharply during the injection flow and keeps nearly constant toward the channel outlet, as reported in our previous study [15]. The persistence of such a nearly constant void fraction near the channel outlet reflects the poor condensation heat transfer therein, which will be demonstrated later. Given local void fraction determined, the corresponding vapor quality and local condensation heat flux in each region may then be determined.

After the condensation heat transfer rates in different regions are obtained, the local condensation heat transfer coefficient can be estimated on the basis of the temperature

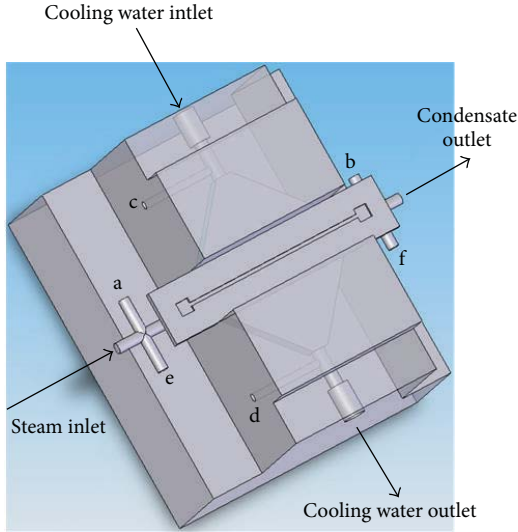


FIGURE 3: Schematic of the test section combined with a cooling chamber. Locations “a” to “d” are points for temperature measurement and “e” and “f” are pressure tap locations in the microchannel.

difference between the saturation temperature ($T_{\text{sat},z}$) of the fluid flowing through the microchannel and the local wall temperature ($T_{\text{ch},z}$) as follows:

$$h_z = \frac{q_z''}{T_{\text{sat},z} - T_{\text{ch},z}}, \quad (7)$$

where $T_{\text{ch},z}$ is extrapolated from the wall temperature measured on the backside, $T_{w,z}$, by considering the total thermal resistances (R'') of the silicon layer and the thin layer of silicon dioxide:

$$T_{\text{ch},z} = T_{w,z} + q_z'' \times R''. \quad (8)$$

The above equation neglects heat conduction in the axial and lateral directions, as the wall thickness ($450 \mu\text{m}$) is much smaller than the channel length (35 mm) and the width of the test section (10 mm).

4. Results and Discussion

4.1. Condensation Two-Phase Flow Pattern. Condensation two-phase flow patterns in microchannels have been investigated in many studies. In the literature, five distinct flow regimes have been reported, namely, mist flow, annular flow, injection flow, slug/plug flow, and bubbly flow. In the present study, three flow regimes, from the inlet to the outlet, can be identified: mist/annular flow (Figure 4(a)), injection flow (Figure 4(b)), and slug/bubbly flow (Figure 4(c)) regions. More detailed discussions on the characteristics of condensation two-phase flow pattern in rectangular microchannels with different cross-section designs have been presented in our previous study [14].

Figure 5 presents the occurrence location for the injection flow as a function of steam mass flow rate in the converging microchannel with $\beta = 0.5^\circ$. This figure indicates that

the location of the injection flow retreats toward the channel inlet with increasing the coolant flow rate (Q_c) at a given steam mass flow rate or decreasing the steam mass flow rate at a given coolant flow rate. Moreover, the occurrence of injection flow moves to downstream with an increase in the convergence angle at a given coolant flow rate. Such movement of the location of injection flow with mass flow rate and/or convergence angle has a significant effect on the characteristics of condensation heat transfer, which will be discussed in the following sections.

Flow pattern maps are used to determine the flow pattern prevailing under a particular operating condition. Figures 6, 7, and 8 further show the flow pattern maps, constructed in the coordinates of superficial vapor and liquid velocities, that is, j_V and j_L , respectively, observed during experiments in microchannels with different convergence angles. In the present study, flow patterns were observed in four different locations, that is, channel inlet, channel outlet, and locations for void fraction of 0.52 and 0.8 corresponding to the transition boundaries between injection flow and slug/bubbly flow and between mist/annular flow and injection flow, respectively. In the channel inlet region, as shown in the figures, the superficial vapor velocity is the highest and greater than 10 m/s. With a decrease in the void fraction, the superficial vapor velocity decreases while the superficial liquid velocity increases. The transition boundaries that separate the mist/annular flow from the injection flow ($\alpha = 0.8$) and the injection flow from the slug/bubbly flow ($\alpha = 0.52$) are also identified in the figure. Figures 6, 7, and 8 demonstrate that the transition boundaries between mist/annular flow and injection flow and between injection flow and slug/bubbly flow become more distinct as the convergence angle is increased. For these two transition boundaries, the superficial liquid velocity increases very rapidly with an increase in the superficial vapor velocity.

4.2. Condensation Heat Transfer. Figure 9 shows the condensation heat transfer rate as a function of steam mass flow rate in the converging microchannel with $\beta = 0.5^\circ$. This figure clearly demonstrates that the condensation heat transfer rate increases with an increase in the steam mass flow rate at a given coolant flow rate, as reported earlier by Odaymet and Louahlia-Gualous [10], but decreases with an increase in the coolant flow rate at a given steam mass flow rate. The decrease of condensation heat transfer rate with increasing coolant flow rate results primarily from the occurrence location of injection flow moves upstream, as shown previously in Figure 5. This shortens the length of mist/annular flow region and decreases the total condensation heat transfer rate, as the mist/annular flow presents the highest heat transfer compatibility among the three possible flow regimes [15].

To further understand the heat transfer characteristics among microchannels with different convergence angles, the condensation heat fluxes (q_c'') are also examined, as shown in Figure 10(a). Note that in this figure the experimental data of the uniform microchannel ($\beta = 0^\circ$) are from our previous study [15]. This figure shows that at a given coolant flow rate and steam mass flux the condensation heat flux increases with an increase in the convergence angle. This

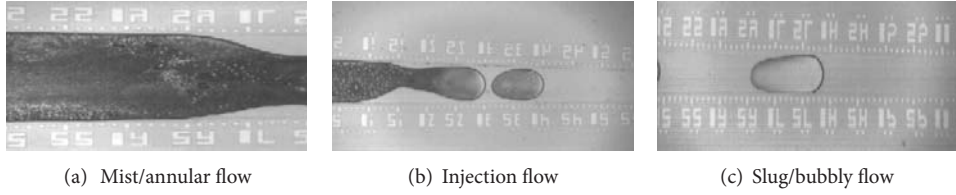
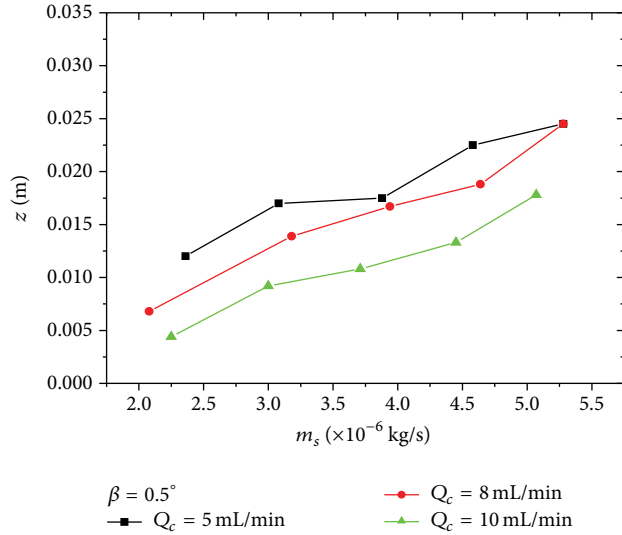
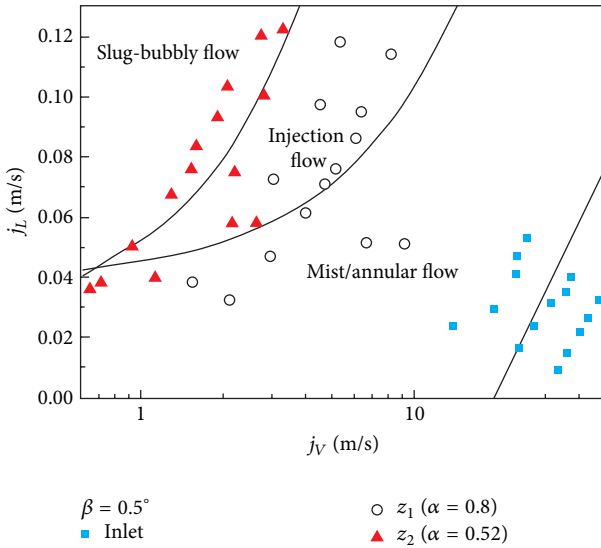
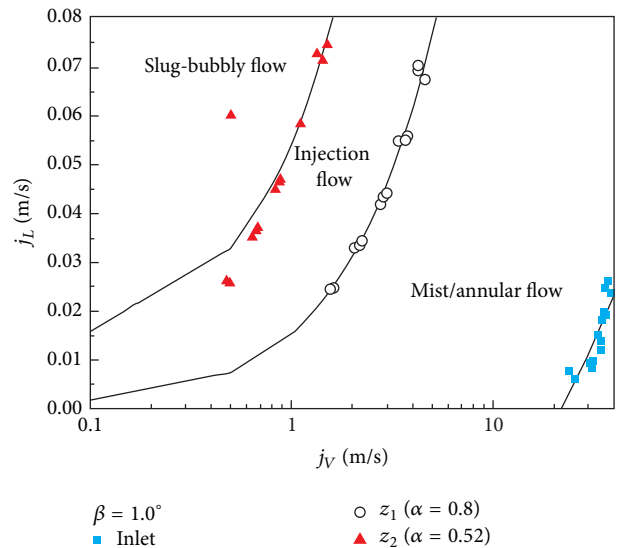


FIGURE 4: Typical condensation flow patterns in the microchannel.

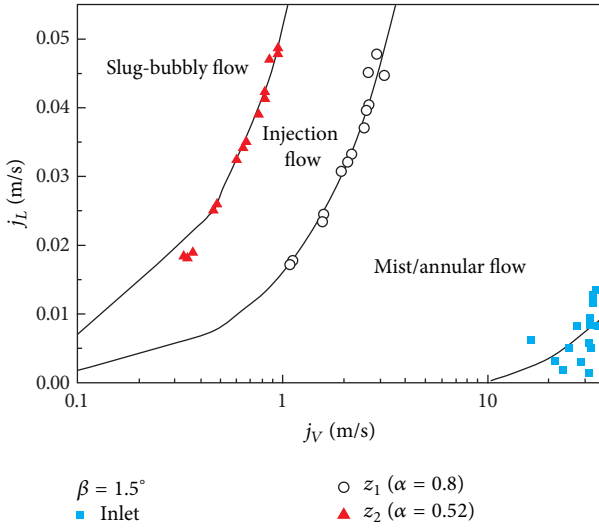
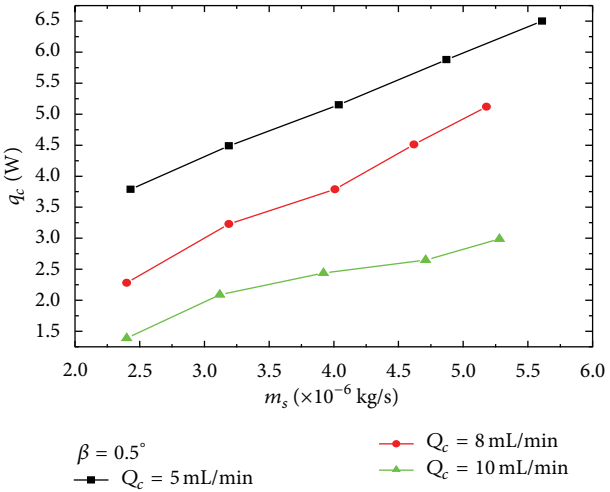
FIGURE 5: Occurrence location of the injection flow as a function of steam mass flow rate in the microchannel with $\beta = 0.5^\circ$.FIGURE 6: Flow pattern map for the microchannel with $\beta = 0.5^\circ$.

is mainly due to the occurrence of injection flow moves to downstream with an increase in the convergence angle, as shown in Figure 10(b). The occurrence of injection flow taking place in a further downstream location indicates that the region of mist/annular flow prevails larger, and, therefore, a much higher bottom heat transfer area for the mist/annular

FIGURE 7: Flow pattern map for the microchannel with $\beta = 1.0^\circ$.

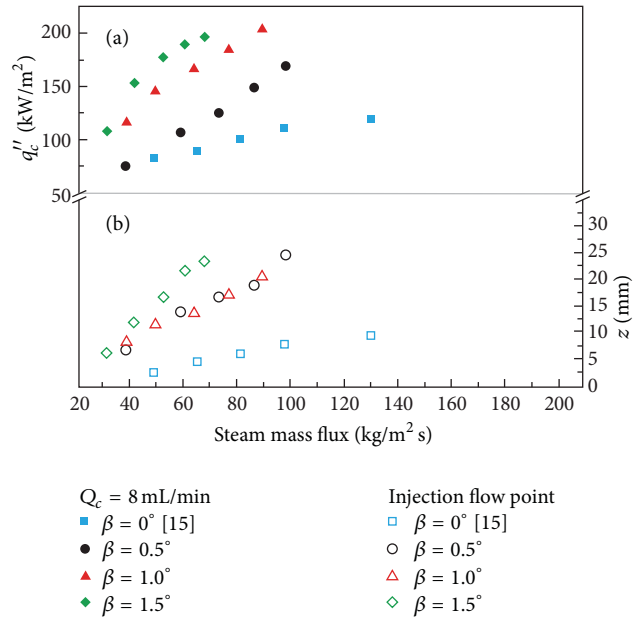
region can be obtained. As the condensation heat transfer rate from the channel is the sum of heat transfer rate from mist/annular flow, injection flow, and bubbly flow regions, that is,

$$q_t = q_1'' A_1 + q_2'' A_2 + q_3'' A_3, \quad (9)$$

FIGURE 8: Flow pattern map for the microchannel with $\beta = 1.5^\circ$.FIGURE 9: Condensation heat transfer rate as a function of steam mass flow rate in the microchannel with $\beta = 0.5^\circ$.

where q_1'' , q_2'' , and q_3'' are the condensation heat flux from the mist/annular flow, injection flow, and bubbly flow regions, respectively, A_1 , A_2 , and A_3 are the corresponding heat transfer area for the mist/annular flow, injection flow, and bubbly flow regions, respectively. The heat flux in the mist/annular flow region is much higher than that in the injection flow and bubbly flow regions due to its much thinner liquid film between the vapor and the cooling wall [15]. Consequently, a much higher heat transfer area for the mist/annular flow region will result in a higher total condensation heat transfer rate, as suggested by [10]. Therefore, the mean condensation heat transfer rate is higher for the microchannel with a larger convergence angle.

Figure 11 shows the effect of convergence angle on the local condensation heat transfer coefficient. This figure indicates that, for the microchannel with a given convergence angle, the mist/annular flow region is much higher than

FIGURE 10: (a) Condensation heat flux and (b) injection flow location as a function of steam mass flux for the microchannels with different convergence angles. Data of $\beta = 0^\circ$ are from Kuo and Pan [15].

that in other condensation regimes, as reported by Kuo and Pan [15]. Moreover, for mist/annular flow and injection flow regimes the local condensation heat transfer coefficient decreases generally with an increase in the convergence angle. Interestingly, the uniform microchannel presents a higher heat transfer coefficient in both mist/annular flow and injection flow regions than those in the converging microchannels with convergence angles from 0.5° to 1.5° . As indicated earlier, the injection flow takes place in a much downstream location as the convergence angle increases; much more steam has been condensed in the mist/annular flow region and the liquid film formed may be thicker. Consequently, the local heat transfer coefficient in the mist/annular flow region decreases with an increase in the convergence angle. However, the mean condensation heat flux in the converging microchannel increases with an increase in the convergence angle. This can be understood by rewriting (9) as

$$q_t = h_1 A_1 (T_{\text{sat},1} - T_{\text{ch},1}) + h_2 A_2 (T_{\text{sat},2} - T_{\text{ch},2}) + h_3 A_3 (T_{\text{sat},3} - T_{\text{ch},3}) \quad (10)$$

The condensation heat transfer rate is primarily influenced by the product of heat transfer coefficient and area in the mist/annular flow region. Although the heat transfer coefficient decreases with an increase in the convergence angle, the heat transfer area increases more significantly with an increase in the convergence angle. This explains why the condensation heat transfer rate and, therefore, the mean condensation heat flux increase with an increase in the convergence angle.

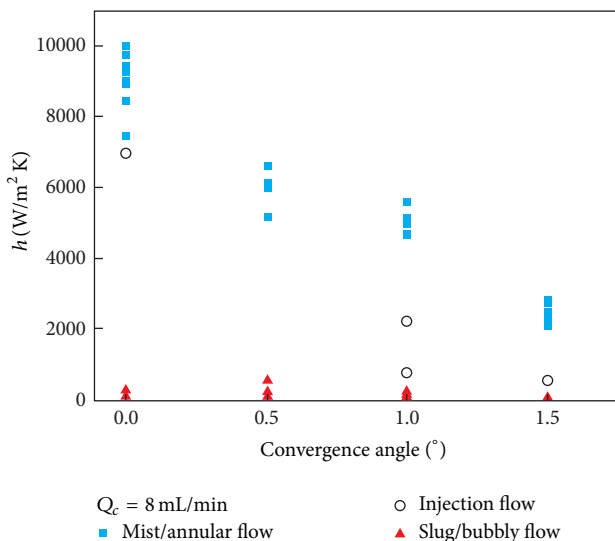


FIGURE 11: Local condensation heat transfer coefficient as a function of convergence angle for different flow regimes. Data of $\beta = 0^\circ$ are from Kuo and Pan [15].

5. Conclusions

This work experimentally investigates the effect of convergence angle of microchannel on two-phase flow and heat transfer during steam condensation. Three convergence angles (0.5° , 1.0° , and 1.5°) of microchannel with the same mean hydraulic diameter of $135\text{ }\mu\text{m}$ are studied. Flow visualization is conducted using a high-speed digital camera. Three condensation regimes, namely, mist/annular flow, injection flow, and slug/bubbly flow can be identified. Flow pattern maps are constructed using coordinates of superficial vapor and liquid velocities, wherein relatively distinct boundaries between the flow patterns are identified. The experimental results show that the condensation heat flux increases with an increase in the convergence angle and/or the steam mass flux at a given coolant flow rate but decreases with an increase in the coolant flow rate at a given steam mass flux. The results further demonstrate that the local condensation heat transfer coefficient in the mist/annular flow region is much higher than that in other condensation regimes. Moreover, the local condensation heat transfer coefficient in the microchannel with a convergence angle of 0.5° is larger than that in the microchannel with a bigger convergence angle under the condition of the same condensation regime.

Nomenclature

A: Condensation heat transfer area (m^2)
 Co: Condensation number (—)
 c_p : Specific heat ($\text{kJ}/\text{kg K}$)
 D_h : Mean hydraulic diameter of a channel (m)
 H: Channel depth (m)
 h: Heat transfer coefficient ($\text{kW}/\text{m}^2 \text{ K}$)
 i_{LV} : Latent heat of vaporization (kJ/kg)
 j: Superficial velocity (m/s)

L: Channel length (m)
 m_c : Mass flow rate of coolant (kg/s)
 m_s : Mass flow rate of steam (kg/s)
 q: Condensation heat transfer rate (W)
 q'' : Condensation heat flux (kW/m^2)
 Q_c : Coolant flow rate (mL/min)
 R'' : Total thermal resistances for conduction through the silicon and silicon dioxide ($\text{m}^2 \text{ K}/\text{W}$)
 Re: Reynolds number (—)
 T: Temperature (K or $^\circ\text{C}$)
 W: Channel width (m)
 x: Quality (—)
 z: Axial distance from the channel inlet (m).

Greek Symbols

α : Void fraction (—)
 β : Convergence angle of a channel ($^\circ$)
 ρ : Density (kg/m^3).

Subscripts

1: Mist/annular flow region
 2: Injection flow region
 3: Slug/bubbly flow region
 c: Coolant or forced convection
 ch: Channel
 h: Homogeneous
 in: Inlet
 L: Liquid
 out: Outlet
 sat: Saturation
 t: Total
 V: Vapor
 w: Wall
 z: Distance from channel inlet in the axial direction.

Acknowledgments

This work was supported by the National Science Council of Taiwan under the contract no. NSC 100-2221-E-007-112-MY3, and Ben-Ran Fu would like to express gratitude to Geothermal Technology Department at Industrial Technology Research Institute. This work is reconstructed based on a proceeding paper presented at the *8th International Symposium on Heat Transfer*, October 21–24, 2012, Beijing, China.

References

- [1] H. Y. Wu and P. Cheng, "Condensation flow patterns in silicon microchannels," *International Journal of Heat and Mass Transfer*, vol. 48, no. 11, pp. 2186–2197, 2005.
- [2] H. Wu, M. Yu, P. Cheng, and X. Wu, "Injection flow during steam condensation in silicon microchannels," *Journal of*

Micromechanics and Microengineering, vol. 17, no. 8, article 027, pp. 1618–1627, 2007.

[3] X. Quan, P. Cheng, and H. Wu, “Transition from annular flow to plug/slug flow in condensation of steam in microchannels,” *International Journal of Heat and Mass Transfer*, vol. 51, no. 3-4, pp. 707–716, 2008.

[4] H. Wu, X. Wu, J. Qu, and M. Yu, “Condensation heat transfer and flow friction in silicon microchannels,” *Journal of Micromechanics and Microengineering*, vol. 18, no. 11, Article ID 115024, 2008.

[5] Y. Chen, R. Wu, M. Shi, J. Wu, and G. P. Peterson, “Visualization study of steam condensation in triangular microchannels,” *International Journal of Heat and Mass Transfer*, vol. 52, no. 21–22, pp. 5122–5129, 2009.

[6] J. Wu, M. Shi, Y. Chen, and X. Li, “Visualization study of steam condensation in wide rectangular silicon microchannels,” *International Journal of Thermal Sciences*, vol. 49, no. 6, pp. 922–930, 2010.

[7] A. Agarwal, T. M. Bandhauer, and S. Garimella, “Measurement and modeling of condensation heat transfer in non-circular microchannels,” *International Journal of Refrigeration*, vol. 33, no. 6, pp. 1169–1179, 2010.

[8] X. Ma, X. Fan, Z. Lan, and T. Hao, “Flow patterns and transition characteristics for steam condensation in silicon microchannels,” *Journal of Micromechanics and Microengineering*, vol. 21, no. 7, Article ID 075009, 2011.

[9] C. Fang, J. E. Steinbrenner, F.-M. Wang, and K. E. Goodson, “Impact of wall hydrophobicity on condensation flow and heat transfer in silicon microchannels,” *Journal of Micromechanics and Microengineering*, vol. 20, no. 4, Article ID 045018, 2010.

[10] A. Odaymet and H. Louahlia-Gualous, “Experimental study of slug flow for condensation in a single square microchannel,” *Experimental Thermal and Fluid Science*, vol. 38, pp. 1–13, 2012.

[11] A. Odaymet, H. Louahlia-Gualous, and M. De Labachelerie, “Local heat transfer and flow patterns during condensation in a single silicon microchannel,” *Nanoscale and Microscale Thermophysical Engineering*, vol. 16, pp. 220–241, 2012.

[12] S.-M. Kim, J. Kim, and I. Mudawar, “Flow condensation in parallel micro-channels—part 1: experimental results and assessment of pressure drop correlations,” *International Journal of Heat and Mass Transfer*, vol. 55, no. 4, pp. 971–983, 2012.

[13] S.-M. Kim and I. Mudawar, “Flow condensation in parallel micro-channels—part 2: heat transfer results and correlation technique,” *International Journal of Heat and Mass Transfer*, vol. 55, no. 4, pp. 984–994, 2012.

[14] C. Y. Kuo and C. Pan, “The effect of cross-section design of rectangular microchannels on convective steam condensation,” *Journal of Micromechanics and Microengineering*, vol. 19, no. 3, Article ID 035017, 2009.

[15] C. Y. Kuo and C. Pan, “Two-phase flow pressure drop and heat transfer during condensation in microchannels with uniform and converging cross-sections,” *Journal of Micromechanics and Microengineering*, vol. 20, no. 9, Article ID 095001, 2010.

[16] J. J. Hwang, F. G. Tseng, and C. Pan, “Ethanol-CO₂ two-phase flow in diverging and converging microchannels,” *International Journal of Multiphase Flow*, vol. 31, no. 5, pp. 548–570, 2005.

[17] R. J. Moffat, “Describing the uncertainties in experimental results,” *Experimental Thermal and Fluid Science*, vol. 1, no. 1, pp. 3–17, 1988.

[18] B. R. Fu, F. G. Tseng, and C. Pan, “Two-phase flow in converging and diverging microchannels with CO₂ bubbles produced by chemical reactions,” *International Journal of Heat and Mass Transfer*, vol. 50, no. 1-2, pp. 1–14, 2007.

[19] A. Kawahara, P.-Y. Chung, and M. Kawaji, “Investigation of two-phase flow pattern, void fraction and pressure drop in a microchannel,” *International Journal of Multiphase Flow*, vol. 28, no. 9, pp. 1411–1435, 2002.

Research Article

Computational Analysis of Droplet Mass and Size Effect on Mist/Air Impingement Cooling Performance

Zhenglei Yu, Tao Xu, Junlou Li, Tianshuang Xu, and Tatsuo Yoshino

College of Mechanical Science & Engineering, Jilin University, Changchun 130025, China

Correspondence should be addressed to Tatsuo Yoshino; yoshinojlu@sina.com

Received 14 June 2013; Accepted 20 August 2013

Academic Editor: Godson Asirvatham Lazarus

Copyright © 2013 Zhenglei Yu et al. This is an open access article distributed under the Creative Commons Attribution License, which permits unrestricted use, distribution, and reproduction in any medium, provided the original work is properly cited.

Impingement cooling has been widely employed to cool gas turbine hot components such as combustor liners, combustor transition pieces, turbine vanes, and blades. A promising technology is proposed to enhance impingement cooling with water droplets injection. However, previous studies were conducted on blade shower head film cooling, and less attention was given to the transition piece cooling. As a continuous effort to develop a realistic mist impingement cooling scheme, this paper focuses on simulating mist impingement cooling under typical gas turbine operating conditions of high temperature and pressure in a double chamber model. Furthermore, the paper presents the effect of cooling effectiveness by changing the mass and size of the droplets. Based on the heat-mass transfer analogy, the results of these experiments prove that the mass of $3E-3$ kg/s droplets with diameters of $5-35\text{ }\mu\text{m}$ could enhance 90% cooling effectiveness and reduce 122 K of wall temperature. The results of this paper can provide guidance for corresponding experiments and serve as the qualification reference for future more complicated studies with convex surface cooling.

1. Introduction

Efficiency is one of the most important parameters in evaluating the performance of a gas turbine engine. With even a 1% efficiency increase, the operating costs can be substantially reduced over the life of a typical power plant. One of the most effective ways to improve the gas turbine system efficiency is to increase the combustor outlet temperature. A higher outlet temperature leads to better system thermodynamic efficiency. However, outlet temperature is limited by the highest temperature that the material of the gas turbine can withstand. Spontaneously, we need to consider the efficiency of cooling technology which plays a significant role in the whole process as the more efficiency it applied, the higher temperature of combustor could exit and the efficiency of gas turbine cycle could reach. Cooling technology has been successfully applied in protecting turbine airfoils from high temperature since the last half century [1, 2]. The majority of the literature has been covered in the book by Han et al. [3]. Such that most of these studies concentrate on blade shower head film cooling; however, less attention is given to the transform piece cooling [4]. As one of most important cooling technology, impingement cooling has been studied on transform piece cooling.

The early investigation on impingement cooling has been summarized by Chupp et al. [5]. They did experimental study on impingement of a single row of circular jets on semicircular concave surface. Their results suggested general increases in heat transfer with approximately the 0.7 power of jet Reynolds number. Dyban and Mazur [6] measured heat transfer coefficient on a parabolic concave surface and investigated the effect of jet flow passage curvature. McCormack et al. [7] found that Nusselt numbers were increased by 100–150% on the concave surface. Hrycak [8] proposed correlations for stagnation and average heat transfer coefficient for a row of impinging jets on a cylindrical concave surface. Wei et al. [9] investigated impingement and serpentine convection cooling under the effect of rotation. Their results suggested that rotation effects increase the serpentine cooling and reduce the jet impingement cooling.

As the working gas temperature continuously increases to augment thermal efficiency, new cooling techniques are needed to surpass incremental improvements of conventional gas turbine cooling technologies. A promising technology is to enhance film cooling with mist (small water droplets) injection. Based on the aforementioned heat transfer mechanisms, mist can be used in gas turbine systems in different

ways, including gas turbine inlet air fog cooling [10], overspray cooling through wet compression in the compressor [11], and airfoils (vanes and blades) internal cooling [12–16]. Recently, Li and Wang [17] conducted the first numerical simulations of air/mist film cooling. They showed that injecting a small amount of droplets (2% of the coolant flow rate) could enhance the cooling effectiveness about 30–50%. Li and Wang [18] continued a more fundamental study on investigating the effect of various models on the computational results including the turbulence models, dispersed phase modeling, different forces models (Saffman, thermophoresis, and Brownian), trajectory tracking model, near-wall grid arrangement, and mist injection scheme.

As a continuous effort to develop a realistic impingement cooling scheme, this paper focuses on using a promising technology to enhance impingement cooling which is to inject water mist into the coolant flow. The main objective of this thesis is to elucidate how the mass and dimension of the droplet affect the mist impingement cooling performance over a curved surface with a hole of double chamber model, calculated by CFD. Earlier studies discussed the mist film performance on the blade and combustor of gas turbine [10–15]. The model created in the paper looks like a flat with two double chambers, simulating the structure of transition piece. Accordingly, the main objectives of the investigation are as follow: (1) model establishment: discrete-hole impingement cooling flat surface with an injection coolant intercalation; (2) model analysis: the droplet mass ratio and dimension on mist impingement cooling effectiveness over a flat surface; (3) results comparison: the temperature of inner wall, film cooling effectiveness, velocity magnitude contours, and droplet particle track in various conditions. The results of this paper can serve as a reference for future experimental validation and technical implementation to real gas turbine applications.

2. Numerical Method

The new transition piece features a rounded body shape that balances the heat transfer loading both internally and externally and eliminates resonant frequency concerns [19], which consists of heavier walls, single-piece aft ends, ribs, seal arrangements, and selective cooling. It has an upstream aperture for the gas flow (which is cylindrical), and it is used to receive the gas flow directly from the corresponding combustion liners with a high level of enthalpy; transition pieces are conjured in a longitudinal direction so that their downstream ends comprise arched segments to form a ring-type configuration which opens toward the first stage of the gas turbine (stator) [20, 21].

A schematic of the flow domain along with boundary conditions and dimensions is given in Figure 1. As shown in the figure, the flat model has two chambers with length of 1050 mm, and the outer and inner height is 38 mm and 162 mm, respectively. The outer chamber in Figure 1 is called coolant chamber as the side is closed. Contrarily, the inner chamber goes by the name of mainstream chamber as the gas could pass through it from one side to another. There is a hole on the surface of the outer wall, and the distance from the hole to the end of the model is 520 mm. The size of all the holes is about 10.26 mm.

2.1. Turbulence Model (Realizable k - ε). The present film cooling study involves flow which is steady, Newtonian, three-dimensional, incompressible, and turbulent. Such flow behaves according to three fundamental laws, namely, the laws of continuity, conservation of momentum, and conservation of energy.

The realizable k - ε model proposed by Shih et al. [22] was intended to address these deficiencies of standard k - ε models by adopting the following: (1) realizable k - ε model contains a new formulation for the turbulent viscosity; and (2) a new transport equation for the dissipation rate, ε , is derived from an exact equation for the transport of the mean square velocity fluctuation. The modeled transport equations for k and ε in the realizable k - ε model are

$$\begin{aligned} \frac{\partial}{\partial x_i} (\rho k u_i) &= \frac{\partial}{\partial x_j} \left[\left(\mu + \frac{\mu_t}{\sigma_k} \right) \frac{\partial k}{\partial x_j} \right] \\ &\quad + G_k + G_b - \rho \varepsilon - Y_M + S_k, \\ \frac{\partial}{\partial x_i} (\rho \varepsilon u_i) &= \frac{\partial}{\partial x_j} \left[\left(\mu + \frac{\mu_t}{\sigma_\varepsilon} \right) \frac{\partial \varepsilon}{\partial x_j} \right] \\ &\quad + \rho C_1 S_\varepsilon - \rho C_2 \frac{\varepsilon^2}{k + \sqrt{v \varepsilon}} - C_{1\varepsilon} \frac{\varepsilon}{k} C_{3\varepsilon} G_b + S_\varepsilon, \end{aligned} \quad (1)$$

where

$$C_1 = \max \left[0.43, \frac{\eta}{\eta + 5} \right], \quad \eta = S \frac{\varepsilon}{k}, \quad S = \sqrt{2S_{ij}S_{ij}}. \quad (2)$$

In these equations, G_k and G_b represent the generation of turbulent kinetic energy due to the mean velocity gradients and buoyancy, respectively. Y_M is the contribution of the fluctuating dilatation in compressible turbulence to the overall dissipation rate, and $C_{1\varepsilon}$ and C_2 are constants. S_k and S_ε are user-defined source terms. The turbulent (or eddy) viscosity μ_t is computed by combining k and ε as follows:

$$\mu_t = \frac{\rho C_\mu k^2}{\varepsilon}. \quad (3)$$

A benefit of the realizable k - ε model is that it better predicts the spreading rate of both planar and round jets. It is also stated that it has superior performance for flows involving rotation, separation, recirculation, and boundary layers under adverse pressure gradients.

2.2. Stochastic Particle Tracking. To track the trajectory of droplets, the hydrodynamic drag, gravity, and forces such as the “virtual mass” force, thermophoretic force, Brownian force, and Saffman’s lift force are combined to accelerate the droplet. The energy equation for any individual droplet can be given as the following equation:

$$m_p c_p \frac{dT}{dt} = \pi d^2 h (T_\infty - T) + \frac{dm_p}{dt} h_{fg}, \quad (4)$$

where h_{fg} is the latent heat. The convective heat transfer coefficient (h) can be obtained with an empirical correlation [23, 24].

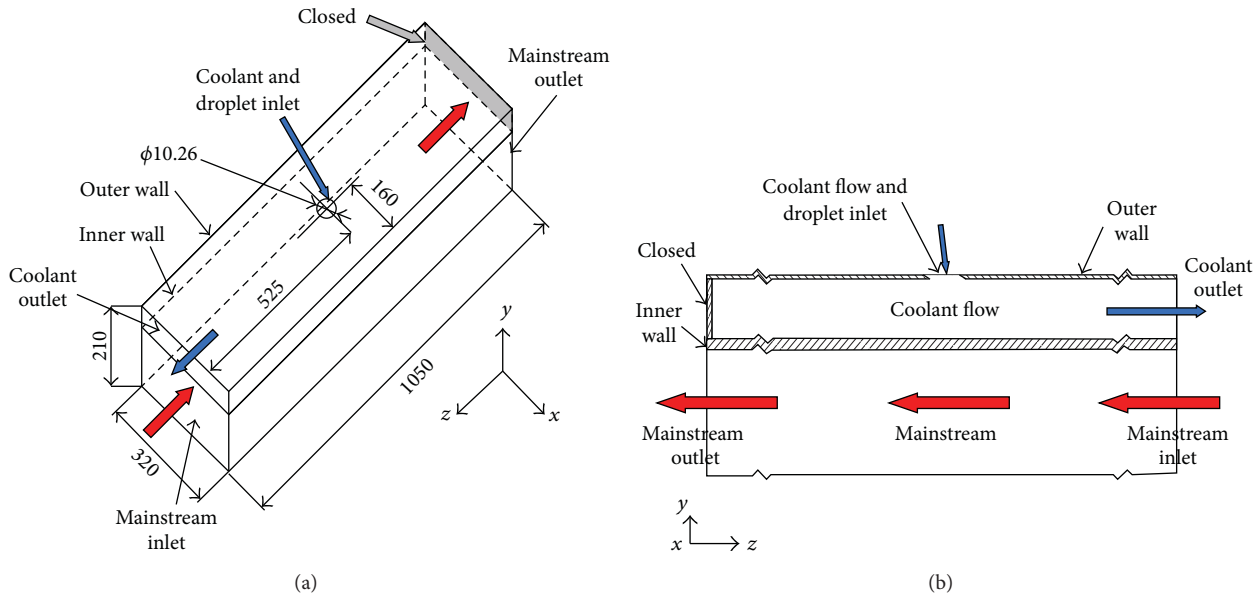


FIGURE 1: Computational domain showing boundary conditions.

The mass change rate or vaporization rate in (4) is governed by concentration difference between droplet surface and the air stream:

$$-\frac{dm_p}{dt} = \pi d^2 k_c (C_s - C_\infty), \quad (5)$$

where k_c is the mass transfer coefficient and C_s is the vapor concentration at the droplet surface, which is evaluated by assuming that the flow over the surface is saturated. C_∞ is the vapor concentration of the bulk flow, obtained by solving the transport equations. When the droplet temperature reaches the boiling point, the following equation can be used to evaluate its evaporation rate [25]:

$$-\frac{dm_p}{dt} = \pi d^2 \left(\frac{\lambda}{d} \right) (2.0 + 0.46 \text{Re}_d^{0.5}) \times \frac{\ln (1 + c_p (T_\infty - T) / h_{fg})}{c_p}, \quad (6)$$

where λ is the gas/air heat conductivity and c_p is the specific heat of the bulk flow.

Stochastic method [26] is used to consider turbulence dispersion effect on droplets tracking. The droplet trajectories are calculated with the instantaneous flow velocity ($\bar{u} + u'$), and the velocity fluctuations are then given as

$$u' = \zeta \left(\bar{u}^2 \right)^{0.5} = \zeta \left(\frac{2k}{3} \right)^{0.5}, \quad (7)$$

where ζ is a normally distributed random number. This velocity will apply during the characteristic lifetime of the eddy (t_e), a time scale calculated from the turbulence kinetic energy, and dissipation rate. After this time period, the instantaneous velocity will be updated with a new ζ value until a full trajectory is obtained.

2.3. Boundary Conditions. Boundary conditions were applied to specific faces within the domain to specify the flow and thermal variables that dictate conditions within the model. They are a critical constituent to the simulation, and it is important that they are specified appropriately. The masses of water droplets are 0, $3E - 6$, $3E - 5$, $3E - 4$, and $3E - 3$ kg/s. The droplet size is given as 5, 15, 25, 35, 45, and $55 \mu\text{m}$.

Figure 1(a) also shows the boundary conditions used for the modeling. Respectively, the cooling air and gas are coursing along the cooling chamber and the mainstream chamber with the opposite direction. In the cooling chamber, the simulation is performed using air as the cooling flow; velocity and temperature contours are set on the jet holes, and then out from the exit mouth. In another chamber, assume that the mainstream is a mixture of O_2 , H_2O , CO_2 , N_2 , and some rare gas. Gas velocity and temperature contours are set on the surface of the sector section; pressure on the exit mouth and natural convection on the outside wall of the model are considered as boundary condition (Table 1) [4]. In gas chamber, egress of the mainstream was fixed and exported free expansion. The assumption of the solid wall of the quarter torus is modeled with a hypothesis of negligible thermal resistance by conduction; the thermal properties of the material were considered by Nimonic 263. The temperature of the coolant and mainstream flow are set as 300 K and 1300 K, respectively.

2.4. Mesh and Simulation Procedures. The computational domain incorporates the model, the HEXA mesh in the software, ICEM/CFD, used to generate the structured multi-block and the body-fitted grid system. This software allows to separate grids generated for different parts of the flow domain, using an appropriate grid system. In this study, the grid system associated with the parts of the mainstream and the coolant supply plenum is H-type. Figure 2 shows the grids

TABLE 1: Boundary conditions.

Component	Boundary conditions	Magnitude
Mainstream inlet	Mass flux rate	31.46 [kg/s]
	Gas temperature	1300 [K]
	Turbulent intensity	5 [%]
	Hydraulic diameter	0.324 [m]
Mainstream outlet	Pressure	1.512 [MPa]
	Turbulent intensity	5 [%]
	Hydraulic diameter	0.324 [m]
	Convection coefficient	10 [W/m ² K]
Coolant chamber	Air temperature	300 [K]
	Pressure	1.4552 [MPa]
	Pressure recovery coefficient	0.95
	Turbulent intensity	5 [%]
Droplet	Hydraulic diameter	0.01026 [m]
	Velocity	0 [m/s]
	Mass	3E - 3, 3E - 4, 3E - 5, and 3E - 6 [kg/s]
	Size	5, 10, 15, 20, 50, and 75 [μm]

of the computational domain. The total number of the cells for the 3D domain is 198,068.

This study uses a commercial CFD code based on the control-volume method, ANSYS-FLUENT 12.0.16, which in order to predict temperature, cooling effectiveness, velocity fields, and droplet particle track at different droplet mass and size. All runs were made on a PC cluster with four Pentium-4 2.8 GHz personal computers. The convergence criteria of the steady-state solution are judged by the reduction in the mass residual by a factor of 6, typically, in 2000 iterations.

3. Result and Discussion

In this section, the results obtained with a different mass ratio and dimension of droplet are presented in order to validate the CFD model above so that the mist impingement cooling physics would be well studied.

3.1. Effect of Droplet Mass. Comparison of the temperature and cooling effectiveness results of four droplet masses (3E - 3, 3E - 4, 3E - 5, and 3E - 6 kg/s) is shown in Figure 3. In this condition, the size of all droplets is 5 μm. Similar to the results under high pressure and temperature conditions [4], the heavier droplets are shown to provide better enhancements. The figure illustrates that the temperature at the starting point of the wall is high, and then it starts to go down. The starting point is cooled by the coolant holes at the Z = 525 mm on the outer wall, while the same temperature is maintained throughout the coolant hole. With the droplet mass increase, the color of temperature distribution in the same region becomes lighter which indicates that the surface has been better protected by the coolant flow. Since the jet flow seems to possess sufficient capacity to receive more mist flow, it is

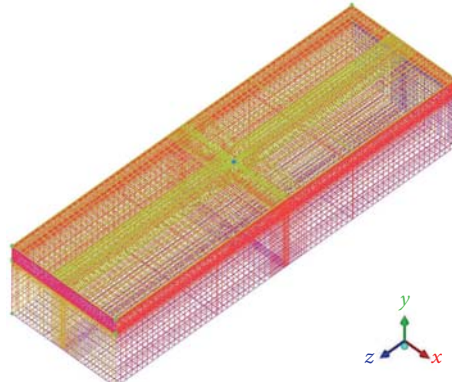


FIGURE 2: Mesh.

interesting to see the effect of injecting more mist into the jet flow.

The adiabatic cooling effectiveness (η) is used to examine the performance of film cooling. The definition of η is

$$\eta = \frac{T_g - T_{aw}}{T_m - T_c}, \quad (8)$$

where T_g is the mainstream hot gas inlet temperature, which is a fixed value for calculation of the adiabatic cooling effectiveness of any location, and T_c is the temperature of the coolant, which is assigned as a constant of 300 K in this issue. T_{aw} is the adiabatic wall temperature.

The cooling effectiveness is defined the same as it was in the previous section. To evaluate the cooling enhancement of adding mist into the air film, the net enhancement is plotted on the secondary y -axis on the right-hand side. The net enhancement is defined as follows:

$$\text{Net Enhancement} = \frac{(\eta_m - \eta)}{\eta}. \quad (9)$$

The subscript “ m ” means mist is added. Without any subscript, it means air-only film is used. From the definition, net enhancement is zero if the mist cooling effectiveness is the same as the air-only cooling effectiveness. Note that mist film cooling itself can be improved by using different droplet masses. Figure 4 shows the cooling effectiveness and enhancement ratio when different droplet masses are employed. For simplicity, it can be seen that when the droplet mass is 3E - 6 kg/s, the adiabatic cooling effectiveness increases significantly. Compared with the normal case, the cooling effectiveness of MIC provides 90% in axis $Z = 550$ mm. The cooling effectiveness lines are almost the same with no MIC case condition when the droplet mass is 3E - 6, 3E - 5, and 3E - 4 kg/s. Therefore, it is plausible that the temperature and cooling effectiveness contours of lighter mass cases (3E - 6, 3E - 5, and 3E - 4 kg/s) are similar to the no MIC case.

3.2. Effect of Droplet Size. In real applications, the size of droplet is another factor that could affect the mist impingement cooling results. Comparison of the cooling effectiveness

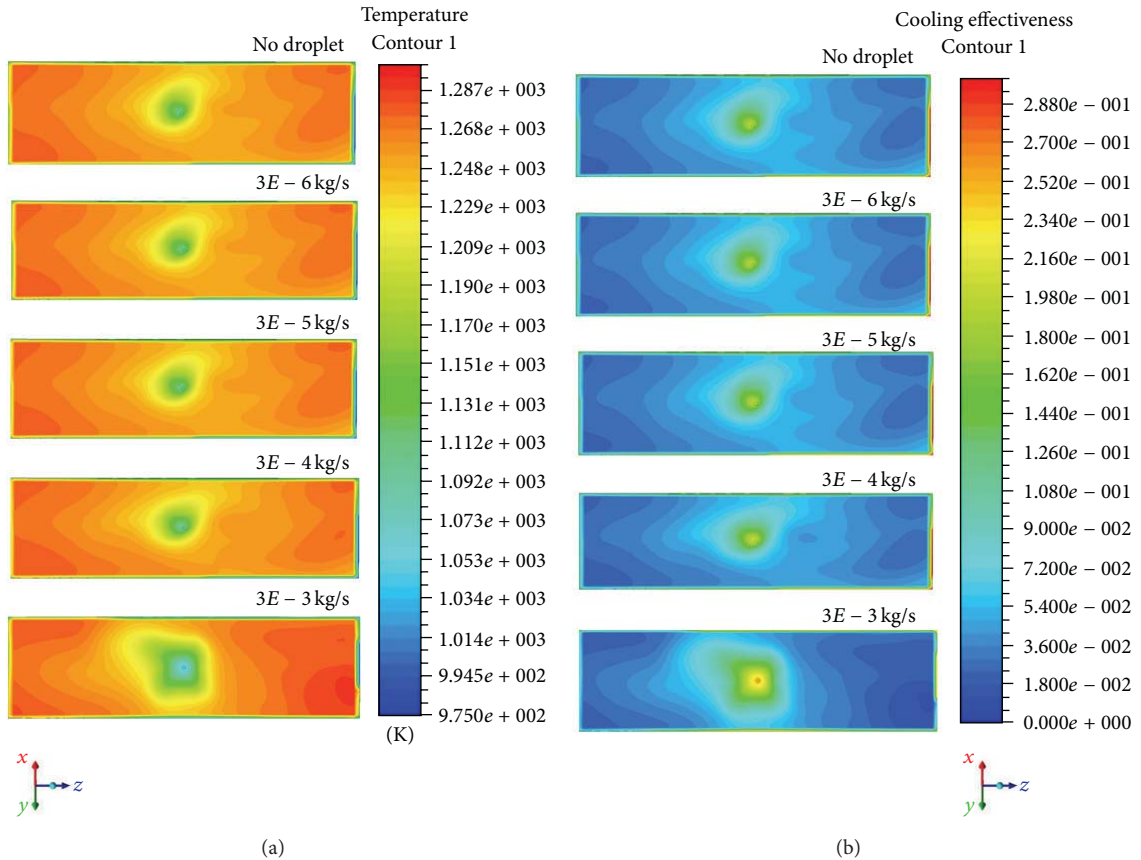


FIGURE 3: Comparative analysis of temperature and cooling effectiveness at different droplet masses (no droplet, $3E - 6$, $3E - 5$, $3E - 4$, and $3E - 3$ kg/s) showing vortex induction towards the inner wall and (a) temperature distribution of inner wall and (b) cooling effectiveness distribution.

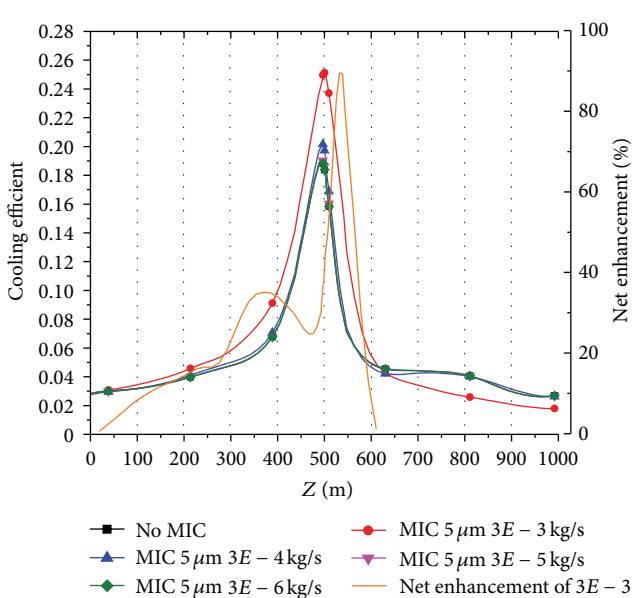


FIGURE 4: Distributions of averaged cooling effectiveness and net enhancement of $3E - 3$ kg/s in the different droplet masses.

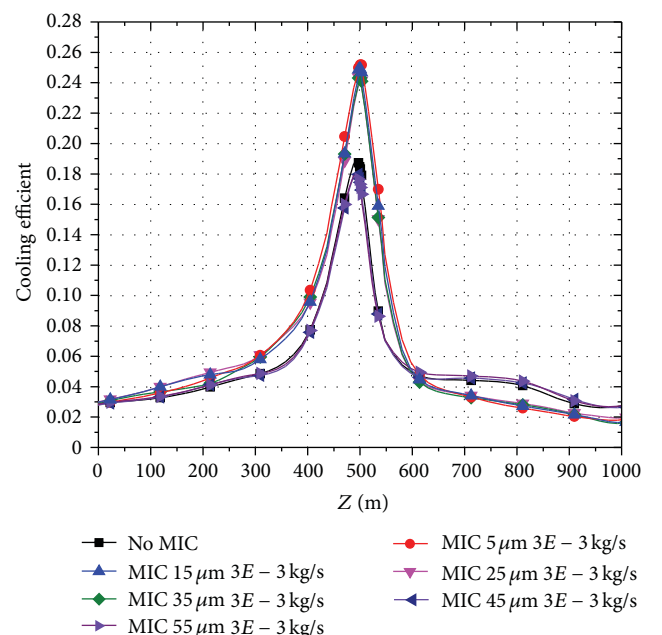


FIGURE 5: Distributions of averaged cooling effectiveness in different sizes with $3E - 3$ kg/s droplet mass.

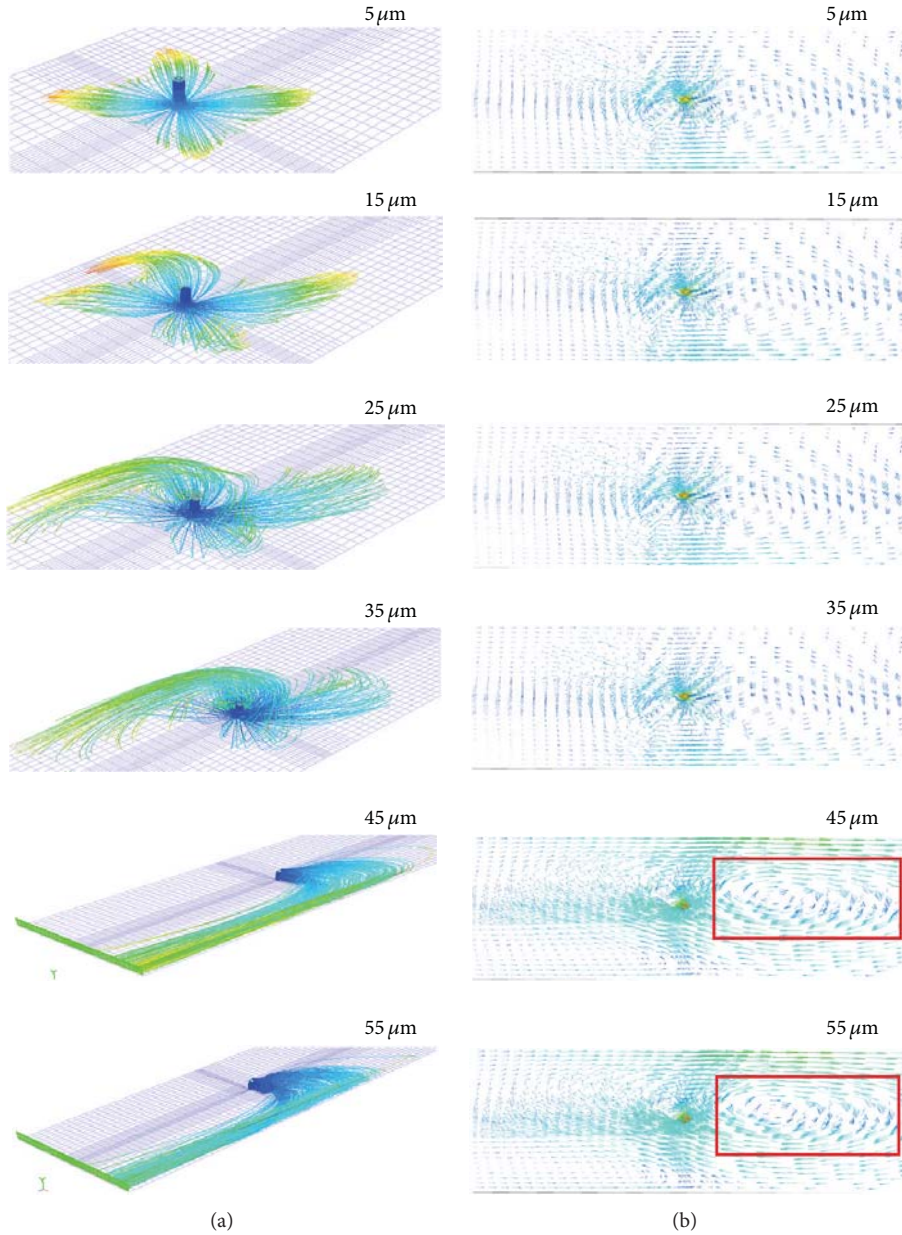


FIGURE 6: Distributions of velocity magnitude contours and droplet particle track in different sizes with $3E-3$ kg/s droplet mass: (a) droplet particle track and (b) velocity vector plot.

in different sizes (5, 15, 25, 35, 45, and 55 μm) with $3E-3$ kg/s droplet mass is shown in Figure 5. In the picture, the cooling effectiveness lines are almost the same when the droplet size is 5, 15, 25, and 35 μm . However, the cooling effectiveness is reduced by increasing the droplet size (45 and 55 μm), and they all have the same trend with the normal case. Before axis $Z = 600$ mm, the smaller droplets are shown to provide better enhancements. The small droplets provide higher surface to volume ratio, so evaporation completes more rapidly and effectively than the larger droplets. The results show that its effect on cooling effectiveness is negligible because the size is found very large (larger than 35 μm) in the currently studied cases.

Figure 6 shows the velocity magnitude contours and the droplet particle track in the different size cases. Figure 6(a) shows that the droplets impact the inner wall, which moved with the coolant jet from the hole. In the small size cases (5, 15, 25, and 35 μm) of Figure 6(a), all the droplets evaporate before axis $Z = 600$ μm in the coolant chamber. However, larger droplets may exit the computational domain without complete evaporation due to low evaporation rate or short residential time. Therefore, it is plausible that the large droplets move farther away from the wall than small droplets under the condition in the current study due to the high inertia force from jet injection. This mechanism of larger droplets moving further away from the wall contributes to

ineffectiveness of producing film cooling protection of the inner wall even though the latent heat absorption can reduce the coolant chamber temperature.

To explain the effect of droplet size on MIC enhancement with flat configuration, velocity vectors at the coolant chamber are plotted and shown in Figure 6(b). The figure shows that the small size cases (5, 15, 25, and 35 μm) jet velocity vectors are much shorter in the coolant chamber than large size cases (45 and 55 μm). The small size cases jet is formed as the impinging jet turning parallel to the surface from the stagnation region. Due to jet-to-jet interaction after impingement, the flow becomes complex with a large 3D recirculation zone in the large size cases. Corresponding to the large recirculation zone, the droplet particle track of the large size cases offsets to one side of coolant chamber.

4. Conclusion

A complete three-dimensional numerical simulation of a mist impingement cooled flat double chamber model is conducted to study coolant structure, and it has been proven that this structure could be influenced by the droplet mass and size. This feature is very favorable in considering applying mist impingement cooling in the transition piece because of the following.

- (i) The liquid droplets in the film provide a more extended impingement cooling coverage effect than the air impingement cooling.
- (ii) Compared with no MIC case, the maximum enhancement of adiabatic cooling effectiveness is about 90% for the $3E - 3 \text{ kg/s}$ droplet mass case, corresponding to an additional adiabatic wall temperature reduction of 122 K.
- (iii) Smaller size droplets (5, 15, 25, and 35 μm) provide 80–90% better cooling performance than larger size droplets (45 and 55 μm).

Nomenclature

D_a : Diameter of coolant chamber
 D_g : Diameter of mainstream chamber
 L : Length of the model
 T : Absolute static temperature
 X, Y, Z : Nondimensional coordinates in diameter, spanwise, and mainstream directions.

Greek Symbols

α : Injection angle
 η : Film cooling effectiveness.

Suffixes

g : Mainstream flow
 c : Coolant flow
 aw : Adiabatic wall
 m : Mist added
 s : Size.

Conflict of Interests

The authors declare that they have no conflict of interests.

Acknowledgments

This research is supported by the Technology Development of Jilin Province (no. 20126001), Key Technologies R&D Program of Changchun (no. 10KZ03), and the National Natural Science Foundation of China (no. 51205159).

References

- [1] R. J. Goldstein, *Advances in Heat Transfer*, Academic Press, New York, USA, 1971.
- [2] R. J. Margason, "Fifty years of jet in cross-flow research," *Computational and Experimental Assessment of Jets in Cross Flow*, vol. 41, pp. 7–34, 1993.
- [3] J. C. Han, S. Dutta, and S. V. Ekkad, *Gas Turbine Heat Transfer and Cooling Technology*, Taylor and Francis, New York, USA, 2000.
- [4] Z. L. Yu, T. Xu, J. L. Li, L. Ma, and T. S. Xu, "Comparison of a series of double chamber model with various hole angles for enhancing cooling effectiveness," *International Communications in Heat and Mass Transfer*, vol. 44, pp. 38–44, 2013.
- [5] R. E. Chupp, H. E. Helms, P. W. McFadden, and T. R. Brown, "Evaluation of internal heat transfer coefficients for impingement cooled turbine airfoils," *Journal of Aircraft*, vol. 6, pp. 203–208, 1969.
- [6] Y. P. Dyban and A. I. Mazur, "Heat transfer from a flat air jet flowing into a concave surface," *Heat Transfer*, vol. 2, pp. 15–22, 1970.
- [7] P. D. McCormack, H. Welker, and M. Keeleher, "Taylor-Goertler vortices and their effect on heat transfer," *ASME Journal of Heat Transfer*, vol. 92, pp. 101–112, 1970.
- [8] P. Hrycak, "Heat transfer from a row of impinging jets to concave cylindrical surfaces," *International Journal of Heat and Mass Transfer*, vol. 24, no. 3, pp. 407–419, 1981.
- [9] H. Wei, D. Chiang, and H. L. Li, "Jet impingement and forced convection cooling experimental study in rotating turbine blades," in *Proceedings of the ASME Turbo Expo 2000 (GT '00)*, Paper No. GT2009-59795, Munich, Germany, May 2000.
- [10] M. Chaker, C. B. Meher-Homji, and T. Mee, "Inlet fogging of gas turbine engines, part A: fog droplet thermodynamics, heat transfer and practical considerations," in *Proceedings of the ASME Turbo Expo 2002 (GT '02)*, pp. 413–428, Amsterdam, The Netherlands, June 2002.
- [11] V. Petr, "Analysis of wet compression in GT's," in *Proceedings of the International Conference on Energy and the Environment (ICEE '03)*, vol. 1, pp. 489–494, Shanghai, China, December 2003.
- [12] T. Guo, T. Wang, and J. L. Gaddis, "Mist/steam cooling in a heated horizontal tube, part 1: experimental system, part 2: results and modeling," *ASME Journal of Turbomachinery*, vol. 122, no. 2, pp. 360–374, 2000.
- [13] T. Guo, T. Wang, and J. L. Gaddis, "Mist/steam cooling in a 180-degree tube bend," *ASME Journal of Heat Transfer*, vol. 122, no. 4, pp. 749–756, 2000.
- [14] X. Li, J. L. Gaddis, and T. Wang, "Mist/steam cooling by a row of impinging jets," *International Journal of Heat and Mass Transfer*, vol. 46, no. 12, pp. 2279–2290, 2003.

- [15] X. Li, J. L. Gaddis, and T. Wang, "Mist/steam heat transfer with jet impingement onto a concave surface," *ASME Journal of Heat Transfer*, vol. 125, no. 3, pp. 438–446, 2003.
- [16] T. Wang and X. Li, "Mist film cooling simulation at gas turbine operating conditions," *International Journal of Heat and Mass Transfer*, vol. 51, no. 21-22, pp. 5305–5317, 2008.
- [17] X. Li and T. Wang, "Simulation of film cooling enhancement with mist injection," *ASME Journal of Heat Transfer*, vol. 128, no. 6, pp. 509–519, 2006.
- [18] X. Li and T. Wang, "Effects of various modeling on mist film cooling," *ASME Journal of Heat Transfer*, vol. 129, no. 4, pp. 472–482, 2007.
- [19] J. Benoit, C. Johnston, and M. Zingg, "Enhancing gas turbine power plant profitability: chronic transition piece and turbine part failures in some 501F gas turbines led to a replacement part redesign," *Power Engineering*, vol. 111, no. 11, pp. 140–144, 2007.
- [20] J. A. Alfaro-Ayala, A. Gallegos-Muñoz, and Z. A. Alejandro, "Thermal and fluid dynamic analysis of the gas turbine transition piece," in *Proceedings of the ASME Turbo Expo 2009: Power for Land, Sea, and Air (GT '09)*, pp. 1387–1396, ASME, Orlando, Fla, USA, June 2009.
- [21] A. Gallegos Muñoz, V. Ayala-Ramírez, J. A. Alfaro-Ayala, and B. M. T. Acosta, "Optimization of the transition piece applying genetic algorithms," *Applied Thermal Engineering*, vol. 31, no. 16, pp. 3214–3225, 2011.
- [22] T. Shih, W. W. Liou, A. Shabbir, Z. Yang, and J. Zhu, "A new κ - ε eddy viscosity model for high reynolds number turbulent flows," *Computers and Fluids*, vol. 24, no. 3, pp. 227–238, 1995.
- [23] W. E. Ranz and W. R. Marshall Jr., "Evaporation from drops, part I," *Chemical Engineering Progress*, vol. 48, pp. 141–146, 1952.
- [24] W. E. Ranz and W. R. Marshall Jr., "Evaporation from drops, part II," *Chemical Engineering Progress*, vol. 48, pp. 173–180, 1952.
- [25] K. Y. Kuo, *Principles of Combustion*, John Wiley and Sons, New York, NY, USA, 1986.
- [26] ANSYS FLUENT 12.1 Documentation, ANSYS Inc.

Research Article

Economic Analysis for Rebuilding of an Aged Pulverized Coal-Fired Boiler with a New Boiler in an Aged Thermal Power Plant

Burhanettin Cetin and Merve Abacioglu

Mechanical Engineering Department, Yildiz Technical University, 34349 Istanbul, Turkey

Correspondence should be addressed to Burhanettin Cetin; cetin@yildiz.edu.tr

Received 25 March 2013; Revised 27 May 2013; Accepted 24 June 2013

Academic Editor: Ahmet Selim Dalkılıç

Copyright © 2013 B. Cetin and M. Abacioglu. This is an open access article distributed under the Creative Commons Attribution License, which permits unrestricted use, distribution, and reproduction in any medium, provided the original work is properly cited.

Fossil-fired thermal power plants (TPPs) produce a significant part of electricity in the world. Because of the aging TPPs and so their equipment (especially boiler), thermal power plants also produce less power than their installed capacities, and there has been power loss in time. This situation affects the supply and demand balance of countries. For this reason, aging equipments such as pulverized coal-fired boiler (PCB) must be renewed and power loss must be recovered, instead of building new TPPs. In this study, economic analysis of rebuilding an aged pulverized coal-fired boiler with a new pulverized coal-fired boiler including flue gas desulfurization (FGD) unit and a circulating fluidized bed boiler (FBB) are investigated in an existing old TPP. Emission costs are also added to model, and the developed model is applied to a 200 MWe pulverized coal-fired thermal power plant in Turkey. As a result, the payback period and the net present value are calculated for different technical and economic parameters such as power loss, load factor, electricity price, discount rate, and escalation rate by using the annual value method. The outcomes of this study show that rebuilding of a pulverized coal-fired boiler with a new one is amortized itself in a very short time.

1. Introduction

Population increment, industrializing, and technologic development result directly in increasing energy consumption. This rapid growing trend brings approximately the very important environmental problems such as air pollution and greenhouse effect. Nowadays, about 80% of electricity in the world is produced from fossil fuel-fired thermal power plants [1–3].

Coal is the most abundant fossil energy resource in the world and exists in almost every major region of the world, but its quality varies greatly from region to region. Coal-fired thermal power plants (TPPs) are the most widely used plants worldwide. Actual electricity production of coal-fired TPPs is 41% of annual world electricity generation, and by 2030 this percentage is expected to rise to 44%. However, many countries use aged pulverized coal-fired boilers (PCBs) (25–40 years) for electricity generation. Moreover, coal (especially poor quality) used in these TPPs for electricity generation

causes crucial environmental problems, such as global warming and acid rain, because the poor quality coal cannot be burned cleanly and efficiently in these boilers and their performance deteriorates. Hence, the thermal efficiency of TPPs is to be lower [1, 4–13].

Although the share of TPPs generating electricity is about 64% within the total installed power in Turkey; its ratio at the compensation of electricity demand is about 75% in 2012. Nowadays, more than 50% of the amount of electricity generated from TPPs is dependent on imported fuel sources, especially natural gas. It is obvious that the main solution of problems like these is efficient utilization of the domestic fuel sources. Therefore, enhancing the performance of the aged coal-fired TPPs is a necessity in terms of energy policy, national security, fuel reserve, and environmental concerns [1, 2, 14–16].

In the present work, firstly, economic analysis of rebuilding an aged pulverized coal-fired boiler (PCB) with a new pulverized coal-fired boiler including flue gas desulfurization

system (FGD) and a circulating fluidized bed boiler (FBB) are examined in an existing old thermal power plant. Secondly, emission costs are added to model, and the developed model is applied to a 200 MWe pulverized coal-fired thermal power plant in Turkey. Thirdly, the payback period and the net present value are calculated for different technical and economic parameters such as power loss, load factor, electricity price, discount rate, and escalation rate by using the annual value method. As a result, the outcomes of this study show that rebuilding of aged pulverized coal-fired boiler is a necessity for aging thermal power plants.

2. The Importance of Rebuilding

Because of the aging thermal power plants (TPPs) and so their equipment, thermal power plants also produce less power than their installed capacities, and there has been power loss in time. For example, boiler is one of the most important equipment in TPPs. Due to the aging of boilers, the problems such as slag and degradation of heat transfer increase and boilers produce less steam than their design values. As a result, TPPs also produce less power than their design values. Developing countries need more power and must build new plants to meet increasing demand. So, countries must recover power loss in aging TPPs, instead of making new investments. Moreover, chronic power shortages and scarcity of capital funds have led many countries to apply them to rebuilding of aging thermal power plants, instead of building new ones, because new power projects go through long environmental assessments and approval processes. Development of infrastructure for these projects, following the approval, also takes considerable time and entails high capital costs, whereas rebuilding of aging TPPs can be done in a relatively short time at a much lower cost. Therefore, TPPs can add more power to grid and benefit from recovering capacity through upgrades of old equipment such as aging boiler. In this connection, upgrading of aged pulverized coal-fired boilers (PCBs) can be one of the urgent needs for many countries because of the economic and environmental pressures [1, 6, 9, 14, 15].

In addition, aged PCBs must deal with both the decreasing quality of fuel and strict environmental standards. Moreover, the performance of these boilers is very bad, and emissions are very high. It is a vital issue to meet the increasing electricity demand and decrease emissions for many countries. Therefore, the rebuilding of aged PCBs with new one can be very important for adding more power to the grid and decreasing emissions.

3. Methodology

In this study, all costs and benefits during the economic lifespan of the system are expressed annually. Then, the payback period and the net present value are calculated for rebuilding of aged pulverized coal boiler (PCB) with a new PCB including flue gas desulfurization (FGD) unit and circulating fluidized bed boiler (FBB).

The rebuilding of aged PCB with a new PCB including flue gas desulfurization unit or a circulating FBB requires

some changes, such as need for more area for FGD unit or replacement of super heaters. In addition, operation and maintenance costs will be different by rebuilding. Also, the thermal power plant is not operated throughout the rebuilding. Therefore, electricity is not sold during the rebuilding. Moreover, the results will change by adding FGD unit, because emissions will decrease. So, emission taxes will decrease. All these factors have been considered in the study. Because the proportion of auxiliary power consumption within total expenditure is very low, it is not taken into consideration in the analysis. Moreover, a similar methodology has been used, and assumptions have been taken as the same for two different technologies except for specific costs. Accordingly, total expenditure (E) and gain (G) can be calculated from (1) and (2), respectively [17–23].

Consider the following:

$$E = (C_I + C_D + C_O) N + R_L \text{ [\$],} \quad (1)$$

$$G = G_E + G_F + G_{EM} \text{ [$/year],} \quad (2)$$

$$R_L = N_o \cdot LF \cdot DP \cdot P_e \text{ [\$],} \quad (3)$$

$$G_E = H \cdot LF \cdot (N - N_o) \cdot P_e \text{ [$/year],} \quad (4)$$

$$G_{EM} = G_{CO_2} + G_{SO_2} + G_{NO_x} \text{ [$/year],} \quad (5)$$

$$G_F = \frac{860 \cdot H \cdot N_o \cdot LF \cdot P_f}{LHV} \cdot \left(\frac{1}{\eta_{tho}} - \frac{1}{\eta_{th}} \right) \text{ [$/year],} \quad (6)$$

where E is the total cost, C_I (\$/kWe) is the specific investment cost for new PCB with FGD, FBB, and auxiliary equipment, C_D (\$/kWe) is the specific cost of dismantling, erection, and commissioning, C_O (\$/kWe) is the specific constant operation and maintenance cost such as employees' salary, R_L is the revenue lost for the downtime period, G is the annual total gain, G_E is the annual additional electricity gain obtained from incremental power production, G_F is the annual additional gain because of fuel savings, G_{EM} is the annual gain due to the decrease in emissions after rebuilding, DP (h) is the downtime period, P_e (\$/kWeh) is the unit electricity price, P_f (\$/kg) is the unit fuel price, LHV (kcal/kg) is the low heat value of fuel, H (h) is the annual average operation duration of the plant, η_{tho} is the thermal efficiency of TPP before rebuilding, η_{th} is the thermal efficiency of TPP after rebuilding, N (kWe) is the installed power of the plant, N_o (kWe) is the operating power before revamping, and LF (%) is the annual average load factor of plant.

Unit emission cost is taken as \$0,22/kgCO₂, \$11/kgSO₂, and \$5,7/kgNO_x for CO₂, SO₂, and NO_x, respectively [17, 19, 20, 22, 23]. Then, annual emission costs are found and added to total gain.

Total expenditure (E) can be converted to annual constant expenditure (E_y) by using amortization factor (AF). Then, payback period (PBP) can be calculated (9). The payback period is the time of equality of the cost and benefit. Therefore, it is calculated with the rate of total annual constant expenditure (E_y) to total annual gain (G). Net present value (NPV) which includes escalation rates for electricity price and fuel price and discount rate can be determined from (10).

TABLE 1: Technical and economic parameters for the case study.

Description	Symbol	Unit	Value
Specific investment cost for FBB and auxiliary equipment	C_I	\$/kWe	220
Specific investment cost for new PCB with FGD and auxiliary equipment	C_I	\$/kWe	200
Specific investment cost for dismantling, erection, and commissioning for FBB rebuilding	C_D	\$/kWe	40
Specific investment cost for dismantling, erection, and commissioning for PCB with FGD rebuilding	C_D	\$/kWe	10
Specific operation and maintenance cost for FBB	C_O	\$/kWe	15
Specific operation and maintenance cost for new PCB with FGD	C_O	\$/kWe	5
Installed power of the plant	N	kWe	200
Existing operating power	N_o	kWe	160
Downtime period	DP	h	720
Load factor	L_f	%	85
Low heat value of fuel (1800 kcal/kg)	LHV	kJ/kg	7535
Thermal efficiency of TPP before revamping	η_{tho}	%	33
Thermal efficiency of TPP after revamping	η_{th}	%	35
Unit electricity price without fuel cost	P_e	\$/kWeh	0.035
Unit fuel price	P_f	\$/kg	0.04
Discount rate	r	%	5
Economic lifespan	n	Year	25

Consider the following:

$$E_y = E \cdot AF \quad [\$/year], \quad (7)$$

$$AF = \frac{(1+r)^n \cdot r}{(1+r)^n - r}, \quad (8)$$

$$PBP = \frac{E_y}{G} \quad [year], \quad (9)$$

$$NPV = \sum_{t=0}^n [B_{(t)} - C_{(t)}] \cdot (1+r)^{-t} \quad [\$], \quad (10)$$

where n (year) is the economic life span, t is the period, and r (%) is the discount rate.

4. Case Study and Discussion

The prior aim of this study is to present a general economic model to evaluate quickly the rebuilding of aged pulverized coal-fired boiler (PCB) with a new one in existing thermal power plants (TPPs). Hence, it can be an important study for the evaluation of aging TPPs for researchers and operators of TPPs. Specific costs such as C_I , C_D , and C_O and technical data for case study have been taken from the literature ([1, 6, 15, 21]), authorities of Turkish Electricity Generation Co., Inc. (EUAS; <http://www.euas.gov.tr/>), and operators of Soma Thermal Power Plant (an institution of EUAS) in Manisa in Turkey. EUAS produces about half of Turkish electricity production, and it is a very important official institution of Turkey. Therefore, they are approximate values for case study. Conclusions of case study depend on these values. Moreover, auxiliary power consumption and boiler efficiency for two firing system are important parameters. Because the proportion of auxiliary power consumption within total expenditures is low and boiler efficiency for two firing system

is very close to each other [6, 12], they are not taken into consideration in the analysis, but more accurate and sensitive solutions can be obtained from the development model by considering real cost values, auxiliary power consumption, and combustion efficiency.

Coal (especially lignite) is an important fuel source for Turkey and it is used mostly for electricity generation. On the basis of the latest estimates, the total lignite reserves of Turkey have reached approximately 11.5 billion ton. However, poor quality lignite (below 2000 kcal/kg) accounts for about 70% of these reserves. Share of better quality lignite (over 3000 kcal/kg) is very low (6%). The other lignite reserve (between 2001 and 3000 kcal/kg) accounts for about 24% [7, 16]. The developed model is applied to a 200 MWe pulverized coal-fired TPP in Turkey. Then, the payback period (PBP) and net present value (NPV) are computed. Coal quality effects PBP and NPV. Coal quality is directly related to lower heating value. The coal used in a 200 MWe thermal power plant example is poor quality coal (lower heating value is 1800 kcal/kg). Therefore, PBP decreases and NPV rises if the coal quality increases. Table 1 taken from the literature shows the technical and economic values for the case study [1, 6, 15, 16].

PBP and net present value NPV can change from country to country. Therefore, the effects of almost all technical and economic parameters, such as power loss, downtime period, escalation rate, and discount rate on PBP and NPV are investigated. As a result, it is seen that power loss has a significant effect on the NPV and PBP. When the power loss increases in the aged pulverized coal-fired TPP, the PBP decreases, and the NPV rises. So, the rebuilding is indispensable if power loss is high in aged pulverized coal-fired TPPs, especially after 30 MWe. NPV and PBP values are closer to each other for FBB and new PCB with FGD system when emission costs are not included (Figures 1 and 2), because TPPs can add more

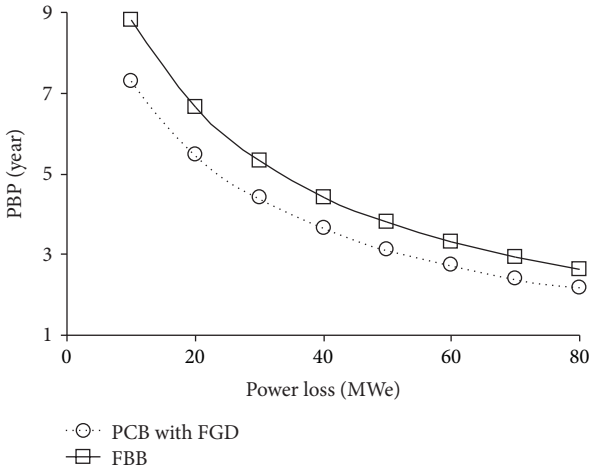


FIGURE 1: The variation of payback period (PBP) with power loss at PCB with FGD and FBB without emission costs.

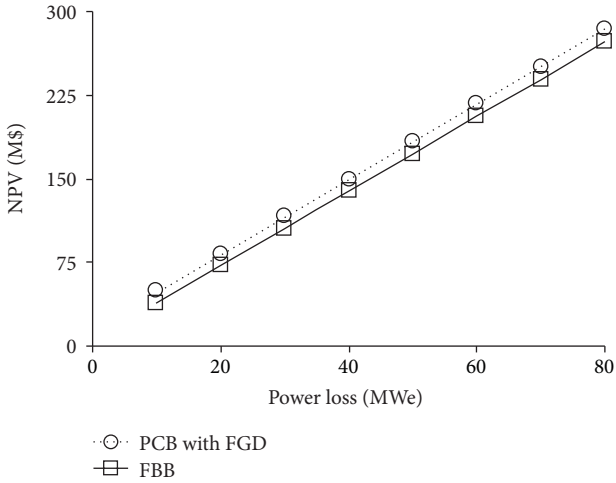


FIGURE 2: The variation of net present value (NPV) with power loss at PCB with FGD and FBB without emission costs.

power to grid and benefit from recovering capacity through upgrades of aging equipment. The other parameters are also investigated in this study. However, their effects are less than power loss effects, so there is no place in this paper.

When the emission costs are added to FBB system, rebuilding is more advantageous (Figures 3 and 4). The results show the necessity of rebuilding with FBB in many countries when the taxes for emissions are engaged in the future. Besides, the results with emission taxes present the necessity of adding an eliminating system, because the PBP is decreasing and the NPV is increasing too much when the emission costs are eliminated. The difference between results includes and excludes emission taxes which are clearly seen from Figures 3 and 4.

Figures 5 and 6 show the variation of the payback period with downtime period and load factor at new PCB with FGD without emission costs, respectively. When the downtime

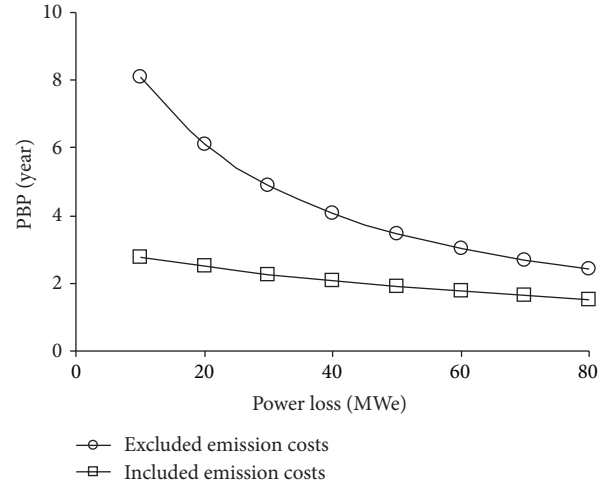


FIGURE 3: The variation of payback period (PBP) with power loss at FBB.

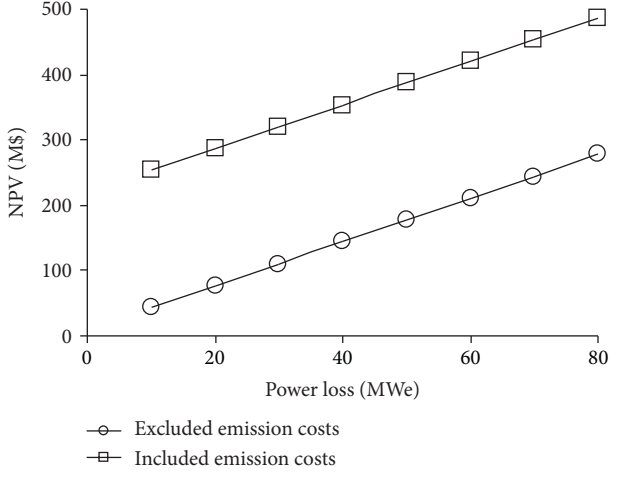


FIGURE 4: The variation of net present value (NPV) with power loss at FBB.

period is decreased and the load factor is increased, payback period is diminished, because after rebuilding, income increases.

5. Conclusions and Suggestions

This study firstly presents a general economic model for the rebuilding of a pulverized coal boiler (PCB) with a new PCB including flue gas desulfurization (FGD) unit and circulating fluidized bed boiler (FBB). Secondly, a case study is performed for a 200 MWe aging pulverized coal-fired thermal power plant (TPP). Finally, the emission taxes are added to the model, and analysis is repeated.

Payback period (PBP) and net present value (NPV) are closer to each other for FBB and new PCB including FGD when emission costs are not included. Of the investigated parameters, power loss has the greatest effect on PBP and NPV. Therefore, if power loss is very high in the existing

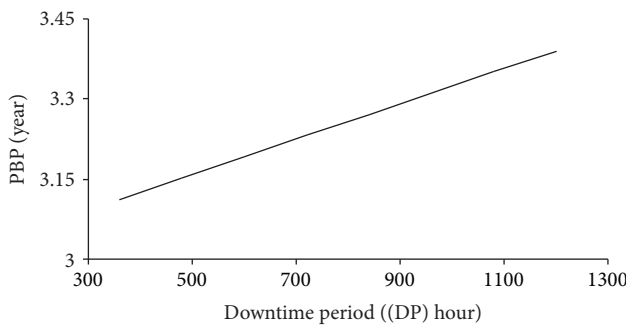


FIGURE 5: The variation of payback period with downtime period at new PCB with FGD without emission costs.

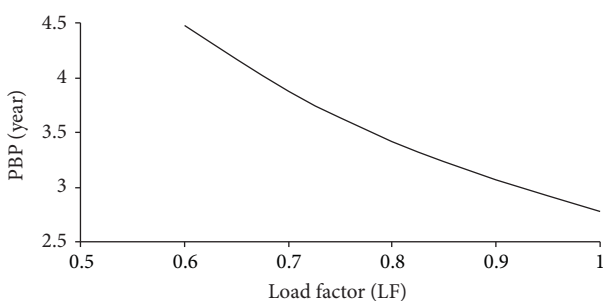


FIGURE 6: The variation of payback period with load factor at new PCB with FGD without emission costs.

TPP, the rebuilding will be very convenient. The more the increase of power loss at the old thermal power plant is, the more advantageous the rebuilding gets, especially after 30 MWe. The results show that the rebuilding of PCB with a new PCB with FGD unit system or FBB system is a cost-effective method, since it is amortized in a very short time.

Moreover, the results show the necessity of rebuilding when the taxes for emissions are engaged in a lot of countries in the future. When the emission costs are added to the model, rebuilding is more advantageous. When the emission taxes are added to the costs, the results are changing very much, the PBP is decreasing and the NPV is increasing too.

The prior aim of this study is to present a general economic model to evaluate quickly rebuilding of aged PCB with a new one in TPPs and to show that rebuilding of a PCB with a new one is a necessity. Technical and economic data in the case study are approximate values. Conclusions of the case study depend on these values. Therefore, more accurate and sensitive solutions can be obtained from the development model by considering real cost values, auxiliary power consumption, and combustion efficiency.

References

- [1] B. Cetin, "Economic model for the revamping of a pulverized coal-fired boiler," *Energy Sources B*. In press.
- [2] H. H. Erdem, A. V. Akkaya, B. Cetin et al., "Comparative energetic and exergetic performance analyses for coal-fired thermal power plants in Turkey," *International Journal of Thermal Sciences*, vol. 48, no. 11, pp. 2179–2186, 2009.
- [3] Ü. Çamdalı and V. S. Ediger, "Optimization of fossil fuel sources: an exergy approach," *Energy Sources A*, vol. 29, no. 3, pp. 251–259, 2007.
- [4] H. H. Erdem, A. Dagdas, S. H. Sevilgen et al., "Thermodynamic analysis of an existing coal-fired power plant for district heating/cooling application," *Applied Thermal Engineering*, vol. 30, no. 2-3, pp. 181–187, 2010.
- [5] B. G. Miller and S. F. Miller, "Fluidized-bed firing systems," in *Combustion Engineering Issues For Solid Fuel Systems*, B. G. Miller and D. A. Tillman, Eds., chapter 8, Elsevier, 2008.
- [6] S. Kavidass, D. J. Walker, and G. S. Norton, "IR-CFB Repowering: a cost-effective option for older pc-fired boilers," in *POWER-GEN International '99*, New Orleans, Lo, USA, December 1999.
- [7] A. Hepbasli, "Coal as an energy source in Turkey," *Energy Sources*, vol. 26, no. 1, pp. 55–63, 2004.
- [8] N. Eskin and A. Hepbasli, "Development and applications of clean coal fluidized bed technology," *Energy Sources A*, vol. 28, no. 12, pp. 1085–1097, 2006.
- [9] P. Basu and P. K. Halder, "New concept for operation of a pulverized coal-fired boiler using circulating fluidized bed firing," *Journal of Engineering for Gas Turbines and Power*, vol. 111, no. 4, pp. 626–630, 1989.
- [10] P. Basu, "Combustion of coal in circulating fluidized-bed boilers: a review," *Chemical Engineering Science*, vol. 54, no. 22, pp. 5547–5557, 1999.
- [11] G. A. Ryabov, O. M. Folomeev, D. S. Litun, D. A. Sankin, and I. G. Dmitryukova, "Prospects for using the technology of circulating fluidized bed for technically refitting Russian thermal power stations," *Thermal Engineering*, vol. 56, no. 1, pp. 31–40, 2009.
- [12] S. Kavidass, G. L. Anderson, and G. S. Norton, "Why build a circulating fluidized bed boiler to generate steam and electric power," in *POWER-GEN Asia '00*, Bangkok, Thailand, September 2000.
- [13] J. Koornneef, M. Junginger, and A. Faaij, "Development of fluidized bed combustion-An overview of trends, performance and cost," *Progress in Energy and Combustion Science*, vol. 33, no. 1, pp. 19–55, 2007.
- [14] P. Basu, "Operation of an existing Pulverized-Coal fired boiler as a circulating fluidized bed boiler—a conceptual study," *Journal of the Institute of Energy*, vol. 60, no. 443, pp. 77–83, 1987.
- [15] M. Abacioglu, *Investigation of a pulverized coal boiler with circulating fluidized bed boiler in an existing thermal power plant* [M.S. thesis], Yildiz Technical University Graduate School of Natural and Applied Science, Istanbul, Turkey, 2012.
- [16] <http://www.euas.gov.tr/Sayfalar/YillikRaporlar.aspx>.
- [17] Å. Karlsson and L. Gustavsson, "External costs and taxes in heat supply systems," *Energy Policy*, vol. 31, no. 14, pp. 1541–1560, 2003.
- [18] T. Berntsson, *Heat Sources-Technology, Economy and Environment*, Department of Heat & Power Technology. Chalmers University of Technology, Göteborg, Sweden, 1999.
- [19] J. Sjödin, "Modelling the impact of energy taxation," *International Journal of Energy Research*, vol. 26, no. 6, pp. 475–494, 2002.
- [20] T. Hamacher, R. M. Sáez, K. Aquilonius et al., "A comprehensive evaluation of the environmental external costs of a fusion power plant," *Fusion Engineering and Design*, vol. 56-57, pp. 95–103, 2001.

- [21] B. Sahin and N. Aybers, *Energy Cost*, Yildiz Technical University Press, Istanbul, Turkey, 1995.
- [22] E. Fahlén and E. O. Ahlgren, "Accounting for external costs in a study of a Swedish district-heating system—an assessment of environmental policies," *Energy Policy*, vol. 38, no. 9, pp. 4909–4920, 2010.
- [23] T. Kosugi, K. Tokimatsu, A. Kurosawa, N. Itsubo, H. Yagita, and M. Sakagami, "Internalization of the external costs of global environmental damage in an integrated assessment model," *Energy Policy*, vol. 37, no. 7, pp. 2664–2678, 2009.

Research Article

Simulation and Experimental Investigation of Thermal Performance of a Miniature Flat Plate Heat Pipe

R. Boukhanouf¹ and A. Haddad²

¹ Department of the Built Environment, University of Nottingham, Nottingham NG7 2RD, UK

² FrigoDynamics GmbH, Bahnhofstraße 16, 85570 Markt Schwaben, Germany

Correspondence should be addressed to R. Boukhanouf; rabah.boukhanouf@nottingham.ac.uk

Received 4 February 2013; Accepted 25 March 2013

Academic Editor: Godson Asirvatham Lazarus

Copyright © 2013 R. Boukhanouf and A. Haddad. This is an open access article distributed under the Creative Commons Attribution License, which permits unrestricted use, distribution, and reproduction in any medium, provided the original work is properly cited.

This paper presents the results of a CFD analysis and experimental tests of two identical miniature flat plate heat pipes (FPHP) using sintered and screen mesh wicks and a comparative analysis and measurement of two solid copper base plates 1 mm and 3 mm thick. It was shown that the design of the miniature FPHP with sintered wick would achieve the specific temperature gradients threshold for heat dissipation rates of up to 80 W. The experimental results also revealed that for localised heat sources of up to 40 W, a solid copper base plate 3 mm thick would have comparable heat transfer performances to that of the sintered wick FPHP. In addition, a marginal effect on the thermal performance of the sintered wick FPHP was recorded when its orientation was held at 0°, 90°, and 180° and for heat dissipation rates ranging from 0 to 100 W.

1. Introduction

Conventional heat sink-fan air coolers in electronics packages are becoming inadequate for use in faster, compact, and more powerful multitasked microprocessors that generate large quantities of attendant heat. This has led current research to focus on high-performance and compact thermal solutions [1]. Heat pipes have been extensively researched and applied in various embodiments for electronics cooling ranging from simple cylindrical geometries to complex configurations [2]. FPHPs in particular have high-heat transfer capability, can maintain a uniform temperature over the evaporator surface when densely packed with heat-generating components, and decrease the thickness of finned heat sinks base material [3–6].

Recent research by Christensen and Graham [7] investigated the performance of heat sinks in packaging high-power (>1 W) light-emitting diode (LED) arrays and concluded that flat plate heat pipes form an important thermal component to achieve long operating life and high reliability. Huang and Liu [8] demonstrated analytically the increased capability of mounting a localised heat source and heat sink on the same

surface of an FPHP. Similarly, Qin and Liu [9] investigated liquid flow in an anisotropic permeability wick of a flat plate heat pipe, determining the effect of heat source location on fluid distribution in the inside of the heat pipe. Further work on finding the optimum location of mounting multiple heat sources on an FPHP evaporator surface was demonstrated by Tan et al. [10] through a simplified analytical solution to a two-dimensional pressure and velocity distribution within the wick. Recently, Sonan et al. [11] developed a simulation model for the transient thermal performance of a $40 \times 40 \times 0.9$ mm FPHP with specific applications to cooling multiple electronics components where space restriction imposes that heat sources and heat sinks need to be mounted on the same surface. The above research agrees that a cost premium associated with a well-designed FPHP for advanced thermal management solution in electronics cooling should be reflected in its superior thermal performance compared to solid copper or aluminium base materials of similar dimensions.

This paper investigates the design and thermal performance of a miniature FPHP as an effective supporting shelf for printed circuit boards (PCB) of radio frequency (RF)

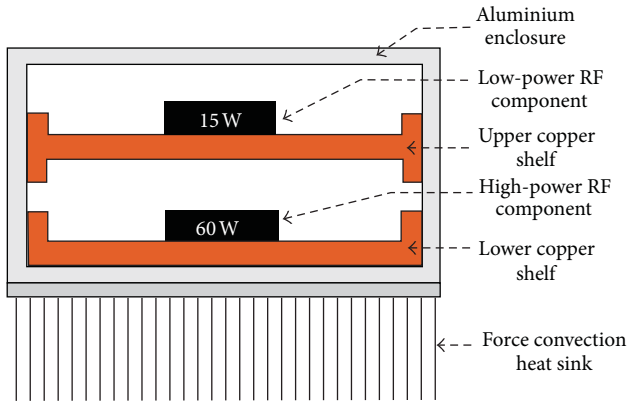


FIGURE 1: Schematic of the electronics cooling enclosure.

components to dissipate and transport heat away to the aluminium enclosure. In this paper, two identical miniature FPHPs configurations one with a sintered copper powder and the other one with a screen copper mesh wick were designed and tested. A further benchmarking exercise, using both CFD analysis and experimental measurements, was carried out by comparing the thermal performance of the FPHP to that of a monolithic solid copper plate with similar dimensions.

2. Description of the Electronics Enclosure Cooling System

The work addresses the cooling requirement to maintain a specified temperature limit for heat-generating RF components that are housed in an existing aluminium enclosure as part of a large telecommunication control system. The aluminium enclosure consists of two separate copper shelves and an air cooled finned base plate, as shown in Figure 1. The PCB of high heat dissipating RF components was mounted on the lower shelf of the enclosure to allow for direct contact with the base heat metal spreader while low-power rated RF components were placed on the top shelf. In the original design, the enclosure's shelves were made of 1 mm thick copper base. However, frequent and premature failures of RF components prompted the review of the enclosure's thermal performance. Hence, a redesign of the copper shelves to keep the operating temperature gradients of the RF components within the specified limits was performed using both CFD simulation and an experimental validation analysis. The work consists in investigating the thermal performance of the enclosure's shelves that are made of a 1 mm and 3 mm solid copper base plates and two miniature FPHPs of 5 mm overall height with one using sintered copper powder wick and the other one a screen mesh wick.

2.1. FPHP Design. The FPHP base material was made of copper material and water was selected as the working fluid for its compatibility and suitable operating temperature range. The outer shell of the constructed prototype miniature FPHPs for the sintered and mesh wicks is shown in Figure 2(a). The inner structure of the sintered wick FPHP with the

condenser cover plate removed to reveal the sintered wick layer and erected pillars on the evaporator surface is shown in Figure 2(b). Similarly, the structure of the miniature FPHP with copper mesh wick is shown in Figure 2(c). The design of the mesh wick FPHP was adopted from Bakke [12] and Rosenfeld et al. [13], which consists of using a fine mesh layer to provide capillary pumping force of the working fluid and a coarse mesh to support and maintain the structural integrity of the vapour space.

2.2. FPHP CFD Simulation. The thermal performance of the miniature FPHP was simulated using FloTHERM, a commercial CFD simulation software. The computer simulation includes analysing the complex flow pattern of the working fluid in the wick and establishing the temperature profiles in the FPHP evaporator. Flotherm is a finite volume-based software package that uses simple Cartesian grid meshing and has built in boundary conditions for common heat transfer devices. The rectangular shape of the FPHP, heater block, and cold plate lend themselves well to meshing using Cartesian coordinates and hence the use of Flotherm for a fast and converging solution. Description of the mathematical model for momentum, mass, and energy conservation that underpin the CFD simulation was not the focus of this paper as similar models are widely available in published literature that can be found in [14–16].

The Flotherm model was built using standard Cuboids and Prism elements for the FPHP components including the evaporator and condenser copper plates, the wick layer, the void (vapour) space, and the supporting solid columns. Planar resistance object model was used to define the thermal properties for each object. This is a useful tool where the thermal resistance of an object can be inserted manually or determined from other thermal parameters such as the thermal conductivity and heat transfer coefficient. Modelling of the porous wick layer, in particular, requires prior knowledge of the permeability of the porous wick structure. The volumetric flow rate, \dot{V} , of the working fluid was also required as an input parameter in the simulation. This was calculated from the following relationship:

$$\dot{V} = \frac{\dot{Q}_H}{\rho_l h}, \quad (1)$$

where \dot{Q}_H is the rate of heat generation in the heat source and h , and ρ_l are the latent heat and density of the working fluid, respectively. In addition, it is well known that the failure of heat pipes is often attributed to operation beyond the device's wick capillary limit. This can be obtained by characterising the actual pressure of the liquid in the wick pores under different heat flux levels using Laplace-Young equation as follows [1]:

$$\Delta p_c = \frac{2\sigma_l}{r_{\text{pore}}}, \quad (2)$$

where Δp_c is the capillary pressure drop in the wick, σ_l is the surface tension of the liquid, and r_{pore} is the pore radius of the wick.



FIGURE 2: Constructed miniature FPHP (a) sealed unit, (b) sintered wick, and (c) mesh wick.

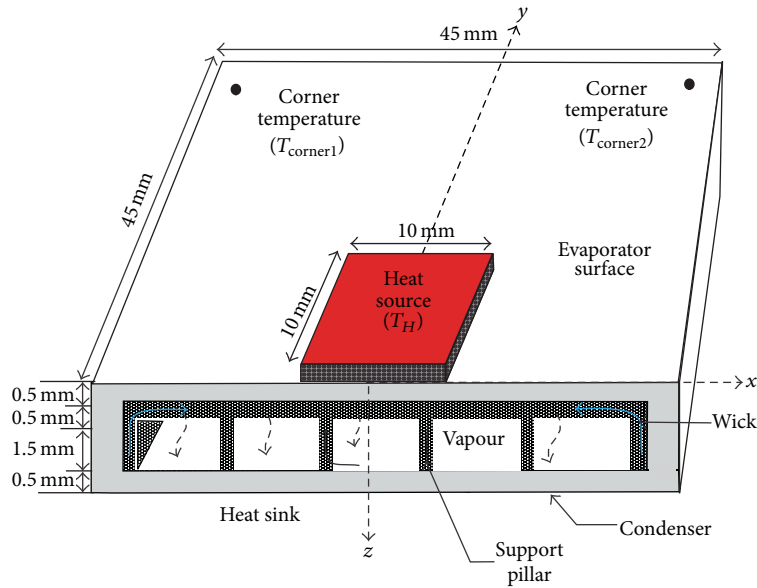


FIGURE 3: A schematic representation of the FPHP.

Equally, the effective thermal conductivity of a saturated wick, k_{eff} , was obtained from the following expression [17, 18]:

$$k_{\text{eff}} = \beta (\varphi k_l + (1 - \varphi) k_s) + \frac{(1 - \beta)}{\varphi/k_l + (1 - \varphi)/k_s}, \quad (3)$$

where φ is the porosity of the wick, k_l and k_s are the thermal conductivity of liquid water and solid wick, respectively. According to Bhattacharya et al. [17], the best-fit data for measuring the effective thermal conductivity of a porous

material is for $\beta = 0.35$ with an overall R^2 value of 0.97. This is consistent with measured thermal conductivities of about 40 W/(mK) in heat pipes with fully saturated wicks, while the vapour space is considered to have a very large heat transfer coefficient of the order of 50000 W/m²K [16, 18].

A schematic representation of the sintered wick heat pipe given in Figure 3 illustrates the location of the heat source, a cross section of the wick layer, the working fluid circulation paths, and the condenser cold plate heat sink.

In this analysis, it was also assumed that the heat source is of constant heat flux type which is applied to the evaporator base plate (at $z = 0$) immediately under the heat source while

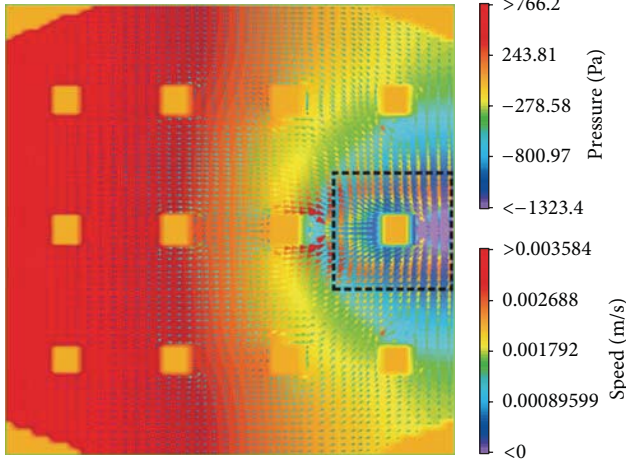


FIGURE 4: CFD simulation of speed and pressure fields of the liquid in the FPHP-sintered wick ($Q_H = 80$ W).

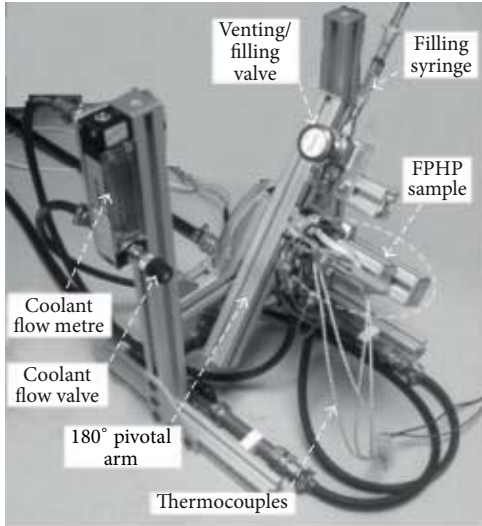


FIGURE 5: The experimental test rig setup.

the remaining outer surface of the evaporator including the edge walls is considered to be adiabatic. In the inner section of the heat pipe, it was assumed that the liquid-vapour interface temperature is equal to the vapour saturation temperature of the working fluid that can be calculated from Clausius-Clapeyron relationship [19]. Similarly, the liquid velocity at the interface of the wick layer-evaporator wall was assumed to equal zero. At the condenser-vapour interface, the temperature of the condenser section was maintained at 35°C using a chilled liquid cold plate with a heat transfer coefficient in the order of 2000 W/(m²K).

A thermocouple placed at the interface surface between the evaporator and heat source was used to measure the temperature of the heater block, T_H , and a further two thermocouples were placed at the two farthest corners on the evaporator to measure $T_{\text{corner}1}$ and $T_{\text{corner}2}$. Furthermore, the heat dissipation from the RF components was simulated

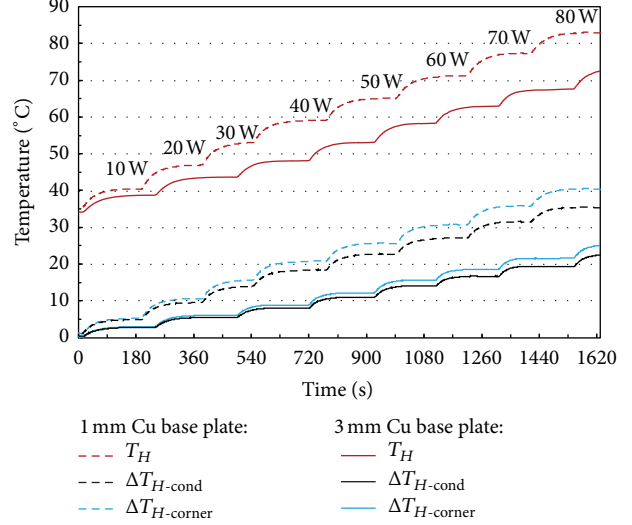


FIGURE 6: Temperature variation of a 1 mm and 3 mm thick copper base plates.

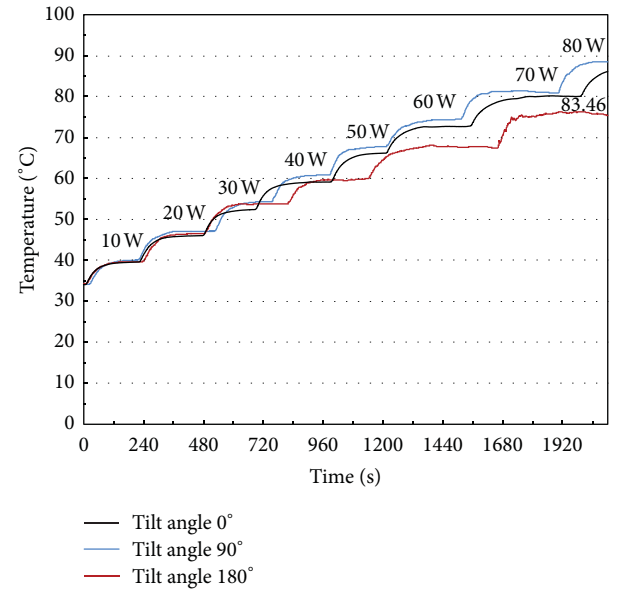
TABLE 1: Design properties of the sintered and mesh wick miniature FPHP.

Casing

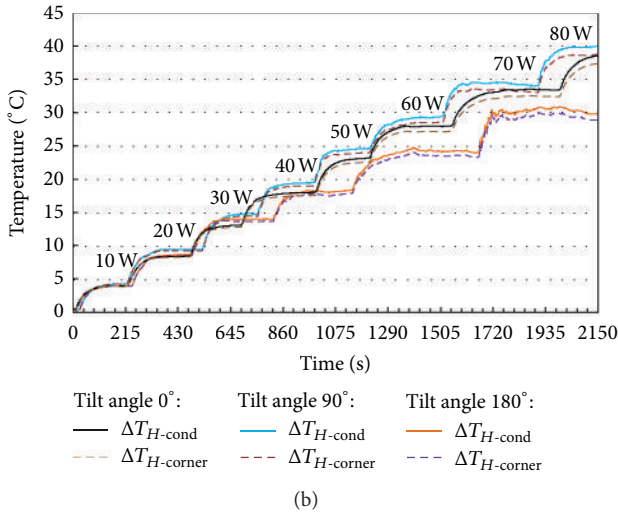
Material	Copper
Height	3 mm
Dimension	45 mm × 45 mm
Heater block size	10 mm × 10 mm
Working fluid	Water
Sintered copper powder wick	
Wick thickness	0.5 mm
Vapour space height	1.5 mm
Porosity	50%
Pore radius	40 μm
Permeability	$1.43 \times 10^{-11} \text{ m}^2$
Screen copper mesh wick	
Fine mesh material	Phosphor bronze 320 mesh/in
Wire diameter	0.03 mm
Porosity	42%
Wick thickness	1 mm
Supporting coarse mesh material	Phosphor bronze 16 mesh/in

using an electric heater cartridge that is inserted in a solid aluminium block of 10 mm × 10 mm with a controlled heat dissipation rates. The condenser surface was maintained to the desired temperature of 35°C by clamping directly onto its surface a chilled water cold plate. The main design properties of the miniature FPHPs with sintered and mesh wicks are given in Table 1.

2.3. CFD Simulation Results. The CFD simulation was used to evaluate the sintered wick FPHP thermal performance by



(a)



(b)

FIGURE 7: Screen mesh wick FPHP temperature variation at various heat dissipation levels and tilt angles: (a) heat source temperature, (b) evaporator surface temperature gradient.

analysing the steady state liquid flow pressure and velocity distribution in the sintered wick as shown in Figure 4. The speed of the liquid flow in the wick structure is presented by arrows pointing towards the heat source (dashed line square) and arranged by colour in contours of equal speeds. It can be seen that the speed of the liquid flow is lowest at regions most distant from the heat source (contours of purple arrows) and increases gradually as the liquid is drawn towards the heat source (contours of orange and red arrows) to replenish the evaporated liquid from the wick pores in the constant heat flux section. The liquid flow speed then drops sharply in the region immediately underneath the heat source as the liquid evaporates from the wick. The effect of the sintered pillars is also visible in that the liquid flow speed field

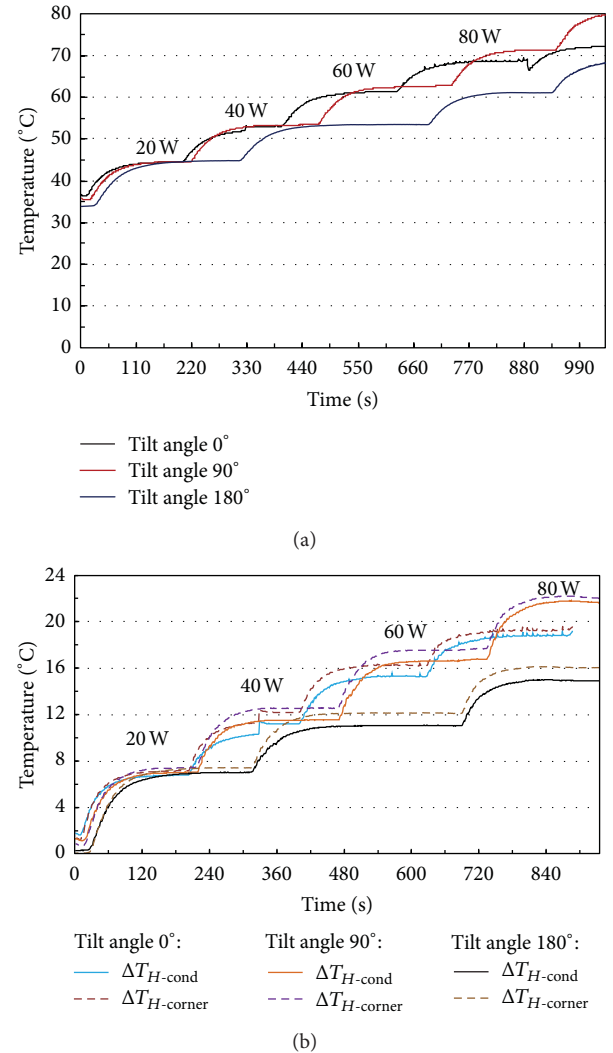


FIGURE 8: Sintered wick FPHP temperature at various heat dissipation levels and tilt angles: (a) heat source temperature, (b) surface temperature gradient.

contours are altered in a way that high-fluid speed spots were developed around the pillars. Furthermore, Figure 4 shows the liquid pressure distribution in the wick with the high pressure region (in red colour) away from the heat source and the low-pressure regions (in blue/purple colour) immediately beneath the heat source.

From the CFD analysis, it was found that the total pressure difference generated by the capillary forces of the wick is 2089.6 N/m^2 . This is markedly lower than the capillarity pumping limit of the wick of 3952 N/m^2 which was calculated using (2) under the working conditions given in Table 2.

3. Experimental Setup and Results

The experimental rig setup to test the thermal performance of the miniature FPHP and solid copper base samples is shown in Figure 5. The rig was equipped with a liquid filling

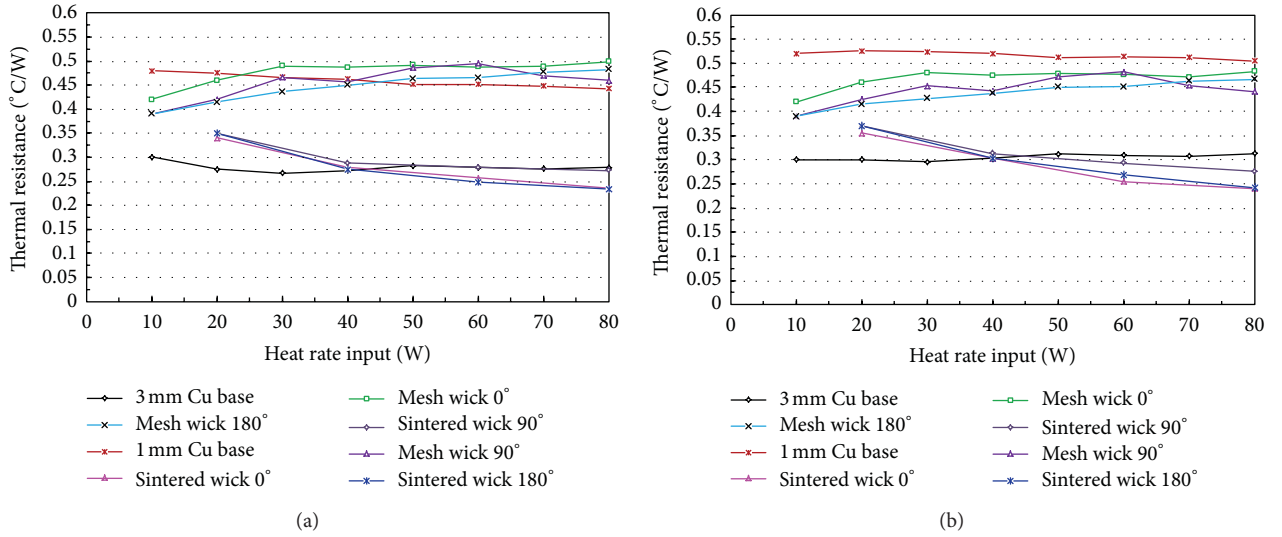


FIGURE 9: Thermal resistance: (a) one dimensional resistance, (b) spreading resistance.

TABLE 2: Saturated wick operating properties.

Heat load \dot{Q}_H (W)	Liquid surface tension σ_l (kg/s ²)	Liquid density ρ_l (kg/m ³)	Liquid latent heat of vaporisation h (kJ/kg)	Sintered powder wick permeability ε_{wick} (m ²)	Liquid flow rate from (1) \dot{V} (m ³ /s)	Pressure drop from (2) ΔP_c (N/m ²)	Pressure drop (CFD) ΔP_{CFD} (N/m ²)
80	0.0626	972	2310	$1.43E - 11$	$3.563E - 08$	3952	2089.6

TABLE 3: Sintered wick FPHP thermal resistance calculation uncertainty.

Heat input (W)	20	40	60	80
Calculated thermal resistance uncertainty (%)	13.60	6.00	4.14	3.80

and venting system for charging the FPHP, a rotating beam for mounting the heat pipe at different tilt angles (0° to 180°), a variable power supply to control heat dissipation from the heat source, a chilled water supply to control the condenser temperature, and associated sensors and data acquisition equipment. The miniature FPHP test sample was clamped onto the tilting beam with 0° angle being designated for operation against gravity (i.e., evaporator is above the condenser). An electric heater cartridge placed inside an aluminium block of 10 mm × 10 mm was used as heat source which heat dissipation rate was controlled by a variable power supply. A thermal interface material 0.5 mm thick was used as an interface between the FPHP test sample, the heater block, and the condenser cold plate to minimise the contact thermal resistances.

The performance of the FPHP test sample was evaluated at various heat dissipation rates by increasing the heat source power at equal increments of 10 W to a maximum of 100 W or until the temperature of the evaporator surface reached a threshold of 100°C. At each heat input increment the temperature of the evaporator surface was allowed to reach steady state. In addition, the effect of orientation on the FPHPs

was evaluated by repeating the experimental measurements at tilt angles of 0°, 90°, and 180°. For comparison, further experimental tests were conducted on a 1 mm and 3 mm thick solid copper base plates under identical controlled conditions. In all tested samples, the operating temperature was measured at the heat source, T_H , evaporator plate corners $T_{corner1}$ and $T_{corner2}$, and at the condenser surface, T_{cond} .

3.1. Solid Copper Base Plate Shelves. The initial tests of two solid copper plates of 45 mm × 45 mm and a thickness of 1 mm and 3 mm were carried out to provide a benchmark data which the thermal performance of the FPHPs was compared to. Results of these tests are shown in Figure 6, where it can be seen that for the same heat dissipation rates the temperature of the heat source in the 1 mm thick copper base is higher than that of the 3 mm thick copper base, particularly at high heat dissipation rates. For example, at a heat dissipation rate of 80 W, the recorded temperature, T_H , is 84°C and 73°C for the 1 mm and 3 mm thick base plates, respectively. Similarly, the temperature gradients between the heat source and the two far end corners, $\Delta T_{H-corner}$, and between the heat source and the heat sink, ΔT_{H-cond} , are approximately 15°C higher for the 1 mm thick copper base than for its 3 mm thick counterpart. This shows that the 3 mm thick copper base plate has superior heat-spreading properties as predicated in the CFD simulation results.

3.2. Screen Mesh Wick Miniature FPHP. The procedure for evaluating the thermal performance of the screen mesh

wick FPHP was similar to that presented in previous case with additional experimental measurements to assess the effect of orientation at tilt angles of 0°, 90°, and 180°. The measured temperature changes at the heat source and across the evaporator surface are shown in Figures 7(a) and 7(b). These show that at 0° and 90° tilt angles the FPHP performance is only comparable to that of the 1 mm thick solid copper base. For example at high-heat dissipation rates (80 W), the temperature of the heat source approaches 90°C and a large temperature gradient (30 to 40°C) appears across the evaporator surface and between the heat source and heat sink, $\Delta T_{H\text{-cond}}$. The thermal performance of the heat pipe has improved marginally for a tilt angle of 180° (gravity assisted wick capillary forces), but it remains that the 3 mm solid copper base plate performed better. This unexpected poor thermal performance may be attributed to the process of fabrication in which poor contact between the fine screen mesh and the inner evaporator wall could have prevented liquid circulation, leading to a high interfacial thermal resistance.

3.3. Sintered Copper Powder Wick FPHP. The sintered wick FPHP thermal performance is shown in Figures 8(a) and 8(b). It can be seen that for a heat dissipation rate of 80 W the measured temperature of the heat source at a tilt angle of 0° is 69°C, which is lower by 15°C and 5°C compared to the 1 mm and 3 mm copper base plates, respectively. For a tilt angle of 180° the temperature of the heat source has dropped even further to 61°C, an improvement of 12°C compared to the 3 mm copper base plate. Similarly, the measured temperature gradients $\Delta T_{H\text{-cond}}$ and $\Delta T_{H\text{-corner}}$ are 6°C and 5°C lower than that of the 3 mm copper base plate for a tilt angle of 0° and 10°C and 8°C for a tilt angle of 180°, respectively.

The high-thermal performance of the sintered wick miniature is due to high heat conduction and spreading capability of the sintered wick compared to a simple monolithic solid copper base plate or screen mesh wick FPHP.

4. Evaluation of Bulk and Thermal Spreading Resistance

The effective thermal resistance of an electronics component mounted on a PCB is the sum of a one-dimensional bulk resistance and a thermal spreading resistance. The one-dimensional bulk thermal resistance is expressed as follows [4, 20, 21]:

$$R_b = \frac{T_H - T_{\text{cond}}}{\dot{Q}_H}. \quad (4)$$

The thermal spreading resistance is associated, however, with discrete heat-generating components when mounted on a cold base plate, as found in electronics packages. The thermal spreading resistance characterises the ability of a base plate to spread the heat uniformly across the base plate surface (or the evaporator surface in the case of FPHP). The thermal spreading resistance could be of a similar magnitude to the one-dimensional bulk resistance in some designs of heat exchangers. Hence, its omission can lead to significant

errors in estimating the temperature of a PCB, resulting in components overheating and failing prematurely. The thermal spreading resistance, R_{sp} , is computed using the following expression [21]:

$$R_{\text{sp}} = \frac{T_H - (T_{\text{corner1}} + T_{\text{corner2}})/2}{\dot{Q}_H}. \quad (5)$$

The variation of the one-dimensional bulk and thermal spreading resistances for the tested copper base plates and miniature FPHPs are shown in Figure 9. It can be seen that for heat dissipation rates of up to 40 W, the sintered wick heat pipe and the 3 mm thick copper base plate have comparable thermal performances in that both the one-dimensional and spreading thermal resistances are of similar magnitude. For higher heat dissipation rates, however, the advantage of a sintered wick FPHP becomes more apparent as the one-dimensional bulk and thermal spreading resistances are lower compared to other designs.

Finally, the uncertainty error of calculating the one-dimensional bulk and thermal spreading resistances is estimated from the measured data and the accuracy of the instruments used in the experiments. The accuracy of the T-type thermocouples is 0.5°C while the average error for power supply reading (wattmeter) is estimated at 2.3 W. Therefore, using the single sample analysis [22], the relative uncertainty error of the thermal resistance is calculated as follows:

$$e_R = \sqrt{\left(\frac{e_T}{\Delta T}\right)^2 + \left(\frac{e_Q}{\dot{Q}_H}\right)^2}. \quad (6)$$

It was assumed that the electrical power input to the heater block was fully dissipated as heat energy and that heat loss by convection and radiation from the test sample was negligible. The relative uncertainty error calculation of the thermal resistances has been limited to the case of the sintered wick FPHP, as shown in Table 3. The uncertainty calculation of the FPHP thermal resistance decreases from 13.6% to 3.8% for heat input rates of 20 W and 80 W, respectively. Although the average reading accuracy of the wattmeter is 2.3 W, the reading scale is nonlinear and the error of measurement is highest at low end of the scale, leading to large uncertainty of the measured thermal resistance for a heat rate input of 20 W.

5. Conclusion

This work investigated the thermal performance of a miniature FPHPs with sintered and screen mesh wicks for application in electronics cooling. The thermal performance of the FPHPs was further compared to that of copper solid base plates 1 mm and 3 mm thick. The ability of each sample to dissipate heat was evaluated by measuring the temperature distribution on the mounting surface and the temperature gradient between the heat source and heat sink. The main findings can be summarised as follows.

- (i) The CFD results of predicting that the sintered wick FPHP would perform better than other arrangements were in good agreement with the experimental measurements.

- (ii) It was found that the 3 mm thick copper base plate thermal performance surpasses that of the 1 mm and achieves higher heat conduction and spreading performance than the screen mesh wick FPHP.
- (iii) The 3 mm thick copper base can perform adequately with heat dissipation rates of up to 40 W.
- (iv) For heat dissipation rates higher than 40 W, the sintered wick FPHP outperforms the 3 mm copper base plate and its application would justify its high cost.
- (v) The temperature measured on the evaporator surface of the sintered wick FPHP shows that there is no sign of liquid dry-out conditions in the wick for the range of heat dissipation rates.
- (vi) The orientation of the sintered wick FPHP had marginal effect on its performance.

Acknowledgments

The authors wish to thank EPSRC (Engineering and Physical Sciences Research Council) for its financial support of the project under Grant EP/P500389/1 and Thermacore Europe Ltd for providing financial and technical help.

References

- [1] D. A. Reay and P. A. Kew, *Heat Pipes: Theory, Design and Applications*, Butterworth-Heinemann, New York, NY, USA, 5th edition, 2006.
- [2] M. Groll, "Heat pipe research and development in western Europe," *Heat Recovery Systems and CHP*, vol. 9, no. 1, pp. 19–66, 1989.
- [3] A. Basiulis, H. Tanzer, and S. McCabe, "Thermal management of high power PWB's through the use of heat pipe substrates," in *Proceedings of the 6th Annual International Electronics Packaging Conference*, vol. 6, p. 501, San Diego, Calif, USA, 1986.
- [4] M. Adami and B. Yimer, "Development and evaluation of a planar heat pipe for cooling electronic systems," *Chemical Engineering Communications*, vol. 90, no. 1, pp. 57–74, 1990.
- [5] S. W. Kang, S. H. Tsai, and H. C. Chen, "Fabrication and test of radial grooved micro heat pipes," *Applied Thermal Engineering*, vol. 22, no. 14, pp. 1559–1568, 2002.
- [6] C. Y. Liu, C. Y. Liu, K. C. Leong, Y. W. Wong, and F. L. Tan, "Performance study of flat plate heat pipe," in *Proceedings of the International Conference on Energy and Environment (ICEE)*, pp. 512–518, Begell House Inc., New York, NY, USA, 1996.
- [7] A. Christensen and S. Graham, "Thermal effects in packaging high power light emitting diode arrays," *Applied Thermal Engineering*, vol. 29, no. 2-3, pp. 364–371, 2009.
- [8] X. Y. Huang and C. Y. Liu, "The pressure and velocity fields in the wick structure of a localized heated flat plate heat pipe," *International Journal of Heat and Mass Transfer*, vol. 39, no. 6, pp. 1325–1330, 1996.
- [9] W. Qin and C. Y. Liu, "Liquid flow in the anisotropic wick structure of a flat plate heat pipe under block-heating condition," *Applied Thermal Engineering*, vol. 17, no. 4, pp. 339–349, 1997.
- [10] B. K. Tan, X. Y. Huang, T. N. Wong, and K. T. Ooi, "A study of multiple heat sources on a flat plate heat pipe using a point source approach," *International Journal of Heat and Mass Transfer*, vol. 43, no. 20, pp. 3755–3764, 2000.
- [11] R. Sonan, S. Harmand, J. Pellé, D. Leger, and M. Fakès, "Transient thermal and hydrodynamic model of flat heat pipe for the cooling of electronics components," *International Journal of Heat and Mass Transfer*, vol. 51, no. 25-26, pp. 6006–6017, 2008.
- [12] A. P. Bakke, "Light weight rigid flat plate heat pipe utilizing copper foil container laminated to heat treated Aluminium plates for structural stability," US Patent No. 6679318 B2, 2004.
- [13] J. H. Rosenfeld, N. J. Gernert, D. V. Sarraf, P. Wollen, F. Surina, and J. Fale, "Flexible heat pipe," US Patent No. 6446706 B1, 2002.
- [14] Y. Koito, H. Imura, M. Mochizuki, Y. Saito, and S. Torii, "Numerical analysis and experimental verification on thermal fluid phenomena in a vapor chamber," *Applied Thermal Engineering*, vol. 26, no. 14-15, pp. 1669–1676, 2006.
- [15] G. Carbajal, C. B. Sobhan, G. P. Bud Peterson, D. T. Queheillalt, and H. N. G. Wadley, "A quasi-3D analysis of the thermal performance of a flat heat pipe," *International Journal of Heat and Mass Transfer*, vol. 50, no. 21-22, pp. 4286–4296, 2007.
- [16] R. Ranjan, J. Y. Murthy, and S. V. Garimella, "Analysis of the wicking and thin-film evaporation characteristics of microstructures," *Journal of Heat Transfer*, vol. 131, no. 10, pp. 1–11, 2009.
- [17] A. Bhattacharya, V. V. Calmudi, and R. L. Mahajan, "Thermophysical properties of high porosity metal foams," *International Journal of Heat and Mass Transfer*, vol. 45, no. 5, pp. 1017–1031, 2002.
- [18] J. Thayer, "Analysis of a heat pipe assisted heat sink," in *Proceedings of the 9th International FLOTHERM Users Conference*, Orlando, Fla, USA, October 2000.
- [19] B. Xiao and A. Faghri, "A three-dimensional thermal-fluid analysis of flat heat pipes," *International Journal of Heat and Mass Transfer*, vol. 51, no. 11-12, pp. 3113–3126, 2008.
- [20] R. Boukhanouf, A. Haddad, M. T. North, and C. Buffone, "Experimental investigation of a flat plate heat pipe performance using IR thermal imaging camera," *Applied Thermal Engineering*, vol. 26, no. 17-18, pp. 2148–2156, 2006.
- [21] Y. S. Muzychka, M. R. Sridhar, M. M. Yovanovich, and V. W. Antonetti, "Thermal spreading resistance in multilayered contacts: applications in thermal contact resistance," *Journal of Thermophysics and Heat Transfer*, vol. 13, no. 4, pp. 489–494, 1999.
- [22] S. J. Kline and F. A. McClintock, "Describing uncertainties in single sample experiments," *Mechanical Engineering*, vol. 75, pp. 3–8, 1953.

Research Article

Numerical Determination of Effects of Wall Temperatures on Nusselt Number and Convective Heat Transfer Coefficient in Real-Size Rooms

Ozgen Acikgoz and Olcay Kincay

Yildiz Technical University, Mechanical Engineering Department, Barbaros Bulvari, Besiktas, 34349 Istanbul, Turkey

Correspondence should be addressed to Ozgen Acikgoz; oacikgoz@yildiz.edu.tr

Received 28 December 2012; Accepted 20 March 2013

Academic Editor: Ahmet Selim Dalkılıç

Copyright © 2013 O. Acikgoz and O. Kincay. This is an open access article distributed under the Creative Commons Attribution License, which permits unrestricted use, distribution, and reproduction in any medium, provided the original work is properly cited.

A modeled room was numerically heated from a wall and cooled from the opposite wall in order to create a real-room simulation. The cooled wall simulated heat loss of the room, and the heated wall simulated the heat source of enclosure. The effects of heated and cooled wall temperatures on convective heat transfer coefficient (CHTC) and Nusselt number in the enclosure were investigated numerically for two- (2D) and three-dimensional (3D) modeling states. Different hot wall and cold wall temperatures were applied in order to obtain correlations that contained characteristic length in Rayleigh numbers. Results were compared with the results of previously reported correlations that have been suggested for vertical room surfaces in enclosures. In addition, new correlations for Nusselt number and average CHTC for enclosures for isothermal boundary conditions within indicated Rayleigh number ranges were derived through solutions. Average deviations of new correlations obtained for CHTC and Nusselt number from the numerical data were found 0.73% and 1.76% for 2D study, 3.01% and 0.49% for 3D study. It was observed that the difference between the 2D and 3D solutions in terms of CHTC and Nusselt number was approximately 10%.

1. Introduction

Because of their importance in industry and living places, natural convection and temperature and velocity distribution problems in enclosures have been widely studied not only numerically but also experimentally in appropriate real-size building geometries. In the era in which we have been encountering many energy crises, natural convection problems in real-size rooms also has great importance since it remarkably affects energy consumption in buildings. Heating and cooling systems with vertical walls, floor, and ceiling (radiant panels) have not been extensively utilized for many years. Nevertheless, especially heating technologies with low water temperature have begun to be reassessed due to the austere energy policies pursued by governments throughout the world. As well as the progression of renewable energy techniques and low temperature heating systems, improving computational methods and descending solution periods for calculation of natural convection problems in real-size building rooms provide us to use computational fluid

dynamics (CFD) programs in order to obtain convective heat transfer coefficients (CHTCs) using proper numerical solution preferences. Although conduction and radiation heat transfer simulation models in room size enclosures have been thoroughly described by numerous researchers, in convection there are still some uncertainties. Difficulties in accurate convection modeling especially analytical and numerical methods arise from complexity of the enclosure geometry, solution of fluid dynamics problems (governing equations), and differences at each air flow pattern in each heating choice.

ASHRAE HVAC Systems and Equipment Handbook—Fundamentals Handbook [1] lists many CHTC values and correlations. However, these equations were derived with the assumption that CHTC in an enclosure is equal to free edge isolated plates. Nonetheless, air flows at surrounding walls, even if they are not heated or cooled, affect the flows on adjacent walls. Also, the air flow on all surfaces affects the overall flow pattern in the enclosure. Thus, correlations for free plates cannot be accurately used for natural convection

problems in enclosures [2]. It can also be correlations derived through 2D enclosure modeling that cannot be utilized due to adjacent wall effects that are neglected in analytical expressions or numerical procedures.

Furthermore, experimental and computational studies have revealed that convection CHTCs of real-room surfaces are affected by the depth or height of the room, boundary conditions of the surface, smoothness/roughness of surfaces, and whether forced convection is present in the room.

In their study, Beausoleil-Morrison [3] showed the effect of CHTC correlations over building heating load predictions. They conducted experimental studies in a well-insulated test buildings that had radiant heating systems. Utilizing measurements from these test buildings and many different CHTC correlations, Beausoleil-Morrison found an 8% difference among the different simulations. He also found that building load amounts were more sensitive to CHTC correlations and the control set point of the room than to building fabric thermal properties or air infiltration. Peeters et al. [2] published an extensive review on experimentally derived CHTCs in enclosures and over free plates. They classified these correlations according to heating conditions, flow intensity, and also reference temperature preference in the enclosure. They questioned robustness of the correlations derived by numerous researchers and carried out new experiments in order to validate correlations. They concluded that large discrepancies were present among existing correlations in the literature. The differences were attributed to values of predicted coefficients, chosen reference air temperatures, and formats of the correlations. They also indicated that determination of appropriate choice of characteristic length was crucial. Nonetheless, it was asserted that choice of these parameters in building simulation programs was limited due to the common single node approach.

Awbi and Hatton [4] studied natural convection in two different enclosures. The enclosures' dimensions were 2.78 by 2.30 by 2.78 m and 1.05 by 1.01 by 1.05 m. One wall in each of the enclosure was used as a "heat sink" through an air conditioner placed in a small room next to the large enclosure. Opposite and adjacent walls to the "heat sink" wall have been heated with impregnated flexible sheets that had a 200 W/m^2 output. Thermal sensors were located inside on both sides of the surfaces. The aim of placing sensors on the outer surface of the enclosure was to calculate heat loss from heated surfaces. Reference air temperature for wall heating system was determined as 100 mm from heated surface and defined as "undisturbed air temperature" or in other words the temperature outside the thermal boundary layer. Thermal radiation was calculated through measuring emissivity of the surfaces and was extracted from total heat flux. Because they also heated the walls partially, characteristic length was determined as equal to hydraulic diameter. The results demonstrated that CHTCs of the heated wall were lower for the small enclosure that had a volume of approximately 1 m^3 than for the larger enclosure. Nonetheless, in order to assess whether the difference was because of the heating plate sizes or enclosure sizes, more experiments were carried out with small plates placed on surfaces. From these experiments, it

was determined that there was a close agreement between CHTCs calculated with whole wall heated and CHTCs calculated with small plates heated. Consequently, the authors asserted that rather than the heated area on a wall, the size of the enclosure significantly affects CHTC. They also compared their results with the correlations in the extant literature and found that their data fell in the middle of the curves. The correlations that they suggested for walls are presented in Table 1.

Awbi [8] presented the results of a CFD study on natural CHTCs of a heated wall, a heated floor, and a heated ceiling. Two turbulence models were used: standard $k-\epsilon$ model using wall functions and low Reynolds $k-\epsilon$ model. The results were compared with experimental results.

Fohanno and Polidori [9] aimed to develop a theoretical model of convective heat transfer between an isolated vertical plate and natural convective flow. They assumed a constant heat flux on surface, and the model they produce allowed average and local CHTCs to be calculated in laminar and turbulent regime. The correlation they derived for average CHTC was produced through local CHTC results. They indicated that there was a good agreement between Alamdari and Hammond's correlations. The applicability of the new correlations to real-size buildings was considered, and despite the three-dimensionality of real-size rooms, a 10% difference was found between data taken from experimental and mathematical work.

To calculate CHTCs for all surfaces in an enclosure, Khalifa and Marshall [5] utilized an experimental enclosure that had dimensions similar to those of a real-size room. Sixty-five aluminium thermistors were used to measure air and surface temperatures in the enclosure. Inner and outer surfaces of the enclosure were coated with aluminium. Radiant heat exchange was not counted in the CHTC calculation process. Also, a sensitive uncertainty analysis was employed. In this analysis, temperature measurements, conductivity of the materials, and the lack of inclusion of long wave radiation in the low emissivity chamber were considered in order to take account of all possible error sources [2]. They derived many general correlations, including the two that are presented in Table 1.

Khalifa and Khudheyer [10] conducted an experimental investigation on the effects of 14 different configurations of partitions on natural convection heat transfer in enclosures. Like other studies, the experiment considered vertical hot and cold walls, while the other walls were insulated. Investigation was conducted for Rayleigh numbers between $6 \cdot 10^7$ and $1.5 \cdot 10^8$ with the aspect ratio of 0.5. Correlations for the test configurations were derived. Khalifa [11] presented an extensive review of studies regarding isolated vertical and horizontal surfaces. Comparisons between correlations for heat transfer coefficients were conducted, and the discrepancies were determined to be up to a factor of 2 for isolated vertical surfaces, up to a factor of 4 for isolated horizontal surfaces facing upward, and up to a factor of 4 for isolated horizontal surfaces facing downward.

Khalifa [12] presented a wide review of two- and three-dimensional natural convection problems, focusing primarily

TABLE 1: Correlations derived for CHTC and Nusselt number in enclosures.

Correlation	Conditions	Reference temperature
Awbi and Hatton [4] $h = \frac{1.823}{D^{0.121}} (\Delta T)^{0.293}$ $\text{Nu} = 0.289(\text{Gr})^{0.293}$	Heated wall ($2.78 \times 2.30 \times 2.78$ m)	Local air temperature (100 mm from wall)
Khalifa and Marshall [5] $h = 2.3(\Delta T)^{0.24}$ $h = 2.10(\Delta T)^{0.23}$	For a room with a heated wall and a room heated by a radiator under a window ($2.35 \times 2.95 \times 2.08$ m)	Average room temperature
ASHRAE [1] $\text{Nu} = 0.117(\text{Gr})^{0.117}$	For a room heated by a fan heater ($2.35 \times 2.95 \times 2.08$ m)	Average room temperature
Li et al. [6] $h = 3.08(\Delta T)^{0.25}$	Turbulent flow $10^8 < \text{Gr} < 10^{12}$ (for free plate)	Average room temperature
Min et al. [7] $h = 1.646 \frac{(\Delta T)^{0.32}}{H^{0.05}}$	Normal conditions, occupied room	Average room temperature
	Heated floor or heated ceiling	Average room temperature

TABLE 2: Change of Nusselt numbers and CHTCs at various wall temperatures (2D solution results, $L \times H \times L = 4.00 \times 2.85 \times 4.00$ m).

T_H (°C)	$T_c = 5^\circ\text{C}$			$T_c = 10^\circ\text{C}$			$T_c = 15^\circ\text{C}$		
	Ra	Nu	h (W/m ² K)	Ra	Nu	h (W/m ² K)	Ra	Nu	h (W/m ² K)
20	$1.1E + 11$	721.52	4.53	$7.03E + 10$	614.2	3.88	$3.38E + 10$	472.16	3.01
25	$1.41E + 11$	783.07	4.96	$1.01E + 11$	695.23	4.43	$6.51E + 10$	590.85	3.8
30	$1.69E + 11$	832.38	5.31	$1.3E + 11$	754.31	4.85	$9.39E + 10$	669.71	4.34
35	$1.95E + 11$	870.14	5.59	$1.57E + 11$	801.39	5.2	$1.21E + 11$	727.26	4.75

on heat transfer in buildings. He determined the discrepancies between correlations to be up to a factor of 5 for vertical surfaces, a factor of 4 for horizontal surfaces facing upward, and up to a factor of 8 for horizontal surfaces facing downward.

In their study, which can be considered as the first experimental investigation for CHTCs in enclosures, Min et al. [7] studied within the range of Rayleigh number 10^9 to 10^{11} and with enclosure dimensions 3.60 by 7.35 by 2.40 m, 3.60 by 7.35 by 3.60 m, and 3.60 by 3.60 by 2.40 m. These correlations were derived for nonventilated conditions. Surfaces which were not heated were kept at constant temperature. Temperatures of the surfaces and heat fluxes applied to the enclosure were measured. Also, radiation effects were recorded. While the temperatures of the surfaces that were not heated varied between 4.4°C and 21.1°C , temperatures of floor surfaces varied between 24°C and 43.3°C and temperatures of ceiling surfaces varied between 32.2°C – 65.6°C [2].

Li et al. [6] investigated natural convection in an occupied office room with normal working conditions up to a temperature difference of 1.5°C .

Karadağ [13] numerically investigated the relationship between radiation and convection heat transfer coefficients at ceilings when the floor surface was isolated. To achieve this goal, first Karadağ neglected radiative heat transfer at surfaces ($\varepsilon_w = \varepsilon_c = 0$) for different room sizes (3 by 3 by 3 m, 4 by 3 by 4 m, and 6 by 3 by 4 m) and thermal boundary conditions ($T_c = 0$ – 25°C , $T_w = 28$ – 36°C). Then Karadağ determined radiative heat transfer for different surface emissivities ($\varepsilon_w =$

$\varepsilon_c = 0.7$ – 0.8 and 0.9). Numerical data were compared with results in the literature. The ratios of radiative heat transfer to convective heat transfer coefficients were calculated, and it was observed that ratios varied from 0.7 to 2.3.

Karadağ et al. [14] numerically analyzed changes in Nusselt number with ceiling and floor temperatures and room dimensions. While wall temperatures were kept at constant, ceiling temperature ranged from 10 to 25°C for different room dimensions. It was observed that when the temperature between the ceiling and air was raised, the Nusselt number over the floor also increased. Correlations in the literature that did not take into account the ceiling and floor temperatures deviated up to 35% from the results of this study. As a result, it was indicated that a new correlation for Nusselt number over the floor that encompasses the effect of thermal conditions and all room dimensions must be explored.

Although many other laminar regime natural problems in an enclosure have been solved in the literature, the turbulence natural convection problem in an enclosure of a similar size as a real room that was heated from one wall and cooled from the opposite wall has not been thoroughly researched with numerical methods, especially due to the length of solution periods. The main purpose of this study is to numerically investigate the effect of hot and cold wall temperatures of the room and characteristic length on average Nusselt number and CHTC for an enclosure modeled two- and three-dimensionally. Then, the results were compared with the correlations in the literature that are presented in Table 1.

TABLE 3: Change of Nusselt numbers and CHTCs at various wall temperatures (3D solution results, $L \times H \times L = 4.00 \times 2.85 \times 4.00$ m).

T_H (°C)	$T_c = 5^\circ\text{C}$			$T_c = 10^\circ\text{C}$			$T_c = 15^\circ\text{C}$		
	Ra	Nu	h (W/m ² K)	Ra	Nu	h (W/m ² K)	Ra	Nu	h (W/m ² K)
20	$1.1E + 11$	647.11	4.06	$7.03E + 10$	550.66	3.48	$3.38E + 10$	423.68	2.7
25	$1.41E + 11$	703.08	4.44	$1.01E + 11$	623.9	3.98	$6.51E + 10$	530.78	3.41
30	$1.69E + 11$	747	4.76	$1.3E + 11$	677.82	4.35	$9.39E + 10$	601.35	3.89
35	$1.95E + 11$	781.9	5.02	$1.57E + 11$	720.13	4.66	$1.21E + 11$	653.27	4.26

The enclosure's right and left walls were heated and cooled with constant wall temperature, while the other walls of the enclosure were kept adiabatic with the heat flux input "0 W/m²".

2. Numerical Method and Mathematical Formulation

Because of long solution periods of governing equations in large geometries, utilization of computational fluid dynamics (CFD) programs has not been practical until a few years ago. However, today's improving computer technology allows us to utilize CFD programs in this field. Despite the frequent mesh density in the boundary layers of room model, CFD programs provide results in reasonable periods, especially in 2D solutions but also in 3D solutions. In this study, we examined numerical methods for calculating average Nusselt number and CHTCs over the heated wall of an enclosure that had similar dimensions to a room of a building. 2D and 3D natural convection problems in enclosure with the dimensions of 4.00 by 2.85 by 4.00 were considered. In order to acquire similar wall temperatures with wall heating systems, the heated sidewall was heated within the range of 20°C to 35°C, while cooled sidewall was cooled to the temperatures between 5°C-15°C. The other walls of the enclosure were kept adiabatic.

The most significant aspect of solving a heat transfer problem in a real-size room by means of a CFD program is to model and properly mesh of the enclosure. For 2D and 3D modeling the enclosure, GAMBIT 2.4.6, a modeling and meshing program, was chosen. In simple geometries as in this study's model, quad/hex meshes provide more qualified solutions with fewer cells than a tri/tet mesh. Thus, all the surfaces of the enclosure were chosen as plane quad/hex meshes in this study. To decrease the meshing effects on the results in each modeling type (two- and three-dimensional) edges of both 2D and 3D modeled rooms have been meshed with different "interval counts." In order to observe whether the mesh effect has been widely diminished, Nusselt numbers were taken from FLUENT for each modeling condition. Since, the difference between the last two solutions is so small, the interval count before the last one (120 × 100) was chosen as appropriate number. In the 2D model, distance between heated and cooled walls (characteristic length, $L = 4.0$ m) was divided into 120 intervals. These intervals were preferred to be frequent near walls due to the rapid temperature differences in surface boundary layers; nonetheless, the intervals were determined less frequent towards the center of the model

(Figures 1 and 2) due to the fact that temperature fluctuation from outside of the boundary layer to center of the room is approximately zero, as can be seen in Figure 3. To achieve this, "first length"—the ratio of midpoint interval size at the edge to the first interval size at the corner of edge—was determined as 0.001. Also, in 3D solution, various interval counts on three axes were employed and appropriate interval counts were found (45 × 40 × 20). Air was chosen as the fluid existing in the enclosure.

FLUENT 6.3 software, one of the most common used codes, was utilized to solve governing equations (energy, momentum, continuity, and turbulence). The program's solution technique is focused on control volume theory turning governing equations into algebraic equations in order to solve them. The control volume technique works by integrating the governing equations for each control volume and then generating discretization of the equations, which conserve each quantity based on control volume [15]. In the model, the key dimension used is characteristic length ($L = 4.0$ m)—which is the difference between heated and cooled walls, that is opposite walls. According to characteristic length, the Rayleigh numbers for the system were calculated, as shown in (1) for one example.

Full Rayleigh numbers table can be seen in Tables 2 and 3. Because all the Rayleigh numbers calculated were greater than 10^9 , a turbulence model was applied in the flow pattern. The first order upwind scheme was utilized to discretize governing equations. The under relaxation factors for density, momentum, turbulence kinetic energy, turbulence dissipation rate, turbulent viscosity, and energy (1.0, 2.0, 0.8, 0.8, 1, and 0.9) were preferred to converge the solution. Simulations were performed on a laptop with an Intel Core i5 processor and the following specifications –2430 M CPU 2.40 GHz, 6 GB Ram, Windows 7 Home Basic 64 Bit SPI operating system. The required solution period for each appropriate (meshing effect minimized) grid model was about 12 hours:

$$\text{Ra} = \frac{g\beta L^3 (T_H - T_C)}{\nu\alpha} = \frac{9.81 \times 0.0034 \times 4^3 (30 - 10)}{15.26 \times 10^{-5} \times 2.15 \times 10^{-5}} = 1.3 \times 10^{11} > 10^9. \quad (1)$$

The governing equations for turbulence 3D flow can be written as follows.

Continuity equation:

$$\frac{\partial u}{\partial x} + \frac{\partial v}{\partial y} + \frac{\partial w}{\partial z} = 0. \quad (2)$$

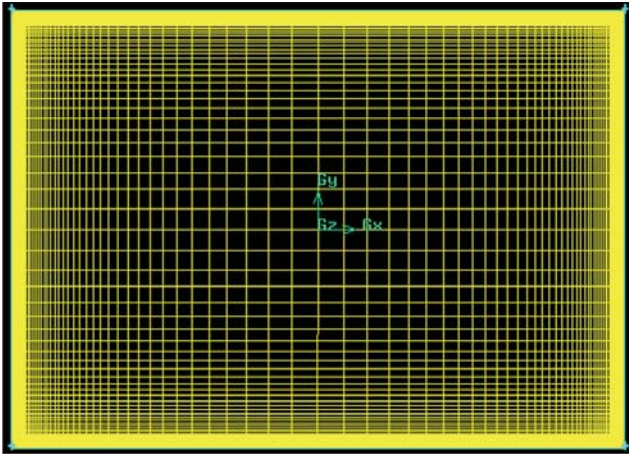


FIGURE 1: Meshing detail of two-dimensional room ($L \times H = 4,0 \text{ m} \times 2,85 \text{ m}$).

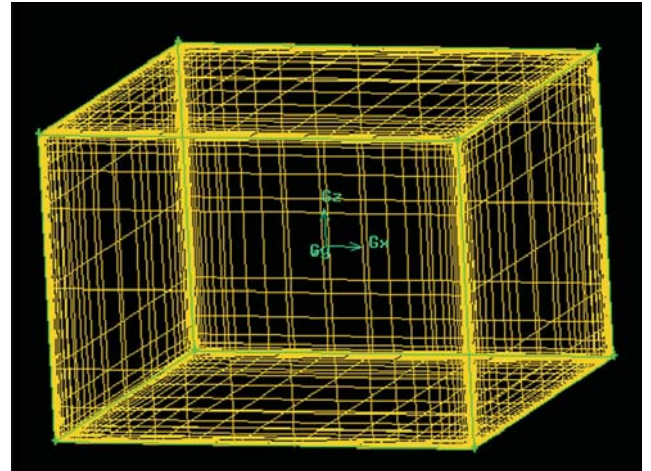


FIGURE 2: Meshing detail of three-dimensional room ($L \times H \times L = 4,0 \text{ m} \times 2,85 \text{ m} \times 4,0 \text{ m}$).

Momentum equations:

$$\begin{aligned} \rho \left(u \frac{\partial u}{\partial x} + v \frac{\partial u}{\partial y} + w \frac{\partial u}{\partial z} \right) &= - \frac{\partial p}{\partial x} + \mu \left(\frac{\partial^2 u}{\partial x^2} + \frac{\partial^2 u}{\partial y^2} + \frac{\partial^2 u}{\partial z^2} \right) \\ \rho \left(u \frac{\partial v}{\partial x} + v \frac{\partial v}{\partial y} + w \frac{\partial v}{\partial z} \right) &= - \frac{\partial p}{\partial y} + \mu \left(\frac{\partial^2 v}{\partial x^2} + \frac{\partial^2 v}{\partial y^2} + \frac{\partial^2 v}{\partial z^2} \right) \\ \rho \left(u \frac{\partial w}{\partial x} + v \frac{\partial w}{\partial y} + w \frac{\partial w}{\partial z} \right) &= - \frac{\partial p}{\partial z} + \rho g \\ &\quad + \mu \left(\frac{\partial^2 w}{\partial x^2} + \frac{\partial^2 w}{\partial y^2} + \frac{\partial^2 w}{\partial z^2} \right). \end{aligned} \quad (3)$$

Energy equation:

$$\rho \left(u \frac{\partial T}{\partial x} + v \frac{\partial T}{\partial y} + w \frac{\partial T}{\partial z} \right) = \alpha \left(\frac{\partial^2 T}{\partial x^2} + \frac{\partial^2 T}{\partial y^2} + \frac{\partial^2 T}{\partial z^2} \right). \quad (4)$$

Residual values were determined as 10^{-6} for energy and 10^{-3} for momentum and continuity equations. The physical properties of air (thermal conductivity, specific heat, density, and viscosity) in the room were written into the program as the average temperature value of hot and cold walls from Incropera and DeWitt's physical properties of air tables [15].

FLUENT has two different solver types, "Pressure Based" and "Density Based." In this study, we chose "Density Based," and the Boussinesq approach was applied. Among many viscous models presented by the program, as suggested by Karadağ [13], " $k-\varepsilon$ " was chosen, and the model of " $k-\varepsilon$ " was indicated as "standard" which was utilized by Awbi as well. Studies in the literature suggest that the $k-\varepsilon$ standard model is the most appropriate for natural convection. It is the most widely used engineering turbulence model for industrial applications, as it is robust and reasonably accurate and contains submodels for compressibility, buoyancy and combustion, and so forth. Also, it is suitable for initial iterations, initial screening of alternative designs, and parametric

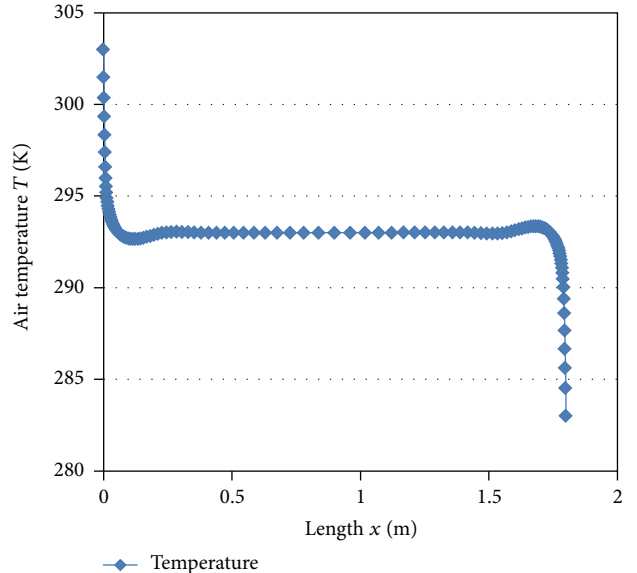


FIGURE 3: Temperature variation along the center of enclosure, from midpoint of hot wall to cold wall ($L \times H \times L = 4,0 \times 2.85 \times 4,0 \text{ m}$).

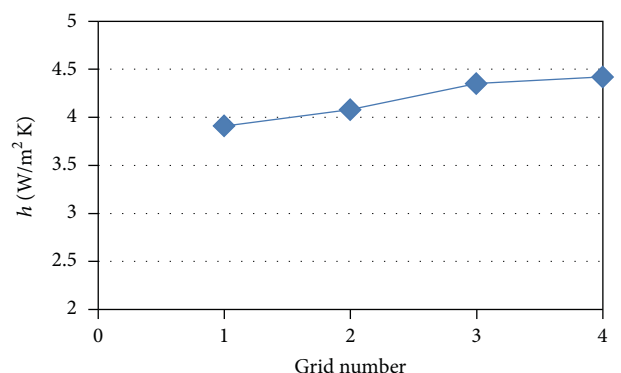


FIGURE 4: Grid independency of 2D results in terms of CHTC.

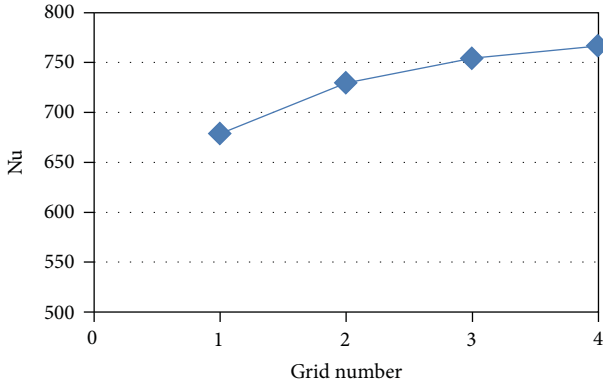


FIGURE 5: Grid independency of 2D results in terms of Nu.

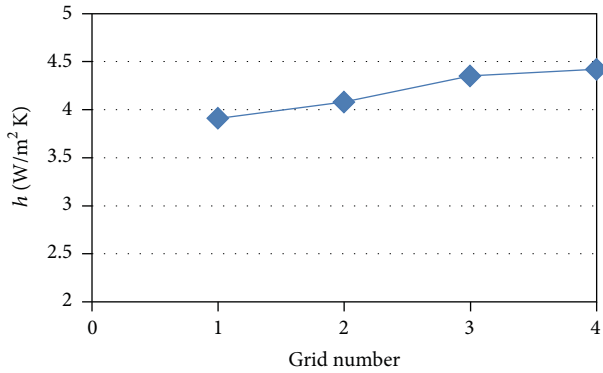


FIGURE 6: Grid independency of 2D results in terms of CHTC.

studies, like this study: Fluent User's Guide, Introductory FLUENT v6.3 notes [16]. Turbulence kinetic energy, k , and dissipation rate, ε , have been calculated through the transport equations (5) and (6), respectively,

$$\frac{\partial}{\partial x} (\rho k u) = \frac{\partial}{\partial y} \left(\left[\left(\mu + \frac{\mu_t}{\sigma_k} \right) \frac{\partial k}{\partial y} \right] \right) + G_k - \rho \varepsilon \quad (5)$$

$$\frac{\partial}{\partial x} (\rho \varepsilon u) = \frac{\partial}{\partial y} \left(\left[\left(\mu + \frac{\mu_t}{\sigma_\varepsilon} \right) + \frac{\partial \varepsilon}{\partial y} \right] \right) + C_{\varepsilon 1} \frac{\varepsilon}{k} G_k - \rho C_{\varepsilon 2} \frac{\varepsilon^2}{k}, \quad (6)$$

where

$$\begin{aligned} \mu_t &= \rho c_p \frac{k^2}{\varepsilon} \\ G_k &= -\rho \bar{v}' u \frac{\partial v}{\partial x} \end{aligned} \quad (7)$$

where $C_{\varepsilon 1}$ and $C_{\varepsilon 2}$ are constants. σ_k and σ_ε are the turbulent Pr numbers for k and ε , respectively. Also, k - ε model constants, C_μ , $C_{\varepsilon 1}$, $C_{\varepsilon 2}$, σ_k , and σ_ε are equal to 0.09, 1.44, 1.92, 1.0, and 1.3, respectively (Fluent User's Guide, Introductory FLUENT v6.3 notes [16], Yilmaz and Öztürk [17]).

Because the object of study was to find average CHTC and because the program gives CHTC with surface radiation heat transfer coefficient and these two could not be separated

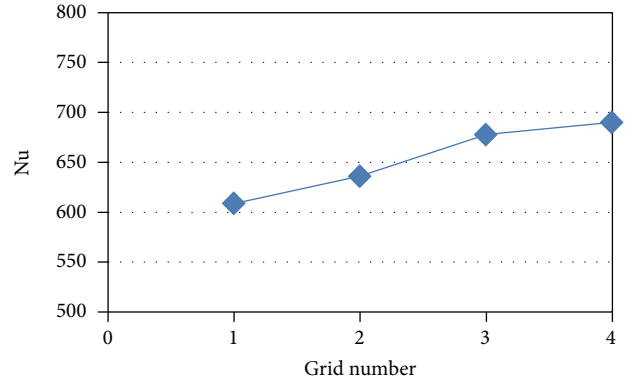
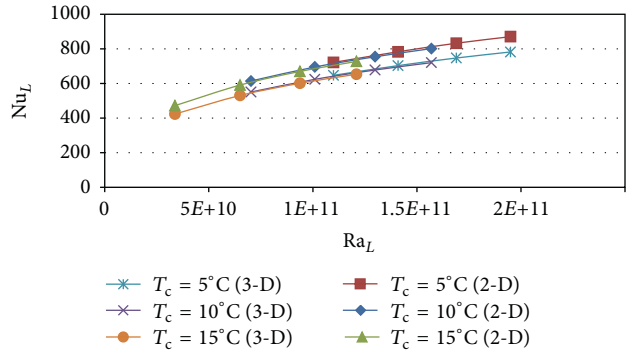


FIGURE 7: Grid independency of 2D results in terms of Nu.

FIGURE 8: Change of Nusselt number at different cold wall temperatures ($T_c = 5\text{--}15^\circ\text{C}$, $T_H = 20\text{--}35^\circ\text{C}$, $L \times H \times L = 4.0 \times 2.85 \times 4.0\text{ m}$).

from each other, no radiation model was chosen from the "models" section of the program. In FLUENT, thermal boundary conditions can be defined with five different methods: constant heat flux, constant temperature, convection, radiation, and mixed. In this study, the wall surfaces that were not heated and cooled were assumed adiabatic and defined as "0 W/m²" to reach adiabatic boundary conditions in the program. In addition, thermal boundary conditions of heated and cooled walls that stood opposite were defined at a constant temperature. As suggested by Karadağ et al. [14], the surface Nusselt numbers of the heated walls were examined as references to decide whether the meshing effect on results was diminished. In Figures 4–7 the CHTC and Nu number results that were obtained at different interval counts were presented and as stated above the optimum interval counts for 2D and 3D models were determined (120×100) and ($45 \times 40 \times 20$), in other words, "Grid Number 3," because the difference between the last two grid number preferences is approximately 1%. To reduce the solution period and since the difference is about 1%, "Grid Number 4" was not chosen as the appropriate model.

Average Nusselt number and CHTC in the enclosure are calculated through the program's "area weighted average" speciality function and β , α , and γ are calculated at film temperature, namely, the average temperature of hot and cold wall temperatures. If we calculate the Rayleigh number for the

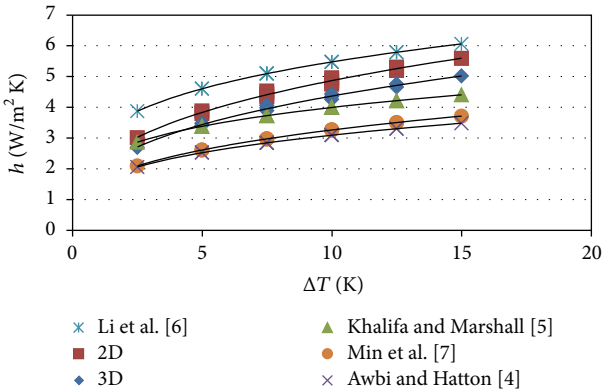


FIGURE 9: Change of CHTC at various temperature difference values between hot and cold walls ($T_c = 5-15^\circ\text{C}$, $T_H = 20-35^\circ\text{C}$, $L \times H \times L = 4.0 \times 2.85 \times 4.0 \text{ m}$).

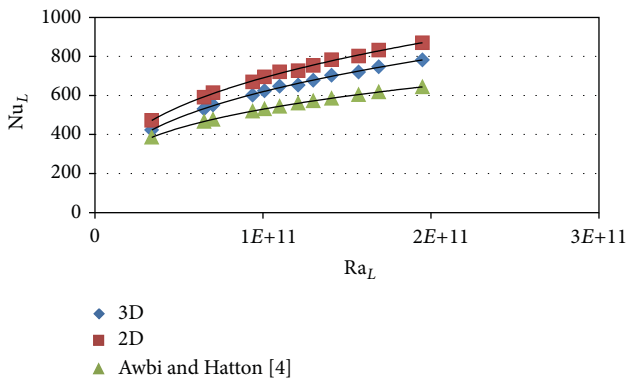


FIGURE 10: Variation of Nusselt number with Rayleigh number in the enclosure ($L \times H \times L = 4.0 \times 2.85 \times 4.0 \text{ m}$).

4,0 by 2,85 by 4,0 m room that can be seen in Figures 1 and 2 when hot and cold wall temperatures are 30°C and 10°C , respectively, it can be seen that Rayleigh number is above 10^9 , and consequently the flow pattern present in the room is turbulent. All calculated Rayleigh numbers at various wall temperatures are presented in Tables 2 and 3. Also, Nusselt numbers and CHTCs at corresponding Rayleigh numbers have been presented in these tables.

3. Results and Discussion

Computational solutions were conducted according to the depictions which were mentioned previously in Section 2. In these solutions, different hot and cold wall temperatures were applied in order to acquire various points on the Nusselt-Rayleigh number diagrams. Figure 8 illustrates the change of hot wall surface average Nusselt number with variation of cold wall temperatures for one constant room dimension (4.0 by 2.85 by 4.0 m), for both (2D) and (3D). The approximate difference between these results is 10% as also can be seen from Tables 2 and 3. It is obvious from the figures that when the cold wall temperature increases, the temperature difference between the hot wall and cold wall decreases, and thus the Nusselt number over the hot wall also decreases. Therefore, it can be stated that the temperature of cold wall

in a room affects the Nusselt number and CHTC in the enclosure.

In Figures 8–10, results of this numerical study, implemented through FLUENT, for appropriate hot and cold wall temperatures similar to real wall temperatures in buildings (hot and cold wall temperatures for real-room surfaces) were compared with the results of correlations presented in the literature. For all the Rayleigh numbers that were presented in Tables 2 and 3, corresponding Nusselt numbers were obtained through the program and are illustrated in Figure 10. It can be deduced that in addition to the Rayleigh number, the Nusselt number depends on hot and cold wall temperatures. According to all these obtained numbers and Figure 10 we have derived two new Nusselt number correlations (8) for an enclosure similar with a real-size room of a building within a Rayleigh number range between $3.38 \cdot 10^9$ and $1.95 \cdot 10^{11}$, while the temperature difference variant of Rayleigh number has been defined as the difference between hot and cold wall temperatures:

$$\begin{aligned} \text{Nu}_L &= 0.1 \text{Ra}_L^{0.349} && \text{(2D solution)} \\ \text{Nu}_L &= 0.09 \text{Ra}_L^{0.349} && \text{(3D solution).} \end{aligned} \quad (8)$$

As the deviations of these new correlations from the Nusselt numbers obtained via 2D and 3D numerical study are 1.76% and 0.49%, deviations of 2D and 3D results from Awbi and Hatton's [4] correlation are 19.34% and 13.43%, respectively. Although 2D solutions have a much more sophisticated meshing infrastructure, 3D solution has a closer agreement with Awbi and Hatton's [4] experimental work. This situation can be explained with "adjacent wall effects." Similar with vertical plate correlations presented and utilized for many years in the literature, 2D solutions also have a disadvantage. In 2D solutions, although the effect of x and y axis can be assessed, third side effect, in other words, "depth of the enclosure," cannot be counted in the solution progression. Studies published in the literature show that all surrounding walls in the enclosure affect CHTCs, since they have significant effect on flow pattern. Hence, the difference between Awbi and Hatton's [4] experimental work and the 3D solutions of this study has better agreement than the 2D solution results as can be seen in Figure 9, although two-dimensional has more detailed meshing frequency especially near walls. Differences may also be interpreted with measurement precision quality of compared experimental study.

Two novel correlations were derived and presented in the figure, written as (9). It can be discerned that CHTC in an enclosure varies with temperature difference between room centre and heated or cooled wall. Figure 9 shows that discrepancies of 3D results of this study and the results of Khalifa and Marshall [5], Li et al. [6], Min et al. [7], and Awbi and Hatton [4] are 6.38%, 21.66%, 25.05%, and 27.7%, respectively. Differences between this study and the aforementioned studies can be interpreted as follows. In Min et al. [7] study no heating equipment on the vertical walls was utilized. Rather, the study used "heated floor on heated ceiling" and the difference can be explained due to this preference. Li et al. [6] worked in an "occupied room under

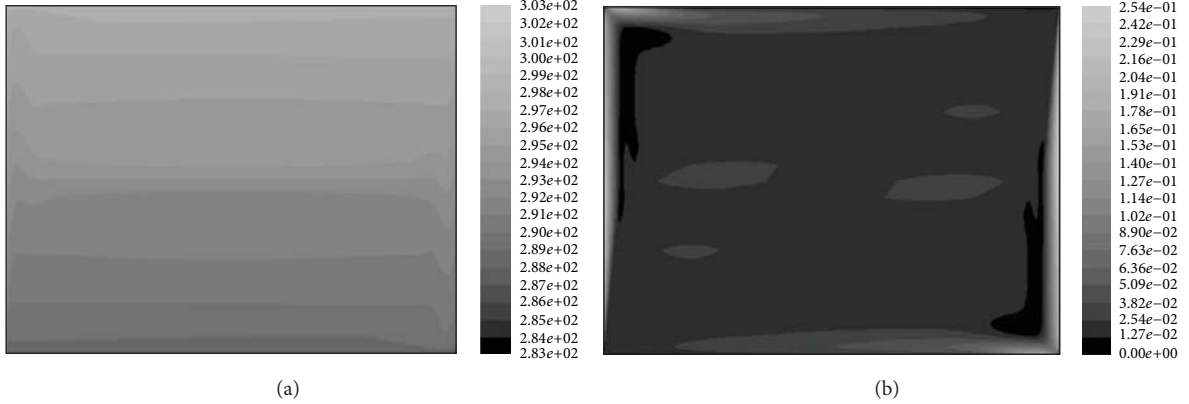


FIGURE 11: CFD predictions of temperature (K) and velocity magnitude (m/s) contours of 2D model's results, respectively ($T_H = 30^\circ\text{C}$, $T_C = 10^\circ\text{C}$; $L \times H \times L = 4.0 \times 2.85 \times 4.0 \text{ m}$).

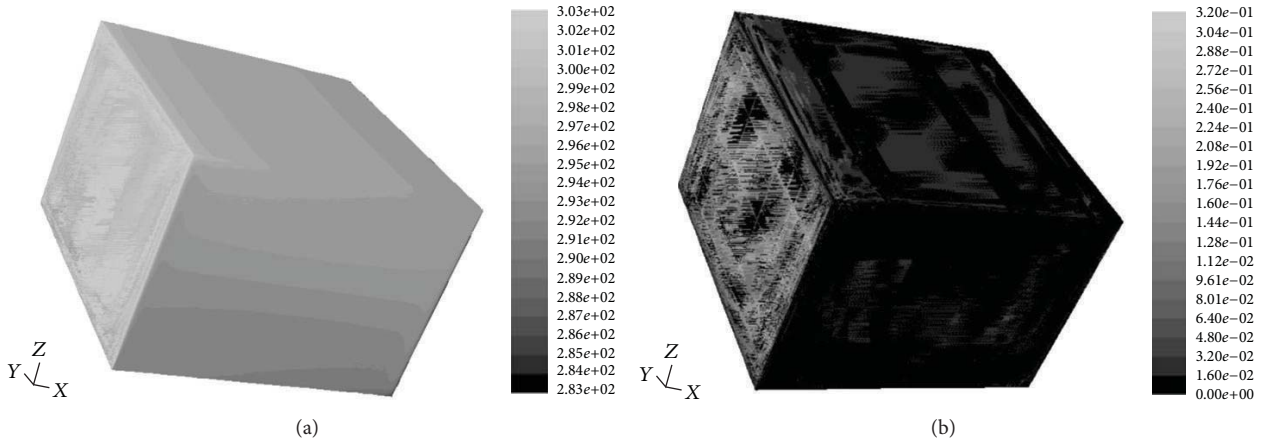


FIGURE 12: CFD predictions of temperature (K) and velocity magnitude (m/s) contours of 3D model's results, respectively ($T_H = 30^\circ\text{C}$, $T_C = 10^\circ\text{C}$; $L \times H \times L = 4.0 \times 2.85 \times 4.0 \text{ m}$).

normal conditions,” which could have caused the differences. Although Awbi and Hatton’s [4] comprehensive study is the most similar to the present work, the researchers of the study preferred “constant heat flux” (200 W/m^2) on vertical walls as boundary conditions. It is thought that this choice could bring about the discrepancy between the two studies. Results have not been compared with correlations derived for free plates, because, as previously stated, it was not appropriate to compare free plate results with enclosure results due to adjacent wall effects:

$$h = 2.21\Delta T^{0.343} \quad (2\text{D solution}) \quad (9)$$

$$h = 1.98\Delta T^{0.343} \quad (3\text{D solution}).$$

In addition, in Figures 11 and 12, 2D and 3D temperature and velocity flow patterns for the studied enclosure can be seen, respectively. Also, according to 2D and 3D models, maximum velocity in the room was found 0.27 m/s and 0.32 m/s , respectively. Both values are about 0.25 m/s , that is, the comfort velocity value in the rooms. Furthermore, velocity at overwhelming part of the enclosure is approximately zero.

4. Conclusions

Numerical case studies have been implemented to acquire Nusselt number and CHTC points on Rayleigh-Nusselt and CHTC- ΔT diagrams within the Rayleigh number range of $3.38 \cdot 10^9$ to $1.95 \cdot 10^{11}$. To attain different points on diagrams and to observe the convective heat transfer behavior in the enclosure, different heated and cooled wall temperatures were applied. Since, all the Rayleigh numbers are above 10^9 , the study involves the area of turbulent convective heat transfer. This study has shown that many correlations are produced by room surfaces, particularly for heated and cooled vertical wall surfaces. Also, two new correlations were derived for both average CHTC and Nusselt number in an enclosure which has the dimensions of 4.00 by 2.85 by 4.00 and heated from one vertical wall and cooled from the opposite wall in order to consist a real-room situation.

The results obtained with this study lie within the range of data obtained from other correlations. The differences between correlation results are thought to be caused by reference temperature determination, whether the study considers

3D or 2D and heat losses and gains that could not be counted by some experimental studies.

Energy consumption and thermal comfort in buildings have great impact on people's productivity, and these factors must be combined at some point. Therefore, parameters for calculating heating and cooling loads in buildings must be well investigated. Correct usage of CHTC does significantly affect losses from wall surfaces to the atmosphere. Also, CHTCs are used with the conduction loss of windows while calculating their total heat transfer coefficient. The effect of correct usage has a significant impact on total heat loss amounts. Also, correct usage has a great impact on thermal comfort in living spaces.

The study carries weight with the determination of the heating load in buildings as well. In this respect, it is thought that this study's results will also be useful for the thermal comfort and energy efficiency in buildings that use wall heating radiant systems and provide an appropriate direction to engineers who calculate heating load via package programs.

Nomenclature

$C_\mu, C_{\varepsilon 1}, C_{\varepsilon 2}, \sigma_k, \sigma_\varepsilon$:	Model constants
C_p :	Specific heat (J/kgK)
D :	Diameter (m)
G :	Generation of turbulence energy
H :	Height (m)
h :	Convective heat transfer coefficient, (W/m ² K)
L :	Length (m)
Nu :	Nusselt number
p :	Pressure (atm)
Ra :	Rayleigh number
T :	Temperature (K)
x, y, z :	Coordinates
u, v, w :	Velocities (m/s).

Greek Letters

ρ :	Density, (kg/m ³)
ε :	Emissivity, turbulence dissipation rate
Δ :	Difference
μ :	Dynamic viscosity (Ns/m ²)
μ_t :	Turbulent viscosity (Ns/m ²).

Subscripts

C :	Cold
H :	Hot, hydraulic
k :	Turbulent energy.

Acknowledgment

The authors gratefully acknowledge the financial support from the Scientific Research Projects Administration Unit of Yildiz Technical University (YTU-BAPK/27-06-01-03, 2007).

References

- [1] "ASHRAE HVAC Systems and Equipment Handbook," in *Panel Heating and Cooling*, chapter 6, American Society of Heating Refrigeration and Air-conditioning Engineers, 2000.
- [2] L. Peeters, I. Beausoleil-Morrison, and A. Novoselac, "Internal convective heat transfer modeling: critical review and discussion of experimentally derived correlations," *Energy and Buildings*, vol. 43, no. 9, pp. 2227–2239, 2011.
- [3] Beausoleil-Morrison, "The adaptive simulation of convective heat transfer at internal building surfaces," *Building and Environment*, vol. 37, no. 8-9, pp. 791–806, 2002.
- [4] H. B. Awbi and A. Hatton, "Natural convection from heated room surfaces," *Energy and Buildings*, vol. 30, no. 3, pp. 233–244, 1999.
- [5] A. J. N. Khalifa and R. H. Marshall, "Validation of heat transfer coefficients on interior building surfaces using a real-sized indoor test cell," *International Journal of Heat and Mass Transfer*, vol. 33, no. 10, pp. 2219–2236, 1990.
- [6] L. D. Li, W. A. Beckman, and J. W. Mitchell, "An experimental study of natural convection in an office room, large time results," Unpublished report, Solar Energy Laboratory, University of Wisconsin, Madison, Wis, USA, 1983.
- [7] T. C. Min, L. F. Schutrum, G. V. Parmelee, and J. D. Vouris, "Natural convection and radiation in a panel heated room," *ASHRAE Transactions*, vol. 62, pp. 337–358, 1956.
- [8] H. B. Awbi, "Calculation of convective heat transfer coefficients of room surfaces for natural convection," *Energy and Buildings*, vol. 28, no. 2, pp. 219–227, 1998.
- [9] S. Fohanno and G. Polidori, "Modelling of natural convective heat transfer at an internal surface," *Energy and Buildings*, vol. 38, no. 5, pp. 548–553, 2006.
- [10] A. J. N. Khalifa and A. F. Khudheyer, "Natural convection in partitioned enclosures: experimental study on 14 different configurations," *Energy Conversion and Management*, vol. 42, no. 6, pp. 653–661, 2001.
- [11] A. J. N. Khalifa, "Natural convective heat transfer coefficient: a review I. Isolated vertical and horizontal surfaces," *Energy Conversion and Management*, vol. 42, no. 4, pp. 491–504, 2001.
- [12] A. J. N. Khalifa, "Natural convective heat transfer coefficient: a review II. Surfaces in two- and three-dimensional enclosures," *Energy Conversion and Management*, vol. 42, no. 4, pp. 505–517, 2001.
- [13] R. Karadağ, "The investigation of relation between radiative and convective heat transfer coefficients at the ceiling in a cooled ceiling room," *Energy Conversion and Management*, vol. 50, no. 1, pp. 1–5, 2009.
- [14] R. Karadağ, I. Teke, and H. Bulut, "A numerical investigation on effects of ceiling and floor surface temperatures and room dimensions on the Nusselt number for a floor heating system," *International Communications in Heat and Mass Transfer*, vol. 34, no. 8, pp. 979–988, 2007.
- [15] F. P. Incropera and D. P. DeWitt, *Fundamentals of Heat and Mass Transfer*, John Wiley & Sons, New York, NY, USA, 4th edition, 1996.
- [16] "Introductory FLUENT v6.3 notes," 2006, <http://www.fluent-users.com>.
- [17] I. Yilmaz and H. F. Öztürk, "Turbulence forced convection heat transfer over double forward facing step flow," *International Communications in Heat and Mass Transfer*, vol. 33, no. 4, pp. 508–517, 2006.

Editorial

Two-Phase Flow and Heat Transfer Enhancement

Somchai Wongwises,¹ Afshin J. Ghajar,² Kwok-wing Chau,³ Octavio García Valladares,⁴ Balaram Kundu,⁵ Ahmet Selim Dalkılıç,⁶ and Godson Asirvatham Lazarus⁷

¹ *Fluid Mechanics, Thermal Engineering and Multiphase Flow Research Lab. (FUTURE), Department of Mechanical Engineering, Faculty of Engineering, King Mongkut's University of Technology Thonburi, Bangkok 10140, Thailand*

² *School of Mechanical and Aerospace Engineering, Oklahoma State University, Stillwater, OK 74078, USA*

³ *Department of Civil & Environmental Engineering, The Hong Kong Polytechnic University Hunghom, Kowloon, Hong Kong*

⁴ *Department of Energy Systems, Centro de Investigación en Energía, CIE-UNAM, Privada Xochicalco S/N, 62580 Temixco, MOR, Mexico*

⁵ *Department of Mechanical Engineering, Jadavpur University, Kolkata 700032, India*

⁶ *Heat and Thermodynamics Division, Department of Mechanical Engineering, Yildiz Technical University, Yildiz, 34349 Istanbul, Turkey*

⁷ *Department of Mechanical Engineering, Karunya University, Coimbatore, Tamil Nadu 641 114, India*

Correspondence should be addressed to Somchai Wongwises; somchai.won@kmutt.ac.th

Received 2 December 2013; Accepted 2 December 2013

Copyright © 2013 Somchai Wongwises et al. This is an open access article distributed under the Creative Commons Attribution License, which permits unrestricted use, distribution, and reproduction in any medium, provided the original work is properly cited.

Gas-liquid two-phase flow and heat transfer processes are commonly encountered in a wide variety of applications, for example, refrigeration and air-conditioning systems, power engineering, and other thermal processing plants. The advantage of high thermal performance in comparison to the single-phase applications leads to various engineering applications including the cooling systems of various types of equipment such as high performance microelectronics, supercomputers, high-powered lasers, medical devices, high heat-flux compact heat exchangers in spacecraft and satellites, and so forth. The aim of this special issue was to collect the original research and review papers on the recent developments in the field of two-phase flow and heat transfer enhancement. Potential topics included advanced heat pipe technologies, boiling and condensation heat transfer, CHF and post-CHF heat transfer, cooling of electronic system, Heat and mass transfer in phase change processes, instabilities of two-phase flow, measurements and modeling of two-phase flow in microchannel, microgravity in two-phase flow, nanofluids science and technology, nuclear reactor applications, passive and active heat transfer enhancement techniques, Refrigeration and air-conditioning technology, two-phase flow with heat and mass transfer, two-phase

refrigerant flow, and special topics on the latest advances in two-phase flow and heat transfer. In this special issue, we have invited a few papers that address such issues.

First paper of special issue investigates the effect of convergence angle of microchannel on two-phase flow and heat transfer during steam condensation experimentally. The experimental results show that the condensation heat flux increases with an increase in the convergence angle and/or the steam mass flux at a given coolant flow rate but decreases with an increase in the coolant flow rate at a given steam mass flux. Second paper focuses on simulating mist impingement cooling under typical gas turbine operating conditions of high temperature and pressure in a double chamber model. The results of this paper can provide guidance for corresponding experiments and serve as the qualification reference for future more complicated studies with convex surface cooling. In third paper, economic analysis of rebuilding an aged pulverized coal-fired boiler with a new pulverized coal-fired boiler including flue gas desulfurization unit and a circulating fluidized bed boiler is investigated in existing old thermal power plants. The fourth paper presents the results of a CFD analysis and experimental tests of two identical miniature flat plate heat pipes using sintered and screen

mesh wicks and a comparative analysis and measurement of two solid copper base plates 1 mm and 3 mm thick. In fifth paper, a modeled room was numerically heated from a wall and cooled from the opposite wall in order to create a real-room simulation. The cooled wall simulated heat loss of the room, and the heated wall simulated the heat source of enclosure. The effects of heated and cooled wall temperatures on convective heat transfer coefficient and Nusselt number in the enclosure were investigated numerically for two- and three-dimensional (3D) modeling states.

In summary, this special issue reflects a variety of contemporary research in heat transfer and is expected to promote further research activities and development opportunities.

Acknowledgment

We thank the authors who prepared the paper within the stringent length and time requirements. We thank the reviewers who provided meaningful suggestions on short notice.

Somchai Wongwises

Afshin J. Ghajar

Kwok-wing Chau

Octavio García Valladares

Balaram Kundu

Ahmet Selim Dalkılıç

Godson Asirvatham Lazarus



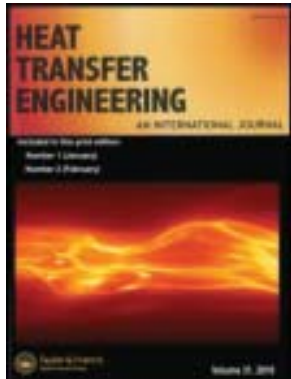
- ▶ Impact Factor **1.730**
- ▶ **28 Days** Fast Track Peer Review
- ▶ All Subject Areas of Science
- ▶ Submit at <http://www.tswj.com>

This article was downloaded by: [Mr Sujoy K. Saha]

On: 18 November 2011, At: 08:10

Publisher: Taylor & Francis

Informa Ltd Registered in England and Wales Registered Number: 1072954 Registered office: Mortimer House, 37-41 Mortimer Street, London W1T 3JH, UK



Heat Transfer Engineering

Publication details, including instructions for authors and subscription information:
<http://www.tandfonline.com/loi/uhte20>

Selected Papers on Advances in Heat Transfer

Sujoy K. Saha ^a, Gian P. Celata ^b & Somchai Wongwises ^c

^a Mechanical Engineering Department, Bengal Engineering and Science University, West Bengal, India

^b ENEA, Energy Department, Institute of Thermal Fluid Dynamics, Rome, Italy

^c Department of Mechanical Engineering, King Mongkut's University of Technology Thonburi, Bangkok, Thailand

Available online: 18 Nov 2011

To cite this article: Sujoy K. Saha, Gian P. Celata & Somchai Wongwises (2012): Selected Papers on Advances in Heat Transfer, Heat Transfer Engineering, 33:4-5, 281-283

To link to this article: <http://dx.doi.org/10.1080/01457632.2012.614157>

PLEASE SCROLL DOWN FOR ARTICLE

Full terms and conditions of use: <http://www.tandfonline.com/page/terms-and-conditions>

This article may be used for research, teaching, and private study purposes. Any substantial or systematic reproduction, redistribution, reselling, loan, sub-licensing, systematic supply, or distribution in any form to anyone is expressly forbidden.

The publisher does not give any warranty express or implied or make any representation that the contents will be complete or accurate or up to date. The accuracy of any instructions, formulae, and drug doses should be independently verified with primary sources. The publisher shall not be liable for any loss, actions, claims, proceedings, demand, or costs or damages whatsoever or howsoever caused arising directly or indirectly in connection with or arising out of the use of this material.

editorial

Selected Papers on Advances in Heat Transfer

SUJOY K. SAHA,¹ GIAN P. CELATA,² and SOMCHAI WONGWISES³

¹Mechanical Engineering Department, Bengal Engineering and Science University, West Bengal, India

²ENEA, Energy Department, Institute of Thermal Fluid Dynamics, Rome, Italy

³Department of Mechanical Engineering, King Mongkut's University of Technology Thonburi, Bangkok, Thailand

Advancement of technology in virtually all fields, in one way or another, has been due to simultaneous advances in thermal engineering. Design objectives of space stations, hazardous-waste destruction, high-speed transport, electronics, materials processing and manufacturing, etc. are fulfilled by proper energy management, heat-flow control, and temperature control.

The scale of thermal engineering ranges from the very large to the near-molecular level and from very high temperatures of thousands of degrees to very low ones approaching absolute zero. Thermal energy transport occurs in every walk of human existence.

In the recent past and of course with the passage of time, tremendous progress has been made in the field of thermal science and engineering. It is a continuous process and the quest of knowledge is truly unending.

In this special issue of the journal, an attempt has been made to collate some scattered knowledge in the advances in heat transfer. Leading international heat transfer experts from the diverse fields of heat transfer have contributed in this special issue. It should be useful to the readers of the journal. This special issue is a compendium of the following 10 papers.

- The first paper is “Thermal Design of Multistream Plate Fin Heat Exchangers—A State-of-the-Art Review” by Prasanta Kumar Das and Indranil Ghosh:

Multistream plate fin heat exchangers are useful and important innovations in the design of heat exchangers. These heat exchangers encounter direct/indirect crossover in temperatures due to several thermal communications among the fluid streams, and their thermal performance depends on “stacking pattern.” Extension of the commonly used design/simulation techniques like ϵ -NTU or the LMTD method, applicable for two-stream heat exchangers, fails miserably in case of multistream units. Though several techniques have been suggested over the years, the “thermal design” method of multistream plate fin heat exchangers is far from being perfect even today.

A state-of-the-art review of the thermal design of multistream plate fin heat exchangers is presented by the authors. Different methods of analysis including “area splitting” and “successive partitioning” along with their merits and demerits are discussed. Basic thermal design methodology and its optimization, the techniques adopted for accounting variable fluid properties, axial heat conduction in the solid matrix, and thermal communication with the environment are discussed. Need for further research is emphasized.

- The second paper is “Dropwise Condensation Studies on Multiple Scales” by Basant Singh Sikarwar, Sameer Khandekar, Smita Agarwal, Sumeet Kumar, and K. Murlidhar:

New surfaces are being engineered by nanotechnology, chemical texturing technologies, thin film coatings, and physical texturing using advanced manufacturing techniques. Dropwise condensation rather than film condensation occurs on those special surfaces. Superior experimental techniques are now available to study the thermo-fluid dynamics of dropwise condensation. Phenomena at different hierarchical length

Address correspondence to Professor Sujoy K. Saha, Mechanical Engineering Department, Bengal Engineering and Science University, Shibpur, Howrah 711 103, West Bengal, India. E-mail: sujoy_k_saha@hotmail.com

scales, e.g., surface modification at the microscale, nuclei formation, formation of clusters, macroscopic droplet ensemble, and drop coalescence, are involved. Atomistic modeling of initial nucleation, droplet–substrate interaction, surface preparation, preliminary results on simulation of fluid motion inside sliding drops, experimental determination of the local and average heat transfer coefficient, and a macroscopic model of the complete dropwise condensation process underneath horizontal and inclined surfaces are discussed.

- The third paper is “Modified Wilson Plots for Enhanced Heat Transfer Experiments: Current Status and Future Perspectives” by E. van Rooyen, M. Christians, and J. R. Thome:

Performance of enhanced heat transfer tubes is evaluated indirectly using the “Wilson plot” method to first characterize the thermal performance of one side (heating or cooling supply) and then obtaining the heat transfer data for the enhanced side based on the Wilson plot results. Wilson plot evolution and alternative methods to the Wilson plot including the advantages and disadvantages are discussed. The existing method has been modified so that the experimental errors can be propagated through the method and the error in the generated correlations may be estimated. A new method based on unconstrained minimization is proposed as an alternative to the least-squares regression.

- The fourth paper is “A State-of-the-Art Review of Compact Vapor Compression Refrigeration Systems and Their Applications” by Jader R. Barbosa, Jr., Guilherme B. Ribeiro, and Pablo A. de Oliveira:

Literature on the fundamentals, design, and application aspects of compact and miniature mechanical vapor compression refrigeration systems has been critically reviewed. Vapor compression enables the attainment of low evaporating temperatures while maintaining a large cooling capacity per unit power input to the system. Miniaturization of system components, particularly the compressor, has been the significant development. When compared with competing cooling technologies, such as flow boiling in microchannels, jet impingement and spray cooling refrigeration is the only one capable of lowering the junction temperature to values below the ambient temperature. The simultaneous use of vapor compression refrigeration with the aforementioned technologies is also possible, necessary, and beneficial, since it increases greatly the potential for reducing the system size. The paper sheds some light on the thermodynamic and thermal aspects of the cooling cycle and on the recent developments regarding its components (compressor, heat exchangers and expansion device). Issues and challenges associated with the different cycle designs have been addressed. An overview of the ongoing efforts in competing technologies is also presented.

- The fifth paper is “Modeling of Evaporation and Combustion of Droplets in a Spray Using the Unit Cell Approach: A Review” by Achintya Mukhopadhyay and Dipankar Sanyal:

Modeling of evaporation and combustion of liquid fuel droplets using “unit cell” approach has been reviewed extensively. Different regimes of droplet combustion and other techniques used for evaluating mutual interaction of droplets are discussed first, followed by the detailed presentation of the cell model. Gas-phase convection, high pressure, and multi-component composition of fuels are reviewed for both dense and dilute sprays.

- The sixth paper is “Loop Heat Pipes: A Review of Fundamentals, Operation, and Design” by Amrit Ambirajan, Abhijit A. Adoni, Jasvanth S. Vaidya, Anand A. Rajendran, Dinesh Kumar, and Pradip Dutta:

The loop heat pipe (LHP) is a passive two-phase heat transport device. LHPs are used in spacecraft thermal control system and in avionics cooling and submarines. A major advantage of a loop heat pipe is that the porous wick structure is confined to the evaporator section, and connection between the evaporator and condenser sections is by smooth tubes, thus minimizing pressure drop. Basic fundamentals, construction details, operating principles, typical operating characteristics, and current developments in modeling of thermohydraulics and design methodologies of LHPs are discussed.

- The seventh paper is “Augmentation of Heat Transfer by Creation of Streamwise Longitudinal Vortices Using Vortex Generators” by Gautam Biswas, Himadri Chattopadhyay, and Anupam Sinha:

A state-of-the-art review of improving heat exchanger surfaces using streamwise longitudinal vortices is presented. Fin-tube cross-flow heat exchangers and the plate-fin heat exchangers are focused on. Protrusions in certain forms such as delta wing or winglet pairs and rectangular winglet pairs act as vortex generators, creating longitudinal vortices, disrupting growth of the thermal boundary layer, and promoting mixing between fluid layers, resulting in enhanced heat transfer from the flat or louvered surfaces. The flow fields are dominated by a swirling motion associated with a modest pressure penalty. Both computational and experimental investigations on flow and heat transfer in the heat exchanger passages with built-in vortex generators are reviewed.

- The eighth paper is “Frictional and Heat Transfer Characteristics of Single-Phase Microchannel Liquid Flows” by Ranabir Dey, Tamal Das, and Suman Chakraborty:

The literature on friction and heat transfer characteristics of single-phase liquid flows through microchannels has been reviewed. The disagreement of experimental results with theoretical predictions has been brought to the fore. Theoretical models and empirical correlations are highlighted. Aspects of microscale liquid flow and heat transfer requiring further scrutiny are identified and possible future research directions are prescribed.

- The ninth paper is “Recent Trends in Computation of Turbulent Jet Impingement Heat Transfer” by Anupam Dewan, Rabijit Dutta, and Balaji Srinivasan:

A review of the current status of computation of turbulent impinging jet heat transfer has been made. Flow and heat transfer characteristics of single jet impingement on a flat surface are considered. The effect of different sub-grid scale models, boundary conditions, numerical schemes, grid distribution, and size of the computational domain adopted in various large eddy simulations of this flow configuration is dealt with in detail. Direct numerical simulation and Reynolds-averaged Navier–Stokes modeling of the same geometry are discussed. Other complex impinging flows are also presented. A listing of some important findings and future directions in the computation of impinging flows is presented.

- The tenth paper is “Two-Phase Natural Circulation Loops: A Review of the Recent Advances” by Souvik Bhattacharyya, Dipankar N. Basu, and Prasanta K. Das:

Experimental and theoretical studies of two-phase natural circulation loops abound in the literature. A comprehensive review has been made by the authors. Different forms of thermal-hydraulic instabilities and coupled nuclear instabilities are discussed. Further research direction is delineated.

We thank the authors for their contributions, and the reviewers, who have played a great role in improving the quality of the papers. We also thank the editor-in-chief of *Heat Transfer Engineering*, Professor Afshin Ghajar, for his willingness to publish this special issue highlighting the current research going on worldwide.



Sujoy K. Saha is a professor of mechanical engineering at Bengal Engineering and Science University Shibpur, India. He specializes in heat transfer enhancement, heat transfer in microchannels, biomimetics, and circulating fluidized bed. Prof. Saha is an associate editor of *ASME Journal of Heat Transfer*, editor of *Experimental Thermal and Fluid Science*, associate editor of *Heat Transfer Engineering*, regional editor of the *Journal of Enhanced Heat Transfer*, and guest editor of *Frontiers of Heat and Mass Transfer*. Prof. Saha has published about 60 articles in international and national peer-reviewed journals and conferences.



Gian P. Celata is director of the Division of Advanced Technologies for Energy and Industry of ENEA, Italy. He is a member of the European Academy of Sciences, of several scientific boards in Italy (UIT, past-President, ANIMP, AIDIC), and also of international scientific boards (EUROTHERM, past president, AIHTC, AWC, vice-president, ICHMT, Executive Committee). Dr. Celata is also the editor-in-chief of the *Journal of Experimental Thermal and Fluid Science* and associate editor of the *International Journal of Thermal Sciences*. He is also the editor of *Thermopedia and Heat Exchangers Design Handbook*. His areas of expertise are heat transfer and two-phase flow, CHEx, microscale heat transfer, bubbly flow, two-phase critical flow, and CHF. He has about 200 articles in international journals and international conferences, and one patent, and is the editor of many scientific books.



Somchai Wongwises is a professor of mechanical engineering at King Mongkut's University of Technology Thonburi, Bangkok, Thailand. He received his Dr.-Ing. (Doktor Ingenieur) in mechanical engineering from the University of Hannover, Germany, in 1994. His research interests include two-phase flow, heat transfer enhancement, and thermal system design. Professor Wongwises is the head of the Fluid Mechanics, Thermal Engineering and Multiphase Flow Research Laboratory (FUTURE).



CONGRATULATIONS!

YOU ARE A HIGHLY-CITED AUTHOR.



REUTERS/Morteza Nikoubazl

Dear Dr. Wongwises,

Congratulations! You have been identified as a highly-cited author according to our Thomson Reuters *Essential Science Indicators*™ and *Web of Science*® (formerly ISI). We are sure your research work in Thailand has motivated many in your field.

As a leading scientist in your field, we are sure you will like to know what other leading scientists are doing, what the hottest topics are affecting research and everyday life, and where the most significant research is taking place. As such, we would also like to bring to your attention our online publication, *Science Watch*®, which provides a behind-the-scenes look at the scientists, journals, institutions, nations, and papers selected by *Essential Science Indicators* from Thomson Reuters.

Science Watch provides a comprehensive, open web resource for science metrics and analysis, along with regularly updated interviews, and commentary source data drawn from *Essential Science Indicators*. Bringing all these resources together in one easily accessible website gives the scientific community an ideal and convenient location for keeping up with the latest developments in science.

We hope you find this useful. If you need more information, please contact Shujie Yu at shujie.yu@thomsonreuters.com

Congratulations once again from all of us at Thomson Reuters.

Best regards

Shujie

.....
Shujie Yu
Account Manager, Academic
Thomson Reuters

Phone: +65 6870 3747
Mobile: +65 9658 9751
Fax: +65 6223 2634



Heat and Mass Transfer

Wärme- und Stoffübertragung

Editor-in-Chief: Andrea Luke

ISSN: 0947-7411 (print version)

ISSN: 1432-1181 (electronic version)

Journal no. 231



  RECOMMEND TO LIBRARIAN



16



0



1



2

[ABOUT THIS JOURNAL](#) | [EDITORIAL BOARD](#)

OPEN ACCESS

Interested in publishing your article in this journal?

Learn about your Open Access option!

CLICK

- » Covers the complete area of heat and mass transfer with relations to engineering thermodynamics and fluid mechanics
- » Publishes results from basic research as well as engineering applications, such as heat exchangers, process and chemical engineering
- » Covers experimental techniques as well as analytical and computational approaches

By publishing original research reports "Heat and Mass Transfer" (Wärme- und Stoffübertragung) serves the circulation of new developments in the field of basic research of heat and mass transfer phenomena, as well as related material properties and their measurements.

Thereby applications to engineering problems are promoted. As of 1995 the title "Wärme- und Stoffübertragung" was changed to "Heat and Mass Transfer".

Related subjects » Classical Continuum Physics - Industrial Chemistry and Chemical Engineering - Mechanical Engineering

ABSTRACTED/INDEXED IN

Science Citation Index, Science Citation Index Expanded (SciSearch), Journal Citation Reports/Science Edition, SCOPUS, INSPEC, Astrophysics Data System (ADS), Chemical Abstracts Service (CAS), Google Scholar, EBSCO, Academic OneFile, CEABA-VTB, Chimica, Current Contents/Engineering, Computing and Technology, El-Compendex, Gale, INIS Atomindex, OCLC, PASCAL, SCImago, Summon by Serial Solutions

POPULAR CONTENT WITHIN THIS PUBLICATION

Natural convection of nano-fluids

Putra, Nandy; Roetzel, Wilfried; Das, Sarit K.

The Blasius and Sakiadis flow with variable fluid properties

Pantokratoras, Asterios

High temperature heat exchanger studies for applications to gas turbines

Min, June Kee; Jeong, Ji Hwan; Ha, Man Yeong Show all authors (4)

Local jet impingement boiling heat transfer with R113

Zhou, D. W.; Ma, C. F.

Heat transfer characteristics of a new helically coiled crimped spiral finned tube heat exchanger

Srisawad, Kwanchanok; Wongwises, Somchai

READ THIS JOURNAL ON SPRINGERLINK

Online First Articles

All volumes & issues

Free: Sample Articles

FOR AUTHORS AND EDITORS

2012 Impact Factor  0.840

Aims and Scope

Submit Online

Open Choice - Your Way to Open Access

Instructions for Authors

Submission information

SERVICES FOR THE JOURNAL

Contacts

Download Product Flyer

Shipping dates

Order back issues

Bulk Orders

Article Reprints

ALERTS FOR THIS JOURNAL

Get the table of contents of every new issue published in Heat and Mass Transfer.

Your E-Mail Address

 SUBMIT

Please send me information on new Springer publications in Engineering Thermodynamics, Heat and Mass Transfer.

ADDITIONAL INFORMATION

How to sign up for ToC alerts

RELATED BOOKS - SERIES - JOURNALS



Journal

Journal of Engineering Physics and Thermophysics

Editor » Zhdanov, S.A.



Experimental Thermal and Fluid Science

International Journal of Experimental Heat Transfer, Thermodynamics, and Fluid Mechanics

Experimental Thermal and Fluid Science provides a forum for research emphasizing experimental work that enhances basic understanding of heat transfer, thermodynamics and fluid mechanics, and their applications...

[View full aims and scope](#)

Editors-in-Chief: G.P. Celata, N. Selçuk

[View full editorial board](#)[Guide for Authors](#)[Submit Your Paper](#)[Track Your Paper](#)[Order Journal](#)[View Articles](#)

Share this page:



ADVERTISEMENT

GIVE
YOUR
PAPER
A VOICE
WITH
AUDIO-
SLIDES

Impact Factor:
1.5955-Year Impact
Factor: 1.777Imprint:
ELSEVIER

ISSN: 0894-1777

Stay up-to-date

Register your interests and receive email alerts tailored to your needs

[Click here to sign up](#)

Follow us



Subscribe to RSS



Latest News

Publish your article
Open Access in
Experimental
Thermal and Fluid
Science

Journal Insights

Discover this journal's metrics

[FIND OUT MORE](#)

Most Cited Articles

Scopus

Measurement of temperature-dependent thermal conductivity and viscosity of TiO₂-water nanofluids
Duangthongsuk, W. | Wongwises, S.

Experimental investigations and theoretical determination of thermal conductivity and viscosity of Al₂O₃/water nanofluid
Chandrasekar, M. | Suresh, S. | ...

An experimental study of convective heat transfer with microencapsulated phase change material suspension: Laminar flow in a circular tube under constant heat flux
Chen, B. | Wang, X. | ...

[VIEW ALL](#)

Most Downloaded Articles

ScienceDirect

1. Cyclic steam generation from a novel zeolite–water adsorption heat pump using low-grade waste heat
Bing Xue | Yoshiho Iwama | ...

2. Two-phase flow in microchannels
Akimi Serizawa | Ziping Feng | ...

3. Fundamental issues related to flow boiling in minichannels and microchannels
Satish G Kandlikar

[VIEW ALL](#)

News

Welcome to four new editors; farewell and thanks as two editors 'retire'

[VIEW ALL](#)

Special Issues

[ORDER NOW](#)

Seventh Mediterranean Combustion Symposium
Volume 43 (2012)

7th ECI-International Conference on Boiling Heat Transfer - ICBHT-2009
Volume 35, Issue 5 (2011)

[ORDER NOW](#)

ECI International Conference on Heat Transfer and Fluid Flow in Microscale
Volume 35, Issue 5 (2011)

[ORDER NOW](#)

Dear Dr. Wongwises,

Congratulations! You have been identified as a highly-cited author according to our Thomson Reuters Essential

ภาคผนวก ช.

ผลงานการนำไปใช้ประโยชน์ เชิงพาณิชย์

บริษัท ไซโจเดนกิ อินเตอร์เนชันแนล จำกัด

ชื่อโครงการ

การออกแบบการทดลองและการทดสอบเครื่องปรับอากาศรุ่น Hybrid Air Hydro (HAH)

ที่มา หรือเหตุผลที่ศึกษา วิจัย คิดค้น หรือปรับปรุงความรู้

บริษัท ไซโจเดนกิ อินเตอร์เนชันแนล จำกัด เป็นบริษัทของคนไทยที่ผลิตเครื่องปรับอากาศที่ใหญ่ที่สุด บริษัทฯผลิตเครื่องปรับอากาศเครื่องหมายการค้าไซโจเดนกิ จำหน่ายภายใต้ประเทศไทยและส่งออกไปจำหน่ายยังต่างประเทศ เนื่องจากเป็นบริษัทของคนไทย จึงไม่มีความช่วยเหลือจากบริษัทแม่ในต่างประเทศ ทำให้ต้องขวนขวยพัฒนาสินค้าของตัวเองเพื่อแข่งกับตลาดทั้งในประเทศและต่างประเทศ

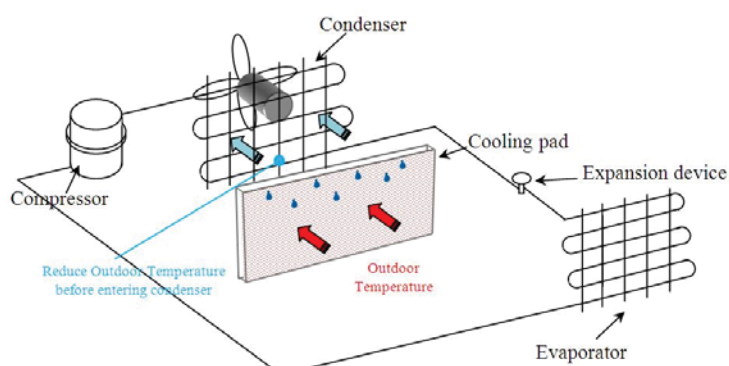
บริษัทฯมียอดการผลิตเครื่องปรับอากาศเป็นอันดับที่ 3-4 ของประเทศ และถือเป็นบริษัทที่มีเจ้าของเป็นคนไทย ใช้ความรู้จากคนไทย พัฒนาโดยคนไทยที่ เห็นความสำคัญของการวิจัยและพัฒนาโดยพยายามหาวิธีการหรือหลักการใหม่ๆมาพัฒนาผลิตภัณฑ์อยู่ตลอดเวลา เครื่องปรับอากาศรุ่น HAH เป็นอีกรุ่นที่บริษัทพัฒนาขึ้นมา อย่างไรก็ตามบริษัทฯยังขาดการทดสอบเครื่องปรับอากาศตามมาตรฐาน เพื่อให้ทราบถึงสมรรถนะที่แท้จริงของเครื่องปรับอากาศ รวมถึงการพัฒนาปรับปรุงแก้ไขข้อบกพร่อง เพื่อให้เครื่องปรับอากาศมีสมรรถนะสูงขึ้น

วัตถุประสงค์ในการศึกษา วิจัย คิดค้น

ออกแบบการทดลองและการทดสอบเครื่องปรับอากาศรุ่น Hybrid Air Hydro (HAH)

วิธีการและขั้นตอนในการคิดค้น ปรับปรุงความรู้ ฯลฯ

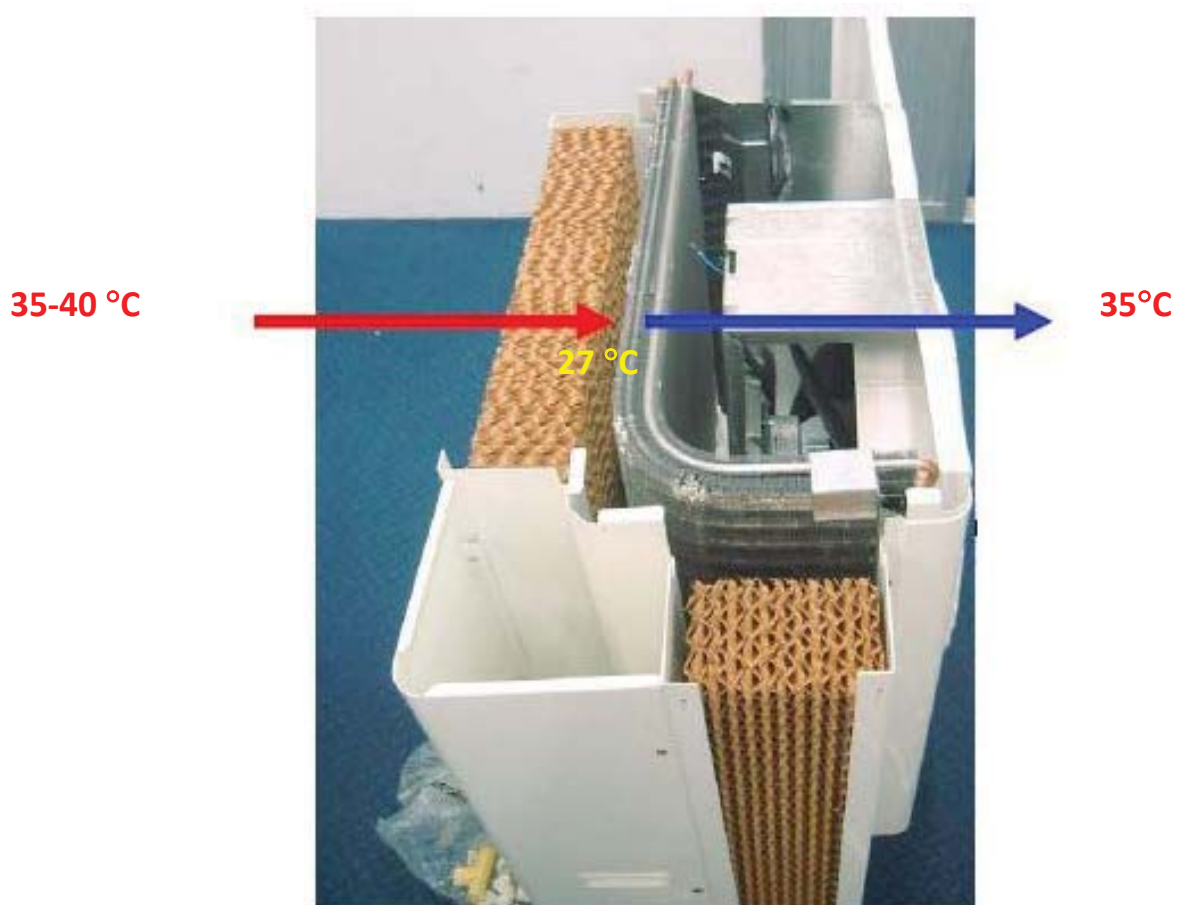
ศาสตราจารย์ ดร. สมชาย วงศ์วิเศษ ได้ช่วย บริษัทไซโจเดนกิ จำกัด ในการออกแบบการทดลอง (Experimental Design) และทำการทดสอบเครื่องปรับอากาศรุ่น Hydro Air Hybrid (HAH) 3 รุ่น ได้แก่ HAH 20 W (SJ-W18-HTGP1/SJ-C18-HTGP1), HAH 15 W (SJ-W13-HTGP1/SJ-C13-HTGP1), และ HAH 12 W (SJ-W10-HTGP1/SJ-C10-HTGP1) โดยได้ทำการวางแผนการทดลอง เก็บข้อมูล คำนวณ วิเคราะห์ผลลัพธ์ และสรุปผล ตามหลักวิชาการ ทั้งนี้รวมถึงการให้คำแนะนำในการปรับปรุงเครื่องปรับอากาศให้มีสมรรถนะสูงขึ้น



ประโยชน์ที่ได้รับ ผลของการคิดค้น ปรับปรุง การใช้วิชาการที่ก่อให้เกิดประโยชน์ต่อประเทศไทย

จากการศึกษาและทดสอบพบว่า เครื่องปรับอากาศรุ่นดังกล่าวสามารถทำงานได้ดีในทุกภาวะอากาศ และมีค่า Coefficient of Performance (COP) และ Energy Efficiency Ratio (EER) โดยเฉลี่ยเท่ากับ 4.36 และ 14.87 ตามลำดับ โดย Performance Index ทั้ง สองค่า สูงกว่ามาตรฐานที่ สำนักงานมาตรฐานอุตสาหกรรม (สมอ) กำหนด และสูงกว่าเครื่องปรับอากาศเครื่องหมายการค้าเดียวกัน และเครื่องหมายการค้าอื่นๆ ในขนาดการทำความเย็นเท่าๆกันโดยเมื่อเปรียบเทียบกับเครื่องปรับอากาศรุ่นปกติในขนาดเท่าๆกันพบว่าสามารถประหยัดได้ประมาณ 40 % นั่นหมายถึงว่าในปริมาณความเย็นเท่าๆกันเครื่องปรับอากาศรุ่นนี้ใช้พลังงานน้อยกว่า ซึ่งถ้ามองภาพรวมทั้งประเทศไทยว่าถ้าประชาชนหันมาใช้เครื่องปรับอากาศรุ่นดังกล่าวจะสามารถประหยัดพลังงานจากการใช้เครื่องปรับอากาศจำนวนมหาศาล ลดความร้อนกับนโยบายประหยัดพลังงานของประเทศไทย

ผลจากการทดสอบและช่วยปรับปรุงเครื่องปรับอากาศทั้ง 3 รุ่นดังกล่าว ทำให้บริษัทใช้โจเกนกิพบจดเด่นของตนเอง บริษัทฯ ได้ใช้จุดเด่นข้อนี้ในการโฆษณา ประชาสัมพันธ์ ผลิตภัณฑ์ชิ้นนี้ ทำให้รู้จักกันไปทั่วทั้งในประเทศไทยและต่างประเทศ โดยสามารถสร้างชื่อเสียงให้กับประเทศไทยเป็นอย่างยิ่ง ถ้าพิจารณาเฉพาะในประเทศไทย ผลิตภัณฑ์ดังกล่าวสามารถช่วยประเทศไทยชาติประหยัดพลังงานได้เป็นปริมาณมหาศาล ทั้งนี้ไม่รวมการรักษาสิ่งแวดล้อมจากการใช้พลังงานอย่างสิ้นเปลืองซึ่งไม่สามารถประเมินมูลค่าได้



บริษัท ชี แอร์คอน เทค จำกัด (โครงการที่ 1)

ชื่อโครงการ

การออกแบบและการทดสอบ Short Tube Orifice เพื่อนำมาใช้เป็น อุปกรณ์ขยายตัว

ที่มา หรือเหตุผลที่ศึกษา วิจัย คิดค้น หรือปรับปรุงความรู้

บริษัท ชี แอร์คอน เทค จำกัด เป็นบริษัทของคนไทย ที่ผลิตชิ้นส่วนเครื่องปรับอากาศและเครื่องปรับอากาศทั้งชุดส่งต่างประเทศ โดยผลิตทั้งตามข้อเสนอของลูกค้าในต่างประเทศและผลิตตามการออกแบบของตนเอง ผลิตภัณฑ์เกือบ 100 % ของบริษัทฯ ส่งออกต่างประเทศ ผลิตภัณฑ์หนึ่งที่บริษัทฯ ผลิตเพื่อการส่งออกคือ อุปกรณ์ขยายตัว (Expansion Device) แบบ Short Tube Orifice และเครื่องปรับอากาศที่ใช้ Short Tube Orifice เป็นอุปกรณ์ขยายตัว อย่างไรก็ตามบริษัทฯ ใช้วิธีการผลิตในลักษณะ Trial and Error ทำให้มีปัญหาในเรื่องของ การออกแบบและการดัดแปลง Short Tube Orifice ตลอดจนการหาระบบติดตั้งของ Short Tube Orifice ที่ใช้กับสารทำความเย็นทางเลือกใหม่ (Alternative Refrigerant) ซึ่งเป็นความต้องการของลูกค้าในต่างประเทศ

วัตถุประสงค์ในการศึกษา วิจัย คิดค้น

สร้างโปรแกรมการคำนวณและสร้าง Chart สำหรับการออกแบบ Short Tube Orifice เพื่อนำมาใช้เป็น อุปกรณ์ขยายตัว (Expansion Device) ในเครื่องปรับอากาศและเครื่องทำความเย็น

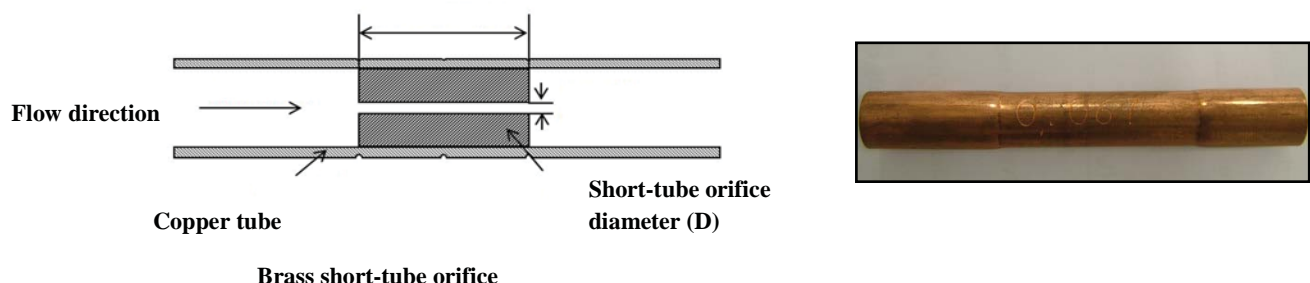
วิธีการและขอบเขตในการคิดค้น ปรับปรุงความรู้ ฯลฯ

ศาสตราจารย์ ดร. สมชาย วงศ์วิเศษ ได้นำมาเป็นหัวข้อวิจัยในโครงการพัฒนา Short Tube Orifice โครงการดังกล่าวเป็นการร่วมทุนระหว่าง โครงการบริษัทฯ เอกภัณฑ์ จำกัด-สำนักงานส่งเสริมวิสาหกิจขนาดกลางและขนาดย่อม (คปภ.-สสว.) ของสำนักงานกองทุนสนับสนุนการวิจัย (สกว.) และบริษัทชี แอร์คอน เทค จำกัด โดยดำเนินการภายใต้รหัสโครงการ เลขที่ 1MKT/50/B1 “สมรรถนะของอิพิซชันด์ท่อสันที่ใช้สารทำความเย็น R-134a สำหรับเครื่องปรับอากาศขนาดเล็ก” ผู้ดำเนินการคือ ศาสตราจารย์ ดร. สมชาย วงศ์วิเศษ และ นักศึกษาบริษัทฯ เอกภัณฑ์ จำกัด ผู้ช่วยวิจัย โดยงานจะครอบคลุมถึงการทดลองเพื่อให้ทราบถึงประสิทธิภาพการณ์การให้ผล ลดลงของความดัน สมรรถนะของตัว Short Tube Orifice และ สมรรถนะของเครื่องปรับอากาศและเครื่องทำความเย็นที่ใช้ Short Tube Orifice ตลอดจนการสร้างแบบจำลองทางคณิตศาสตร์ โปรแกรมคำนวณและ Chart สำหรับการออกแบบ Short Tube Orifice ให้สามารถใช้ได้กับภาระการทำงานต่างๆ กับสารทำความเย็นทางเลือกใหม่ต่างๆ สมการต่างๆ ที่ใช้ในแบบจำลองทางคณิตศาสตร์คือสมการที่เป็นผลจากการที่เป็นผลจากการวิจัยในส่วนของ อุปกรณ์ขยายตัว (Expansion Device) ซึ่งได้ตีพิมพ์เผยแพร่แล้วในวารสารระดับนานาชาติ ผู้ได้รับผลกระทบจากการวิจัยคือ บริษัท ชี แอร์คอน เทค จำกัด ในฐานะผู้ต้องการผลลัพธ์จากโครงการและผู้มีส่วนสนับสนุน และสำนักงานกองทุนสนับสนุนการวิจัย (สกว.) ในฐานะองค์กรของรัฐที่มีส่วนในการสนับสนุน

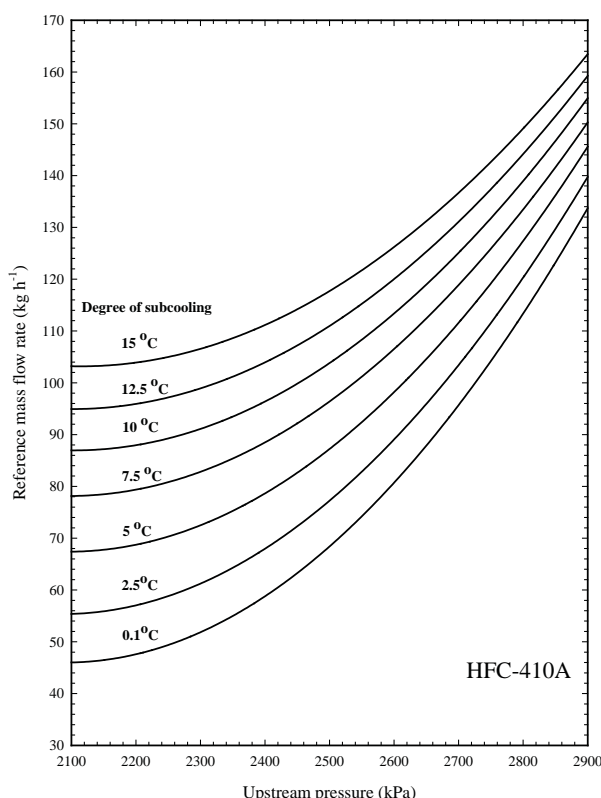
ประโยชน์ที่ได้รับ ผลของการคิดค้น ปรับปรุง การใช้วิชาการที่ก่อให้เกิดประโยชน์ต่อประเทศไทย

สามารถนำ Short Tube Orifice ไปใช้ในเครื่องปรับอากาศหรือเครื่องทำความเย็นทำให้สมรรถนะโดยรวมของอุปกรณ์ดังกล่าวสูงขึ้น และมีราคาต่ำลงเนื่องจากเป็นอุปกรณ์ที่ไม่มีความซับซ้อนเหมือนอุปกรณ์ขยายประเภทต่างๆ ที่ใช้กันในปัจจุบัน ผลจากการศึกษาสามารถนำมาใช้ประโยชน์และช่วยพัฒนาอุตสาหกรรมการผลิตเครื่องปรับอากาศและเครื่องทำความเย็นเป็นอย่างดี เพราะจะทำให้ได้ทั้งรูปร่างและขนาดของ Short Tube Orifice มีเหมาะสมกับสภาพการทำงานและสามารถทำความเย็นทางเลือกใหม่ ซึ่งนอกจากจะช่วยประหยัดพลังงาน รักษาสิ่งแวดล้อม แล้วยังเป็นการเพิ่มคุณภาพ สินค้าไทยที่ส่งออกไปยังตลาดต่างประเทศ เพิ่มมูลค่าการส่งออกและทำชื่อเสียงให้กับประเทศไทยอีกด้วย

ผลลัพธ์ที่ได้มีประโยชน์โดยตรงอย่างยิ่งต่อบริษัทซี แอร์คอน เทค จำกัด และต่อประเทศไทย เพราะจะช่วยในการออกแบบให้ได้ Short Tube Orifice ที่มีทั้งขนาดและรูปร่างที่เหมาะสมกับเครื่องปรับอากาศขนาดต่างๆ สำหรับการทำความเย็นประเภทใหม่ที่ไม่ทำลายสิ่งแวดล้อมต่างๆ ซึ่งนอกจากจะสามารถสร้างเครื่องปรับอากาศที่ประหยัดพลังงาน รักษาสิ่งแวดล้อมในภาพรวมแล้วยังเป็นการเพิ่มคุณภาพ สินค้าไทยที่ส่งออกไปยังตลาดต่างประเทศอีกด้วย



Brass short-tube orifice



บริษัท ชี แอร์คอน เทค จำกัด (โครงการที่ 2)

ข้อโครงการ

การออกแบบคุณเดนเซอร์ที่ระบบความร้อนด้วยอากาศให้กับบริษัทชี แอร์คอน เทค จำกัด

ที่มา หรือเหตุผลที่ศึกษา วิจัย คิดค้น หรือปรับปรุงความรู้

บริษัท ชี แอร์คอน เทค จำกัด เป็นบริษัทของคนไทย ผลิตภัณฑ์ของบริษัทฯคือชิ้นส่วนเครื่องปรับอากาศและเครื่องปรับอากาศทั้งชุด ผลิตภัณฑ์เกือบ 100 % ของบริษัทฯ ส่งออกต่างประเทศเนื่องจากอนาคตอันใกล้บริษัทฯต้องออกแบบและผลิตเครื่องปรับอากาศที่ใช้กับสารทำความเย็นทางเลือกใหม่ (Alternative refrigerant) ที่ไม่เป็นภัยต่อสิ่งแวดล้อม ในขณะที่ต้องรักษาให้เครื่องปรับอากาศมีสมรรถนะสูง ตามที่ประเทศลูกค้าต้องการ ด้วยเหตุนี้ແงคุณเดนเซอร์ ซึ่งเป็นส่วนสำคัญส่วนหนึ่งของเครื่องปรับอากาศ ซึ่งปกติต้องทำงานภายใต้ความดันสูงอยู่แล้วต้องได้รับการปรับปรุงเพื่อให้ทนความดันที่สูงขึ้น เมื่อเป็นเช่นนี้ จำเป็นต้องมีการออกแบบคุณเดนเซอร์ใหม่ทั้งหมด อย่างไรก็ตามการออกแบบเชิงการทดลองเสียค่าใช้จ่ายสูงและใช้เวลามาก เพื่อหลีกเลี่ยงอุปสรรคดังกล่าวจึงพยายามใช้แบบจำลองทางคณิตศาสตร์เข้าช่วยในการออกแบบ.

วัตถุประสงค์ในการศึกษา วิจัย คิดค้น

สร้างโปรแกรมสำหรับการออกแบบคุณเดนเซอร์ที่ระบบความร้อนด้วยอากาศ

วิธีการและขอบเขตในการคิดค้น ปรับปรุงความรู้ ฯลฯ

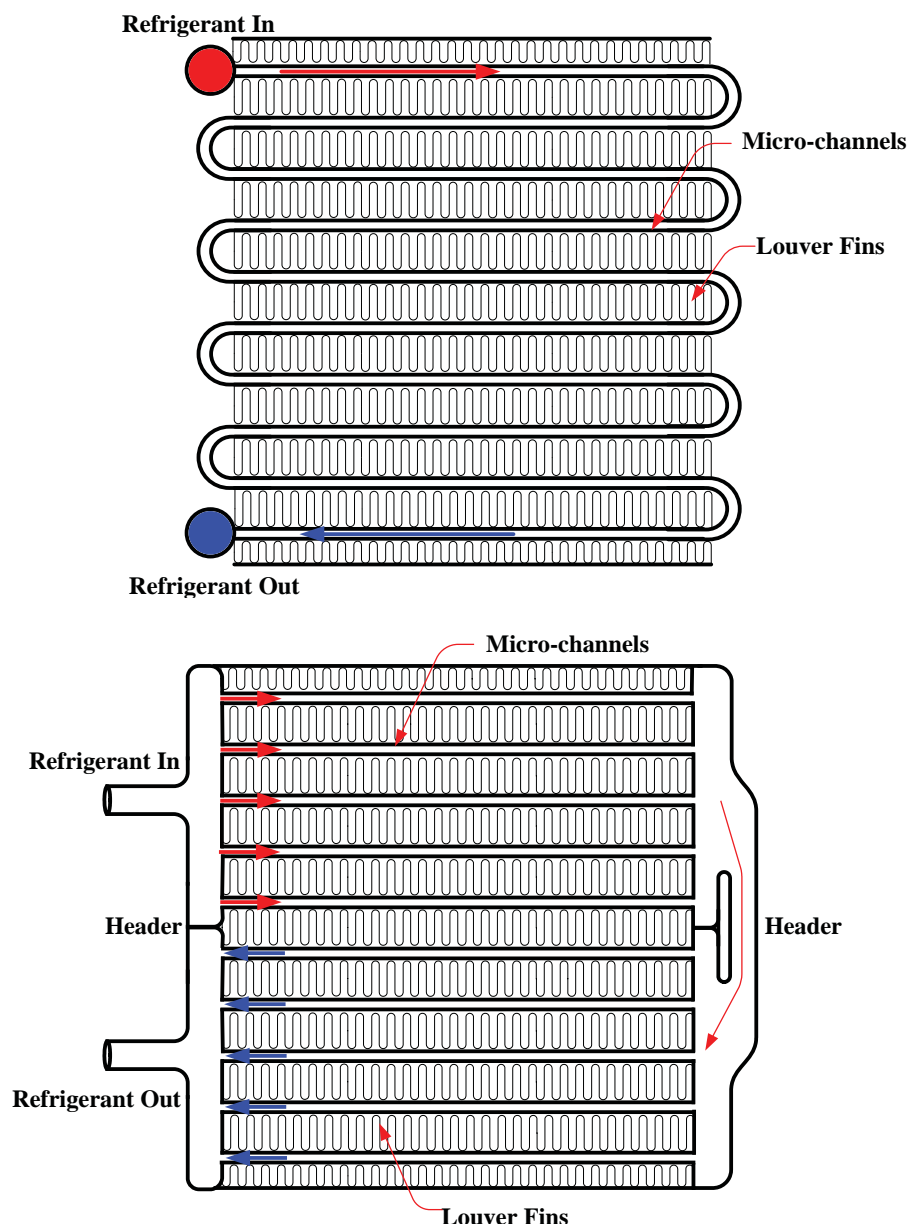
ศาสตราจารย์ ดร. สมชาย วงศิริเศษ ได้ออกเป็นหัวข้องานวิจัย ในโครงการ เลขที่ I350A13002 “การจำลองการทำงานของคุณเดนเซอร์ที่ระบบความร้อนด้วยอากาศที่ใช้ในระบบปรับอากาศและระบบทำความเย็น” ภายใต้การร่วมทุนระหว่าง สำนักงานกองทุนสนับสนุนการวิจัย (สกาว) และบริษัทชี แอร์คอน เทค จำกัด โดยผู้ดำเนินการคือ ศาสตราจารย์ ดร. สมชาย วงศิริเศษ และ คณะทำงาน โดยขอบเขตของงานจะจำกัดอยู่ที่การสร้างแบบจำลองทางคณิตศาสตร์และโปรแกรมคำนวณสำหรับการออกแบบคุณเดนเซอร์ที่ติดครีบ (Finned Tube Condenser) และระบบความร้อนด้วยอากาศ สมการต่างๆที่ใช้ในแบบจำลองทางคณิตศาสตร์คือสมการที่เป็นผลจากการวิจัยในส่วนของคุณเดนเซอร์ซึ่งได้ตีพิมพ์เผยแพร่แล้วในวารสารระดับนานาชาติ โดยผู้ได้รับผลประโยชน์จากการวิจัยคือ บริษัท ชี แอร์คอน เทค จำกัดในฐานะผู้ต้องการผลลัพธ์จากการและผู้มีส่วนสนับสนุน และสำนักงานกองทุนสนับสนุนการวิจัย (สกาว) ในฐานะองค์กรของรัฐที่มีส่วนในการสนับสนุน

ประโยชน์ที่ได้รับ ผลของการคิดค้น ปรับปรุง การใช้วิชาการที่ก่อให้เกิดประโยชน์ต่อประเทศไทย

สามารถนำไปสร้างคุณเดนเซอร์ให้มีประสิทธิภาพในการทำงานสูงขึ้น แต่เมื่อราคามาลง ทำให้โดยรวมจะทำให้เครื่องปรับอากาศมีความสามารถในการประหยัดพลังงานมากขึ้น สามารถนำมาใช้

ประโยชน์และ ช่วยพัฒนาอุตสาหกรรมการผลิตเครื่องปรับอากาศได้เป็นอย่างดี เพราะจะช่วยเป็นแนวทางในการออกแบบให้ได้ แผนกอนเดนเซอร์ ที่มีขนาดเหมาะสมกับสภาพการทำงานและสามารถทำความเย็น ทางเลือกใหม่ ซึ่งนอกจากจะช่วยประหยัดพลังงาน รักษาสิ่งแวดล้อม แล้วยังเป็นการเพิ่มคุณภาพ สินค้า ไทยที่ส่งออกไปยังตลาดต่างประเทศอีกด้วย

ผลลัพธ์ที่ได้มีประโยชน์โดยตรงอย่างยิ่งต่อบริษัทซี แอร์คอน เทค จำกัด และต่อประเทศไทย สามารถ ทำให้ประเทศไทยและประชาชนลดการใช้พลังงานฟอสซิลในรูปของน้ำมันและก๊าซธรรมชาติ ทำให้ ค่าใช้จ่ายของประชาชนและประเทศไทยในการใช้พลังงานลดลง ซึ่งเท่ากับช่วยประหยัดเงินตราในการ สั่งซื้อเชื้อเพลิงจากต่างประเทศได้ในระดับหนึ่ง ลดการก่อปัญหามลภาวะต่าง ๆ เพิ่มขีดความสามารถ ในการผลิตและพัฒนามาตรฐานของสินค้าให้สูงขึ้นในการแข่งขันกับประเทศโลกในภูมิภาคต่าง ๆ และ นำเงินตราเข้าประเทศ



บริษัท สมชายอินดัสตรี จำกัด

ชื่อโครงการ

การตรวจสอบการออกแบบอุปกรณ์แลกเปลี่ยนความร้อนแบบท่อติดครีบ (Finned Tube Heat Exchanger)

ที่มา หรือเหตุผลที่ศึกษา วิจัย คิดค้น หรือปรับปรุงความรู้

บริษัทสมชายอินดัสตรีจำกัด เป็นบริษัทของคนไทย ที่ผลิตอุปกรณ์แลกเปลี่ยนความร้อนประเภทต่างๆที่ใช้งานในอุตสาหกรรมต่างๆรวมถึง อุตสาหกรรมเครื่องปรับอากาศและความเย็นด้วย ผลิตภัณฑ์ส่วนใหญ่ผลิตตามความต้องการของลูกค้า (made to order) ซึ่งส่วนใหญ่คือลูกค้าในประเทศไทย อย่างไรก็ตามบริษัทฯยังขาดความรู้พื้นฐานทางวิศวกรรมเพื่อพัฒนาหรือปรับปรุงให้ผลิตภัณฑ์มีคุณภาพมากขึ้น

วัตถุประสงค์ในการศึกษา วิจัย คิดค้น

ตรวจสอบการออกแบบอุปกรณ์แลกเปลี่ยนความร้อนแบบท่อติดครีบ (Fin and Tube Heat Exchanger) เพื่อนำเสนอขายกับลูกค้าภายในประเทศ

วิธีการและขอบเขตในการคิดค้น ปรับปรุงความรู้ฯลฯ

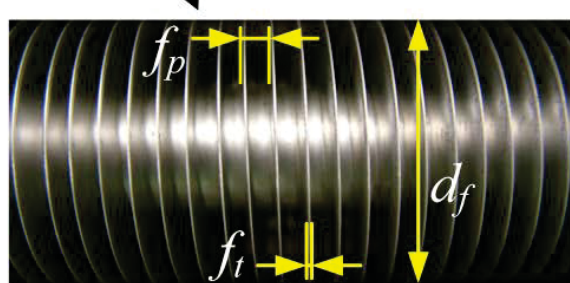
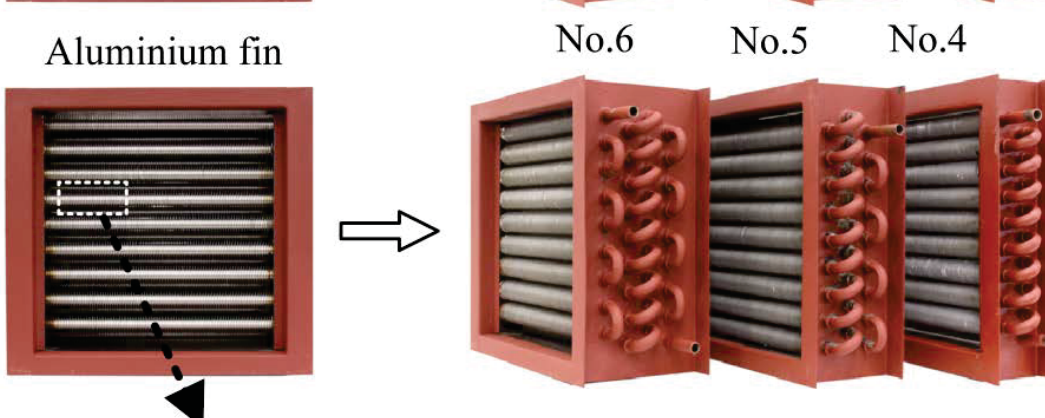
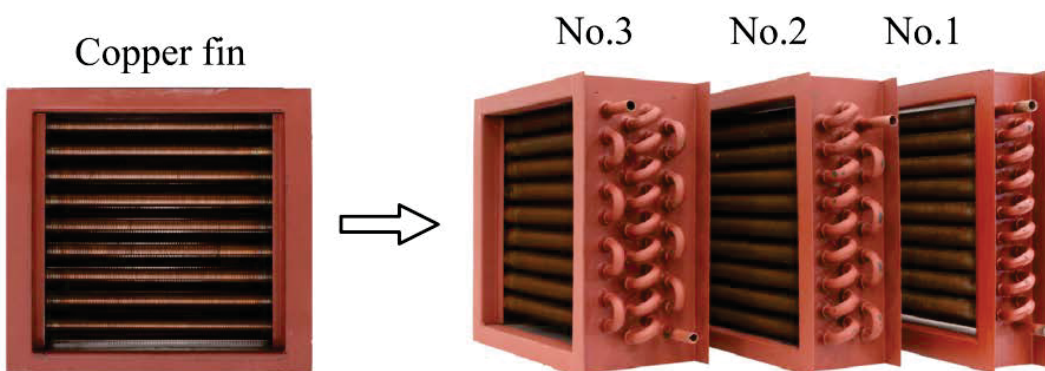
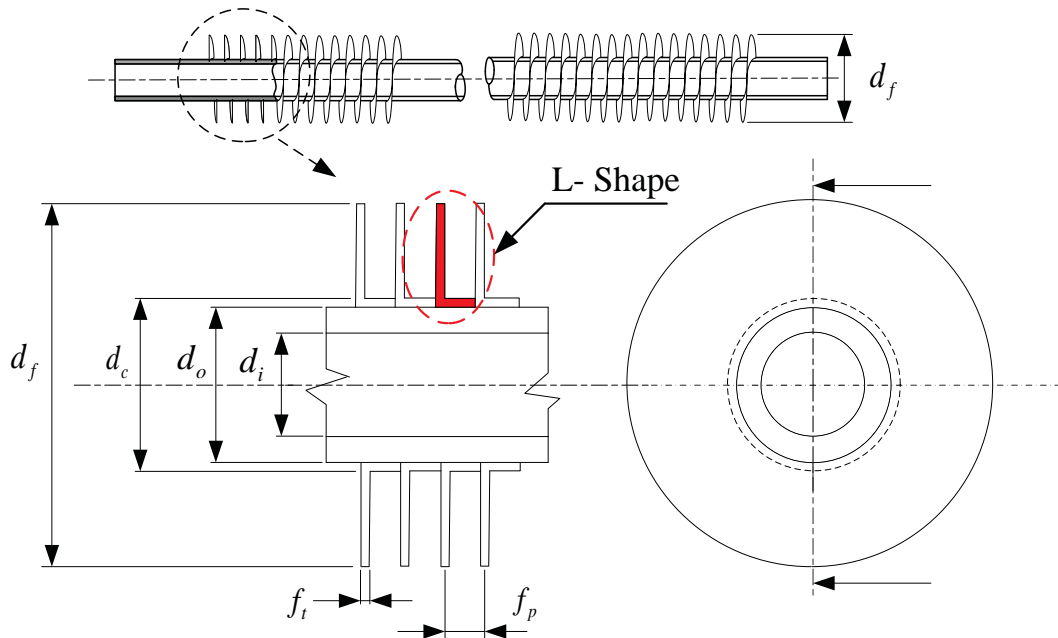
ศาสตราจารย์ ดร. สมชาย วงศ์เศษ ได้ใช้พื้นฐานทางวิศวกรรมเครื่องกลในส่วนของ การถ่ายเทความร้อน (Heat Transfer) ช่วยบริษัท สมชายอินดัสตรี จำกัด ใน การให้ความรู้ในการออกแบบ อุปกรณ์แลกเปลี่ยนความร้อนแบบท่อติดครีบ โดยทำการตรวจสอบการคำนวณก่อนที่จะนำไปสร้างจริง หรือ คำนวณสมรรถนะการถ่ายเทความร้อนจากอุปกรณ์แลกเปลี่ยนความร้อนที่มีอยู่แล้วจากข้อมูลจริงที่เก็บได้ข้างในส่วนของภาคสนาม การอาศัยวิชาการในการแก้ปัญหาช่วยยกระดับให้ผลิตภัณฑ์มีคุณภาพทัดเทียมกับผลิตภัณฑ์จากประเทศอุตสาหกรรม ทำให้ลูกค้าในประเทศหันมาใช้ผลิตภัณฑ์ที่ผลิตขึ้นเองในประเทศไทย เพราะมีคุณภาพดีและราคาถูกกว่ามาก เป็นการช่วยลดการนำเข้าสินค้าจากต่างประเทศได้ในระดับหนึ่ง

ผลของการคิดค้นหรือปรับปรุงหลังจากการทดลองคิดค้น ก่อให้เกิดการเปลี่ยนแปลงอย่างไร

ตัวอย่างหนึ่งของงานที่ได้ช่วยเหลือทางด้านวิชาการแก่บริษัทสมชายอินดัสตรีจำกัด ได้แก่ กรณีที่ โรงงานผลิตสินค้าแห่งหนึ่งซึ่งเดิมใช้อุปกรณ์แลกเปลี่ยนความร้อนแบบท่อติดครีบที่ผลิตในประเทศญี่ปุ่น โดยทำการแลกเปลี่ยนความร้อนระหว่างน้ำกับอากาศ หลังใช้งานไปจนอุปกรณ์แลกเปลี่ยนความร้อนเสื่อมคุณภาพ โรงงานดังกล่าวต้องการซื้อและติดตั้งใหม่โดยเลือกที่จะใช้อุปกรณ์แลกเปลี่ยนความร้อนแบบเดิมจากประเทศญี่ปุ่นอีก ศาสตราจารย์ ดร. สมชาย วงศ์เศษ ได้ช่วยบริษัท บริษัท สมชายอินดัสตรี จำกัด ใน การนำเสนออุปกรณ์แลกเปลี่ยนความร้อนที่ผลิตขึ้นเองภายในประเทศ ซึ่งมีราคาถูกกว่าที่ผลิตในญี่ปุ่นมาก (โดยมีราคาเพียง 2,500,000 บาท ต่อหนึ่งเครื่อง) แต่มีคุณภาพทัดเทียมกัน ทำให้สามารถลดการนำเข้าสินค้าได้ในระดับหนึ่ง

ประโยชน์ที่ได้รับ ผลของการคิดค้น ปรับปรุง การใช้วิชาการที่ก่อให้เกิดประโยชน์ต่อประเทศไทย

ผลของการช่วยเหลือทำให้บริษัทฯสามารถขยายผลิตภัณฑ์ได้และสามารถพัฒนาเทคโนโลยีการผลิตอุปกรณ์แลกเปลี่ยนความร้อน ซึ่งสามารถนำไปประยุกต์ใช้ได้มากกับอุตสาหกรรมอุณหภูมิ (Thermal Industry) ทำให้ในอนาคตอาจสามารถพัฒนาจนถึงขั้น เป็นอุตสาหกรรมส่งออกของประเทศไทย เพิ่มมาตรฐานสินค้าให้สูงขึ้นสามารถแข่งขันกับตลาดโลกได้ อันจะส่งผลต่อรายได้จากการติดตั้งในประเทศ และการจ้างงานของแรงงานในประเทศไทย อันจะส่งผลดีต่อระบบเศรษฐกิจและสังคมของประเทศโดยส่วนรวม



d_f = Outside diameter of fin (m)

f_p = Fin pitch (m)

f_t = Fin thickness (m)

บริษัท ไทย-เยอรมัน โปรดักส์ จำกัด (มหาชน)

ชื่อโครงการ

การออกแบบ และทดสอบห่อท่อที่มีเกลียวภายใน ที่ใช้กับสารทำความสะอาดเย็นขณะเปลี่ยนเฟส

ที่มา หรือเหตุผลที่ศึกษา วิจัย คิดค้น หรือปรับปรุงความรู้

บริษัท ไทย-เยอรมัน โปรดักส์ จำกัด (มหาชน) เป็นบริษัทของคนไทยที่ผลิตห่อ stainless steel รายใหญ่ที่สุดของประเทศไทย ทั้งเพื่อการส่งออกและจำหน่ายภายในประเทศ ห่อที่ผลิตจะมีหลายขนาดและเป็นท่อเรียบ (smooth tube) อย่างไรก็ตามบริษัทฯได้มีความร่วมมือกับ ศ.ดร.สมชาย วงศิริเศษ ในความพยายามที่จะผลิตห่อท่อที่มีร่องเกลียวภายใน เพื่อใช้ในอุปกรณ์แลกเปลี่ยนความร้อนที่ใช้ในกระบวนการแลกเปลี่ยนความร้อนในอุตสาหกรรมต่างๆ เนื่องจากเป็น stainless steel การผลิตหรือขึ้นรูปได้มาก ประกอบกับ มีพารามิเตอร์ต่างๆ มาก การทดสอบในห้องทดลองก่อนเป็นสิ่งจำเป็น

วัตถุประสงค์ในการศึกษา วิจัย คิดค้น

ออกแบบห่อ Grooved tube และ ทดสอบหา ผลกระทบของตัวแปรต่างๆรวมทั้งขนาดและรูปร่างของห่อ grooved tube ที่มีผลต่อสมรรถนะทางการถ่ายเทความร้อนและการลดของความดันในขณะไหลของของไหล เพื่อเป็นแนวทางในการออกแบบอุปกรณ์แลกเปลี่ยนความร้อน รวมทั้งคุณเดนเซอร์และอีว่าปอเรเตอร์ที่ใช้กับสารทำความสะอาดเย็น

วิธีการและขอบเขตในการคิดค้น ปรับปรุงความรู้ ฯลฯ

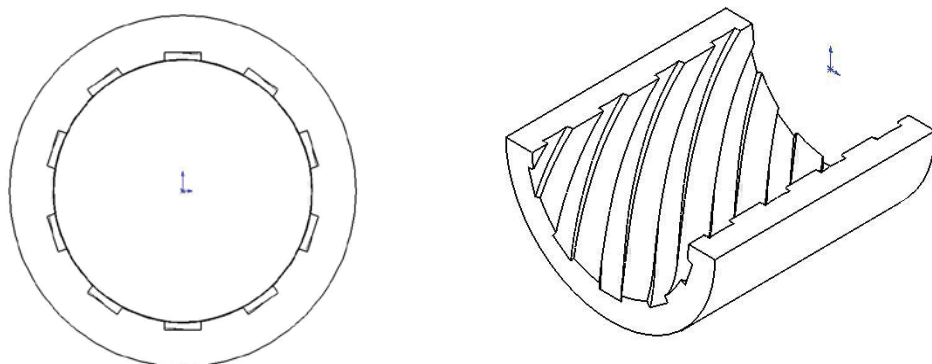
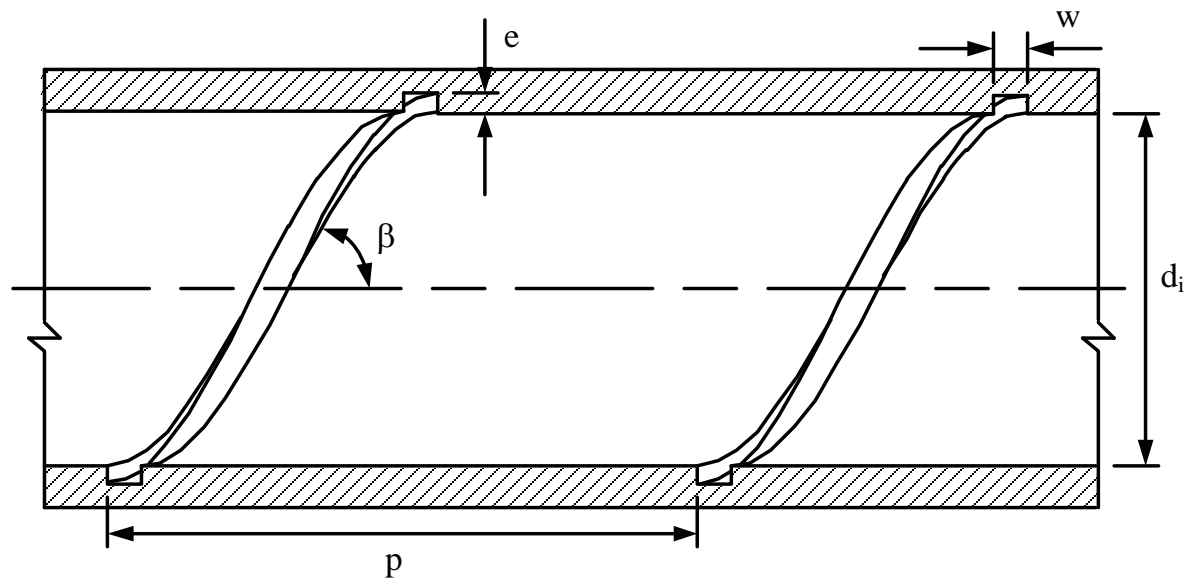
ศ. ดร. สมชาย วงศิริเศษ ได้ช่วยบริษัทฯในการออกแบบห่อ Grooved Tube โดยพิจารณาถึง ผลของตัวแปรต่างๆต่อสมรรถนะในการแลกเปลี่ยนความร้อน อาทิ เช่น Grooved Pitch, Grooved Depth and Helix Angle และสภาวะการใช้งานต่างๆ โดยได้สร้างอุปกรณ์ทดลองและทำการทดลองกับสารทำความสะอาดเย็น R134a โดยทางบริษัทฯ ได้ช่วยเหลือด้าน Hard Ware ทุกอย่างตามที่ร้องขอ ศ.ดร.สมชาย วงศิริเศษ ได้แยกงานส่วนต่างๆออกเป็น วิทยานิพนธ์ สำหรับ นักศึกษาระดับบัณฑิตศึกษา โดยได้มีการสร้างอุปกรณ์การทดลองขึ้นที่มหาวิทยาลัยฯ ทำการทดสอบ คำนวณและวิเคราะห์ผลลัพธ์ที่ได้ ผลจากการทดสอบได้ถูกส่งกลับยังบริษัทฯ เพื่อใช้ประกอบการออกแบบอุปกรณ์แลกเปลี่ยนความร้อน นอกจากนั้น ผลการศึกษาจังได้ถูกนำมาตีพิมพ์ในวารสารวิชาการระดับนานาชาติ (International Journal) จำนวนมาก โดยใช้ชื่อร่วมกันทั้งผู้วิจัยและเจ้าของบริษัทไทย-เยอรมัน โปรดักส์ จำกัด (มหาชน)

ประโยชน์ที่ได้รับ ผลของการคิดค้น ปรับปรุง การใช้วิชาการที่ก่อให้เกิดประโยชน์ต่อประเทศไทย

เนื่องจากบริษัท ไทย-เยอรมัน โปรดักส์ จำกัด (มหาชน) เป็นบริษัทที่ได้รับความเชื่อถือทั้งในประเทศไทยและต่างประเทศ บริษัทฯมียอดการผลิตและยอดการส่งออกจำนวนมากในแต่ละปี การได้รับความ

ช่วยเหลือทางวิชาการทำให้บริษัทฯ เชื่อมั่นใน ท่อ grooved tube โดยบริษัทฯ ถือว่าเป็นผลงานชิ้นสำคัญ และมุ่งมั่นว่าจะได้รับการตอบรับอย่างดีในอนาคต ซึ่งถ้ามองภาพรวมแล้วถ้าอุตสาหกรรมในประเทศไทยใช้ ผลิตภัณฑ์ดังกล่าวแล้วจะทำให้ประเทศไทยติดการใช้พลังงานจำนวนมหาศาล นอกจากนั้นยังช่วยเพิ่ม มาตรฐานสินค้านำเสนอและชื่อเสียงมาสู่ประเทศไทยติดจำนวนมหาศาล

ทางบริษัทฯ ได้ทำ brochure โดยนำเสนอ และได้อ้างอิงผลลัพธ์จากการศึกษาโดย ศ.ดร.สมชาย วงศิริเชษฐ์ ดังเอกสารแนบ





บริษัท ไทย-เยอรมัน โปรดักส์ จำกัด (มหาชน)
THAI-GERMAN PRODUCTS PUBLIC COMPANY LIMITED

16 กันยายน 2556

เรื่อง ขอขอบพระคุณ การสนับสนุนงานวิจัยผลิตท่อ EXTUBA

เรียน ศาสตราจารย์ ดร.สมชาย วงศิริเชษา

สิ่งที่ส่งมาด้วย 1. สำเนาประกาศเกียรติคุณ "EXTUBA TUBE ท่อสแตนเลสช่วยประยัดพลังงาน"

ตามที่คณะกรรมการวิจัยการวิทยาศาสตร์ เทคโนโลยี การสื่อสารและโทรคมนาคม วุฒิสภा ได้ดำเนินโครงการวิทยาศาสตร์สู่ความเป็นเลิศ พ.ศ.2556 เพื่อมอบใบประกาศเกียรติคุณให้แก่ บุคคล องค์กรภาครัฐ และองค์กรภาคเอกชน ซึ่งมีคุณสมบัติครบถ้วนในการประดิษฐ์ คิดค้น และนำวิทยาศาสตร์และเทคโนโลยีมาใช้ ประกอบกิจกรรมหรือประกอบกิจการงานก่อให้เกิดรายได้ทางเศรษฐกิจ และก่อให้เกิดประโยชน์ต่อสังคมและสิ่งแวดล้อมอย่างเป็นรูปธรรมนั้น บัดนี้การพิจารณาและประเมินผลงานได้เสร็จสิ้นลงและได้ประกาศผลเป็นที่เรียบร้อย เมื่อวันที่ 2 กันยายน 2556 ที่ผ่านมา ผู้จัดขึ้นแจ้งให้ทราบทราบว่า บริษัท ไทย-เยอรมัน โปรดักส์ จำกัด (มหาชน) เป็นหนึ่งในองค์กรเอกชนที่ได้รับการคัดเลือกให้เข้ารับใบประกาศเกียรติคุณดังกล่าวจากประธานวุฒิสภा ด้วยผลิตภัณฑ์ "EXTUBA TUBE ท่อสแตนเลสช่วยประยัดพลังงาน"

หลายปีที่ผ่านมา บริษัทฯได้คิดค้นและทำการพัฒนาท่อ EXTUBA TUBE อย่างต่อเนื่อง โดยได้รับ คำแนะนำจากท่าน และเพื่อให้แน่ใจในคุณภาพของผลิตภัณฑ์ บริษัทฯได้นำส่งท่อดังกล่าวไปทำการวิจัยกับท่าน ในห้องปฏิบัติการ ณ มหาวิทยาลัยเทคโนโลยีพระจอมเกล้าธนบุรี จังหวัดบริษัทฯ ได้นำผลการศึกษาวิจัยในครั้งนั้น ไปต่อยอดปรับปรุงพัฒนาผลิตภัณฑ์ท่อ EXTUBA จนเข้าสู่กระบวนการผลิตจริง หลังจากนั้นท่านยังได้นำผลการวิจัยบางส่วนไปตีพิมพ์ในวารสารระดับนานาชาติ ในนามของมหาวิทยาลัยเทคโนโลยีพระจอมเกล้าธนบุรีร่วมกับบริษัทฯ ซึ่งสิ่งนี้ถือได้ว่าเป็นการสร้างชื่อเสียงให้กับบริษัทฯ ทั้งในระดับชาติและนานาชาติ นอกเหนือจากการเผยแพร่ประชาสัมพันธ์แล้ว ท่านยังมีส่วนช่วยสร้างการรับรู้ผลการวิจัยดังกล่าวผ่านสื่อโซเชียลมีเดีย ทำให้สามารถสร้างความมั่นใจในผลิตภัณฑ์ได้เพิ่มมากขึ้น จนทำให้ท่อ EXTUBA ได้รับความสนใจและถูกนำไปใช้จริงในอุตสาหกรรมต่าง ๆ อย่างต่อเนื่อง และในช่วงที่บริษัทฯ ติดตามผลการใช้งานจริง ท่านก็ให้ความช่วยเหลือในการวิเคราะห์ผลและให้คำปรึกษา เพื่อให้บริษัทฯนำผลที่ได้รับไปปรับปรุงพัฒนาผลิตภัณฑ์ ดังกล่าว ให้สามารถนำมายังการสร้างประโยชน์ต่อสังคมและสิ่งแวดล้อมได้อย่างสมบูรณ์สูงสุด

จากส่วนที่ได้รับ ทราบได้ว่า บริษัทฯได้รับความช่วยเหลือและความร่วมมือของท่านที่เกิดขึ้นอย่างต่อเนื่องนี้เอง เป็นส่วนสำคัญอย่างยิ่งที่ทำให้บริษัท ไทย-เยอรมัน โปรดักส์ จำกัด (มหาชน) ได้รับการคัดเลือกให้เข้ารับประกาศเกียรติคุณจากวุฒิสภานี้

Hartsfield
Premium Lifestyle

THAI-GERMAN PRODUCTS PUBLIC COMPANY LIMITED
170/25-28 Ocean Tower 1, 10th Floor, Soi Sukhumvit 16 New Ratchadaphisek Rd.,
Klongtoey, Bangkok 10110 THAILAND Tel: (66 2) 261 3990 Fax: (66 2) 261 2769-70

Twitter



บริษัท ไทย-เยอรมัน โปรดักส์ จำกัด (มหาชน)
THAI-GERMAN PRODUCTS PUBLIC COMPANY LIMITED

ผมในฐานะกรรมการผู้จัดการ บริษัท ไทย-เยอรมัน โปรดักส์ จำกัด (มหาชน) พร้อมทั้งพนักงานและเจ้าหน้าที่ของบริษัทฯ รู้สึกซาบซึ้งในความมีน้ำใจ ความเอาใจใส่และความทุ่มเทของท่าน ผู้จังขอแสดงความขอบคุณอย่างจริงใจ มาก ณ โอกาสนี้ และหวังเป็นอย่างยิ่งว่า ท่านจะให้ความอนุเคราะห์ ช่วยเหลือทางวิชาการในการพัฒนาผลิตภัณฑ์ของบริษัทฯ อย่างต่อเนื่องเช่นนี้ตลอดไป

จึงเรียนมาเพื่อทราบ

ขอแสดงความนับถือ

(นายจารุ ลีลาประชากุล)
กรรมการผู้จัดการ

บริษัท ไทย-เยอรมัน โปรดักส์ จำกัด (มหาชน)

Hartsfield
Premium Lifestyle

THAI-GERMAN PRODUCTS PUBLIC COMPANY LIMITED
170/25-28 Ocean Tower 1, 10th Floor, Soi Sukhumvit 18, New Ratchadaphisek Rd.,
Klongtoey, Bangkok 10110 THAILAND Tel: (66 2) 261 3300 Fax: (66 2) 261 2769-70



บริษัท ไทย-เยอรมัน โปรดักส์ จำกัด (มหาชน)
THAI-GERMAN PRODUCTS PUBLIC COMPANY LIMITED

16 กันยายน 2556

เรื่อง ขอขอบพระคุณ การสนับสนุนงานวิจัยผลิตท่อ EXTUBA
เรียน ศาสตราจารย์ ดร.สมชาย วงศิริเชษฐ์
สิ่งที่ส่งมาด้วย 1. สำเนาประกาศเกียรติคุณ "EXTUBA TUBE ท่อสแตนเลสช่วยประหยัดพลังงาน"

ตามที่คณะกรรมการการวิทยาศาสตร์ เทคโนโลยี การสื่อสารและโทรคมนาคม วุฒิสภा ได้โครงการวิทยาศาสตร์สู่ความเป็นเลิศ พ.ศ.2556 เพื่อมอบใบประกาศเกียรติคุณให้แก่ บุคคล องค์กร และองค์กรภาคเอกชน ซึ่งมีคุณสมบัติครบถ้วนในการประดิษฐ์ คิดค้น และนำวิทยาศาสตร์และเทคโนโลยี ประกอบกิจกรรมหรือประกอบกิจการจนก่อให้เกิดรายได้ทางเศรษฐกิจ และก่อให้เกิดประโยชน์ต่อสังคมอย่างเป็นรูปธรรมนั้น บดีนี้การพัฒนาและประเมินผลงานได้เสร็จสิ้นลงแล้วได้ประกาศ เรียบร้อย เมื่อวันที่ 2 กันยายน 2556 ที่ผ่านมา ณ จังหวัดเชียงใหม่ ให้ท่านทราบว่า บริษัท ไทย-เยอรมัน จำกัด (มหาชน) เป็นหนึ่งในองค์กรเอกชนที่ได้รับการคัดเลือกให้เข้ารับใบประกาศเกียรติคุณดังกล่าว ประธานวุฒิสภा ด้วยผลิตภัณฑ์ "EXTUBA TUBE ท่อสแตนเลสช่วยประหยัดพลังงาน"

หลายปีที่ผ่านมา บริษัทฯได้คิดค้นและทำการพัฒนาท่อ EXTUBA TUBE อย่างต่อเนื่อง ในการออกแบบน้ำจากท่อ และเพื่อให้แน่ใจในคุณภาพของผลิตภัณฑ์ บริษัทได้นำส่งท่อดังกล่าวไปทำการวิจัย ในห้องปฏิบัติการ ณ มหาวิทยาลัยเทคโนโลยีพระจอมเกล้าธนบุรี ซึ่งทางบริษัทฯ ได้นำผลการศึกษาวิจัย นั้น ไปต่อยอดปรับปรุงพัฒนาผลิตภัณฑ์ท่อ EXTUBA จนเข้าสู่กระบวนการผลิตจริง หลังจากนั้นท่าน ผลการวิจัยบางส่วนได้รับการเผยแพร่ในวารสารระดับนานาชาติ ในนามของมหาวิทยาลัยเทคโนโลยีพระจอมเกล้าธนบุรีร่วมกับบริษัทฯ ซึ่งสิ่งนี้ถือได้ว่าเป็นการสร้างชื่อเสียงให้กับบริษัทฯ ทั้งในระดับชาติและนานาชาติ นอกเหนือจากการเผยแพร่ประชาสัมพันธ์แล้ว ท่านยังมีส่วนช่วยสร้างการรับรู้ผลการวิจัยดังกล่าวสู่ผู้บริโภค ให้สามารถสร้างความมั่นใจในผลิตภัณฑ์ได้เพิ่มมากขึ้น จนทำให้ท่อ EXTUBA ได้รับความสนใจนำไปใช้จริงในอุตสาหกรรมต่างๆ อย่างต่อเนื่อง และในช่วงที่บริษัทฯ ติดตามผลการใช้งานจริง ท่านก็ช่วยเหลือในการวิเคราะห์ผลและให้คำปรึกษา เพื่อให้บริษัทฯนำผลที่ได้รับไปปรับปรุงพัฒนาผลิตภัณฑ์ ให้สามารถนำมาใช้สร้างประโยชน์ต่อสังคมและส่งแวดล้อมได้อย่างสมบูรณ์สูงสุด

จากนี้ไป คาดว่า บริษัทฯจะสามารถดำเนินการอย่างต่อเนื่อง สำหรับโครงการนี้ ท่านจะได้รับความช่วยเหลือและความร่วมมือของท่านที่เกิดขึ้นอย่างต่อเนื่องนี้ ทางบริษัทฯ ขอขอบคุณจากวุฒิสภามหาวิทยาลัยเทคโนโลยีพระจอมเกล้าธนบุรี จำกัด (มหาชน) ที่ได้รับการคัดเลือกให้เข้ารับประกาศเกียรติคุณในครั้งนี้

เอกสารแนบท้ายเลข 2

ความเชื่อมโยงกับภาคการผลิตและการบริการ



กฎสีกา

ประกาศศักดิ์สิทธิ์กฎหมายฉบับใหม่

บริษัท ไทย-ยุโรปัน โปรดักส์ จำกัด (มหาชน)
"Extruda" ที่ได้จดทะเบียนจดทะเบียน
เพื่อขายส่งเชื้อชุมชนที่ไม่ดูดซึมและสามารถ
ในการซึมซานดูดซึมยาเสื่อมและยาไม่ถูก
เข้าห้องน้ำและไม่สามารถย่างเป็นรูปห้องน้ำที่ประยุกต์
ของแต่ละห้องน้ำที่มีลักษณะที่ไม่สามารถรับและดูดซึมไป
ให้ไว ณ วันที่ ๒ กันยายน พุทธศักราช ๒๕๖๒

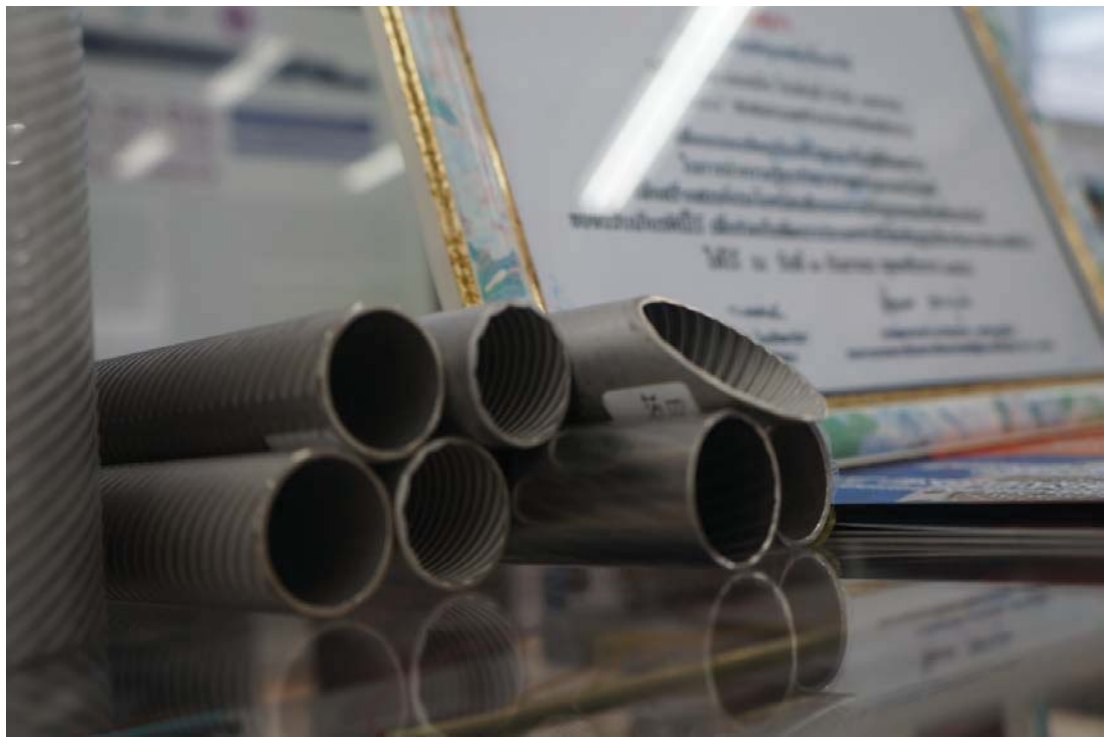
มูลนิธิ
อนามัย

นายพิมพ์ ไวยรัชชานนท์
ประธานสภานิติบัญญัติ

(นายกราชวิทย์ ดร.นิสราตน พะรุษภานัน)
ประชานาคราชวิทย์ราษฎร์ด้วยความเชื่ันลึก ข.ร. ๒๕๖๒

เอกสารแนบท้ายเลข 2

ความเชื่อมโยงกับภาคการผลิตและการบริการ



รูป Extuba Turbo Tube ที่ ศ.ดร. สมชาย วงศ์วิเศษ มีส่วนในการพัฒนาจนกระทั้งบริษัท
ไทย-เยอรมัน โปรดักส์ ได้รางวัลเชิดชูเกียรติจากรัฐสภาเมื่อ 2 ก.ย. 2556



รูป Extuba Turbo Tube ที่ ศ.ดร. สมชาย วงศ์วิเศษ มีส่วนในการพัฒนาจนกระทั้งบริษัท
ไทย-เยอรมัน โปรดักส์ ได้รางวัลเชิดชูเกียรติจากรัฐสภาเมื่อ 2 ก.ย. 2556